RAMAN SPECTRAL STUDIES OF

SOLUTIONS OF FORMIC ACID AND METHYL FORMATE

By

Richard J. Bartholomew, M.Sc.

A thesis
presented to the University of Waterloo
in fulfilment of the
thesis requirement for the degree of
Doctor of Philosophy
in
Chemistry

Waterloo, Ontario, Canada, 1996

© Richard J. Bartholomew 1996

National Library of Canada
Bibliothèque nationale du Canada

Acquisitions and Bibliographic Services
Acquisitions et services bibliographiques

395 Wellington Street
Ottawa ON K1A 0N4
Canada

395, rue Wellington
Ottawa ON K1A 0N4
Canada

Your file Votre référence

Our file Notre référence

The author has granted a non-exclusive licence allowing the National Library of Canada to reproduce, loan, distribute or sell copies of his/her thesis by any means and in any form or format, making this thesis available to interested persons.

L'auteur a accordé une licence non exclusive permettant à la Bibliothèque nationale du Canada de reproduire, prêter, distribuer ou vendre des copies de sa thèse de quelque manière et sous quelque forme que ce soit pour mettre des exemplaires de cette thèse à la disposition des personnes intéressées.

The author retains ownership of the copyright in his/her thesis. Neither the thesis nor substantial extracts from it may be printed or otherwise reproduced with the author's permission.

L'auteur conserve la propriété du droit d'auteur qui protège sa thèse. Ni la thèse ni des extraits substantiels de celle-ci ne doivent être imprimés ou autrement reproduits sans son autorisation.

0-612-21409-5

Canada

The University of Waterloo requires the signatures of all persons using or photocopying this thesis. Please sign below, and give address and date.

ABSTRACT

Raman Spectral Studies of Solutions of Formic Acid and Methyl Formate

Raman spectroscopy was used to study solutions of formic acid in water, acetonitrile, 1,4-dioxane, and dichloromethane and solutions of methyl formate in methyl d-formate and acetonitrile.

A very clear non-coincidence effect, NCE (i.e., $\nu_{aniso.} - \nu_{iso.} \neq 0$), exists for formic acid. Dilution in water led to a reduction of the NCE. Such behaviour is indicative of resonance energy transfer, which implies significant intermolecular coupling in formic acid and short range, short term order in the liquid. Dilution in acetonitrile and 1,4-dioxane led to the development of peaks at ~1735 cm^{-1} and ~1765 cm^{-1}. By comparison with methyl formate, the band at ~1735 cm^{-1} was assigned to uncoupled formic acid monomer. The band at ~1765 cm^{-1} was assigned to a formic acid---solvent complex. Independent evidence (perturbations of the solvent spectra) was found to support the existence of a complex. In the case of acetonitrile, this complex was investigated more deeply. A "Job" plot gave ambiguous results concerning the co-ordination number, n, of the "complex". "Equilibrium constants" were calculated for several possible

stoichiometries. At high relative amounts of acetonitrile the "equilibrium constant" increased dramatically (for each of the stoichiometries). At high concentrations of acetonitrile, a mixture of complexes may exist.

A non-coincidence effect also exists in methyl formate but is much smaller than in formic acid. The NCE was studied as a function of concentration and compared with several models in the literature. The behaviour of the NCE for the isotopic dilution (in methyl d-formate) conformed with the model tested. However, the non-isotopic dilution (in acetonitrile) did not conform with the models. The full width at half maximum of the carbonyl band exhibited unusual behaviour, first increasing and then decreasing, indicating a change in the nature of the intermolecular potential with dilution.

ACKNOWLEDGEMENTS

First of all, I thank Dr. D. E. Irish for his help, patience and guidance through the course of this project and the preparation of this thesis.

I wish to thank Dr. M. Brooker of Memorial University for advice and suggestions at the beginning of this project. He originally suggested the polarization studies of formic acid, but I expected those experiments to last about three weeks. Little did I realize this would mushroom into an entire thesis!

Without technical help of Andy Barber, Dave Bowen, Chris Gendron, Norm Harrison, John Selwood and Jacek Szubra this thesis could never have been completed.

I must, of course, thank my many co-workers over last few years: Dr. Marek Odziemkowski, Dr. Gerry Toogood, Dr. Grzegorz Szymanski, Dr. Zhongyi Deng, Brian Smith, Alexandre G. Brolo, Feng Guo, Y-K Ha, Joanne Gruithuizen, Jean Hein, Linda Fytche, Darrin Mayhew, Wendy Stevenson, Greg Keech, Kenneth Friesen and Sandra Brownlee. Not enough good things can be said. From the first day I joined this group (in September, 1990), the atmosphere in the group has been open, cheerful and supportive. We have been told our laughter can be heard down the corridor and that must say a lot.

If anyone in authority ever found out just how much fun we have, an investigation would probably be launched! If I ever work with as good a group of people again, I shall count myself extraordinarily lucky.

A thesis is a bit like a marathon; some faltering can be expected. Fortunately, the support and encouragement of my family and friends has helped me reach the finish line and I must thank them for it.

TABLE OF CONTENTS

ABSTRACT iv

ACKNOWLEDGEMENTS vi

LIST OF TABLES xi

LIST OF FIGURES xiv

LIST OF ABBREVIATIONS AND FORMULAE xix

1. INTRODUCTION 1

1.1 Preface 1

1.2 Raman Spectroscopy 3

1.2.1 Theory of Raman Spectroscopy 4

1.2.2 Practical Aspects of Raman Spectroscopy. 14

1.2.3 Instrumentation 17

1.2.4 Applications of Raman Spectroscopy 20

1.3 Resonance Energy Transfer 21

1.3.1 Theory of Scheibe 23

1.3.2 Theory of Fini and Mirone 24

1.3.3 Theory of McHale 29

1.3.4 Theory of Logan 33

1.3.5 Summary 40

1.4 References 42

2. EXPERIMENTAL 45

2.1 Chemicals and Solutions 45

2.2 Spectra Recorded at less than 100°C 45

2.3 High Temperature Furnace 47

2.4 Experimental Problems 51

2.5 Excitation and Detection 52

2.6 Computers and Software 57

2.7 References 63

2.8 Appendix I - Computer Programs 64

3. SOLUTIONS OF FORMIC ACID 82

3.1 Introduction 82

3.2 Experimental 86

3.3 Results and Discussion 89

3.3.1 Formic acid / Water 89

3.3.2 Formic Acid / Acetonitrile 102

3.3.3 Formic Acid / 1,4-dioxane 117

3.3.4 Formic Acid / Dichloromethane 128

3.3.5 Discussion of Binary Results 132

3.3.6 Formic Acid + Acetonitrile / Dichloromethane 140

3.4 Summary 166

3.5 References 168

4. SOLUTIONS OF METHYL FORMATE 171

4.1 Introduction 171

4.2 Experimental 176

4.3 Results and Discussion 180

4.3.1 Methyl Formate / Methyl d-Formate 183

4.3.2 Solutions of Methyl Formate / Acetonitrile 202

4.4 Summary 224

4.5 References 226

5. SUMMARY AND CONCLUSIONS 228

5.1 Formic Acid 228

5.2 Methyl Formate 230

5.3 References 233

LIST OF TABLES

Table 3.1: Partial Assignment of Formic Acid 85

Table 3.2: Concentrations of Formic Acid / Water Solutions 90

Table 3.3: Non-Coincidence Effect for Formic Acid / Water 97

Table 3.4: Concentration Summary for Formic Acid / Acetonitrile Solutions 103

Table 3.5: Summary of Bandfitting for Formic Acid / Acetonitrile (Carbonyl Region) 107

Table 3.6: Fraction of Total Area of 2270 cm^{-1} Band in Formic Acid / Acetonitrile Solutions (Nitrile Stretch) 112

Table 3.7: Summary of Concentrations for Formic Acid / 1,4-dioxane 118

Table 3.8: Assignment of 1,4-dioxane Spectrum 120

Table 3.9: Concentration Summary for Formic Acid / Dichloromethane Solutions 129

Table 3.10: Concentrations for (Formic Acid + Acetonitrile) / Dichloromethane (Job Plot) 145

Table 3.11: Relative Integrated Intensities of the "Bound" Acetonitrile for the (Formic Acid + Acetonitrile) / Dichloromethane System 149

Table 3.12: Summary of 'α' Values for the (Formic Acid + Acetonitrile) / Dichloromethane System 156

Table 3.13: Summary of Fraction of Bound Acetonitrile and "Equilibrium Constant" for (Formic Acid + Acetonitrile) / Dichloromethane 158

Table 3.14: Average Solvation Numbers of Formic Acid in the (Formic Acid + Acetonitrile) / Dichloromethane System 162

Table 4.1: Comparison of Physical Properties of Formic Acid and Methyl Formate 172

Table 4.2: Concentration Summary for Methyl Formate / Methyl d-Formate 178

Table 4.3: Concentrations Summary for Methyl Formate / Acetonitrile 179

Table 4.4: Assignment of Methyl Formate and Methyl d-Formate 182

Table 4.5: Summary of Band Maxima Frequencies for Methyl Formate / Methyl d-Formate (Carbonyl Mode) 189

Table 4.6 Summary of Band First Moments for Methyl Formate / Methyl d-Formate (Carbonyl Mode) 193

Table 4.7: Half Widths at Half Maxima and Full Widths at Half Maxima for Methyl Formate / Methyl d-Formate (Carbonyl Mode) 198

Table 4.8: Summary of Band Maxima Positions, Non-coincidence Effect, and Relative Non-coincidence Effect for Methyl Formate / Acetonitrile (Carbonyl Mode) 204

Table 4.9: Summary of Band First Moments, Non-coincidence Effect and Relative Non-coincidence Effect for Methyl Formate / Acetonitrile (Carbonyl Mode) 215

Table 4.10: Indices of Refraction for Methyl Formate / Acetonitrile Solutions 218

Table 4.11: Half Widths at Half Maxima and Full Widths at Half Maxima for Methyl Formate / Acetonitrile (Carbonyl Mode) 222

LIST OF FIGURES

Fig. 1.1: Schematic Layout of a Typical Raman Experiment 18

Fig. 2.1: Copper Block for Holding Capillary Tubes 46

Fig. 2.2: High Temperature Furnace 48

Fig. 2.3: Comparison of Parallel and Perpendicular Orientations of the Furnace Sample Cell for 2.8 m $ZnSO_4$ 50

Fig. 2.4: The Sample Compartment of the Jarrell-Ash Spectrometer 54

Fig. 2.5: Spectral Resolution as a Function of Raman Shift 56

Fig. 3.1: Survey Spectrum of 98% Formic Acid 84

Fig. 3.2: Survey Spectrum of Formic Acid / Water (X(HCOOH) = 0.501) 91

Fig. 3.3: Carbonyl Modes of Formic Acid / Water 92

Fig. 3.4: Polarization Studies of Formic Acid / Water 94

Fig. 3.5: Polarization Studies of Formic Acid at ~100°C 95

Fig. 3.6: Non-Coincidence Effect as a Function of Mole Fraction 96

Fig. 3.7: Effect of Dilution on the "Association" Band of Formic Acid 99

Fig. 3.8: Effect of Dilution on the O-C=O Deformation Modes of Formic Acid 101

Fig. 3.9: Spectra of Formic Acid / Acetonitrile (X(HCOOH) = 0.503) 104

Fig. 3.10: Carbonyl Region of Formic Acid / Acetonitrile 106

Fig. 3.11: Variation of the Band Parameters for the Carbonyl Region of Formic Acid / Acetonitrile 108

Fig. 3.12: Nitrile Stretching Region for Formic Acid / Acetonitrile 110

Fig. 3.13: Variation of the Fraction of the Total Intensity of the Nitrile Stretch due to "Bound" Acetonitrile with Mole Fraction of Formic Acid 111

Fig. 3.14: Spectra of Solutions of Methyl Formate / Acetonitrile 114

Fig. 3.15: Spectra of Formic Acid + Acetonitrile / 1,4-dioxane 116

Fig. 3.16: Survey Spectra of 1,4-dioxane and Formic Acid / 1,4-dioxane 119

Fig. 3.17: Spectra of 1,4-dioxane and Formic Acid / 1,4-dioxane (350 - 750 cm^{-1}) 122

Fig. 3.18: Spectra of 1,4-dioxane and Formic Acid / 1,4-dioxane (900 - 1275 cm^{-1}) 124

Fig. 3.19: Carbonyl Region of Formic Acid / 1,4-dioxane 125

Fig. 3.20: Variation of the Band Parameters for the Carbonyl Region of Formic Acid / 1,4-dioxane 127

Fig. 3.21: Carbonyl Region of Formic Acid / Dichloromethane 131

Fig. 3.22: Effect on "Association" Band of Formic Acid of Dilution in Dichloromethane 133

Fig. 3.23: Variation of the Band Parameters for the 1735 cm^{-1} Band of Formic Acid in Acetonitrile and in 1,4-dioxane 136

Fig. 3.24: Variation of the Fraction of Total Carbonyl Intensity and Relative Intensity of the 1765 cm^{-1} of Formic Acid in Acetonitrile and in 1,4-dioxane 138

Fig. 3.25: ν_3 and ν_9 Modes of CH_2Cl_2 in (Formic Acid + Acetonitrile) / Dichloromethane 147

Fig. 3.26: Job Plot for the (Formic Acid + Acetonitrile) / Dichloromethane 148

Fig. 3.27: Determination of J_B and J_F for the Nitrile Bands in the (Formic Acid + Acetonitrile) / Dichloromethane 154

Fig. 3.28: Fraction of "Bound" Acetonitrile as a Function of 'α' and 'R' for the (Formic Acid + Acetonitrile) / Dichloromethane 157

Fig. 3.29: "Equilibrium Constants" for the Formic Acid--Acetonitrile Complex for Different Stoichiometries 161

Fig. 3.30: Average Solvation Number of Formic Acid in the (Formic Acid + Acetonitrile) / Dichloromethane System vs. the Free Acetonitrile Concentration 164

Fig. 3.31: The Carbonyl Region of Formic Acid for the (Formic Acid + Acetonitrile) / Dichloromethane and the Variation of the Intensity of the 1760 cm^{-1} Band with the Concentration of the Complex 165

Fig. 4.1: Spectra of Pure Methyl Formate 181

Fig. 4.2: Isotropic and Anisotropic Spectra of Methyl Formate and Methyl d-Formate 184

Fig. 4.3: Isotropic and Anisotropic Spectra of Methyl Formate / Methyl d-Formate 186

Fig. 4.4: Bandfitting Results for Methyl Formate / Methyl d-Formate 187

Fig. 4.5: Overall Calculated Contour and Component Bands for the Carbonyl Stretch of Methyl Formate / Methyl d- Formate 188

Fig. 4.6: Isotropic and Anisotropic Peak Positions for Methyl Formate / Methyl d-Formate 190

Fig. 4.7: Non-Coincidence Effect for Methyl Formate / Methyl d-Formate 192

Fig. 4.8: (Isotropic Spectral First Moment - Band Maximum) vs. Mole Fraction for Methyl Formate / Methyl d-Formate 194

Fig. 4.9: Test of Logan's Model for the NCE of Methyl Formate / Methyl d-Formate 196

Fig. 4.10: Effect of Dilution on Bandwidth of Methyl Formate / Methyl d-Formate 199

Fig. 4.11: Bandfitting in the Carbonyl Region of Methyl Formate / Acetonitrile 203

Fig. 4.12: Isotropic and Anisotropic Band Positions for Carbonyl Band for Methyl Formate / Acetonitrile 205

Fig. 4.13: Non-Coincidence Effect for Methyl Formate / Acetonitrile vs. Mole Fraction 207

Fig. 4.14: Non-Coincidence Effect for Methyl Formate / Acetonitrile vs. Volume Fraction 210

Fig. 4.15: Test of Fini and Mirone's Model for the Non-Coincidence Effect of Methyl Formate / Acetonitrile 211

Fig. 4.16: Test of McHale's Model for the Non-Coincidence Effect of Methyl Formate / Acetonitrile 213

Fig. 4.17: Test of Mirone's Modification of McHale's Model for the Non-Coincidence Effect of Methyl Formate / Acetonitrile 214

Fig. 4.18: Index of Refraction of Methyl Formate / Acetonitrile Solutions 217

Fig. 4.19: (Isotropic Spectral First Moment - Band Maximum) vs. Mole Fraction for Methyl Formate / Acetonitrile 220

Fig. 4.20: Effect of Dilution on Bandwidth for Methyl Formate / Acetonitrile 223

LIST OF ABBREVIATIONS AND FORMULAE

C . . . . . Formal Concentration

[ ] . . . . . Equilibrium Concentration

FWHM . . . . . Full Width at Half Maximum

HWHM . . . . . Half Width at Half Maximum

NCE . . . . . Non-coincidence Effect

RET . . . . . Resonance Energy Transfer

ν . . . . . Vibrational Energy (cm^{-1})

ω . . . . . Angular Frequency (rad s^{-1})

M . . . . . Spectral First Moment

X . . . . . Mole Fraction

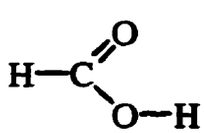

. . . . . Formic Acid (HCOOH), FA

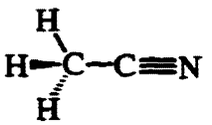

. . . . . Acetonitrile (CH_3CN), AN

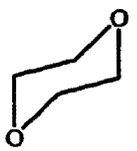

. . . . . 1,4-dioxane ($C_4H_8O_2$)

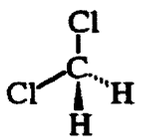

. . . . . Dichloromethane (CH_2Cl_2)

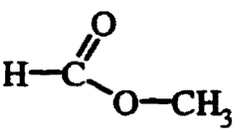

. . . . . Methyl Formate ($HCOOCH_3$), MF

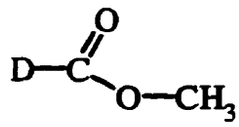

. . . . . Methyl d-Formate ($DCOOCH_3$), d-MF

1. INTRODUCTION

1.1 Preface

A goal of the research described in this thesis was to attain a better understanding of the "structure" of liquid formic acid, methyl formate, and their solutions; the principal technique has been Raman spectroscopy. Results from neat formic acid at room temperature and at elevated temperatures have already been reported (1); the study of formic acid solutions is a natural extension. Previously in our group acetic acid was studied as a function of concentration and temperature (2) and formic acid was a natural choice for a similar study. The high temperature results indicated formic acid, while structurally similar to acetic acid, has a significantly different liquid structure. The explanations presented for acetic acid were not applicable to liquid formic acid. In an attempt to further elucidate the structure of liquid formic acid, the study was extended to include polarization results and solution studies. The inclusion of methyl formate may appear, at first glance, somewhat arbitrary. However, methyl formate is closely related to formic acid. The acidic proton is replaced by a methyl group, precluding hydrogen bonding. Hydrogen bonding is obviously present in formic acid and methyl formate is the closest structural analogue where hydrogen bonding is absent. By studying this non-

hydrogen bonded analogue, some light may be shed on the liquid structure of formic acid. Furthermore, methyl formate is a solvent of intrinsic interest. Methyl formate has been suggested as a solvent for the preparation of electrolytes for lithium batteries (3). As such, further understanding of its liquid structure and interactions with other species is desirable.

This thesis is organized as follows. The first chapter gives a brief overview of the theory and application of Raman spectroscopy, followed by a discussion of resonance energy transfer. The second chapter outlines the general experimental procedures. Experimental details are presented in the following chapters as required. The third and fourth chapters present the studies of formic acid and methyl formate, respectively. Each chapter has been written, as much as possible, as a self-contained "unit". Consequently, there is no central list of references - they are presented at the end of each chapter. Throughout this thesis 'ν' has been used to represent frequency in wavenumber units. Conventionally, ν with a horizontal bar is used for this. Unfortunately, the limitations of the text editor used to prepare this thesis prevent the easy generation of such a character.

1.2 Raman Spectroscopy

Raman spectroscopy is a form of optical spectroscopy which, like infrared spectroscopy, provides information about the vibrational modes of molecules. Smekal (4) theoretically predicted the Raman effect (or combination scattering) in 1923 but it was not observed until 1928. Simultaneously, Raman and Krishnan (5) and Landsberg and Mandelstam (6) observed combination scattering. Raman later won a Nobel prize for the achievement. Initially, Raman spectroscopy enjoyed a period of widespread use because, at the time, it was experimentally easier than infrared spectroscopy. However, infrared instrumentation advanced rapidly and Raman spectroscopy was pushed into the background, becoming the territory of specialists (7). In the late 1960's and early 1970's, the invention of the laser and its subsequent replacement of the mercury arc lamp as a source of sample excitation led to rebirth of Raman spectroscopy as a practical technique. Since then, advances in detector technology, computer control, and data analysis have led to its popularity and a respected position among the tools for the characterization of matter.

1.2.1 Theory of Raman Spectroscopy

Raman spectroscopy is based on a light scattering phenomenon. A monochromatic source (usually a laser) illuminates the sample. When an incident photon interacts with a molecule, it can be scattered either elastically (with no change in energy) or inelastically (with a change in energy). The former process is known as Rayleigh scattering and the latter is called Raman scattering. The Rayleigh scatter is much less intense than the incident radiation and the intensity of the Raman scattering is much weaker (ca. 10^{-3} times) than the Rayleigh scattering.

The following short discussion of the (classical) theory of Raman spectroscopy has been adapted from Guillory (8).

Rayleigh scattering may be thought of in terms of the following equation:

$$M(z=0) + hc\nu_0 \rightarrow M(z=0) + hc\nu_0 \qquad [1]$$

where M(z = 0) represents a molecule in the ground vibrational state and $h\nu_0$ is the energy of the incident photon. Normal Raman (Stokes) scattering, on the other hand, may be written as:

$$M(z=0) + hc\nu_0 \rightarrow M(z=1) + hc(\nu_0 - \nu_s) \qquad [2]$$

where M ($z = 1$) represents a molecule in a first excited vibrational state and $hc(\nu_0 - \nu_s)$ is the energy difference between the incident and scattered photons. The difference is referred to as a Raman shift and is equal to a vibrational, rotational or electronic energy change of the molecule. The difference in energy between the incident radiation and the scattered radiation is independent of the energy of the incident photon. It is, in fact, the energy difference between the ground state and a first excited state - a characteristic property of the molecule.

The Raman effect arises because of an induced oscillating dipole moment, μ, generated in the molecules by the interaction of the electric field vector, **E**, of the incident radiation. The induced dipole moment is given by:

$$\mu = \alpha E \qquad [3]$$

where α is the polarizability - a tensor quantity. If the medium is anisotropic, then

$$\mu = \begin{pmatrix} \alpha_{xx} & \alpha_{xy} & \alpha_{xz} \\ \alpha_{yx} & \alpha_{yy} & \alpha_{yz} \\ \alpha_{zx} & \alpha_{zy} & \alpha_{zz} \end{pmatrix} \begin{pmatrix} E_x \\ E_y \\ E_z \end{pmatrix} \qquad [4]$$

(α is a symmetric matrix).

As the molecule vibrates the polarizability will change. For small variations about the equilibrium position, α_{xx} (or any element of α) can be expanded as a Taylor series in normal co-ordinates:

$$\alpha_{xx} = \alpha_{xx}^{e} + \sum_{k=1}^{3N-6} \left(\frac{\partial \alpha_{xx}}{\partial Q_k} \right)_e Q_k \qquad [5]$$

where α_{xx}^{e} is the equilibrium polarizability along the x direction induced by E_x. Higher terms in this expansion have been neglected.

For a normal mode undergoing simple harmonic motion:

$$Q_k = Q_k^0 \cos(2\pi c \nu_k t) \qquad [6]$$

where Q_k^0 is the amplitude of vibration and ν_k is the frequency of the vibration. Therefore,

$$\alpha_{xx} = \alpha_{xx}^{e} + \sum_{k=1}^{3N-6} \left(\frac{\partial \alpha_{xx}}{\partial Q_k} \right)_e Q_k^0 \cos(2\pi c \nu_k t) \qquad [7]$$

If the x component of the electric field of the incident radiation can be expressed by

$$E_x = E_x^0 \cos(2\pi c \nu_0 t) \qquad [8]$$

where E_x^0 is the amplitude of the electric vector and ν_0 is the frequency of the incident light, then

$$\alpha_{xx} E_x = \alpha_{xx} E_x^o \cos(2\pi c \nu_0 t) \qquad [9]$$

$$\alpha_{xx} E_x = \left[\begin{array}{l} \alpha_{xx}^e E_x^0 \cos(2\pi c \nu_0 t) \\ + E_x^0 \sum_{k=1}^{3N-6} \left(\frac{\partial \alpha_{xx}}{\partial Q_k} \right)_e Q_k^0 \cos(2\pi c \nu_0 t) \cos(2\pi c \nu_k t) \end{array} \right] \qquad [10]$$

(this is the 'x' component of the induced dipole). Using the trigonometric relation cos(a)cos(b)=½[cos(a+b)+cos(a-b)]:

$$\alpha_{xx} E_x = \left[\begin{array}{l} \alpha_{xx}^e E_x^0 \cos(2\pi c \nu_0 t) + E_x^0 \sum_{k=1}^{3N-6} \frac{1}{2} \left(\frac{\partial \alpha_{xx}}{\partial Q_k} \right)_e \cdot \\ \left(Q_k^0 \left[\cos(2\pi c(\nu_0 + \nu_k) t + \cos(2\pi c(\nu_0 - \nu_k) t] \right) \right] \end{array} \right] \qquad [11]$$

The first term on the right hand side of this equation characterizes the intensity of the Rayleigh line and is proportional to α_{xx}^e. The second term gives the Raman intensity and is proportional to $(\partial\alpha_{xx} / \partial Q_k)_e$. Thus, for a vibration to be Raman active it must have a non-zero fluctuating polarizability at equilibrium. The derivation also shows that Raman intensity occurs at $\nu_0 - \nu_k$ and $\nu_0 + \nu_k$, the Stokes and anti-Stokes lines respectively. This derivation implies equal intensity for both the Stokes and anti-Stokes lines. This, however, is not true as will be discussed later. It also allows only fundamental

transitions. These flaws arise from restriction to a classical derivation and use of the simple harmonic oscillator approximation. The expression above was derived using only one element of the tensor. A full treatment requires the use of all the tensor elements, but the derivation for each element is essentially the same.

When Raman scattering takes place, the scattered light can be of higher or lower frequency than the incident light. When it is higher, it is referred to as anti-Stokes scattering and when it is lower, Stokes scattering. Anti-Stokes scattering occurs when a molecule in an excited vibrational state surrenders energy to the incident photon, thereby relaxing to a lower energy state. For Stokes scattering the opposite is true: a molecule in a vibrational ground state obtains energy from the incident photon and is excited to a higher state. Boltzmann statistics dictate that at low temperatures most molecules are in vibrational ground states, so, because intensity is related to the number of molecules making the transition, Stokes lines are normally far more intense than anti-Stokes lines. In light of this fact, most Raman spectroscopy is done by studying the Stokes lines. The intensity of Raman scattering depends on the *absolute* frequency of the scattered light raised to the fourth power (see equation [17]). Consequently, excitation is usually in the visible region (commonly at 488.0 nm or 514.5 nm from an argon ion laser).

The classical treatment of the Raman effect gives an incomplete picture. A complete study requires the use of time-dependent perturbation theory and is given by

Long (9). Only a brief comment on the results will be given here.

Placzek (10) derived the expressions for Raman scattering for different geometries. The polarizability is divided into two parts: a symmetric part, α, and an asymmetric part, β:

$$\alpha_T = \alpha + \beta \qquad [12]$$

The symmetric part is defined as:

$$\alpha = \frac{1}{3}(\alpha_{xx} + \alpha_{yy} + \alpha_{zz}) \qquad [13]$$

and the asymmetric part as:

$$\beta = \frac{1}{\sqrt{2}}\left[(\alpha_{xx} - \alpha_{yy})^2 + (\alpha_{yy} - \alpha_{zz})^2 + (\alpha_{zz} - \alpha_{xx})^2 + 6(\alpha_{xy}^2 + \alpha_{yz}^2 + \alpha_{zx}^2)\right]^{\frac{1}{2}} \qquad [14]$$

(α_{ij} being the elements of the polarizability tensor defined in equation [4]). A transformation of the basis vectors can always be found that will diagonalize the tensor matrix. If this is done, the expression for β is greatly simplified:

$$\beta = \frac{1}{\sqrt{2}}\left[(\alpha_{xx} - \alpha_{yy})^2 + (\alpha_{yy} - \alpha_{zz})^2 + (\alpha_{zz} - \alpha_{xx})^2\right]^{\frac{1}{2}} \qquad [15]$$

In Raman spectroscopy the polarizability derivatives are the important quantities. These are defined as:

$$\alpha'_i = \frac{\partial \alpha}{\partial Q_i} \quad ; \quad \beta'_i = \frac{\partial \beta}{\partial Q_i} \qquad [16]$$

where 'Q' is the vibrational normal coordinate for a given mode.

For 90° scattering geometry, the intensity of the Stokes scattered light is (9):

$$I_i = C \frac{(\nu_0 - \nu_{mn})^4}{\nu_{mn}} \frac{NI_0}{1 - \exp\left(\frac{-hc\nu_{mn}}{kT}\right)} [45(\alpha'_i)^2 + 7(\beta'_i)^2] \qquad [17]$$

where

C	=	constant.
ν_0	=	incident frequency in cm^{-1}
$hc\nu_{mn}$	=	the energy difference between an initial state 'm' and a final state 'n'
N	=	number of molecules initially in state 'm'
I_0	=	the incident intensity.

For anti-Stokes "$(\nu_0 + \nu_{mn})^4$" replaces "$(\nu_0 - \nu_{mn})^4$" and "$\exp(hc\nu_{mn} / kT) - 1$" replaces "$1 - \exp(-hc\nu_{mn} / kT)$". The constants 45 and 7 arise from orientational averaging and are a result of the particular experimental geometry. From this result, the ratio of Stokes to

anti-Stokes intensity is found:

$$\frac{I_{Stokes}}{I_{anti-Stokes}} = \left(\frac{\nu_0 - \nu_{mn}}{\nu_0 + \nu_{mn}}\right)^4 \exp\left(\frac{hc\nu_{mn}}{kT}\right) \qquad [18]$$

This expression is found to be valid at thermal equilibrium (11). The exciting frequency is assumed to be well separated from any electronic transitions. If not, the intensities can be greatly enhanced by the resonance Raman effect (11).

In Raman spectroscopy the polarization characteristics of the incident light are known. Light scattered from a randomly oriented liquid will have electric vectors whose orientation is parallel ($I_{\parallel}$) and perpendicular ($I_{\perp}$) to the orientation of the incident electric vector. By using a simple Polaroid film either one of these orientations can be selectively studied. A quantity known as the depolarization ratio, defined as:

$$\rho = \frac{I_{\perp}}{I_{\parallel}}$$

can be calculated and can be used to determine structural information. With 90° scattering geometry, polarized incident light (as from an argon ion laser), and a Polaroid filter to analyze the scattered radiation, the depolarization ratio will have a value between 0 and 0.75. For totally symmetric vibrations $\rho < 0.75$ (in theory, for cubic point groups, it should be zero) while for non-totally symmetric vibrations $\rho = 0.75$ (the value depends on the experimental geometry (12)). Therefore, the number of totally symmetric modes

can be found easily. This helps elucidate the structure of the species under investigation. In addition to this rather simple analysis, two intensity functions may be defined as follows:

$$I_{iso.} = I_{\parallel} - \frac{4}{3} I_{\perp} \qquad [20]$$

$$I_{aniso.} = I_{\perp} \qquad [21]$$

These are the isotropic and anisotropic intensities, respectively. The anisotropic spectrum depends on both vibrational and reorientational motion of the molecule while the isotropic depends only on vibrational motion (13). In some cases information about vibrational and reorientational relaxation can be extracted from the data - vibrational and reorientational relaxation times may be determined from the half-widths of the isotropic and anisotropic spectra. The phenomenon of resonance energy transfer (see section 1.3) can be studied by examining the isotropic and anisotropic spectra as a function of concentration. Valuable conclusions can then be drawn about intermolecular forces and liquid structure.

At low Raman shifts a problem arises in separating the Rayleigh scatter from the Raman scatter. This is particularly pronounced over the range 0 - 200 cm^{-1}. For gases this low frequency region will display discrete lines from rotational transitions. With solids, discrete lines from the lattice normal modes are clearly observed. For liquids and solutions, however, sharp lines are not observed and separating the Raman from the

Rayleigh scatter becomes more difficult. Brooker, Nielsen and Praestgaard (14) and Murphy et al. (15) have asserted that most low frequency intensity above 10 cm^{-1} should be regarded as Raman scatter. To extract the low frequency Raman data from the Rayleigh wing they proposed a so called "reduced" function:

$$R(\nu) = I(\nu)(\nu_0 - \nu)^{-4}\nu B \qquad [22]$$

$$B = 1 - \exp\left(\frac{-hc\nu}{kT}\right) \qquad [23]$$

where

ν	=	Raman shift in cm^{-1}
ν_0	=	frequency of the exciting line in cm^{-1}
$I(\nu)$	=	intensity at ν
h	=	Planck constant
c	=	speed of light
k	=	Boltzmann constant
T	=	temperature in Kelvin.

This function corrects the intensity for separation from the exciting line and for variations in the Boltzmann distribution with temperature. Its utility is greatest when studying bands at low frequency or solutions at high temperature. An expression can, just as above in the intensity format, be written for the isotropic spectrum:

$$R_{iso} = R_{\parallel} - \frac{4}{3} R_{\perp} \qquad [24]$$

1.2.2 Practical Aspects of Raman Spectroscopy.

Raman spectroscopy has some very useful advantages which make it applicable to a wide variety of situations. These advantages can be crudely classified into three categories: chemical, instrumental, and sampling.

Raman spectroscopy has some important "chemical" advantages. First of all, like infrared spectroscopy, it can be used for "fingerprinting". All molecules will have a characteristic spectrum and the spectrum can be used to determine a molecule's presence. In practice, however, because of band overlap, weakness of bands, and other problems, it may be difficult to distinguish a given molecule in a complex system. A second "chemical" advantage is that water is a weak Raman scatterer, while it is a very strong infrared absorber. Consequently, Raman spectra of aqueous systems are quite easy to collect. Studies of important biological and biochemical systems where, clearly, aqueous species are of great importance, are quite straightforward. A further "chemical" advantage is that the intensity is linearly dependent on the concentration of the scattering species. This is a great benefit for analytical applications.

Most Raman spectroscopy is done using excitation frequencies in the visible region of the electromagnetic spectrum leading to important instrumental benefits. Although the frequency *difference* between the incident and the scattered light is in the infrared, the light analyzed by the spectrometer is in the visible. Therefore, all the optical components and sample cells involved in the Raman experiment can be made from glass. There is no need for special optical materials which may be fragile, expensive or difficult with which to work. In addition, the entire vibrational spectrum (0 - 5000 cm^{-1}) can be studied easily without having to change the optics of the spectrometer. The use of glass as a material for cell construction means cells for non-ambient conditions can be fairly easily constructed. The use of lasers and visible light leads to another advantage of Raman spectroscopy: the use of fibre optics. Fibre optics allow the collection of *in situ* data without having the spectrometer *in situ* (16). Data can then be collected from *in vivo* systems (obviously very important in biological applications) or from hostile (either to the spectrometer or the operator!) environments.

Sample handling in Raman spectroscopy is generally very easy. For example, solutions and liquids can be contained in a melting point capillary tube or a glass test tube. Sample preparation for solids can be equally easy. Using a microscope attachment and assuming the solid is neither moisture nor air sensitive, a spectrum can be collected of a sample placed on a microscope slide. Even when the solid is sensitive, collection of a spectrum may be possible through the walls of the cell containing it without

disturbing the solid. Single crystals can be mounted and positioned with a goniometer head. The amount of sample required for a Raman spectrum is, in general, very small. For example, when studying liquids or solutions and using melting point capillary tubes, spectra can routinely be collected from 0.25 - 0.50 mL of sample. Raman spectroscopy has the further advantage of being a non-destructive technique; the sample can be recovered and used again.

Unfortunately, Raman spectroscopy is saddled with some disadvantages. First, and most seriously, it is a very weak effect. Because of this, the concentration of the species must be fairly high to obtain a good spectrum. Even when the concentration of the analyte is quite high a good spectrum may only be obtained with large time constants and signal averaging. Consequently, considerable time may be required to obtain a good spectrum. This is especially true with a monochannel instrument. The second big problem with Raman spectroscopy is fluorescence. Visible radiation is commonly used for excitation in Raman spectroscopy and radiation at these frequencies can sometimes induce fluorescence. Fluorescence may be particularly pronounced for highly conjugated systems. Compared to the Raman effect, fluorescence is a very strong effect and can simply overwhelm the Raman signal. Extraction of useful data may then be impossible. Even small concentrations of fluorescent impurities can cause serious problems. Fortunately, the development of FT-Raman techniques have reduced this problem because near-infrared frequencies are used for excitation. Similarly, experiments on coloured

samples can be difficult. If the sample absorbs at the frequency of the exciting radiation, unwanted thermal or photochemical effects may occur. Fluorescence may also be a more serious problem in coloured samples. These problems can be overcome by using longer wavelength excitation (e.g., krypton or helium-neon lasers), but this leads to a loss of sensitivity as governed by the ν^4 factor in the intensity expression (equation **[17]**).

1.2.3 Instrumentation

A schematic diagram of the typical Raman experiment is shown in Fig. 1.1 (13). In the early days of Raman spectroscopy the excitation source was often a mercury arc lamp (the "Toronto" arc lamp). Since the 1960's the arc lamps have been replaced by lasers and all Raman spectroscopy is now done with lasers. The most common types of lasers are the argon ion (lines at 514.5 nm and 488.0 nm) and krypton (568.2 nm and 647.1 nm). Other lasers are also used including the helium - neon laser and dye lasers. In choosing an exciting line a trade-off must be made between the so-called "ν^4 advantage" and the possibility of photochemical reaction. The "ν^4 advantage" refers to the fact that the intensity of the scattered light increases in proportion to the fourth power of the frequency of the exciting light. Unfortunately, the use of higher frequency exciting radiation may lead to unwanted photochemical effects. Furthermore, using ultraviolet radiation takes away the advantage of being able to use glass cells and optics. To have

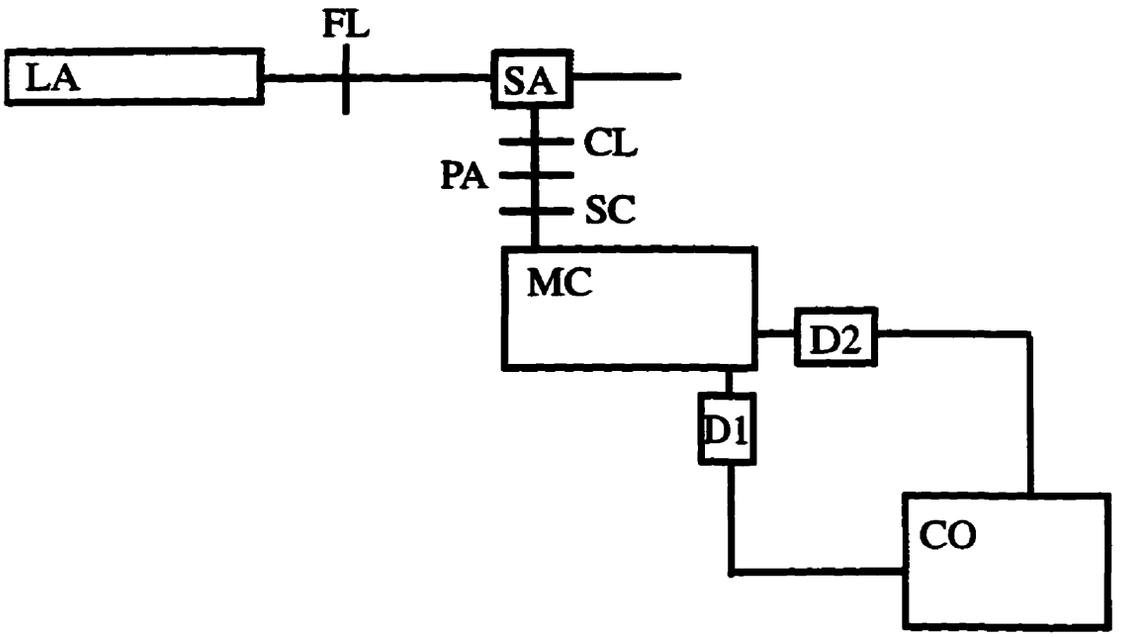

LA	-	laser (often argon ion or krypton ion)
FL	-	focusing lens
SA	-	sample
CL	-	camera lens
PA	-	polarization analyzer
SC	-	scrambler
MC	-	monochromator
D1, D2	-	detectors, either monochannel or multi-channel
CO	-	computer for acquisition and analysis of spectral data

Fig. 1.1: Schematic of Layout of a Typical Raman Experiment.

a choice of exciting lines is useful in order to overcome possible fluorescence and colour problems.

In principle, the light scattered from the sample can be analyzed at any angle relative to the incident radiation. In practice, three geometries are used 90°, 180°, and 360° (back scattering). The 90° scattering geometry is the most common. The light is focused into the spectrometer by a camera lens through the entrance slit. If polarization measurements are being performed, the polarization analyzer is mounted in front of the entrance slit. Between the polarization discriminator and the slit there is a quarter wave plate. The plate converts the linearly polarized light to circularly polarized light, effectively "scrambling" it. Scrambling is necessary because spectrometer gratings often have different transmission efficiencies for the two different orientations of the electric vector of the scattered light. The monochromator then splits the light into its component wavelengths. In the case of monochannel detection, the intensity of the light at each wavelength is measured sequentially and the detector is usually a photomultiplier tube. Multichannel detection is also possible. In this case, the exit slit from the spectrometer is eliminated and all the wavelengths of the scattered light can be dispersed over a multichannel detector such as a photodiode array or a charge coupled device detector. The multichannel detector provides a multiplex advantage so that an entire spectrum (or any part thereof) can be recorded in the time required for a single point on a single channel device. Thus, a large number of spectra may be averaged to improve the signal-

to-noise ratio.

In most modern Raman instruments a computer controls the spectrometer and acquires spectral data. Photon counters can be easily connected to microcomputers to collect data in a digital format. Once collected the data can be easily treated on the computer. Baseline correction, spectral averaging, bandfitting, etc., allow the extraction of useful information (both qualitative and quantitative) even from relatively weak peaks.

1.2.4 Applications of Raman Spectroscopy

Because of its several advantages Raman spectroscopy has found widespread application. It is a technique that may be applied to gases, liquids or solids. In practice, gases, because of their low densities and the inherent weakness of the Raman effect, are not as commonly studied as liquids and solids. Raman spectroscopy is often used in the study of solutions. Because water is such a poor Raman scatterer, Raman spectroscopy is especially good for studying aqueous systems (13,17). Application to biological systems follows quite naturally from this property (18). Bands may shift, change intensity, or develop in response to structural changes in the solution. In some cases kinetic (1) or thermodynamic (2) variables can be quantified. Raman spectroscopy has also found application in the study of electrodes and processes occurring at electrode

surfaces. Certain molecules when adsorbed on particular metals (gold, silver, and copper being the primary examples) have greatly enhanced Raman signals - an effect known as surface enhanced Raman scattering (SERS). It allows the study of species adsorbed on metal surfaces at mono- or sub-monolayer concentrations (19). Raman spectroscopy can also be used in the study of the dynamics of non-electrolytes. Results from the anisotropic and isotropic spectra can be used to calculate vibrational and reorientational correlation functions (20). Clearly, based even on this short list, Raman spectroscopy is a technique of great utility.

1.3 Resonance Energy Transfer

In pure liquids vibrations of neighbouring molecules are coupled because of the intermolecular interactions between them (21). If the molecular orientations are random, the net effect is the broadening of vibrational bands. If, however, the alignment of the molecules is not random, then the transition dipole moments of two neighbouring molecules may couple. This will give rise to in-phase and out-of-phase modes of this larger unit. When this phenomenon occurs, resonance energy transfer (RET) has taken place, and it can be observed spectroscopically. RET most clearly manifests itself in a Raman non-coincidence effect (NCE) which is a difference in the maxima of the isotropic and the anisotropic components of the spectral bands. The difference, defined as $\Delta\nu$ =

$\nu_{aniso.} - \nu_{iso.}$ (in cm^{-1}), is almost always positive. When the difference is negative, it is referred to as the anomalous NCE (22) and this has been observed in alcohols (23). Furthermore, RET provides a "new" pathway for vibrational dephasing, so it may affect vibrational bandwidths.

Changes in the conditions of the substance under investigation lead to changes in the spectra. If the species is diluted in some inert solvent, the NCE gradually disappears. Mirone and Fini (24) reported that $\Delta\nu$ becomes zero at a finite, non-zero concentration, somewhat dependent on the nature of the solvent. They reported that the shape of the $\Delta\nu$ vs. concentration graph depends on the relative values of the dielectric constants of the solute and solvent. The slope increases with increasing concentration of the solute if the solvent has a higher dielectric constant than the solute. The slope decreases when the reverse is true. Also, when the solute is diluted, the frequency of the maximum in the anisotropic spectrum was found not to change significantly (25). However, the frequency of the isotropic maximum increased and tended toward the frequency of the anisotropic maximum. Secondly, when the temperature was raised, $\Delta\nu$ decreased (21). Thirdly, increasing the pressure usually causes the frequency maxima of both the isotropic and anisotropic spectra to shift in the same direction (26) but not necessarily by the same amount.

Different workers have taken different approaches to the development of a theory

to explain the non-coincidence effect (NCE) (24,27-36). In chapter 4 only some of these models (24,29-34) are applied to solutions of methyl formate in methyl d-formate and in acetonitrile. However, for the sake of completeness, each of these approaches will be briefly summarized here.

1.3.1 Theory of Scheibe (27,28)

Scheibe and Döge (27) and Scheibe (28) developed a theoretical treatment of the non-coincidence effect. Their treatment did not include the effects of dilution. They began by writing the dipole potential between two molecules 'A' and 'B' as:

$$V_{AB} = \frac{-\mu_A \mu_B}{R^3} K_{AB} \qquad [25]$$

where

R = the distance between the dipoles

K_{AB} = a factor related to the orientation of the dipole moment vectors.

This dipole interaction can cause an additional energy difference between the ground and the first excited vibrational states. By applying perturbation theory to molecule 'A' this additional energy difference is given by:

$$V_{odd} = \frac{K_{AB}}{R^3}\left[\begin{array}{l} \frac{\partial \mu_A}{\partial Q_A}\,\mu_B\,(\langle 1|\,Q\,|1\rangle - \langle 0|\,Q\,|0\rangle) \\ \quad + \frac{1}{2}\left[\frac{\partial^2 \mu_A}{\partial Q_A^{\,2}}\,\mu_B\,(\langle 1|\,Q^2\,|1\rangle - \langle 0|\,Q^2\,|0\rangle)\right] \\ \qquad + \left(\frac{\partial \mu_A}{\partial Q_A}\right)\left(\frac{\partial \mu_B}{\partial Q_B}\right)(|\langle 1|\,Q\,|0\rangle|^2) \end{array}\right] \quad [26]$$

The first term in the large square brackets arises from mechanical anharmonicity and disappears if a harmonic potential is used. The second term is from the electrical anharmonicity and occurs if the dipole moment is not a linear function of the normal co-ordinate. A vibrating molecule will interact with the field created by the dipole moments of its neighbours. The first and second terms in the large square brackets arise from this interaction and the interaction leads to a shift in the unperturbed frequency. The last term originates from transition dipole coupling between 'A' and 'B'. This will only occur if 'A' and 'B' are identical and the same vibrational mode for each is considered. This will lead to splitting of modes which are normally singly degenerate, i.e., a non-coincidence effect. The size of the splitting will be directly affected by 'R' and 'K_{AB}'.

1.3.2 Theory of Fini and Mirone (21,24,29)

Fini and Mirone (21) proposed a fairly simple model to explain RET. They assumed aprotic, dipolar liquids consist of small molecular clusters within which there

exists some partial order. The molecular dipoles of the molecules in each cluster can align themselves either parallel or anti-parallel to a common direction. The presence of a permanent dipole moment, therefore, allows the formation of some short range order. The transition dipole moments may then couple and resonance energy transfer can take place. The orientational order will exist up to a distance such that the energy of electrostatic interaction between the two dipoles equals the thermal agitation energy (21). Typically, this distance is a value that allows the molecules in the first coordination shell to attain a preferential orientation with respect to the central molecule. Because RET only occurs between identical molecules, dilution (which replaces solute molecules in a co-ordination shell with solvent molecules) will decrease the ability of the solute molecules to couple. As dilution continues, RET will decrease and the non-coincidence effect will diminish. Eventually, as mentioned above, $\Delta\nu$ vanishes at a finite, non-zero concentration. At this point the isotropic, anisotropic, and infrared peak maxima should all coincide. This model can also explain the effect of increased temperature. As the temperature increases, the greater thermal agitation reduces the size of the clusters and disrupts alignment of the molecular dipoles inside them. This reduces the extent of resonance energy transfer and reduces $\Delta\nu$.

Fini and Mirone derived an empirical equation to relate the non-coincidence ($\Delta\nu$) to the concentration of the solute and the dielectric constants of the solute and solvent (24):

$$\Delta\nu = \Delta\nu_{neat} \frac{\varepsilon_2}{1-\phi_0} \frac{\phi-\phi_0}{\varepsilon_2\phi+\varepsilon_1(1-\phi)} \quad [27]$$

for $\phi > \phi_0$

$$\Delta\nu = 0 \quad [28]$$

for $\phi < \phi_0$

where

$\Delta\nu$	=	$\nu_{aniso.} - \nu_{iso.}$ (in cm^{-1})
$\Delta\nu_{neat}$	=	$\nu_{aniso.} - \nu_{iso.}$ for the pure solute
ε_1	=	dielectric constant of the solvent
ε_2	=	dielectric constant of the solute
ϕ	=	volume fraction
ϕ_0	=	"threshold" volume for non-coincidence to occur.

Giorgini and Fini later stated (29), based on this observation, that the NCE was related to the interaction between the permanent dipoles of the dissolved species. They noticed two important points. First, $\Delta\nu$ decreased as the solution became more dilute and there was a certain "threshold" concentration below which the NCE did not take place. Second, the shape of the $\Delta\nu$ vs. ϕ graphs depended on the relative values of the dielectric constants of the solute and solvent.

They explained their first observation as follows. There are two competing

processes for vibrational dephasing. The first is resonance energy transfer in which a quantum of vibrational energy is transferred from one oscillator to another. The second is simple energy dissipation through collisions and the like. If two oscillators are coupled at time t = 0, there is a finite, non-zero probability of vibrational energy transfer from the excited oscillator to the second oscillator. As time passes the probability that transfer has occurred increases. At some time, τ, the probability will be unity. If τ is long relative to the time for simple energy dissipation resonance energy transfer does not take place. As the solution is diluted, τ becomes longer and longer so RET becomes less "efficient". At some finite concentration τ is so large RET does not take place and the splitting disappears.

The explanation of the second observation (that the shape of the $\Delta\nu$ vs. ϕ graphs depended on the dielectric constants of the "active" and "solvent" species) was based on two assumptions. First, the coupling of the two modes takes place by transition dipole - transition dipole (TD-TD) coupling. Each molecule will contribute to $\Delta\nu$ a term which is proportional to:

$$\frac{\left(\frac{\partial\mu}{\partial Q}\right)^2}{\nu r^3} \qquad [29]$$

where 'r' is the distance from the reference molecule. Secondly, the isotropic - anisotropic separation is directly related to the orientational correlation induced by static dipolar interactions. Under these assumptions, they showed that:

$$\Delta\nu \propto \left(\frac{\partial\mu}{\partial Q}\right)^2 \frac{N}{V} \frac{\mu^2}{3\varepsilon d^3 kT}\left[1-\left(\frac{\mu^2}{3\varepsilon d^3 kT}\right)^2\right] \qquad [30]$$

where

ε	=	dielectric constant of the solution
N	=	number density of solute
d	=	minimum distance of approach between two molecules

Therefore, the $\Delta\nu$ versus concentration curve will have a dependence on ε. This value can be calculated assuming a linear relationship between the solution dielectric constant and the volume fraction of the active species (31):

$$\varepsilon = \varepsilon_1 (1-\phi) + \varepsilon_2\phi \qquad [31]$$

where

ε_1	=	dielectric constant of the solvent
ε_2	=	dielectric constant of the solute
ϕ	=	volume fraction of the "active" species

In some cases they found their model did not agree with the observed results. Two possible explanations were given. First, ε might not be a linear function of volume fraction. Second, and most importantly, specific, possibly short range, interactions might

not be adequately described by the bulk dielectric constant. Furthermore, such interactions could affect the transition dipole moments leading to even greater errors.

1.3.3 Theory of McHale (30,31,32)

If the vibrational coupling which leads to RET occurs through the transition dipole moment, then $\Delta\nu$ should be proportional to $|\partial\mu/\partial Q|^2$ (37). In other words, the separation of the isotropic and anisotropic peak maxima should be related to the intensity of the infrared transition. Indeed, it is generally the case that the largest non-coincidence effects are observed for strongly absorbing modes (e.g., the carbonyl stretch). The NCE has been observed, however, for the ν_6 vibration of 1,2,5-thiadiazole (38) which is very weak in the infrared. McHale has asserted (30,31) that the transition dipole - transition dipole interactions are not the only means of coupling. Other possible sources are hydrogen bonding, quadrupole-quadrupole, and dipole-dipole interactions. McHale determined that orientation-dependent intermolecular forces can give rise to an NCE even in the absence of local order.

Wang and McHale (30) performed an extensive and detailed theoretical analysis of the non-coincidence effect. They concluded, contrary to the prevailing wisdom, that short range order is unnecessary for a non-coincidence effect to be observed. Short range

order may enhance the non-coincidence effect, but it is not at the root of the effect. The fundamental reason is that the resonance coupling potential between two molecules is angle dependent. The angle dependent intermolecular forces modify the force constants of the harmonic oscillators leading to an anisotropic frequency distribution. Isotropic Raman scattering samples the average of the frequency distribution but anisotropic Raman scattering samples the anisotropy of the distribution. Because of this, the first spectral moments in the isotropic and the anisotropic are different and a NCE is observed. Further, Wang and McHale's derivation showed the splitting is proportional to the number density ("concentration") of the solute and inversely proportional to both the free oscillator frequency and the effective mass. At infinite dilution the splitting should vanish and this is commonly observed. In addition, McHale and Wang showed that if the coupling is assumed to arise from induced dipole interactions the relative splitting (i.e., the non-coincidence splitting for a given solution divided by the non-coincidence splitting for the pure solute) relies linearly on the infrared intensity parameter $|\partial\mu/\partial Q|^2$ and is always positive. Therefore, the size of the NCE should be related to the infrared intensity. As was mentioned above, strongly intense infrared transitions are most likely to have a large NCE.

In a subsequent paper (31) McHale examined the dependence of the non-coincidence effect on the concentration of the active (solute) species. She argued that a strong angle dependent intermolecular potential could result in concentration-dependent

peak positions for the isotropic and anisotropic spectra. Furthermore, any intermolecular forces strong enough to give an NCE could also be expected to cause the bandwidths in both the infrared and Raman spectra to depend on the concentration.

The derivations carried out in this paper (31) were tested for a mixture at dilute concentration (the so called "weak interaction regime") where the effects of molecular association can be neglected; the primary means of vibrational coupling is through the transition dipoles. (However, this is not the only means by which resonance energy transfer may occur. Hydrogen bonding is another type of interaction which can lead to a large isotropic-anisotropic splitting (39-41)). Within these assumptions the following expression was derived for the splitting:

$$M_{aniso.} - M_{iso.} = \Delta M = \frac{8\mu^2\gamma^2}{25m\omega kTd^3} \frac{N_o}{V_m} \frac{\phi}{\epsilon^2} \qquad [32]$$

where

N_o	=	Avogadro's number
V_m	=	molar volume
m	=	reduced oscillator mass
ϕ	=	volume fraction of the active species
γ	=	$\lvert \partial\mu / \partial Q \rvert$
μ	=	the dipole moment
ω	=	free oscillator angular frequency

ε = static dielectric constant of the solution

d = minimum intermolecular distance

$M_{aniso.}$ = anisotropic spectral first moment (in angular frequency)

$M_{iso.}$ = isotropic spectral first moment (in angular frequency)

To make comparisons to experimental observations, it is necessary to know the dependence of the dielectric constant on concentration. McHale assumed ε is a function of the volume fraction (see equation [31]). It is then possible to re-write equation [32]:

$$\Delta M = \Delta M_{neat} \frac{\epsilon_2^2 \phi}{(1-\phi)^2 \epsilon_1^2 + 2\epsilon_1\epsilon_2\phi(1-\phi) + (\phi\epsilon_2)^2} \qquad [33]$$

Putting

$$x = \frac{\epsilon_1}{\epsilon_2} \qquad [34]$$

gives

$$\frac{\Delta M}{\Delta M_{neat}} = \frac{\phi}{(\phi(1-x) + x)^2} \qquad [35]$$

For systems in which x>1 or x=1 this result is in fairly good agreement with experimental results. For x<1 the application of McHale's model (because of some underlying assumptions) is not really appropriate. This is the case for polar molecules in a non-polar solvent where molecular association (short range order effects) may be important.

Mirone (33) disputed McHale's result given above. He believed McHale's equation (equation [32]) was too simplistic and needed to be replaced. He suggested McHale's equation should be re-written as:

$$\Delta M = \frac{8\mu_v^2\gamma^2}{25m\omega_0 kTd^3}\,\frac{N_o}{V_m}\,\phi\left(\frac{n^2+2}{2\varepsilon+n^2}\right)^2 e \qquad [36]$$

where

n = refractive index of the solution.

Mirone compared the splitting (for neat acetone) predicted by his equation with that of McHale and found his modification gave a better result.

1.3.4 Theory of Logan (34,35)

Logan outlined his theories on the non-coincidence effect in two papers. One of these (34) dealt with isotopic binary mixtures and the second (35) with more general systems. Logan accepted Wang and McHale's (30) hypothesis of an angle dependent interaction potential (arising from permanent dipolar interactions) which preferentially weights the relative alignment of a pair of molecules between which resonance energy transfer can take place. He stated that many-body molecular interactions are responsible for the details of liquid structure and thus the appearance of the non-coincidence effect.

Logan set out to examine the thermodynamic dependencies of the NCE.

In his first paper (34), Logan derived an expression for the dependence of the NCE on the concentration of the active species for mixtures of isotopomers. His derivation was predicated on a number of assumptions. First, he used a model of a simple, dipolar, hard sphere liquid. Second, to apply the theory, the mode studied must be non-degenerate and sufficiently separated from all other vibrational transitions that population relaxation effects can be neglected. Third, he assumed the permanent dipole moment of the active species lies along the principal molecular axis and that vibration modulates the dipole moment along this axis. He stated that this is a common situation for singly-degenerate vibrational modes in dipolar molecules. In addition to these assumptions, Logan made use of the mean spherical approximation (42). Within these assumptions Logan derived a following dependence of the NCE on concentration:

$$M_{aniso.} - M_{iso.} = \Delta M = \frac{48}{25\pi\epsilon_0} \frac{\gamma^2}{m\omega_\alpha\sigma^3} X_A \, \xi(\rho,T) \qquad [37]$$

where

m	=	reduced mass
σ	=	hard sphere diameter
ω_α	=	angular frequency of the isolated, uncoupled α mode of 'A'
γ	=	$\lvert \partial\mu / \partial Q \rvert$, the dipole moment derivative

ρ = number density of the solution

ε_0 = permittivity of a vacuum

M = spectral first moment of the anisotropic or isotropic spectrum

X_A = mole fraction of the active species, 'A'.

$\xi(\rho,T)$ is a value found by solving:

$$\frac{\beta\mu_0^2\rho}{3\epsilon_0} = \frac{(1+4\xi)^2}{(1-2\xi)^4} - \frac{(1-2\xi)^2}{(1+\xi)^4} \qquad [38]$$

where

μ_0 = permanent dipole moment

ξ = $\xi(\rho,T)$

$$\beta = \frac{1}{k_B T} \qquad [39]$$

$\xi(\rho,T)$ is a function of ρ and T alone, independent of X_A. Therefore, if number density and temperature are constant,

$$\Delta M = X_A \, \Delta M_{neat} \qquad [40]$$

where

ΔM_{neat} = splitting for pure species 'A'.

This linearity only applies to an isotopic mixture.

Logan then extended his study to examine non-isotopic mixtures (35). His

analysis was based on the same assumptions as in his previous paper (34). Unlike the isotopic mixtures, the splitting does not necessarily have a linear dependence on the mole fraction of the active species (see, for example, (21,24,43,44)). For a non-isotopic dilution the abilities of the solute and solvent molecules to orient a solute pair differ. Dilution can cause new intermolecular forces to become important. These new forces may arise from sources other than the active pair and will have differing abilities to align the active pair than for the original, pure solvent. Therefore, there is no simple linear dependence of the NCE on the mole fraction even at constant temperature and number density. Furthermore, most experimental work is done at constant temperature and pressure, so the mole fraction and number density dependencies of the NCE become entwined.

In this second paper (35) Logan examined a simple dipolar, hard sphere mixture (of the "active" species, 'A', and the "solvent" species, 'B') in which the interaction potential consisted of two parts: 1) a sum of pairwise additive hard sphere interactions with hard sphere diameters σ_A and σ_B; 2) a dipolar part arising from the mutual interaction of the permanent dipole moments of both species. Logan then defined a function:

$$\xi(X_A,\rho,T) = \frac{\pi\rho\sigma_A^3}{6}\int_0^\infty \frac{h_D^A(R)}{R}\,dR \qquad [41]$$

where

ρ = total number density

R = distance between interacting molecules.

The function $h_D^A(R)$ gives the 'R' dependence of the contribution of an angular function (which is related to the relative orientation of the active species) to the pairwise distribution function. The splitting depends on $\xi(X_A,\rho,T)$:

$$c t_{\alpha,A} \, \Delta M_{\alpha,A} \, (X_A,\rho,T) = X_A \, \xi(X_A,\rho,T) \qquad [42]$$

where

$$t_{\alpha,A} = \frac{25\pi^2 \, \epsilon_0 \, m_{\alpha,A} \, \omega_{\alpha,A} \, \sigma_A^{\,3}}{24\gamma_{\alpha,A}^{\,2}} \qquad [43]$$

c = speed of light

$\Delta M_{\alpha,A}$ = $M_{aniso.} - M_{iso.}$ for the α mode of species 'A' - a function of X_A, ρ and T

$m_{\alpha,A}$ = effective mass for the α mode of species 'A'

$\omega_{\alpha,A}$ = free oscillator angular frequency for the α mode of species 'A'

σ_A = hard sphere diameter of 'A'

$\gamma_{\alpha,A}$ = $|\partial\mu / \partial Q_\alpha|$ for the α mode of species 'A'

ε_0 = permittivity of a vacuum

(and $t_{\alpha,A}$ has dimensions of time). In the low number density limit:

$$\xi_A (X_A, \rho, T) \sim \xi_{A,0} (\rho, T) = \frac{\beta \mu_A^2 \rho}{72 \epsilon_0} \qquad [44]$$

where

$$\beta = \frac{1}{k_B T} \qquad [45]$$

The splitting can then be written as

$$\Delta M_{\alpha,A} (X_A, \rho, T) = \Delta M_{\alpha,A}^0 (X_A, \rho, T) \, \zeta(X_A, \rho, T) \qquad [46]$$

where

$$\Delta M_{\alpha,A}^0 (X_A, \rho, T) = \frac{X_A \, \xi_{A,0} (\rho, T)}{ct_{\alpha,A}} = \frac{\beta \mu_A^2 \rho X_A}{72 \epsilon_0 c t_{\alpha,A}} \qquad [47]$$

and

$$\zeta(X_A, \rho, T) = \frac{\xi(X_A, \rho, T)}{\xi_{A,0} (\rho, T)} \qquad [48]$$

($\xi_{A,0}(\rho,T)$ is defined by equation [44]). In the low number density domain the alignment effects which facilitate resonance energy transfer (and therefore non-coincidence splitting) arise from the interaction of the permanent dipoles on a pair of "active" molecules. The quantity $\xi_{A,0}(\rho,T)$ embodies the pair-wise alignments of the active molecules. Outside the low number density limit, other molecules of other species will act to preferentially weight the relative alignment of any pair of RET active molecules. $\zeta(X_A,\rho,T)$ may be

calculated (within the MSA) from:

$$24y_0 = \frac{(1+4\zeta y_0)^2}{(1-2\zeta y_0)^4} - \frac{(1-2\zeta y_0)^2}{(1+\zeta y_0)^4} \qquad [49]$$

where

$$y_0 = X_A\ \xi_{A,0}\ (\rho,T) + X_B\ \xi_{B,0}\ (\rho,T) \qquad [50]$$

$$\zeta = \zeta(X_A,\rho,T)$$

These equations are, strictly speaking, only valid when the diameters of 'A' and 'B' are the same. However, Logan states they should be reasonably successful if the hard sphere diameters are within 5 - 10%. For a given set of X_A, ρ, and T, y_0 is obtained from equations **[44]** and **[50]** and $\Delta M_{\alpha,A}{}^0$ from **[47]** and **[43]**. Knowing y_0, equation **[49]** gives $\zeta(X_A,\rho,T)$. The experimentally observable $\Delta M_{\alpha,A}(X_A,\rho,T)$ is then found from equation **[46]**. Using an approximate method to solve for $\zeta(X_A,\rho,T)$ the following relationship can be written:

$$ct_{\alpha,A}\ \Delta M_{\alpha A}\ (X_A\ ,\rho,T) = X_A\ \xi_{A,0}\ (\rho,T)\ \frac{1+\frac{5}{4}\ y_0\ (X_A,\ \rho,T)}{(1+\frac{5}{2}\ y_0\ (X_A\ ,\rho,T))^2} \qquad [51]$$

Application of this theory requires the experimenter to measure the number density of the solutions at each concentration.

According to Logan, previous workers (24,29,31,32,33) tried to simplify this result. Simple dielectric screening or continuum dielectric theory arguments were employed to scale the low number density pair alignment effects embodied in $\xi_{A,0}(\rho,T)$ by a function dependent on the index of refraction and/or the dielectric constant of the solution. Logan feels this approach is not likely to adequately reflect the microscopic origins of the NCE.

Logan made some important assumptions. First, the dominant anisotropic intermolecular forces responsible for alignment effects are from dipolar interactions. Second, the species involved are dipolar hard spheres with comparable effective hard sphere diameters. Furthermore, Logan omitted from his theoretical treatment the effects of short range anisotropic intermolecular interactions. Such interactions can lead to orientational alignment and either a positive or negative contribution to the non-coincidence effect.

1.3.5 Summary

The preceding sections have presented a brief overview of the three main

theoretical approaches to the NCE and its dependence on concentration. The main result of the treatments of Wang and McHale (30) and McHale (31) is that short range order in the liquid is not necessary for the non-coincidence effect to occur. The *fundamental* reason is because of an angle dependent intermolecular potential. Fini et al. (24,29) derived an empirical equation for the dependence of the splitting on the concentration. They also postulated the existence of a "threshold volume" below which the NCE does not appear. These two approaches made use of dielectric screening arguments to simplify the interaction of two dipoles in the solution. On the other hand, Logan developed a theory to explain the effect without using this type of simplification. He derived a more detailed equation for the dependence of the splitting on concentration using a more rigorous model of liquid structure. Because of this, its range of application is narrower and certain more restrictive conditions must be met. Later in this thesis the data for methyl formate in methyl d-formate are compared to Logan's theory for isotopic dilution (34) while the data for methyl formate in acetonitrile are compared with the models of Fini and Mirone (24,29), McHale (31-32) and Mirone's modification of McHale (33). Without knowing the hard sphere diameters of methyl formate and acetonitrile, comparison to Logan's model for non-isotopic dilution (35) is pointless.

1.4 References

1. R. J. Bartholomew, *M.Sc. Thesis*, **1992**, University of Waterloo

2. J. Semmler, *Ph. D. Thesis*, **1989**, University of Waterloo
   J. Semmler, D. E. Irish, *J. Solution Chem.*, **1988** 17 805
   J. Semmler, D. E. Irish, *J. Mol. Liquids*, **1990** 46 1

3. E. Plichta, M. Salomon, S. Slane, M. Uchiyama *J. Sol. Chem.* **1987** 16 225

4. A. Smekal, *Naturwiss.* **1923** 11 873

5. C. V. Raman, K. S. Krishnan, *Nature* **1928** 121 501

6. G. Landsberg, L. Mandelstam, *Naturwiss.* **1928** 16 557

7. R. N. Jones in *Chemical, Biological and Industrial Applications of Infrared Spectroscopy*, Chap. 1 (J. R. Durig Ed.), John Wiley and Sons Inc., Toronto, 1985

8. W. A. Guillory, *Introduction to Molecular Structure and Spectroscopy*, Allyn and Bacon, Boston, 1977

9. D. A. Long, *Raman Spectroscopy*, McGraw-Hill, London, 1977

10. G. Placzek, *Handbuch der Radiologie* (E. Marx, Ed.) Vol. 6, p. 205, Akademie-Verlag, Leipzig, 1934

11. B. J. Bulkin in *Analytical Raman Spectroscopy*, Chap. 1 (J. G. Grasselli and B. J. Bulkin Eds.), John Wiley and Sons Inc., Toronto, 1991

12. J. R. Scherer in *Analytical Raman Spectroscopy*, Chap. 3 (J. G. Grasselli and B. J. Bulkin Eds.), John Wiley and Sons Inc., Toronto, 1991

13. M. H. Brooker in *The Chemical Physics of Solvation* Part B (J. Ulstrup, R. R. Dogonadze, E. Kálmán, A. A. Karnyshev Eds.), Elsevier, Netherlands, 1986

14. M. H. Brooker, O. F. Nielsen, E. Praestgaard, *J. Raman Spectrosc.*, **1988** 19 71

15. W. F. Murphy, M. H. Brooker, O. F. Nielsen, E. Praestgaard, J. E. Bertie, *J. Raman Spectrosc.*, **1989** 20 695

16. D. L. Gerrard in *Analytical Raman Spectroscopy*, Chap. 9 (J. G. Grasselli and B. J. Bulkin (Eds.), John Wiley and Sons Inc., Toronto, 1991

17. D. E. Irish, M. H. Brooker in *Advances in Infrared and Raman Spectroscopy*, Vol. 2, Chap. 6, (R. J. H. Clark, R. E. Hester Eds.), Heyden and Son Ltd., London, 1976

18. *Biological Applications of Raman Spectroscopy*, Vol. 1 - 3, T. G. Spiro Ed., John Wiley and Sons Inc., Toronto, 1987

19. E. S. Brandt, T. M. Cotton in *Investigations of Surfaces and Interfaces - Part B*, Chap. 8, (B. W. Rossiter, R. C. Baetzold Eds.), John Wiley and Sons Inc., Toronto 1993

20. J. Yarwood, *N.A.T.O. A.S.I. Series, Series C*, **1992** 379 275

21. G. Fini, P. Mirone, *J. Chem. Soc. Faraday Trans.* **1974** 70 1776

22. S. A. Kirillov, *J. Raman Spectrosc.* **1993** 24 167

23. H. D. Thomas, J. Jonas, *J. Chem. Phys.* **1989** 90 4632

24. P. Mirone, G. Fini, *J. Chem. Phys.* **1979** 71 2241

25. M. Kamoun, P. Mirone, *Chem. Phys. Lett.* **1980** 75 287

26. W. Schindler, T. W. Zerda, J. Jonas, *J. Chem. Phys.* **1984** 81 4306

27. D. Scheibe, G. Döge, *Ber. Bunsenges. Phys. Chem.* **1981** 85 520

28. D. Scheibe, *J. Raman Spectrosc.* **1982** 13 103

29. M. G. Giorgini, G. Fini, *J. Chem. Phys.* **1983** 79 639

30. C. H. Wang, J. McHale, *J. Chem. Phys.* **1980** 72 4039

31. J. L. McHale, *J. Chem. Phys.* **1981** 75 30

32. J. L. McHale, *J. Chem. Phys.* **1982** 77 2705

33. P. Mirone, *J. Chem. Phys.* **1982** 77 2704

34. D. E. Logan, *Chem. Phys.* **1986** 103 215

35. D. E. Logan, *Chem. Phys.* **1989** 131 199

36. V. Shelley, J. Yarwood, *Mol. Phys.* **1991** 72 1407

37. G. Fini, P. Mirone, *Spectrochim. Acta.* **1976** 32A 625

38. D. R. Jones, C. H. Wang, O. F. Nielsen, *J. Chem. Phys.* **1976** 64 4475

39. B. Desbat, P. V. Huong, *J. Chem. Phys.* **1983** 78 6377

40. C. Perchard, J. P. Perchard, *Chem. Phys. Lett.* **1974** 27 445

41. J. P. Perchard, *Chem. Phys. Lett.* **1976** 44 169

42. M. S. Wertheim, *J. Chem. Phys.*, **1971** 55 4291

43. V. M. Shelley, J. Yarwood, *Chem. Phys.* **1989** 137 277

44. G. Fini, P. Mirone, *J. Chem. Soc. Faraday Trans. 2* **1973** 69 1243

2. EXPERIMENTAL

2.1 Chemicals and Solutions

In general chemicals were used "as received" from suppliers - no further purification was performed. The details of the chemicals and the preparation of solutions will be discussed in the relevant chapters.

2.2 Spectra Recorded at less than 100°C

For spectra collected of samples under 100°C, the samples were sealed in glass capillary tubes held in a thermostatted copper block. The sample was placed in the tube using a syringe and a length of Teflon tubing. As the plunger of the syringe was pressed, the tubing was slowly removed. Next, using the syringe and tubing, some of the sample was removed from the top half of the capillary. This made sealing the tube somewhat easier. Any bubbles in the tube were removed by tapping the tube. After this, the capillary tube was sealed using a Bunsen burner. The copper block is illustrated in Fig.

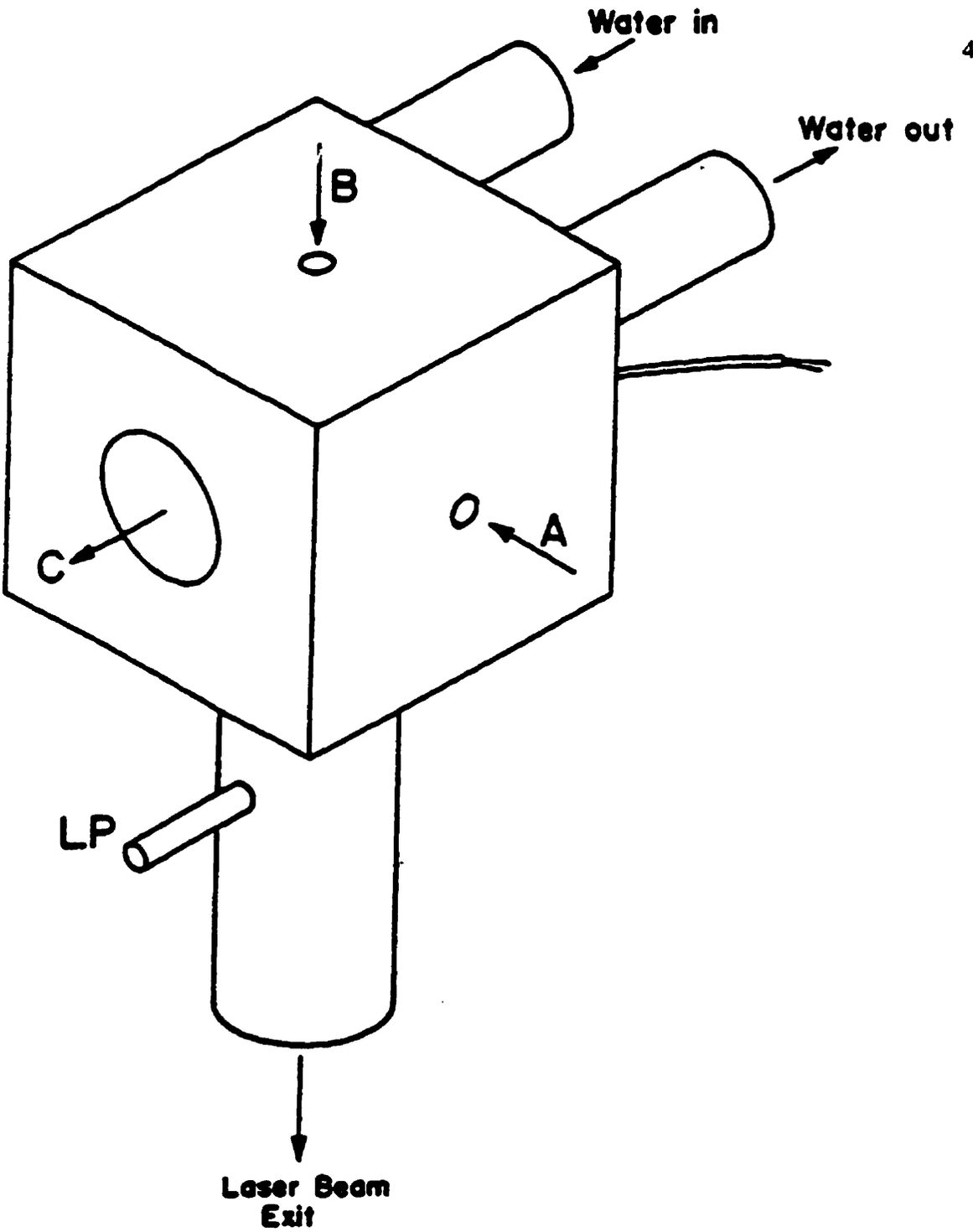

Fig. 2.1: Copper Block for Holding Capillary Tubes (2)
A - Sample Tube Entrance; B - Laser Beam Entrance; C - Raman Scattered Light; LP - Locking Pin to Hold Copper Block in Place.

2.1. Water from a regulated bath circulated through the block to maintain a constant temperature.

2.3 High Temperature Furnace

At the beginning of this project it was anticipated that high temperature (i.e., > 100°C), high pressure experiments would play a significant role. The furnace used to generate the high temperatures is illustrated in Fig. 2.2. To perform these experiments, the furnace was re-designed to give better spectra (as described below). Detailed descriptions of the furnace, the high pressure apparatus, and their use are readily available elsewhere (1-4) and are not provided here. However, a brief description of the re-designed furnace is given. As the project evolved, the role of the high temperature, high pressure equipment greatly diminished.

Originally the furnace was positioned in the sample chamber so that the sample tube was perpendicular to the floor of the sample chamber. It was subsequently pointed out this did not take full advantage of the slit geometry (5). To improve the signal, the furnace was reconstructed by rotating it and mounting it on its side. In this way the sample tube was parallel to the floor. As shown in Fig. 2.3, a tube parallel to the floor gives much better signal than one perpendicular to the floor. There is, however, a trade-

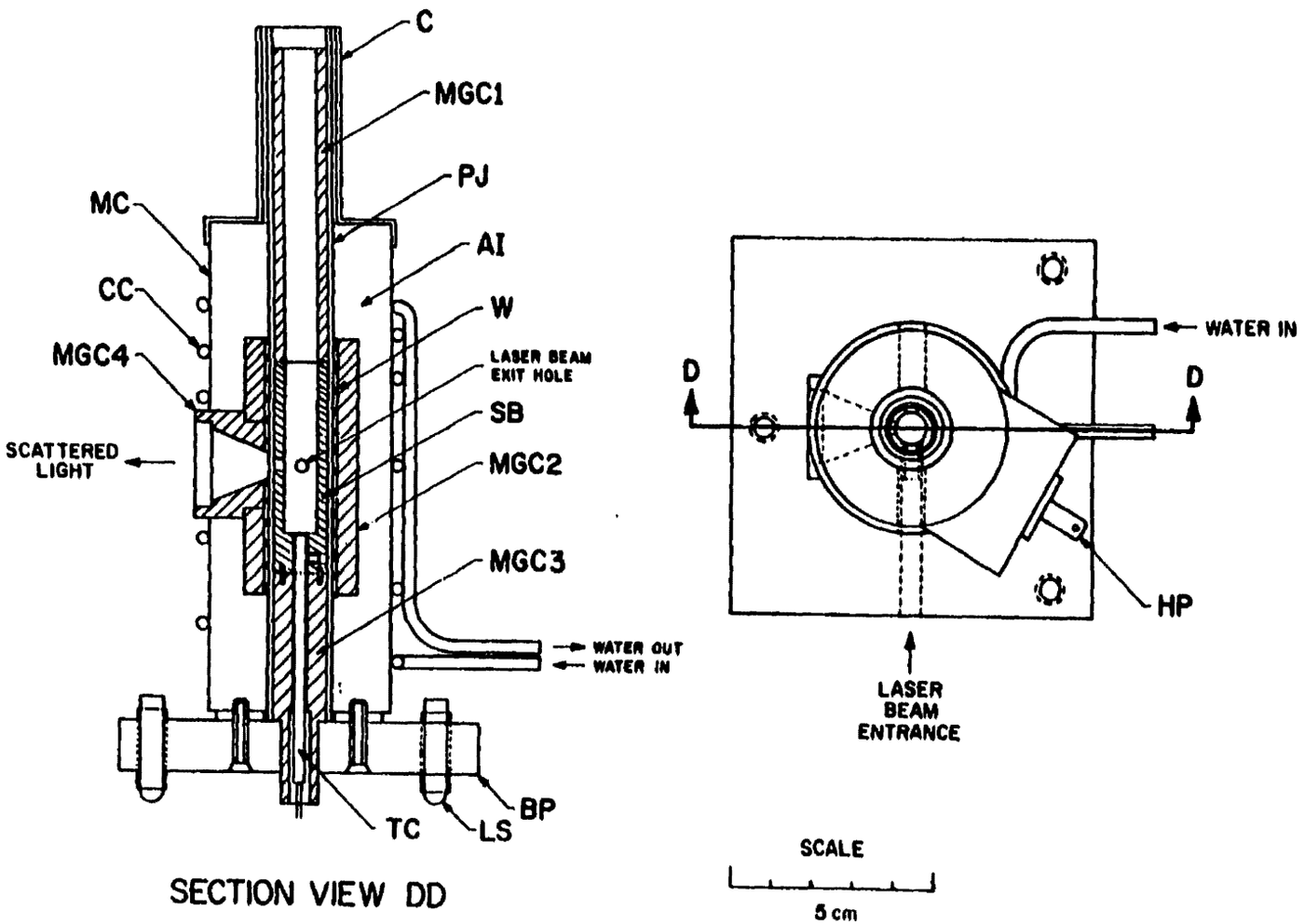

Fig. 2.2: High Temperature Furnace (2).

High Temperature Furnace

AI	-	asbestos based insulation
BP	-	base plate
C	-	removable metal cap
CC	-	copper coils for cooling water
HP	-	plug connecting heating wire to temperature controller
LS	-	furnace feet
MC	-	metal casing
MGC1-4	-	machinable glass ceramic sections surrounding furnace
PJ	-	Pyrex jacket
SB	-	silver block to minimize heating gradients along sampling region
TC	-	chromel-alumel thermocouple
W	-	heater wire

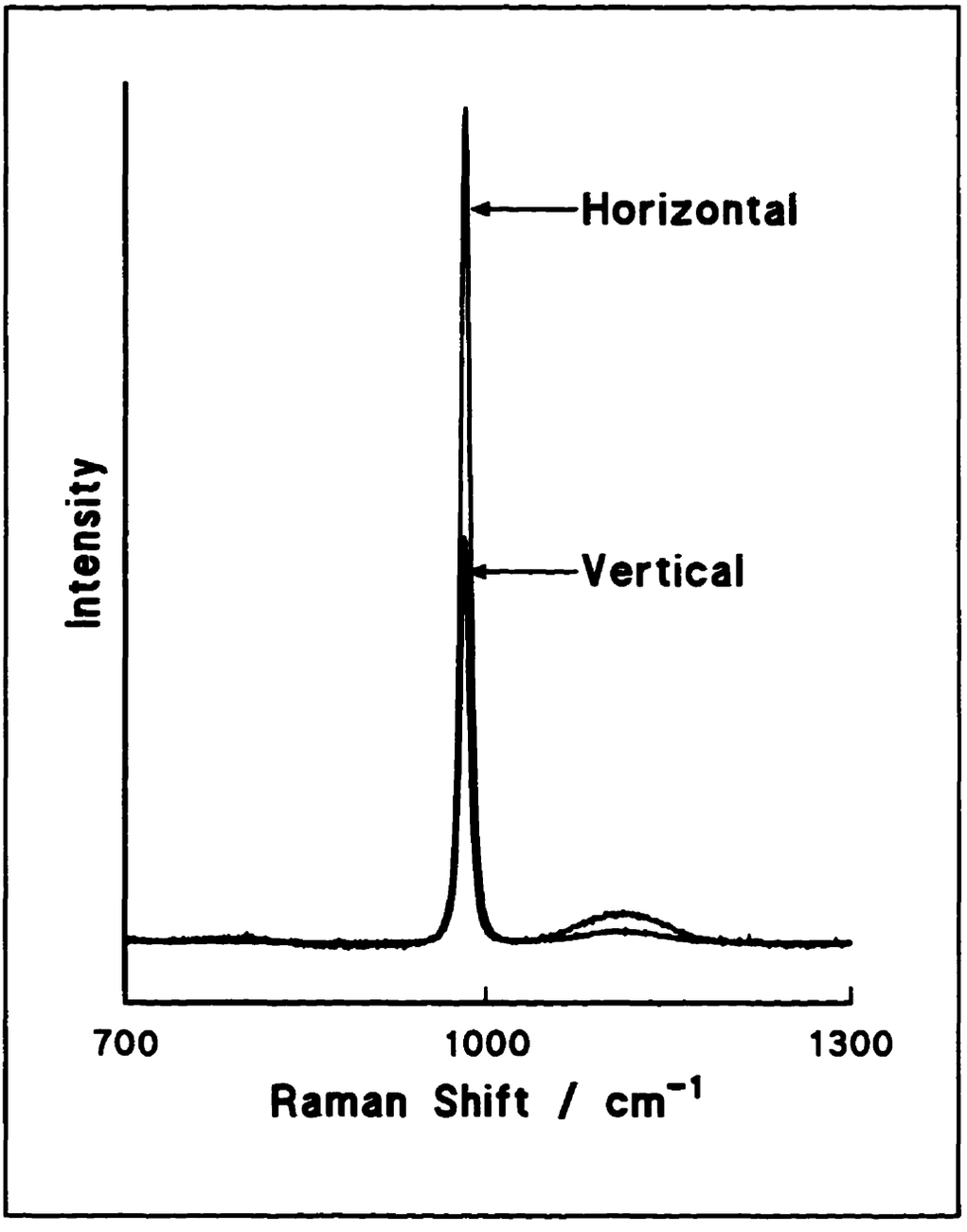

Fig. 2.3: Comparison of Horizontal (Parallel to the Floor) and Vertical (Perpendicluar to the Floor) Orientations of the Furnace Sample Cell for 2.8 m $ZnSO_4$.

off. When the tube is perpendicular, any bubbles which may form will rise to the top of the tube and their residence time in the beam will be very short. Obviously this will not happen when the tube is parallel to the floor. Second, mixing of the sample and the hydraulic fluid (generally, water) can be a greater problem in the parallel arrangement, leading to contamination of the sample.

2.4 Experimental Problems

Raman spectroscopy is based on an inherently weak effect and this leads to weak signals. It is frequently difficult to obtain spectra with a good signal-to-noise (S/N) ratio. Improvements to the signal-to-noise ratio can generally be made in two ways: 1) mathematically by the use of smoothing and 2) experimentally. Experimentally, the signal-to-noise ratio can be improved by 1) increasing the measurement time, 't', at each point; 2) increasing the number of measurements (which are averaged) at each point; 3) increasing the number of scans of the spectrum which are then averaged. More will be said about these options in the section, "Computers and Software". It is, in general, better to improve signal-to-noise experimentally rather than mathematically.

The laser and spectrometer performed admirably over the course of this research causing no special problems. There is, however, a small recurring problem with the

detector housing and window. The photomultiplier tube must be kept cold (-40°C) to reduce thermal emission of electrons from the photocathode. Under humid conditions (such as a southern Ontario summer!) this leads to condensation and formation of ice across the lens and the lens holder in front of the photomultiplier tube. Leaks (which develop over time) in the dry argon-filled holder cause this problem. This leads to a dramatic loss of signal. In severe cases this can lead to cracking of the lens holder. When this problem is evident, it is necessary to dry out the housing, lens, and lens holder. The detector must be disassembled in such a way that the photomultiplier tube is not exposed to bright light. It must be stored in a cool, dark, dry place. The lens and lens holder are removed from the housing and dried and cleaned. The housing is "baked out" at ~30°C overnight. Then, the detector is re-assembled.

2.5 Excitation and Detection

The configuration used in these experiments was typical for Raman spectroscopy. Excitation was achieved with a Coherent Model 305 argon ion laser operating at either 488.0 nm (in air, blue) or 514.5 nm (in air, green) with the latter being used for the majority of the experiments. The blue line was occasionally employed to avoid problems with laser plasma lines interfering with spectral bands. Powers were measured with the laser's internal meter and were set at 1.5 W or 2.0 W depending on the experiment. In

general, low temperature (< 100°C) capillary work was done at 1.5 W and high temperature, high pressure work was done at 2.0 W. In some cases, because of the volatility of species, the laser power was reduced to prevent bubble formation. No problems with fluorescence were encountered. The laser light followed the path illustrated by the dashed line in Fig. 2.4.

The light scattered from the sample was collected and focused on the entrance slit of the monochromator by a simple camera lens. A Jarrell-Ash spectrometer with a 1.0 m focal length scanning Czerny-Turner double monochromator was used. The 1180 grooves mm^{-1} grating is blazed for 514.5 nm to give a linear dispersion of 8.2 Å mm^{-1}. Mechanical slitwidths were normally set at 100 μm or 150 μm depending on the particular experiment. Where signal strength made it practical, the narrower width was used. These mechanical slitwidths translate to ~3 cm^{-1} and ~4.5 cm^{-1} (at 514.5 nm) spectral slitwidths, respectively. Spectral slitwidths become smaller for a given mechanical slitwidth as the absolute wavenumber decreases. In other words, spectral slitwidth improves as the monochromator moves from the exciting line to greater Raman shift. This is illustrated in Fig. 2.5. Control of the monochromator and acquisition of spectral data were by an I.B.M. PS/2 286 computer.

The detector was a thermoelectrically cooled R.C.A. 31034 photomultiplier tube. Photon counting was employed using a combination of an SSR Instruments model 1120

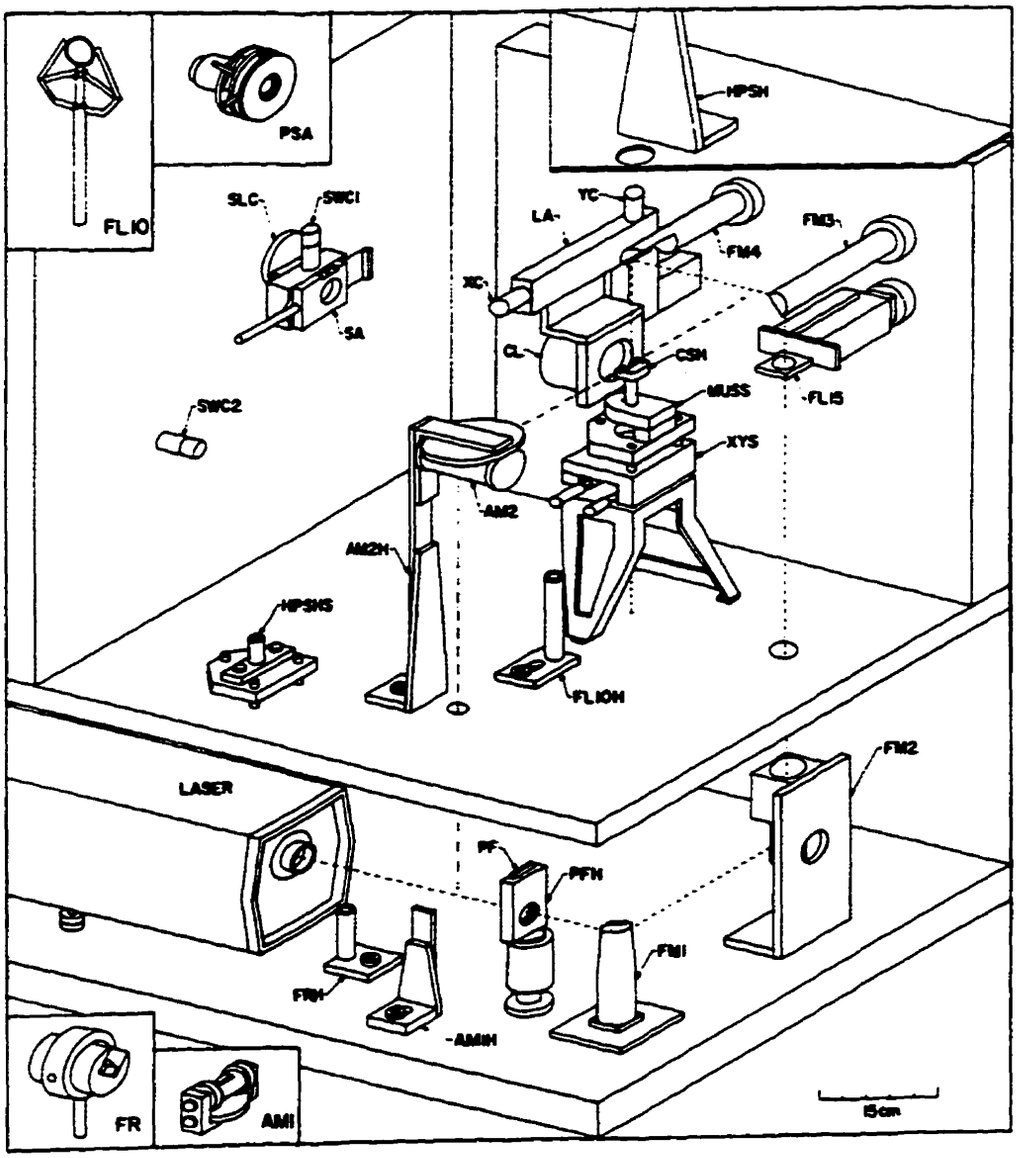

Fig. 2.4: The Sample Compartment of the Jarrell-Ash Spectrometer (2).

The Jarrell-Ash Sample Compartment

AM1-2	-	adjustable mirrors*
AM1H-2H	-	adjustable mirror holders*
CL	-	collection lens
CSH	-	capillary sample holder
FL10	-	10 cm focal length lens*
FL10H	-	10 cm focal length lens holder*
FL15	-	adjustable lens
FM1-4	-	fixed mirrors
FR	-	Fresnel prism*
FRH	-	Fresnel prism holder*
LA	-	lens assembly
MUSS	-	multiple use sample stage
PF	-	plasma filter
PFH	-	plasma filter holder
PSA	-	polarization and scrambler assembly
SA	-	slit assembly
SLC,SWC1-2	-	slit width and length controls
XC,YC	-	X,Y controls of lens assembly
XYS	-	translation stage

(* not required in the parallel arrangement for high temperature, high pressure work.)

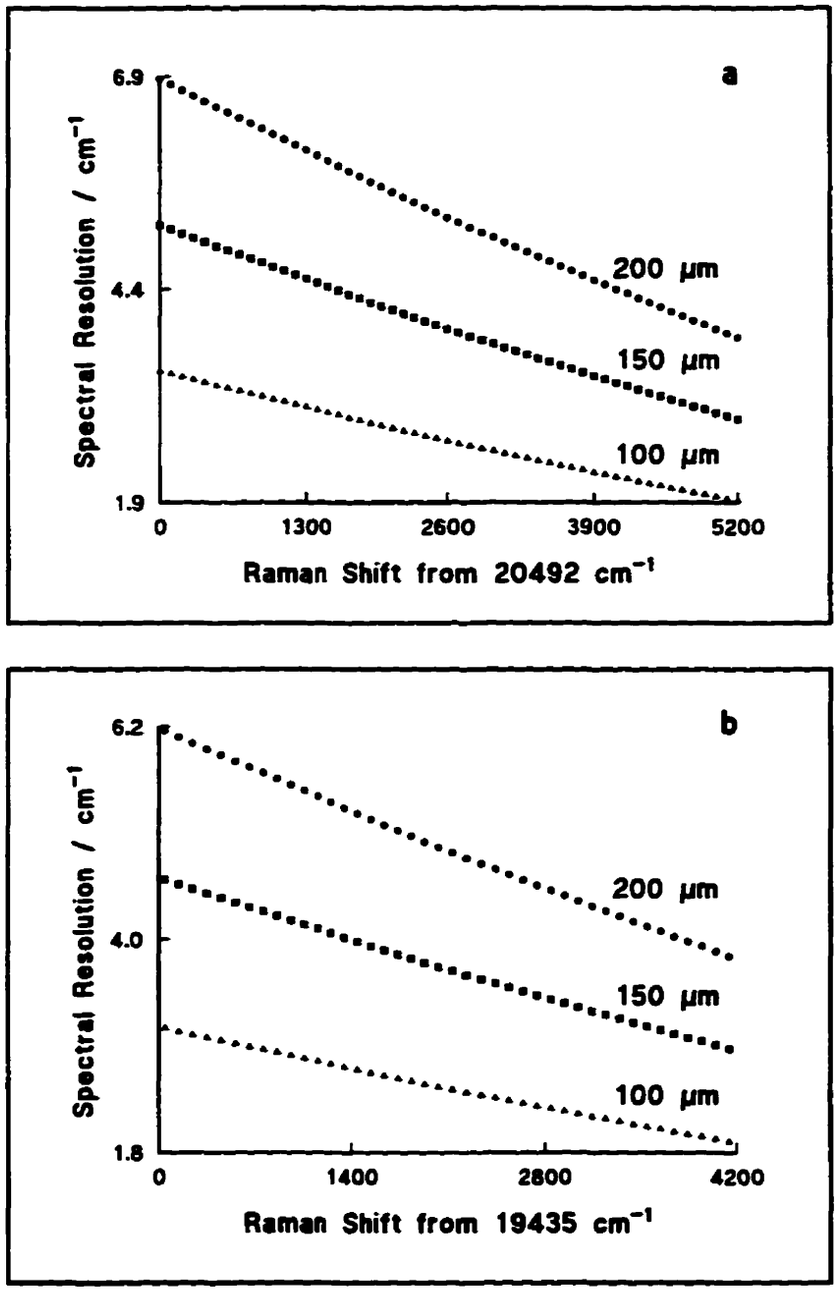

Fig. 2.5: Spectral Resolution as a Function of Raman Shift
a) Shift from 20492 cm^{-1} (488.0 nm, in air)
b) Shift from 19435 cm^{-1} (514.5 nm, in air)

amplifier / discriminator and a model 1105 data converter.

For conducting polarization studies, a polarization analyzer was used. This apparatus was attached at the entrance slit to the monochromator and consisted of two parts: a thin piece of Polaroid film to discriminate one polarization from another and a scrambler plate just after the Polaroid film. The Polaroid film had a circular holder which allowed easy rotation of the film to select either parallel or perpendicular radiation for analysis. Because gratings do not have equal transmission efficiencies for parallel and perpendicular radiation, a "scrambler" (see section 1.2.3) is necessary. In these experiments, a quarter wave plate made from calcite was used as the scrambler.

2.6 Computers and Software

All data collection and manipulations were performed on IBM PC's or compatibles using software designed (or adapted) and written in our laboratory.

Most important among the programs was the aptly named "Raman" program. This program controlled the monochromator and acquired spectral data. This program allows the collection of spectral data in four independent regions with a maximum of 2000 points in each region. The user enters five experimental parameters: i) the spectral region; ii)

the number of points per wavenumber; iii) the time constant; iv) the number of measurements at each point and v) the number of scans. Collecting a spectrum is then a matter of optimizing each of these parameters to get the best spectra (in terms of quality and quantity) in the shortest time. The user's choice of the first parameter is, obviously, a matter of which spectral region is being studied. It is the latter four parameters where the real "juggling" takes place. By increasing the number of points per wavenumber, the spectrum is sampled more frequently. Clearly, sampling more often is desirable as it will give a more accurate representation of the spectrum. Furthermore, when applying statistical tools such as bandfitting, it is desirable to have as many points as possible. Equally obvious, of course, is that the total experimental time will increase markedly. The time constant is the length of time for a given measurement at a given point. Increasing this variable increases the total signal (which is good) but also the total time (which is bad). The number of measurements is perhaps the most important parameter. This sets the number of measurements of time constant, 'TC', at each point. These measurements are then averaged to give a final intensity value at each point. Because signal rises as n and noise rises as $\sqrt{n}$, the S/N ratio rises as $\sqrt{n}$. Therefore, increasing the number of measurements increases the S/N ratio. Unfortunately, it also increases the total experimental time quite dramatically. Varying the number of scans should achieve the same result as changing the number of measurements at each point. In this case, however, it is the entire spectrum which is averaged by co-adding several different scans. Unfortunately, if any flaws exist in the monochromator drive, the monochromator may

not be re-set to precisely the same position at the beginning of each run and this might lead to poor spectra. Therefore, this parameter was always set to one.

In addition to collecting data, the "Raman" program was used for some data manipulation. The first of these is baseline correction. Baseline correction using this program is interactive. The user chooses points in the spectrum which model the baseline and then chooses a function to which to fit these points. The available functions are a line and polynomials to the fifth degree. There is also an option to model the baseline using line segments drawn from point to point. A least squares procedure is used to fit the chosen function to the chosen points. Once an acceptable (to the user) fit is found it is subtracted and the modified data can be stored. Good baseline correction is important because, if poorly applied, it can lead to misleading or erroneous results when bandfitting is applied. A second type of data modification possible using this program is the generation of "reduced" or "R" spectra (see section 1.2.1). This correction was suggested by Brooker, Nielsen and Praestgaard (6).

Frequently in Raman spectroscopy vibrational bands overlap. This is especially pronounced when working with condensed phase systems such as solutions. This is a problem which may be overcome, in some cases, by applying statistical methods to decompose the spectral contour into its component bands. Bandfitting was performed using a routine originally written by Pitha and Jones (7), modified by Murphy and

Bernstein for Raman spectroscopy (8), and slightly modified in our laboratory to run on PC's. In Raman spectroscopy, the bandshape is the convolution of two functions: a Lorentzian function, which accounts for homogeneous line broadening, and a Gaussian function, which accounts for inhomogeneous line broadening. The Lorentzian function is given by:

$$I(\nu) = \frac{x_1}{1 + x_3^2(\nu - x_2)^2} \qquad [1]$$

where

$I(\nu)$	=	intensity at Raman shift of ν
x_1	=	peak height
x_2	=	peak position
x_3	=	bandwidth parameter.

The Gaussian function is given by:

$$I(\omega) = x_1 \exp(-x_4^2(\omega - x_2)^2) \qquad [2]$$

x_4 = Gaussian bandwidth parameter

Murphy and Bernstein's routine replaces the convolution of equations [1] and [2] with a simple product of Lorentzian and Gaussian functions. When using this routine, the user is required to enter the band position, intensity, half width at half maximum and the relative Lorentzian "character". This "character" is embodied by a quantity 'R' - the Gauss - Lorentz shape ratio:

$$R = \frac{x_3}{x_3 + x_4} \qquad [3]$$

When R = 1 the band is completely Lorentzian and when R = 0 the band is completely Gaussian. The fitting routine uses a non-linear, least squares method and varies the parameters until a best fit of the spectrum is constructed. It was found there was some variation in the calculated parameters. This was especially true if a large number of bands was used or if overlap of component bands was quite significant. Generally, band positions were reproducible and the largest variations were found with band areas and widths. Furthermore, the final results were somewhat dependent on the initial guesses of the user. To alleviate this problem, bandfitting was applied to a given file several times and averages used. The error bars used in this thesis represent the spread of results obtained from these repeated bandfits. In some cases the differences between bandfit solutions was greater than in other cases and the wider error bars are seen. In some cases the spread of results was very small and the sizes of the error bars are smaller than the markers themselves. In light of these problems it is necessary to apply careful judgement in the evaluation of bandfitting results.

In the course of this project, two other computer routines had to be developed (see Appendix I). The first of these was to perform spectral subtraction. As mentioned in chapter 1, the isotropic spectrum is defined as:

$$I_{iso.} = I_{\parallel} - \frac{4}{3} I_{\perp} \qquad [4]$$

The subtraction routine simply subtracts the second from the first on a point by point basis. The user enters a subtraction factor by which the second file is multiplied prior to subtraction. By changing the sign of this factor, two spectra may be added. The second routine developed was to calculate spectral moments. It is necessary to calculate first moments to test the theories of resonance energy transfer. The nth spectral moment of a band is defined as (9):

$$M(n) = \frac{\int_{band} I(\nu)\nu^{n}\, d\nu}{\int_{band} I(\nu)\, d\nu} \qquad [5]$$

where

I(ν) = intensity at a Raman shift of ν

ν = the Raman shift (in cm^{-1})

such that M(0) = 1. If the band is symmetric, the first moment and the band centre will be equal. Because the spectral data are digitized, the integrals are evaluated over a selected range (chosen by the user) using Simpson's rule. The user may also choose which spectral moment to calculate.

2.7 References

1. D. E. Irish, T. Jarv, C. I. Ratcliffe, *Appl. Spectrosc.* **1982** 36 137
2. T. Jarv, *Ph. D. Thesis,* **1980** University of Waterloo
3. J. Semmler, *Ph. D. Thesis,* **1989** University of Waterloo
4. R. J. Bartholomew, *M. Sc. Thesis,* **1992** University of Waterloo
5. M. H. Brooker, *private communication*
6. M. H. Brooker, O. F. Nielsen, E. Praestgaard, *J. Raman Spectrosc.* **1988** 19 71
7. J. Pitha, R. N. Jones, *Can. J. Chem.* **1966** 44 3031
8. W. F. Murphy, H. J. Bernstein, *J. Phys. Chem.* **1972** 76 1147
9. M. H. Brooker in *The Chemical Physics of Solvation* Part B (J. Ulstrup, R. R. Dogonadze, E. Kálmán, A. A. Karnyshev Eds.), Elsevier, Netherlands, 1986

2.8 Appendix I - Computer Programs

This program (SPTOOLII.BAS) will add and subtract spectra, calculate band areas using Simpson's Rule, and calculate spectral moments.

```
30  DIM Y(2000, 4), S(4), F(4), SS(4), NS(4), TC(4), COL(8)
    DIM Y2(2000), S2(4), F2(4), SS2(4), NS2(4), TC2(4), AI(2000)
    NUL$ = ""
    ECH$ = CHR$(27)
    COL(1) = 9: COL(2) = 14: COL(3) = 12: COL(4) = 13: COL(5) = 7: COL(6) = 11:
    COL(7) = 10: COL(8) = 14
    SMIN = 20000: YMIN = 150000
    FMAX = 0: YMAX = 0
110 CLS
120 PRINT : PRINT : PRINT
130 PRINT TAB(32); "SPECTRAL TOOLS II"
140 PRINT : PRINT : PRINT
150 PRINT TAB(28); "PRESS ANY KEY TO CONTINUE"
160 A$ = INKEY$: IF A$ = "" THEN 160

'*********** GET THE INPUT FILENAME *******************

209 FLAG = 0: CLS
210 PRINT
    ON ERROR GOTO 220
    IF SOU$ = "" THEN DEFDIR$ = "B:\" ELSE DEFDIR$ = SOU$
211 PRINT : PRINT "What is the source directory (def. = "; DEFDIR$; ")";
    INPUT SOU$
    IF SOU$ = "" THEN SOU$ = DEFDIR$
    IF RIGHT$(SOU$, 1) <> "\" THEN SOU$ = SOU$ + "\"
    DEFDIR$ = SOU$
    PRINT : PRINT "Files on "; SOU$; " disk:": FILES SOU$ + "*.*"
212 PRINT : PRINT "What is the name of the file (def. ext. is 'RAM')";
```

```
    INPUT Q$

    IF Q$ = "" OR LEN(Q$) > 12 THEN
      PRINT "Filename is to long"
      GOTO 212
    END IF
    EXT$ = ".RAM"

    FOR IA1 = 1 TO LEN(Q$)
    IF MID$(Q$, IA1, 1) = "." THEN
       IF IA1 = 1 THEN BEEP: GOTO 212
       EXT$ = MID$(Q$, IA1)
       Q$ = LEFT$(Q$, IA1 - 1)
    END IF
    NEXT IA1

    IF LEN(EXT$) <> 4 THEN
      FOR IA1 = LEN(EXT$) + 1 TO 4
       EXT$ = EXT$ + " ":
      NEXT IA1
    END IF

    L$ = SOU$ + Q$ + EXT$

    PRINT
    PRINT "Opening file "; L$
    OPEN L$ FOR INPUT AS #1
      INPUT #1, SA$, TE$, CL$, D$, E$, G$, RE$, NR

      FOR J = 1 TO NR
        INPUT #1, S(J), F(J), SS(J), T(J), NS(J)

          FOR I = 0 TO NS(J)
            INPUT #1, Y(I, J)
          NEXT I

      NEXT J

    CLOSE #1
    DEFDIR$ = SOU$
218 PRINT : PRINT : PRINT " Filename     : "; L$
```

```
   PRINT " Temperature  : "; TE$
   PRINT " Line/power   : "; CL$
   PRINT " Polarization : "; D$
   PRINT " Slits        : "; E$
   PRINT " Remarks      : "; RE$
   PRINT " Region       Start        End        Step Size    Time/step"

   FOR J = 1 TO NR: PRINT J, S(J), F(J), SS(J), T(J): NEXT

219 PRINT
   INPUT "1) Add/Subtraction  2) Simpson's Rule Area 3) Spectral Moment 4) Run 5)
   Exit"; TC
   PRINT : ON TC GOSUB 25222, 30000, 40000, 60000, 61000
   CLS : GOTO 218

60000 GOTO 110

61000 END

220  '********** error trapping ************************************

    IF ERR = 53 THEN
      LOCATE CSRLIN - 1, 30: PRINT "---->     FILE DOES NOT EXIST !!!"
      BEEP
      IF FLAG = 1 THEN RESUME 26011 ELSE RESUME 210
    END IF

    IF ERR = 71 OR ERR = 72 THEN
     PRINT : PRINT "Disk not ready."
     BEEP
     PRINT "Insert disk and press any key to continue"

      DO UNTIL K$ <> ""
         K$ = INKEY$
      LOOP

     IF K$ = ECH$ AND FLAG = 1 THEN RESUME 26011
     IF K$ = ECH$ AND FLAG <> 1 THEN RESUME 211
     IF K$ <> ECH$ THEN RESUME
    END IF
```

```
IF ERR = 75 OR ERR = 76 THEN
  BEEP: PRINT
  PRINT "Path does not exist or cannot be found!"
  IF FLAG = 1 THEN RESUME 26011 ELSE RESUME 210
END IF

IF ERR = 68 OR ERR = 24 OR ERR = 25 OR ERR = 57 THEN
   BEEP: PRINT
   PRINT "Some form of device error has occurred."
   PRINT "Check disk drive connections etc. then press any key to continue"
   K$ = ""

   DO UNTIL K$ <> ""
     K$ = INKEY$
   LOOP

  IF K$ = ECH$ AND FLAG = 1 THEN RESUME 26011
  IF K$ = ECH$ AND FLAG <> 1 THEN RESUME 211
  IF K$ <> ECH$ THEN RESUME

END IF

IF ERR = 64 OR ERR = 52 THEN
  PRINT : PRINT "Bad filename"
  BEEP
  IF FLAG = 1 THEN RESUME 26011 ELSE 210
END IF

IF ERR = 11 THEN RESUME 1000
ON ERROR GOTO 0 '                          turn off error trapping
'****************** end of error trapping ******************************

25222 '************ SUBTRACTION ******************************

PRINT : PRINT "The addition/substraction feature will replace all the original data.
Continue";
INPUT AN$
IF LEFT$(AN$, 1) = "N" OR LEFT$(AN$, 1) = "n" THEN RETURN
```

```
25225 IF NR = 1 THEN
        OREG = 1
        GOTO 26000
      END IF


25500 PRINT : INPUT "Which region do you want to use in the subtraction"; OREG

      IF OREG > NR THEN
        BEEP
        GOTO 25500
      END IF

      IF OREG <= 0 THEN 209


26000 'CLS
26010 'CLS : PRINT
26011 FLAG = 0
      ON ERROR GOTO 220
      FLAG = 1
      PRINT : INPUT "Which directory do you want to search for the file to be subtracted
      "; DIR$
      IF DIR$ = "" THEN DIR$ = DEFDIR$
      IF RIGHT$(DIR$, 1) <> "\" THEN DIR$ = DIR$ + "\"
      PRINT : PRINT "Files on "; DIR$; "  disk:": FILES DIR$ + "*.*"
26012 PRINT : INPUT "What is filename  (default extension is  RAM !!!) "; Q$
      IF Q$ = "" THEN 26011

      IF LEN(Q$) > 12 THEN
        BEEP: PRINT "Filename is to long"
        GOTO 26000
      END IF

    EXT$ = ".RAM"

    FOR IA1 = 1 TO LEN(Q$)
```

```
 IF MID$(Q$, IA1, 1) = "." THEN
   IF IA1 = 1 THEN BEEP: GOTO 26012
   EXT$ = MID$(Q$, IA1)
   Q$ = LEFT$(Q$, IA1 - 1)
 END IF

NEXT IA1

IF LEN(EXT$) <> 4 THEN

  FOR IA1 = LEN(EXT$) + 1 TO 4
    EXT$ = EXT$ + " "
  NEXT IA1

END IF

L$ = DIR$ + Q$ + EXT$
PRINT : REFLAG = 1
PRINT "Opening file "; L$

OPEN L$ FOR INPUT AS #1
INPUT #1, SA2$, TE2$, CL2$, d2$, E2$, MG2$, RE2$, NR2
FOR J = 1 TO NR2
  INPUT #1, S2(J), F2(J), SS2(J), T2(J), NS2(J)
  FOR I = 0 TO NS2(J)
    INPUT #1, Y2(I)
  NEXT I
NEXT J
CLOSE #1:

DISPFL = 0
PRINT : PRINT : PRINT " Filename      : "; SA2$
PRINT " Temperature  : "; TE2$
PRINT " Line/power   : "; CL2$
PRINT " Polarization : "; d2$
PRINT " Slits        : "; E2$
PRINT " Remarks      : "; RE2$
PRINT " Region       Start        End        Step Size    Time/step"
FOR J = 1 TO NR2: PRINT J, S2(J), F2(J), SS2(J), T2(J): NEXT
PRINT
```

```
  IF NR2 = 1 THEN
   SREG = 1
   GOTO 26018
  END IF

26017   PRINT : INPUT "Which region do you want to use for subtraction"; SREG

      IF SREG <= 0 THEN 26000

      IF SREG > NR2 THEN
        BEEP
        GOTO 26017
      END IF

26018  IF SS(OREG) <> SS2(SREG) AND NR2 > 1 THEN
        BEEP
        PRINT : PRINT "The step size is different from the original spectrum!"
        GOTO 26017
      END IF

     IF SS(OREG) <> SS2(SREG) AND NR2 = 1 THEN
        BEEP
        PRINT : PRINT "The step size is different from the original spectrum!"
        GOTO 26011
     END IF


      IF S2(SREG) <> S(OREG) THEN
        BEEP
        PRINT : PRINT "The starting wavenumbers are different!"
        IF NR2 > 1 THEN 26017 ELSE 26011
      END IF

      E = VAL(E$): E2 = VAL(E2$)

      IF T2(SREG) <> T(OREG) THEN
        BEEP: PRINT
        PRINT "The time constant is not the same for the two spectra!  Continue";
        INPUT AN$
        IF LEFT$(AN$, 1) <> "y" AND LEFT$(AN$, 1) <> "Y" AND NR2 = 1 THEN
26000
```

```
    IF LEFT$(AN$, 1) <> "y" AND LEFT$(AN$, 1) <> "Y" AND NR2 > 1 THEN
26017
  END IF

  IF E2 <> E THEN
    BEEP: PRINT
    PRINT "The slits are not the same for the two spectra!  Continue";
    INPUT AN$
    IF LEFT$(AN$, 1) = "N" OR LEFT$(AN$, 1) = "n" THEN 26000
  END IF



  IF NS2(SREG) > NS(OREG) THEN INS = NS(OREG) ELSE INS = NS2(SREG)

  SSI = SS(SREG)
  SI = S(OREG)
  FI = SI + SSI * INS

  OPEN L$ FOR INPUT AS #2
  INPUT #2, SA2$, TE2$, CL2$, d2$, E2$, MG2$, RE2$, NR2
  FOR J = 1 TO SREG
    INPUT #2, S2(J), F2(J), SS2(J), T2(J), NS2(J)
      FOR I = 0 TO NS2(J)
        INPUT #2, Y2(I)
      NEXT I
  NEXT J
  CLOSE #2


  PRINT : INPUT "What is the scaling factor (default = - 4/3)"; SF

  IF SF = 0 THEN SF = -4 / 3

  FOR J = 0 TO INS
    Y(J, 1) = Y(J, OREG) + SF * Y2(J)
  NEXT J

  FOR T = INS + 1 TO 2000
    Y(T, 1) = 0
  NEXT T
```

```
      FOR R = 2 TO NR
        FOR J = 0 TO NS(R)
          Y(J, R) = 0
        NEXT J
      NEXT R


      NR = 1: SS(1) = SSI: S(1) = SI: F(1) = FI: NS(1) = INS

      NR = 1

      REFLAG = 0
      PRINT : INPUT "Do you want to view the results"; AN$

IF LEFT$(AN$, 1) = "Y" OR LEFT$(AN$, 1) = "y" OR AN$ = "" THEN GOSUB 1050

      CLS
      PRINT : INPUT "Do you want to store the results"; AN$
      IF LEFT$(AN$, 1) = "N" OR LEFT$(AN$, 1) = "n" THEN RETURN

      GOSUB 26200

1000    RETURN

   '********************** Plotting on screen of results *******************

1050  CLS
     XV = SI: NSP = SI
     SW = SI: EW = FI
     NNS = INS
     TSS = SSI

     YMAX = 0: YMIN = 1500000

   FOR T = 0 TO INS
     IF Y(T, 1) > YMAX THEN YMAX = Y(T, 1)
     IF Y(T, 1) < YMIN THEN YMIN = Y(T, 1)
   NEXT T

     MX = YMAX
```

```
    MI = YMIN
1150 CLS
   SCREEN 12                          '640x480 pixels
   LOCATE 1, 1                        'set up the plot screen
   PRINT "   "; SA$; " - "; SA2$        '(identify the files)

1155 VIEW (20, 43)-(620, 413), 0, 0       'set view port at 600x370 pixels
   LOCATE 27, 1                       'set x axis label
   PRINT TAB(3); USING "####"; SW; TAB(75); EW
   PRINT TAB(35); "SHIFT (CM-1)"
   LINE (0, 0)-(0, 370), 11           'draw axes
   LINE -(600, 370), 11
   PPWN = 600 / (EW - SW)               'determine pixels/waveno.
   PPINT = 370 / (MX - MI)             'determine pixels/intensity
   XHS = (EW - SW) / 5: YHS = (MX - MI) / 5
   XH = SW: YH = MI

   FOR T = 1 TO 5                     'place hatchmarks
     XHP = (XH - SW) * PPWN
     XHPI = INT(XHP)
     IF (XHP - XHPI) >= .5 THEN XHPI = XHPI + 1
     YHP = (YH - MI) * PPINT
     YHPI = INT(YHP)
     IF (YHP - YHPI) >= .5 THEN XHPI = XHPI + 1
     PSET (XHP, 370)
     LINE -(XHPI, 365), 11
     PSET (0, YHPI)
     LINE -(5, YHPI), 11
     XH = XH + XHS
     YH = YH + YHS
   NEXT T


1165 YV = Y(0, 1)                     'determine first x pixel position
   FX = (NSP - SW) * PPWN               'and find integral value for it.
   FXI = INT(FX)                      'Round it off if necessary.
   IF (FX - FXI) >= .5 THEN FXI = FXI + 1 'do the same for the first y
   FY = 370 - ((YV - MI) * PPINT)     'position
   FYI = INT(FY)
   IF (FY - FYI) >= .5 THEN FYI = FYI + 1
```

```
    PSET (FXI, FYI), COL(PC)                'set the first point in the spectrum
   FOR J = 1 TO NNS                       'draw the spectrum by drawing lines
    XV = XV + TSS                         'to the next pixel position
    YV = Y(J, 1)
    XP = ((XV - SW) * PPWN)
    XPI = INT(XP)
    IF (XPI - XP) >= .5 THEN XPI = XPI + 1
    YP = 370 - ((YV - MI) * PPINT)
    YPI = INT(YP)
    IF (YP - YPI) >= .5 THEN YPI = YPI + 1
    LINE -(XPI, YPI), COL(2)
   NEXT J

1175 VIEW PRINT 29 TO 30
    K$ = ""
    PRINT "Press any key to continue"

    DO WHILE K$ = ""
     K$ = INKEY$
    LOOP

    SCREEN 0

    RETURN

'******************* ROUTINE TO STORE THE RESULTS *****************

26200  PRINT : PRINT "The spectra will be recorded with the following descriptors:"
      PRINT
      D$ = "Isotropic"
      PRINT " Temperature  : "; TE$
      PRINT " Line/power   : "; CL$
      PRINT " Polarization : "; D$
      PRINT " Slits        : "; E$
      PRINT " Remarks      : "; RE$
      PRINT : INPUT "Do you want to change any of this information"; AN$

      IF LEFT$(AN$, 1) = "Y" OR LEFT$(AN$, 1) = "y" THEN
        PRINT
        PRINT "'ENTER' does not change the default value."
        PRINT : INPUT "Temperature"; AN$
```

```
    IF AN$ <> "" THEN TE$ = AN$
    INPUT "Line/power"; AN$
    IF AN$ <> "" THEN CL$ = AN$
    INPUT "Polarization"; AN$
    IF AN$ <> "" THEN D$ = AN$
    INPUT "Slits"; AN$
    IF AN$ <> "" THEN E$ = AN$
    INPUT "Remarks"; AN$
    IF AN$ <> "" THEN RE$ = AN$
  END IF

  RE$ = DATE$ + " " + RE$
  LRE = LEN(RE$)

  IF LRE >= 70 THEN RE$ = LEFT$(RE$, 70)

26500  EXT$ = "ISO"
  IF DEST$ = "" THEN DDIR$ = SOU$ ELSE DDIR$ = DEST$
26505  DEF$ = SA$: DEFEX$ = EXT$
  LSA = LEN(SA$)

  FOR T = 1 TO LSA

    S$ = MID$(SA$, T, 1)

    IF S$ = "." THEN
      SA$ = LEFT$(SA$, (T - 1))
      EXIT FOR
    END IF

  NEXT T

  DEF$ = SA$: DEFEX$ = EXT$
  PRINT : PRINT "If all the defaults are chosen, the results will be stored as: "
  PRINT DDIR$ + DEF$ + "." + DEFEX$
  PRINT : PRINT "What is the destination directory (def. is "; DDIR$; " )";
  INPUT DEST$
  IF DEST$ = "" THEN DEST$ = DDIR$
  IF RIGHT$(DEST$, 1) <> "\" THEN DEST$ = DEST$ + "\"
26510  PRINT : PRINT "What is the permanent name for the file (def. is "; DEF$; " )";
  INPUT F$
```

```
     IF F$ = "" THEN F$ = DEF$

     IF LEN(F$) > 8 THEN
       BEEP: PRINT : PRINT "Filename is too long"
       GOTO 26510
     END IF

     DEFEX$ = EXT$
26511  PRINT : PRINT "What is the extension (def. is "; DEFEX$; " )";
     INPUT EXT$

     IF LEN(EXT$) > 3 THEN
       BEEP: PRINT
       PRINT "Extension is too long"
       GOTO 26511
     END IF

    IF EXT$ = "" THEN EXT$ = "." + DEFEX$ ELSE EXT$ = "." + EXT$
    FILEN$ = DEST$ + F$ + EXT$

    ON ERROR GOTO 26512

    PRINT : FILES FILEN$
    PRINT "File already exists": BEEP: EXT$ = RIGHT$(EXT$, 3): GOTO 26510

26513  PRINT "Saving file as "; FILEN$: PRINT
26514    OPEN FILEN$ FOR OUTPUT AS #1
       PRINT #1, F$; ","; TE$; ","; CL$; ","; D$; ","; E$; ","; MG$; ","; RE$; ","; NR
       PRINT #1, S(1); F(1); SS(1); T(1); NS(1)

       FOR I = 0 TO NS(1)
         PRINT #1, Y(I, 1)
       NEXT I

      PRINT #1, ZE

      CLOSE #1

      RETURN
```

```
26512 '****************** error handling ************************************

      IF ERR = 53 AND REFLAG = 0 THEN
        PRINT : PRINT "New file"
        RESUME 26513
      END IF

     IF ERR = 61 OR ERR = 71 OR ERR = 72 OR ERR = 57 OR ERR = 68 OR
      ERR=24 OR ERR = 25 AND REFLAG = 0 THEN
        BEEP: PRINT
        PRINT "Disk full or not ready"
        PRINT "Check drive and/or insert a new diskette"
        PRINT "Press any key to continue"
        K$ = ""

        DO UNTIL K$ <> ""
          K$ = INKEY$
        LOOP

        CLOSE #1
        IF K$ = ECH$ THEN RESUME 26500 ELSE RESUME 26514
    END IF

      IF (ERR = 64 OR ERR = 52) AND REFLAG = 0 THEN
        PRINT : PRINT "Bad filename"
        BEEP: EXT$ = RIGHT$(EXT$, 3)
        RESUME 26510
      END IF

      IF ERR = 75 OR ERR = 76 THEN
        PRINT : PRINT "Path not found or access error"
        BEEP: EXT$ = RIGHT$(EXT$, 3)
        RESUME 26505
      END IF


    ON ERROR GOTO 0 '                          turn off error trapping
'************************ end of error trapping ******************************

'************************ Simpson's Rule Area Determination ******************
```

```
30000  IF NR = 1 THEN
         CH = 1
         GOTO 31000
       END IF

       PRINT : INPUT "For which region do you wish to calculate the area"; CH

       IF CH > NR OR CH <= 0 THEN 219

31000  GOSUB 35100  'arrange array for integration

       GOSUB 50000  'perform Simpson's Rule integration"

       PRINT : PRINT "The calculated area is"; AREA
       PRINT : PRINT

       IF NR > 1 THEN
         PRINT : INPUT "Do you want to calculate the area of another region"; AN$
         IF AN$ = "Y" OR AN$ = "y" THEN 30000
       END IF

       RETURN

'********* ROUTINE TO SET UP ARRAYS FOR INTEGRATION ***************

35100  PRINT : INPUT "What is the starting wavenumber"; SWN

       IF SWN < S(CH) OR SWN > F(CH) THEN
         BEEP
         PRINT : PRINT "Starting wavenumber is not within the range of the data"
         GOTO 35100
       END IF

35200  PRINT : INPUT "What is the final wavenumber "; EWN

       IF EWN < S(CH) OR EWN <= SWN OR EWN > F(CH) THEN
         BEEP
         PRINT : PRINT "Final wavenumber is invalid!"
         GOTO 35200
       END IF
```

```
      SPA = (SWN - S(CH)) / SS(CH)
      EPA = (EWN - S(CH)) / SS(CH): NSA = (EWN - SWN) / SS(CH)

      FOR T = 0 TO NSA
       AI(T) = Y(SPA + T, CH)
      NEXT T

      RETURN
'*********************************************************************


40000 '************ SPECTRAL MOMENT CALCULATION *******************

      IF NR = 1 THEN
        CH = 1
        GOTO 40100
      END IF

   PRINT : INPUT "In which region do you wish to calculate the spectral moment"; CH

   IF CH > NR OR CH <= 0 THEN 219

40100  PRINT : INPUT "Which spectral moment to calculate"; SM

      IF SM < 0 THEN
        BEEP
        PRINT : PRINT "Invalid spectral moment!": PRINT
        GOTO 40100
      END IF

40200  PRINT : INPUT "What is the band maximum"; BM

      IF BM < 0 THEN
        BEEP
        PRINT "Invalid frequency!": PRINT
        GOTO 40200
      END IF

      GOSUB 35100
```

```
    GOSUB 50000

    BA = AREA


    FOR T = 0 TO NSA
      IN = (SWN + T * SS(CH))
      AI(T) = Y(SPA + T, CH) * (IN) ^ SM
    NEXT T

    GOSUB 50000

    BSM = AREA / BA

    PRINT : PRINT "The band maximum is "; BM
    PRINT : PRINT "The spectral moment is "; BSM

    PRINT : PRINT "Press any key to continue"
    K$ = ""
    DO WHILE K$ = ""
      K$ = INKEY$
    LOOP

    RETURN
'************** SIMPSON'S RULE APPLICATION ***********************

50000  AREA = 0: A1 = 0: A2 = 0: A3 = 0

    H = SS(CH)

    IF NSA / 2 <> INT(NSA / 2) THEN M = .5 * (NSA - 1) ELSE M = .5 * NSA

    A1 = AI(0) + AI(2 * M)

    FOR T = 1 TO (2 * M - 1) STEP 2
      A2 = A2 + AI(T)
    NEXT T

    FOR T = 2 TO (2 * M - 2) STEP 2
      A3 = A3 + AI(T)
    NEXT T
```

```
AREA = H / 3 * (A1 + 4 * A2 + 2 * A3)

RETURN
```

3. SOLUTIONS OF FORMIC ACID

3.1 Introduction

An isolated formic acid molecule has C_S symmetry and nine normal modes of vibration spanning the representation:

$$\Gamma_{vib.} = 7A' + 2A''$$

All the vibrations are both Raman and infrared active and seven of the Raman bands are polarized. Four of the vibrations are stretches, four are deformations, and one is a torsion. If the 'OH' group is taken as a point mass, C_S symmetry is retained and

$$\Gamma_{vib.} = 5A' + A''$$

Therefore, three vibrations are associated with the 'OH' group: the O-H stretch, the COH deformation, and the OH torsion. The remaining modes are the C-H stretch, C=O stretch, C-OH stretch, CH in-plane bend, O-C=O deformation, and the CH out-of-plane bend. A normal coordinate analysis of monomeric formic acid has been conducted by Susi and Scherer (1).

In practice, the Raman and infrared spectra are complicated by intermolecular interactions (hydrogen bonding or dipole - dipole forces) between formic acid molecules.

This problem is particularly pronounced for liquid formic acid. The existence of strong intermolecular forces can lead to the coupling of normal modes and to the resonance energy transfer effect. This may further complicate the spectrum of formic acid.

Liquid formic acid has been studied by a number of methods including infrared spectroscopy (2,3,4), low frequency Raman spectroscopy (5,6), Raman spectroscopy (4), X-ray analysis (7), NMR spectroscopy (8), dielectric measurements (9), and neutron diffraction methods (10). The conclusions regarding the structure of liquid formic acid have been almost as diverse. Several workers have concluded the liquid contains polymeric species (2,4,5,7,9,10). Tomlinson, Curnutte and Hathaway were specific in concluding the liquid consists of helical polymers (4). Other workers have concluded liquid formic acid contains of dimers (3,8,11). Waldstein and Blatz concluded liquid formic acid was composed of either polymers, an open dimers, or a mixture of the two (6). Clearly, the structure of formic acid is not well characterized.

Pure formic acid was studied both at room temperature and at elevated temperatures and pressures in a previous work (12). A survey spectrum (100 - 2000 cm^{-1}, in R(v) format) is presented here for completeness (Fig. 3.1) and partial assignments are given in Table 3.1.

Dr. Murray Brooker (13) suggested a series of experiments on formic acid diluted

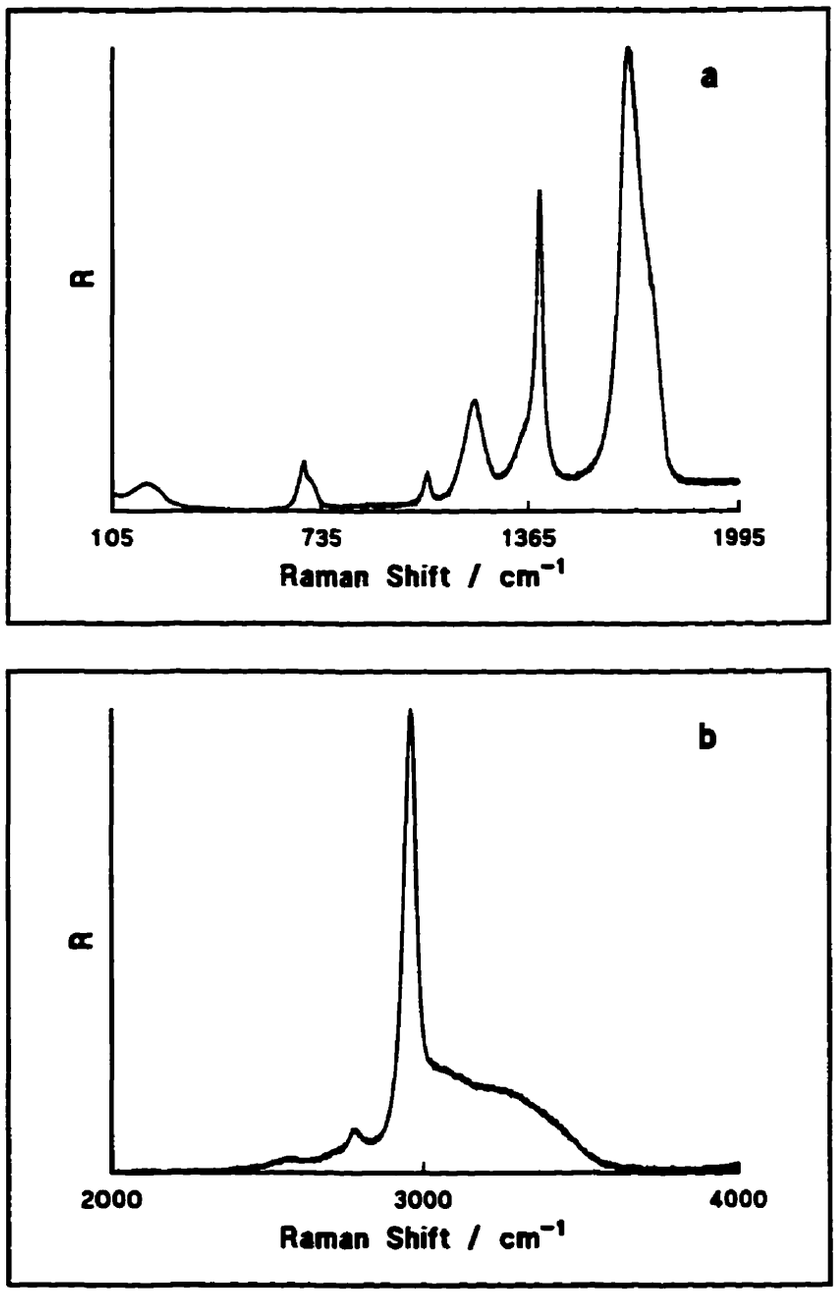

Fig. 3.1: Survey Spectrum of 98% Formic Acid.

Table 3.1: Partial Assignment of Formic Acid (4).

Frequency / cm^{-1}	Assignment
1600 - 1750	C=O stretch
1398	C-H bend
1333	δ(OHO) + C-O stretch
1208	C-O stretch
650 - 725	OCO bend
~210	OH···H out of plane bend
1060	C-H bend

in water. Dilution should lead to a reduction of any intermolecular coupling (which gives rise to resonance energy transfer) and therefore to consequent changes in the spectrum. As the "active" species is diluted the degree of association should decrease and this should be observable in the spectrum. Similar work has already been done in our laboratory on acetic acid (14,15). Those studies showed a dependence on concentration of the nature and relative amounts of the associated species in acetic acid. Studies of solutions of formic acid were undertaken, in part, to see if similar effects might be observed. Such effects, if they do occur, may shed some light on the structure of pure formic acid. However, as was found from the previous work (12), the behaviour of formic acid is quite different from that of acetic acid.

3.2 Experimental

The chemicals used in these experiments were: 98 - 100% formic acid, 99% acetonitrile, 99.9% dichloromethane (all supplied by B.D.H), 99.9% 1,4-dioxane (Fisher) and Milli-Q water. The formic acid and the organic solvents were used "as received", i.e., without further purification. The small amount of water present in the formic acid is not expected to have a significant effect on the results. Binary solutions of formic acid with each of the solvents were prepared. Ternary solutions of formic acid, acetonitrile and dichloromethane were prepared to construct a Job plot. As shown in section 3.3.2

(formic acid / acetonitrile) formic acid and acetonitrile form some sort of "complex". The "method of continuous variations" (which generates a Job plot) (16) allows the determination of the relative amounts of "ligand" and "metal" in a complex. This method was applied to the formic acid - acetonitrile system with the objective of determining the relative amounts of formic acid and acetonitrile in the "complex". More will be said about this later (section 3.3.6).

The binary solutions of formic acid were prepared on a mole fraction basis using 25 mL volumetric flasks. The required volume of formic acid was measured using a graduated cylinder and poured into the flask. The mass of the formic acid was then determined. The volumetric flask was filled to the mark with solvent and the mass of the solvent was recorded. The volumetric flasks were capped, wrapped with Parafilm and stored in a refrigerator.

Portions of the solutions were added to thin-walled capillary tubes using a syringe and a length of Teflon tubing. The binary solutions were added using a plastic syringe and this did not appear to have any adverse effect on the spectra. For the solutions containing dichloromethane, however, the use of plastic syringes gave quite high backgrounds. A glass syringe was tried and it alleviated the problem. The syringes (both plastic and glass) were rinsed thoroughly with the intended solutions before filling the capillary and rinsed with Milli-Q water afterwards. The capillary was then placed in the

thermostatted copper block that has already been described (section 2.2).

All spectra were collected using the 514.5 nm line at 1.5 W (measured at the laser head) as the excitation source. Survey spectra and spectra of the C=O stretching region of the binary solutions were collected with a mechanical slitwidth of 150 μm. For solutions involving acetonitrile, spectra of the C≡N stretching region (2100 - 2400 cm^{-1}) were collected with slits of 100 μm. For the ternary solutions, spectra were collected in three spectral regions. The first was 585 - 885 cm^{-1}. This region includes a band from the solvent, dichloromethane, that was used as an intensity standard. It exactly overlaps the O-C=O bending bands of formic acid but is very strong while the O-C=O bending bands are very weak. The error in intensity from the contribution of the O-C=O bands was estimated to be less than 1% and therefore not significant. The second region was the C≡N stretching region of the acetonitrile. For both of these regions the slits were set at 100 μm. The third region was the carbonyl region of formic acid (1500 - 1900 cm^{-1}) where the slits were set at 200 μm. The binary solution spectra were collected at 25°C while the spectra for solutions containing dichloromethane were collected at 20°C. The temperature was reduced for the latter solutions because of the low boiling point of dichloromethane (40°C).

3.3 Results and Discussion

Solutions of formic acid in four different solvents (water, acetonitrile, 1,4-dioxane and dichloromethane) were studied. The results for each solvent will be presented in turn.

3.3.1 Formic acid / Water

A series of solutions of HCOOH / H_2O was prepared from X(HCOOH) = 0.900 to X(HCOOH) = 0.510. The concentrations are summarized in Table 3.2.

Figure 3.2 shows a survey spectrum for formic acid at X = 0.510. The most dramatic effects are in the O-C=O deformation region (600 - 750 cm^{-1}) and the carbonyl region (1475 - 1875 cm^{-1}). Also, some slight change appears in the low frequency band at ~200 cm^{-1}.

The carbonyl spectral region was studied in the greatest depth. Figure 3.3 shows the effect of dilution on this spectral region. As the formic acid is diluted the band maximum moves to higher frequency and the high frequency shoulder becomes less prominent. The band maximum moves towards coincidence with the high frequency shoulder. In the spectra of more dilute formic acid, low frequency asymmetry occurs

Table 3.2: Concentrations of HCOOH / H_2O Solutions.

Code	X(HCOOH) / mol L^{-1}	C(HCOOH) / mol L^{-1}	C(H_2O) / mol L^{-1}
RB940207A	0.900	25.10	2.774
RB940204B	0.803	23.82	5.857
RB940204C	0.700	22.06	9.440
RB940204D	0.591	20.21	14.01
RB940204A	0.510	18.29	17.64

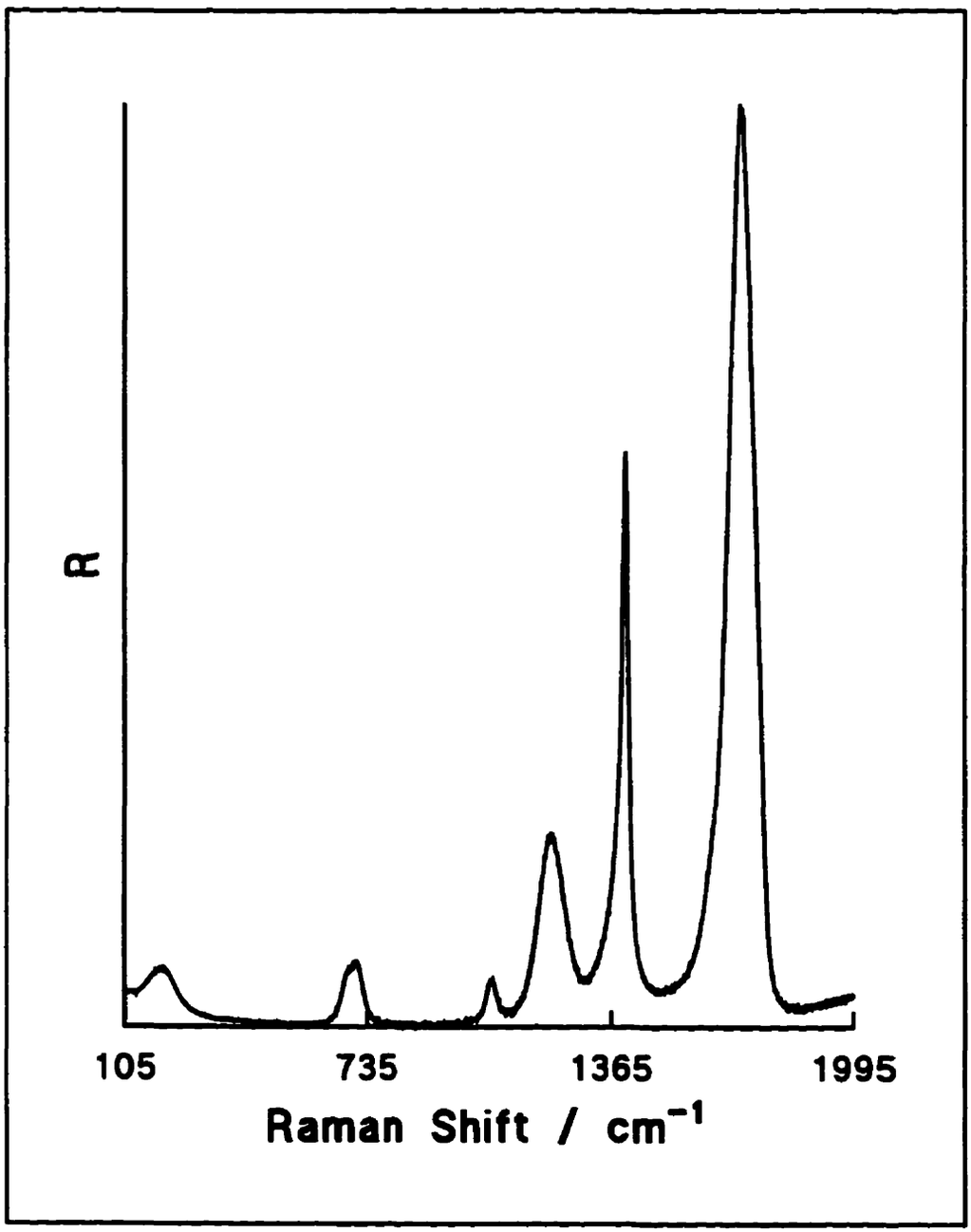

Fig. 3.2: Survey Spectrum of HCOOH / H_2O X(HCOOH) = 0.501.

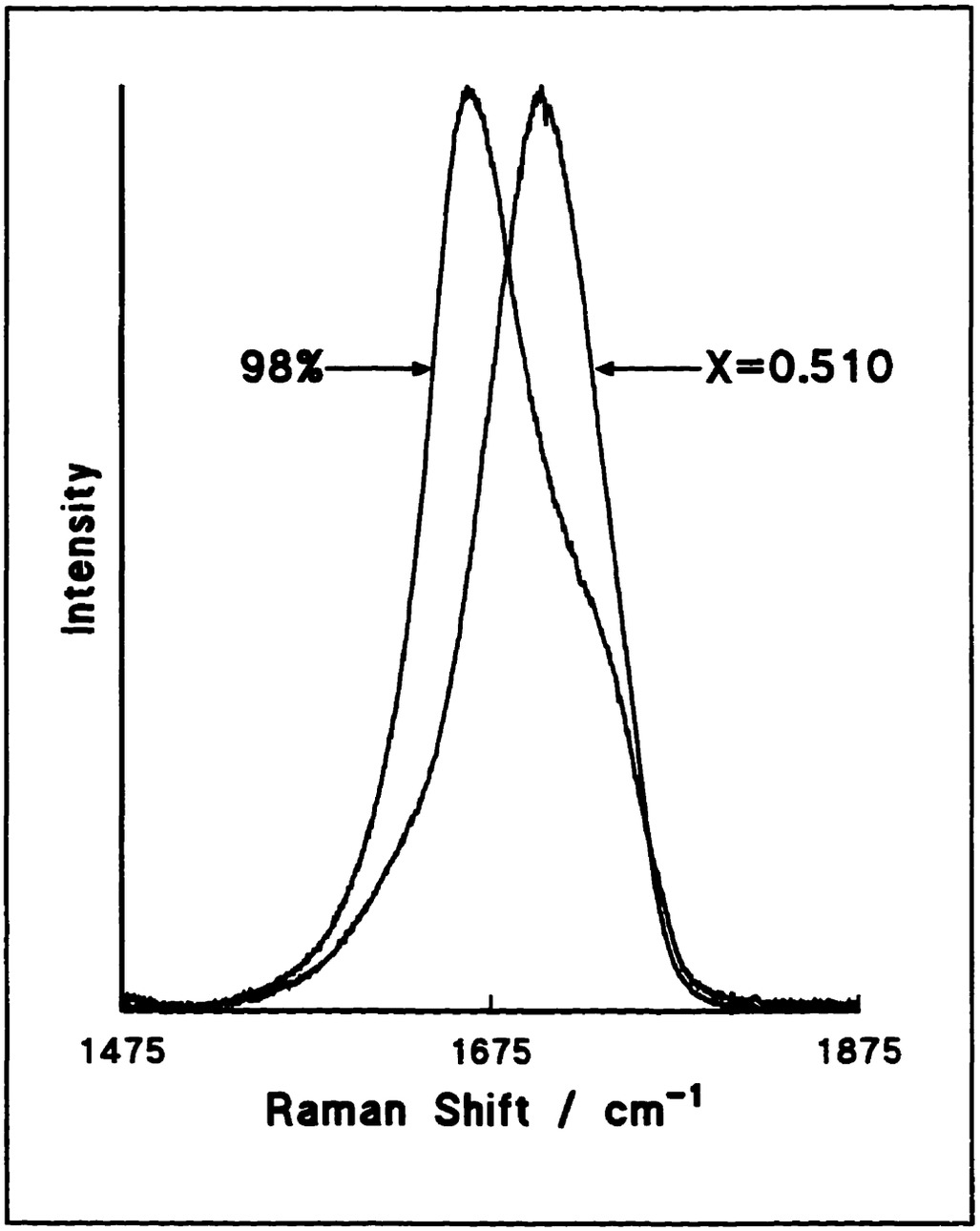

Fig. 3.3: Carbonyl Modes of HCOOH / H_2O.

because of overlap with the ν_2 mode of water. The appearance of this mode necessarily precludes continuing studies below X(HCOOH)~0.5 for HCOOH / H_2O.

Figures 3.4 - 3.5 show the isotropic and anisotropic spectra of formic acid under various conditions. A non-coincidence of the isotropic and anisotropic band maxima is very clear. From the spectrum of 98% formic acid it is evident the maximum in the isotropic spectrum corresponds to a shoulder in the anisotropic and vice versa. The maximum in the anisotropic is at ~1725 cm^{-1} and this frequency is essentially constant throughout the concentration range. At 100°C (98% HCOOH) the anisotropic maximum is at ~1728 cm^{-1}. Tomlinson, Curnutte, and Hathaway (4) report an infrared maximum at 1715 cm^{-1} that shifts upward by 4 cm^{-1} when the temperature is raised from 10°C to 80°C. They assigned this to C=O stretching. In the Raman, however, they assigned the peak at 1654 cm^{-1} to C=O stretching and a shoulder at 1740 cm^{-1} to a combination of CH bending (1060 cm^{-1}) and OCO bending (675 cm^{-1}). Unfortunately, these assignments seem to be based on spectra at 0°C and pure formic acid freezes at 8°C!

Figure 3.6 shows the separation of band maxima as a function of formic acid mole fraction. The separations are given in Table 3.3. At X(HCOOH)~1 (98% B.D.H. formic acid) the separation is ~64 cm^{-1}. In other molecules with carbonyl groups the non-coincidence is typically < 15 cm^{-1} (17). However, all the other evidence suggests a resonance energy transfer (RET) effect is taking place in formic acid. As the acid is

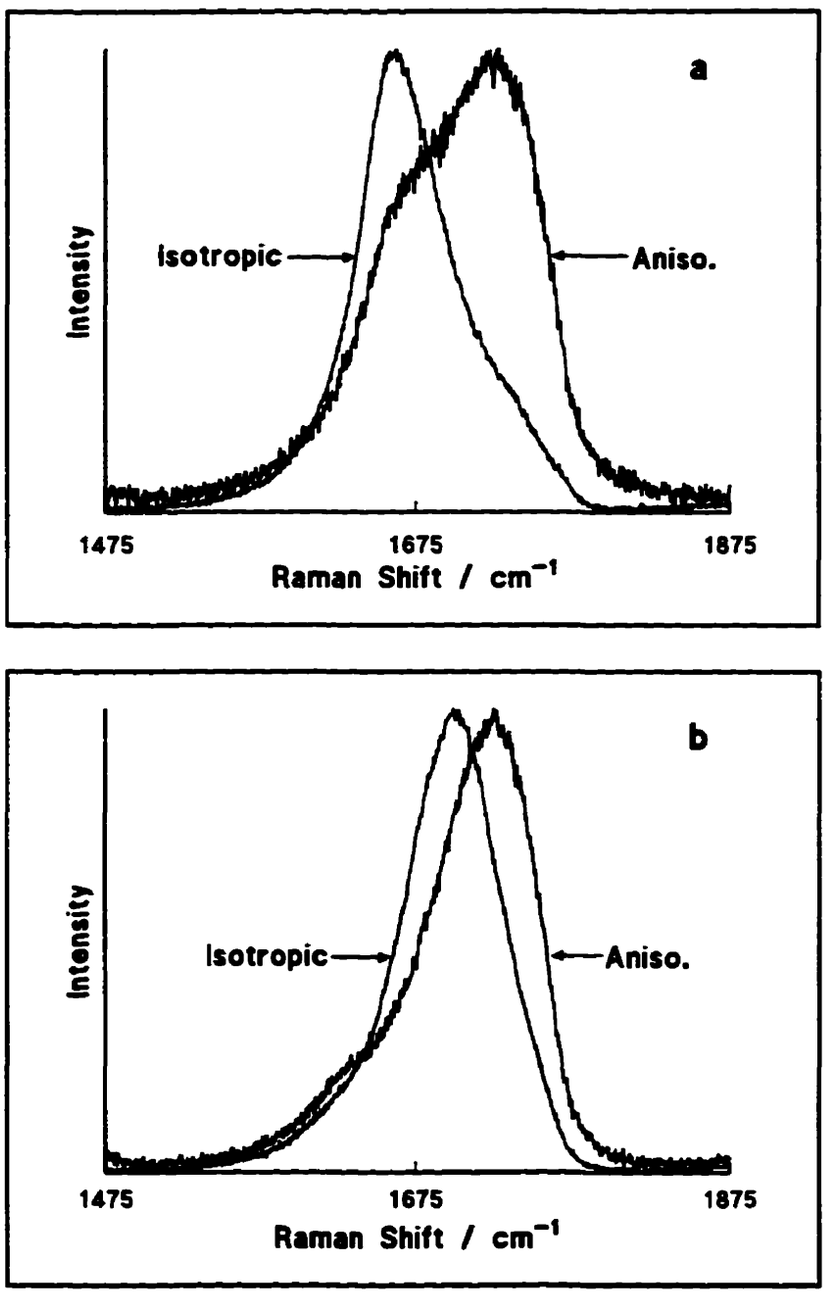

Fig. 3.4: Polarization Studies of HCOOH / H_2O:
a) 98% HCOOH b) X(HCOOH) = 0.510
(normalized).

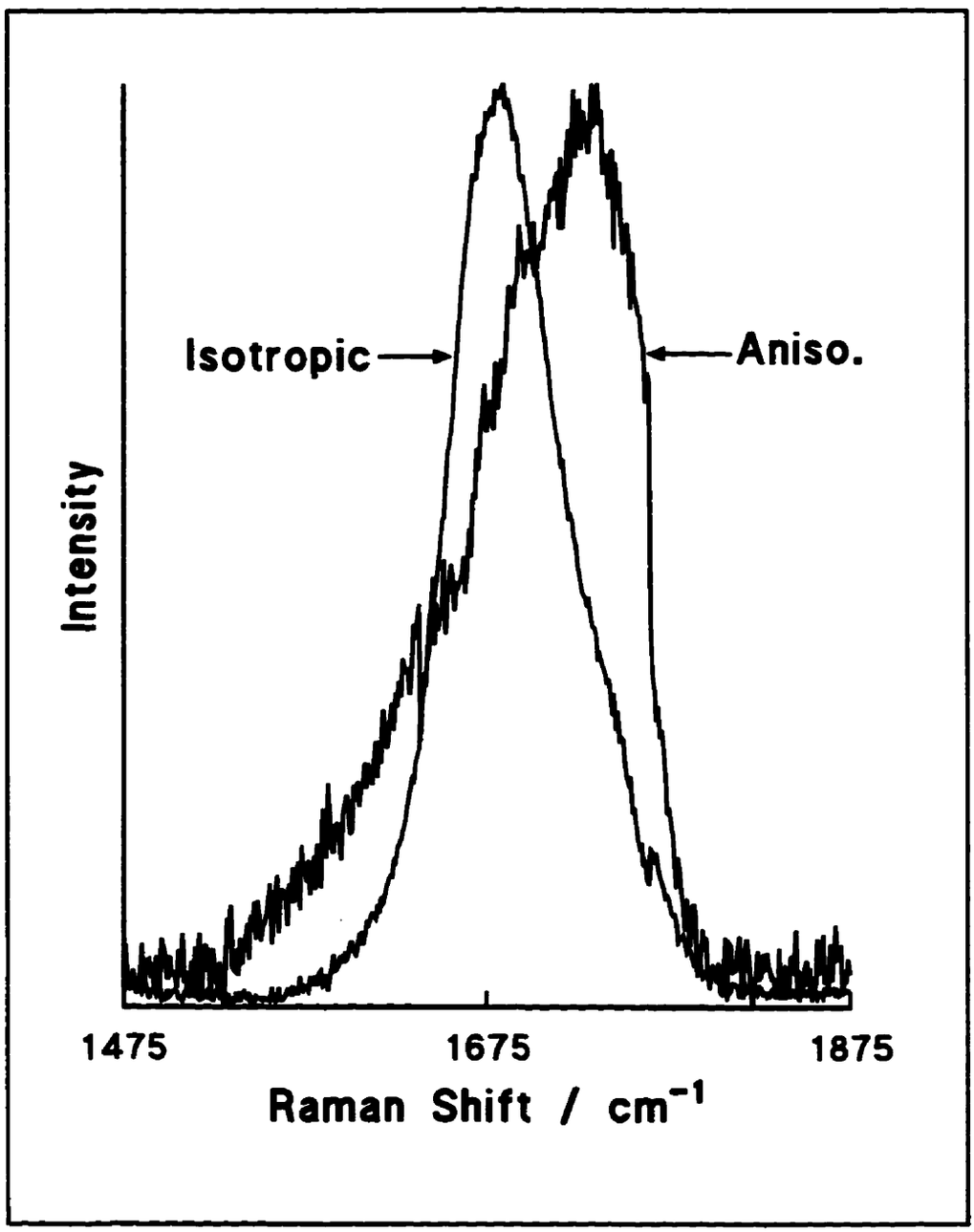

Fig. 3.5: HCOOH (98%) Polarization Studies at ~100°C (normalized).

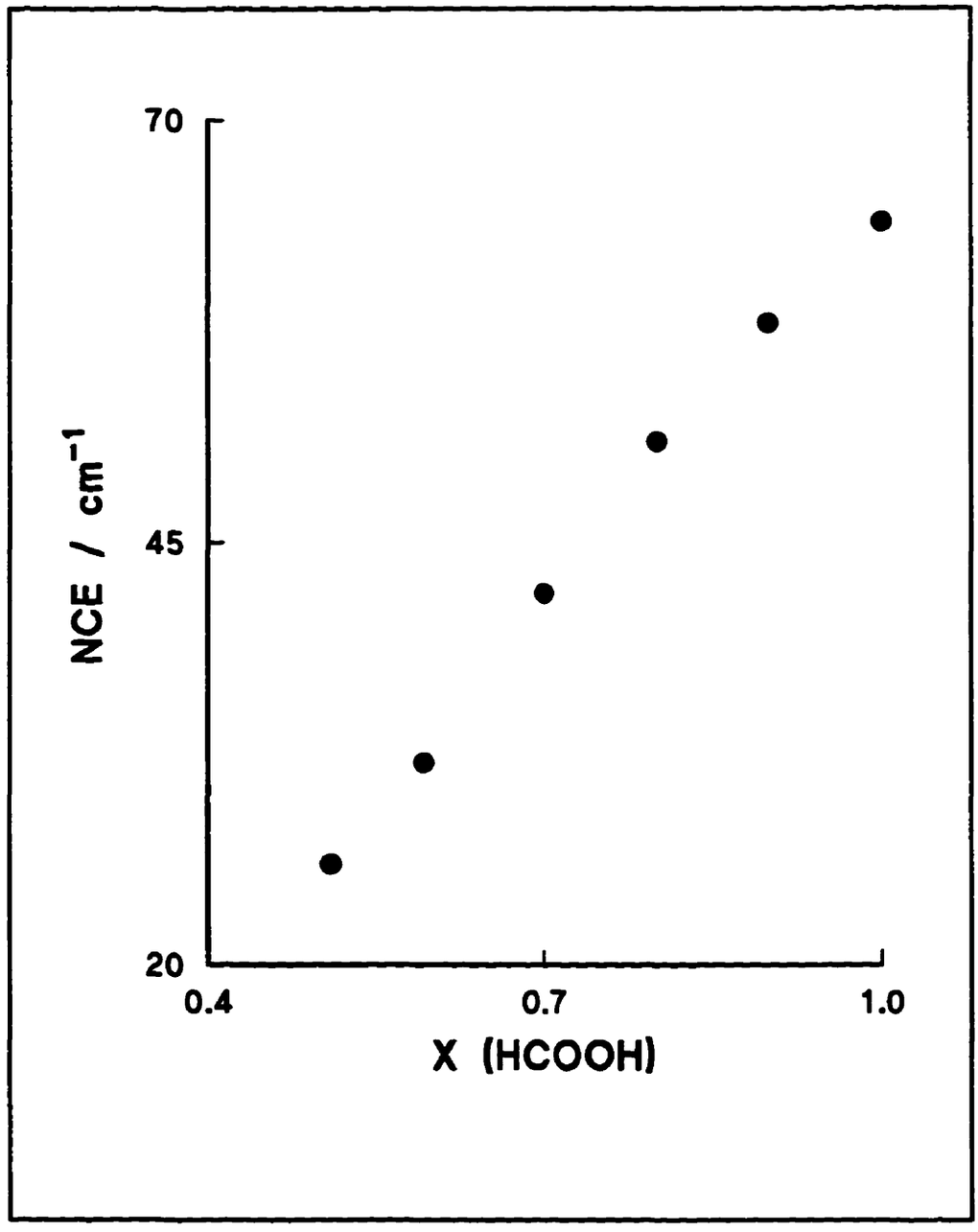

Fig. 3.6: NCE in HCOOH as a Function of Mole Fraction.

Table 3.3: NCE for HCOOH / H_2O.

X(HCOOH)	NCE / cm^{-1}
1.000	64
0.900	56
0.803	50
0.700	40
0.591	29
0.510	24

diluted, the separation of the isotropic and anisotropic peaks decreases and has a fairly strong dependence on the mole fraction. The anisotropic peak position does not change as the formic acid is diluted, remaining fixed at ~1725 cm^{-1}. The isotropic peak shifts. Concentrations of formic acid below X(HCOOH)~0.5 were not used because of the overlap with ν_2 of water at ~1600 cm^{-1}. Further, the NCE at ~100°C is smaller than at 25°C. A reduction in NCE as temperature is raised is characteristic of resonance energy transfer (18). The splitting in formic acid is very large and indicates a significant interaction between formic acid molecules. This is not surprising considering the possibility of quite strong hydrogen bonding in this system.

The low frequency band at ~200 - 210 cm^{-1} shifts very slightly from 208 cm^{-1} (98% HCOOH) to 201 cm^{-1} (X(HCOOH) = 0.510) as the concentration falls. The "R" spectrum (19) suggests some high frequency asymmetry in this band (see Fig. 3.7). This band has been assigned to an H-O--H bending mode associated with hydrogen bonding (Blatz and Waldstein (6)). The presence of this band throughout the dilution range implies the continuation of hydrogen bonding. Therefore, the hydrogen bonding in formic acid is quite strong and may partially explain the very large non-coincidence effect.

The third region studied in detail was the O-C=O deformation region (625 - 750 cm^{-1}). In neat formic acid this band envelope had an unusual shape suggesting the possibility of three underlying bands. At lower concentrations (X(HCOOH) < 0.7) this

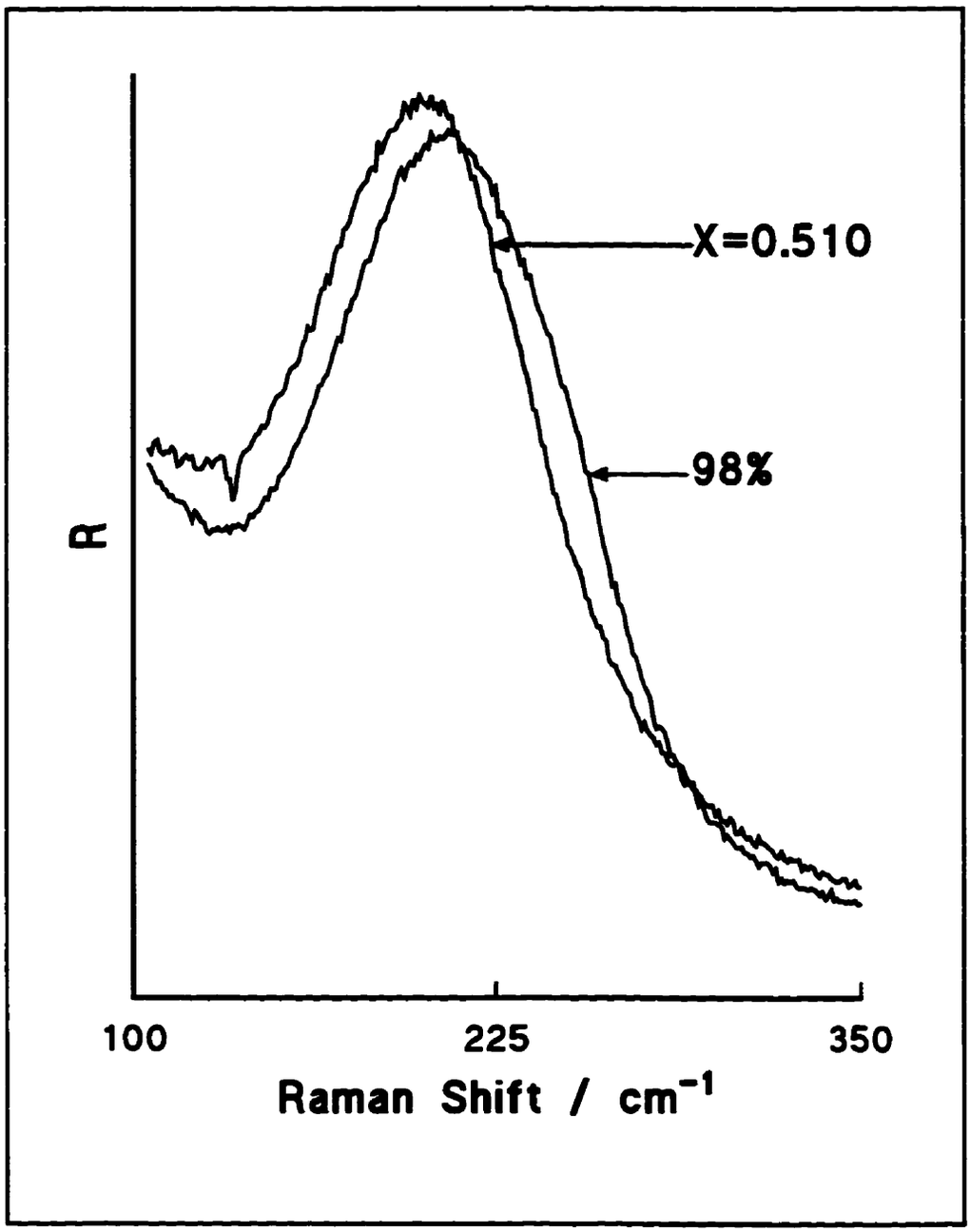

Fig. 3.7: Effect of Dilution on the "Association" Band of HCOOH.

envelope had a more "conventional" appearance (see Fig. 3.8). Using three band fits on all the spectra reveal interesting changes. The lowest frequency band shifted to higher frequency (from ~672 cm^{-1} to ~679 cm^{-1}), but the change occurs almost entirely below X(HCOOH)~0.7. The relative intensity also decreased. The second band shifted (681 cm^{-1} to 693 cm^{-1}) but, again, the change is greatest for concentrations below X(HCOOH)~0.7. The relative intensity of this band increased. The third band increased in frequency, but the change was spread more evenly. The relative intensity of this band increased and then decreased. The O-C=O bending band, just like the C=O band, is likely to change as the intermolecular forces change. Therefore, these spectral changes indicate changes in the nature of the intermolecular forces.

Formic acid in aqueous solutions behaves differently from acetic acid. Semmler (14,15) studied acetic acid at elevated temperatures and in solutions. She concluded neat acetic acid was a mixture of polymers, cyclic dimers, open dimers, and monomers. As the acetic acid was heated or diluted, the level of association decreased. No polarization results were reported. In formic acid the results strongly suggest resonance energy transfer is occurring. The isotropic and the anisotropic peaks are non-coincident and the separation is quite large. The separation decreases with dilution and with a rise in temperature. Both observations strongly suggest RET because diluting or heating the formic acid should lead to a disruption of order, a decoupling of the oscillators, a reduction in the effectiveness of RET and consequently a decrease in the non-coincidence

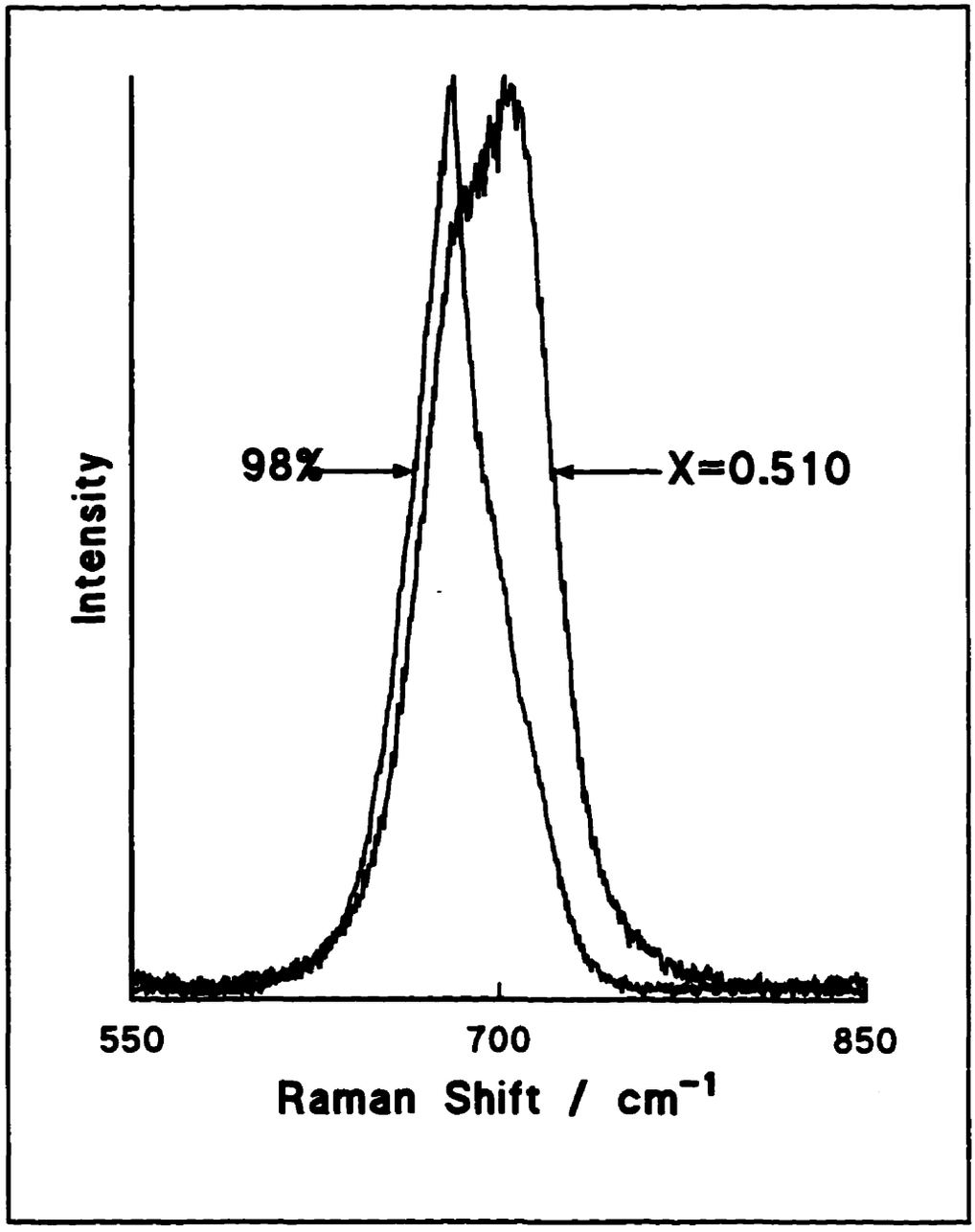

Fig. 3.8: Effect of Dilution on the O-C=O Deformation Modes of HCOOH.

effect. The occurrence of RET suggests some type of order in the liquid that allows the oscillators to couple. This local order is induced by dipole - dipole forces in conjunction with hydrogen bonding. The hydrogen bonding is present throughout the dilution range (as proven by the continued presence of the "association" band at ~200 cm^{-1}). This observation suggests formic acid forms very stable hydrogen bonds.

3.3.2 Formic Acid / Acetonitrile

These experiments were originally undertaken to study the RET effect in formic acid using a solvent whose bands do not overlap those of formic acid. The ideal solvent must meet other conditions as well. It should not react with formic acid and should provide a wide range of formic acid solubility. Acetonitrile seemed an appropriate choice and a series of solutions (X(HCOOH) = 0.898 to X(HCOOH) = 0.157) of formic acid in acetonitrile was prepared. A summary of the concentrations is presented in Table 3.4.

The results were unexpected. The changes in the formic acid spectra (see Fig. 3.9a) are completely different from those seen for dilution in water. The first impression was that the acetonitrile and the formic acid had reacted. Hydrolysis of acetonitrile (to form acetic acid) occurs under acidic conditions but is very slow (20). Furthermore, in this system only small amounts of water and few protons are present. Other possible

Table 3.4: Concentration Summary for HCOOH / CH_3CN Solutions.

Code	X(HCOOH)	C(HCOOH) / mol L^{-1}	C(CH_3CN) / mol L^{-1}
RB940520A	0.898	22.75	2.577
RB940520B	0.702	16.54	7.010
RB940520C	0.503	11.09	10.94
RB940520D	0.305	6.327	14.41
RB940520E	0.157	3.106	16.69
RB940526A	0.782	18.96	5.283
RB940526B	0.580	13.10	9.482
RB940526C	0.397	8.468	12.88
RB940526D	0.198	3.988	16.11

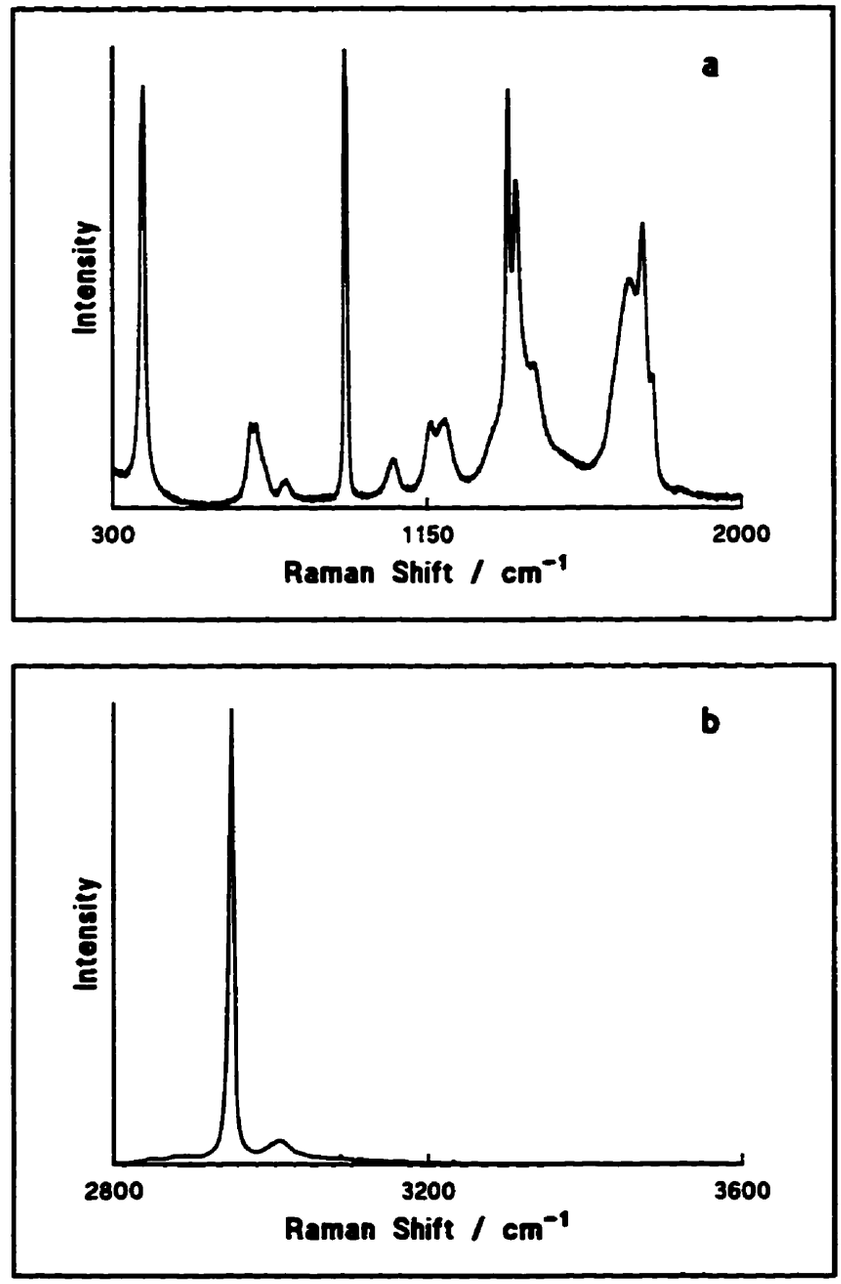

Fig. 3.9: Spectra of HCOOH / CH_3CN X(HCOOH) = 0.503:
a) Survey Spectrum
b) Spectral Region where an NH Stretching Band would be Expected (above 3200 cm^{-1}).

reactions between formic acid and acetonitrile might reasonably be expected to lead to a product exhibiting an NH stretching mode. Therefore, a spectrum of X(HCOOH) = 0.503 solution was recorded between 2800 cm^{-1} and 3600 cm^{-1}. This spectrum shows no evidence of an NH stretch (see Fig. 3.9b). Furthermore, if proton transfer had taken place the C=O vibrations would disappear and two vibrations from the CO_2^- group would appear (21). This is not the case. These results suggest no reaction took place and so the carbonyl (1500 - 1900 cm^{-1}) and the nitrile (2100 - 2400 cm^{-1}) regions were examined more closely.

In the carbonyl region of pure formic acid a maximum with a high frequency shoulder is evident. As formic acid is diluted in acetonitrile, this profile changes dramatically. Figure 3.10 illustrates this very well. Three bands are obviously present and low frequency asymmetry suggests a fourth band underlying this profile. Bandfitting was applied to the spectra using four-band fits and the results are summarized in Table 3.5. At X(HCOOH) = 0.898 the spectrum suggested only three bands. Figure 3.11a shows the dependence of each band position on mole fraction. The band positions of the two higher frequency bands (ν_c and ν_d) are virtually independent of concentration. The lowest frequency band (ν_a) appears to pass through a maximum at X(HCOOH) = 0.580. The remaining band's (ν_b) position decreases with increasing formic acid concentration. Another set of parameters that is of interest in this study is the fraction of the total carbonyl intensity from each band, α. As can be seen in Fig. 3.11b, the intensity of band

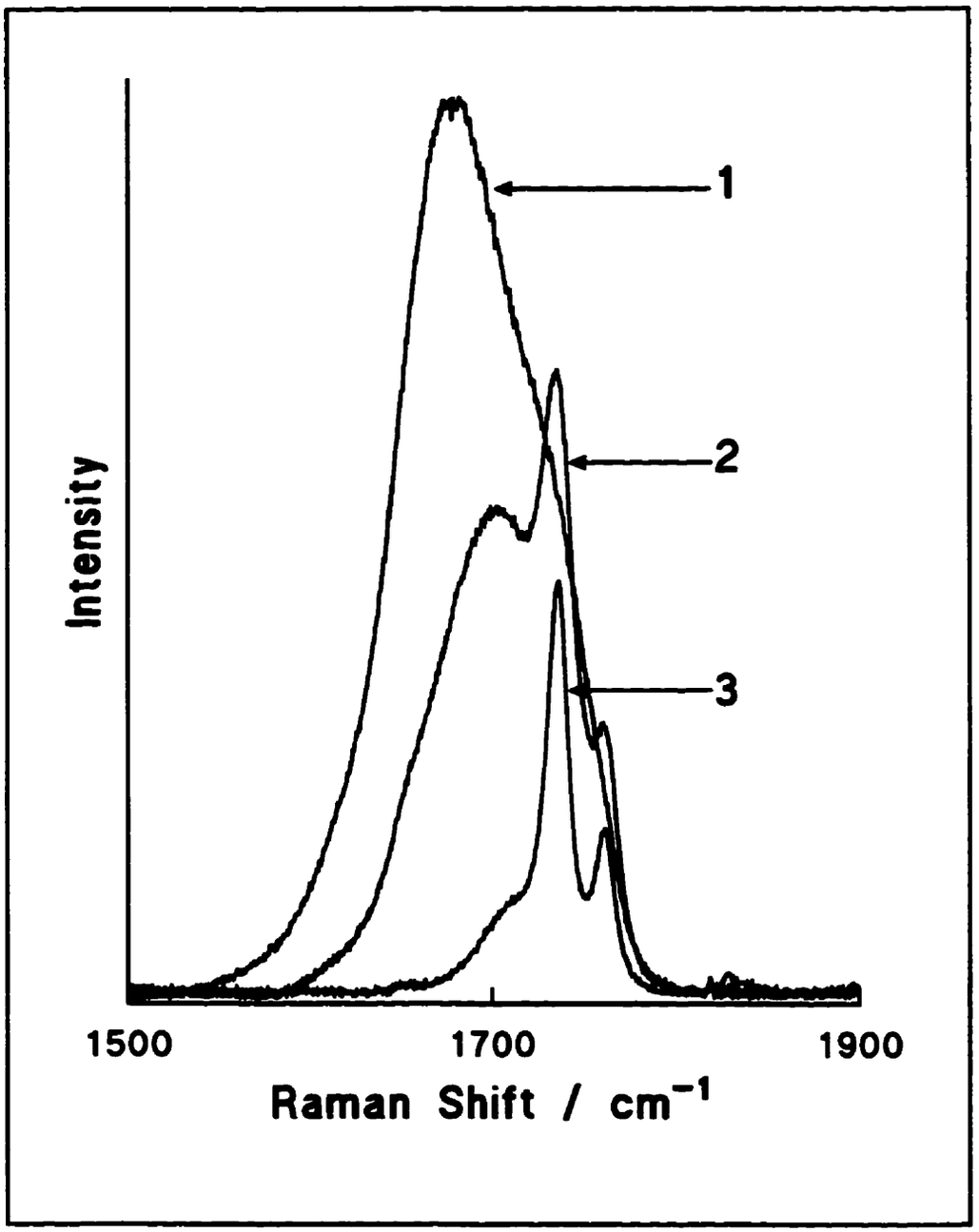

Fig. 3.10: Carbonyl Region of HCOOH / CH_3CN:
1 - X(HCOOH) = 0.898; 2 - X(HCOOH) = 0.503;
3 - X(HCOOH) = 0.157.

Table 3.5: Summary of Bandfitting for HCOOH / CH_3CN.

X	ν_a / cm^{-1}	ν_b / cm^{-1}	ν_c / cm^{-1}	ν_d / cm^{-1}	α(a)	α(b)	α(c)	α(d)
0.898	1658	1682	1731	-	0.363	0.357	0.280	-
0.782	1663	1696	1738	1765	0.450	0.362	0.170	0.018
0.702	1664	1697	1738	1764	0.346	0.414	0.197	0.043
0.580	1668	1701	1737	1763	0.286	0.448	0.222	0.044
0.503	1666	1703	1737	1763	0.255	0.395	0.271	0.070
0.397	1662	1704	1736	1762	0.131	0.447	0.325	0.097
0.305	1659	1707	1737	1763	0.069	0.484	0.327	0.119
0.198	1655	1712	1736	1762	0.010	0.409	0.411	0.169
0.157	1653	1715	1737	1763	0.008	0.360	0.455	0.187

Note:

α is the fraction of the total carbonyl band intensity.

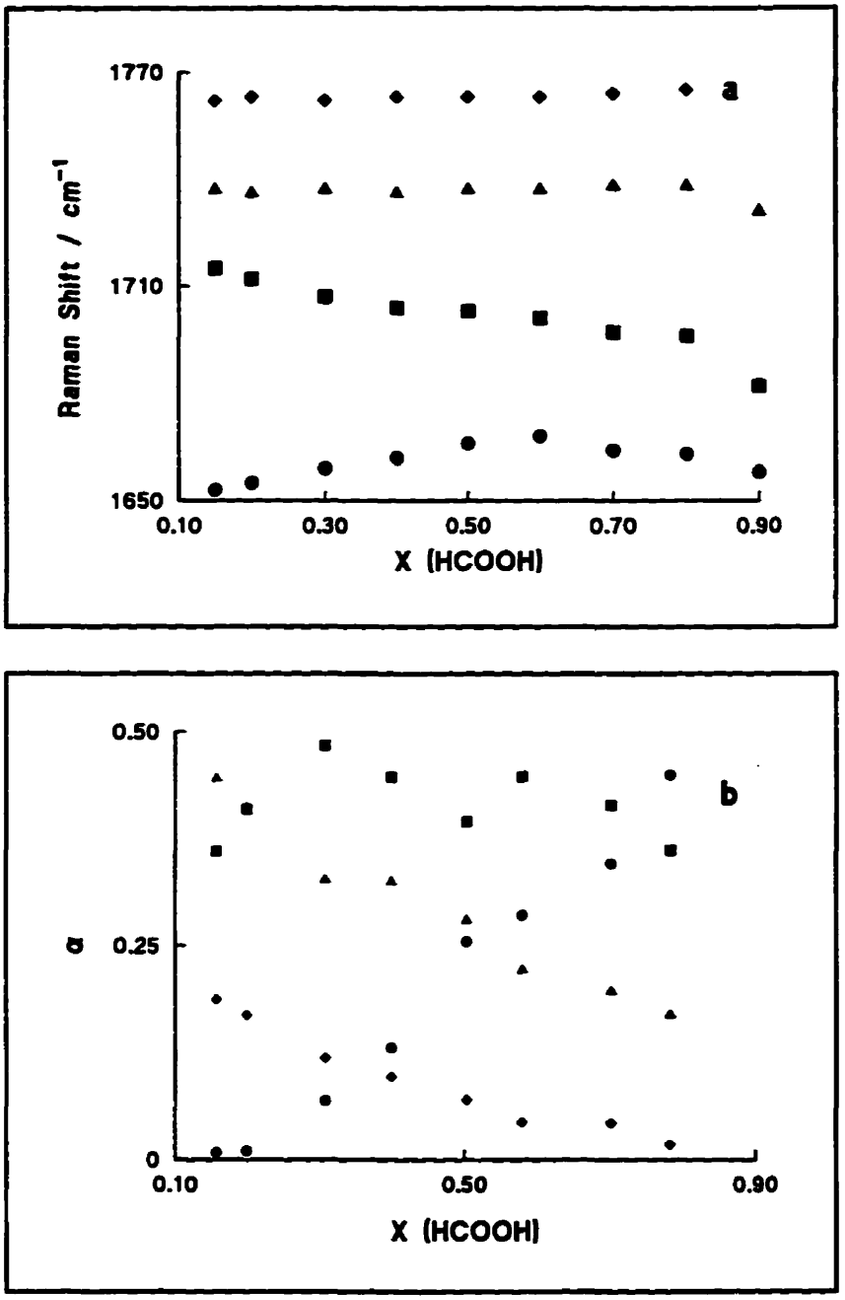

Fig. 3.11: Variation of the Band Parameters for the Carbonyl Region of HCOOH / CH_3CN:
a) Position b) Fraction of Total Intensity
● - Band a; ■ - Band b; ▲ - Band c; ♦ - Band d.

(a) increases with increasing formic acid concentration whereas bands (c) and (d) decrease. Band (b) shows considerable fluctuation but no systematic trend. The reason for this variation is unknown. Because of the occurrence of four bands (as opposed to two in neat formic acid) and the behaviour of their relative integrated intensities, the formation of some sort of formic acid - acetonitrile association or complex was hypothesized. Evidence in the C≡N stretching region gave further support to this hypothesis.

Clearer evidence to support the existence of some sort of "association" is found in the nitrile (2100 - 2400 cm^{-1}) region. In pure acetonitrile the strongest band in this region is the C≡N stretch. It is a very intense band. When formic acid is added to acetonitrile, a shoulder appears at higher frequency (see Fig. 3.12). This shoulder (~2270 cm^{-1}) increases in intensity relative to the band at ~2255 cm^{-1} as the formic acid concentration increases (see Fig. 3.13 and Table 3.6). This band has also been observed for solutions of acetonitrile with silver ions (22), methanol (23), ortho-cresol (24), IBr (25), and phenol (26) and suggests significant formic acid - acetonitrile binding. Fawcett (27) studied the interaction of acetonitrile with a wide range of solvents of varying Lewis basicity or acidity. He found a solvent induced frequency shift (SIFS) of the C≡N band. For solvents more basic than acetonitrile, the SIFS was negative but for more acidic solvents the SIFS was positive. Formic acid is more acidic than acetonitrile, so the development of the peak at 2270 cm^{-1} is consistent with the results of Fawcett.

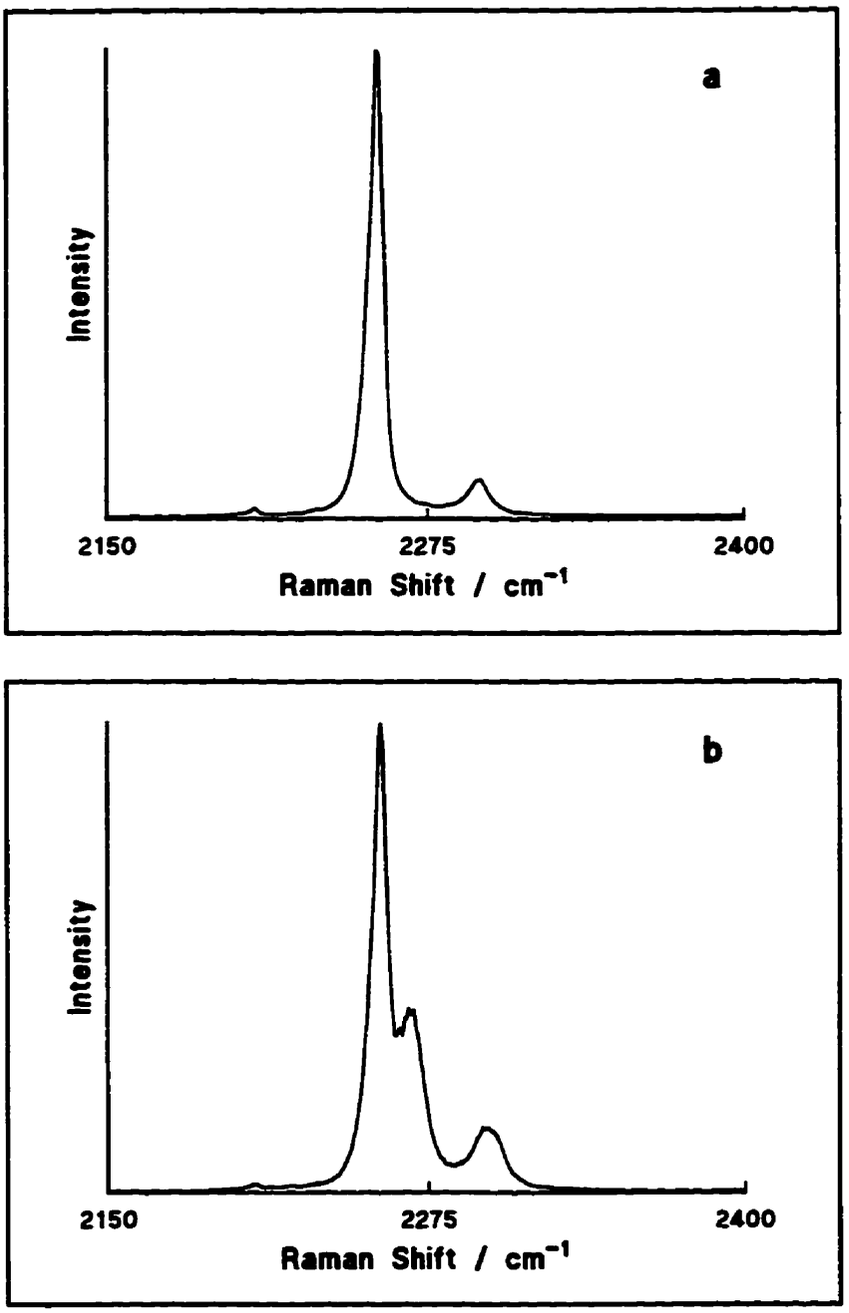

Fig. 3.12: C≡N Stretching Region of:
a) Pure CH_3CN b) HCOOH / CH_3CN (X(HCOOH) = 0.510).

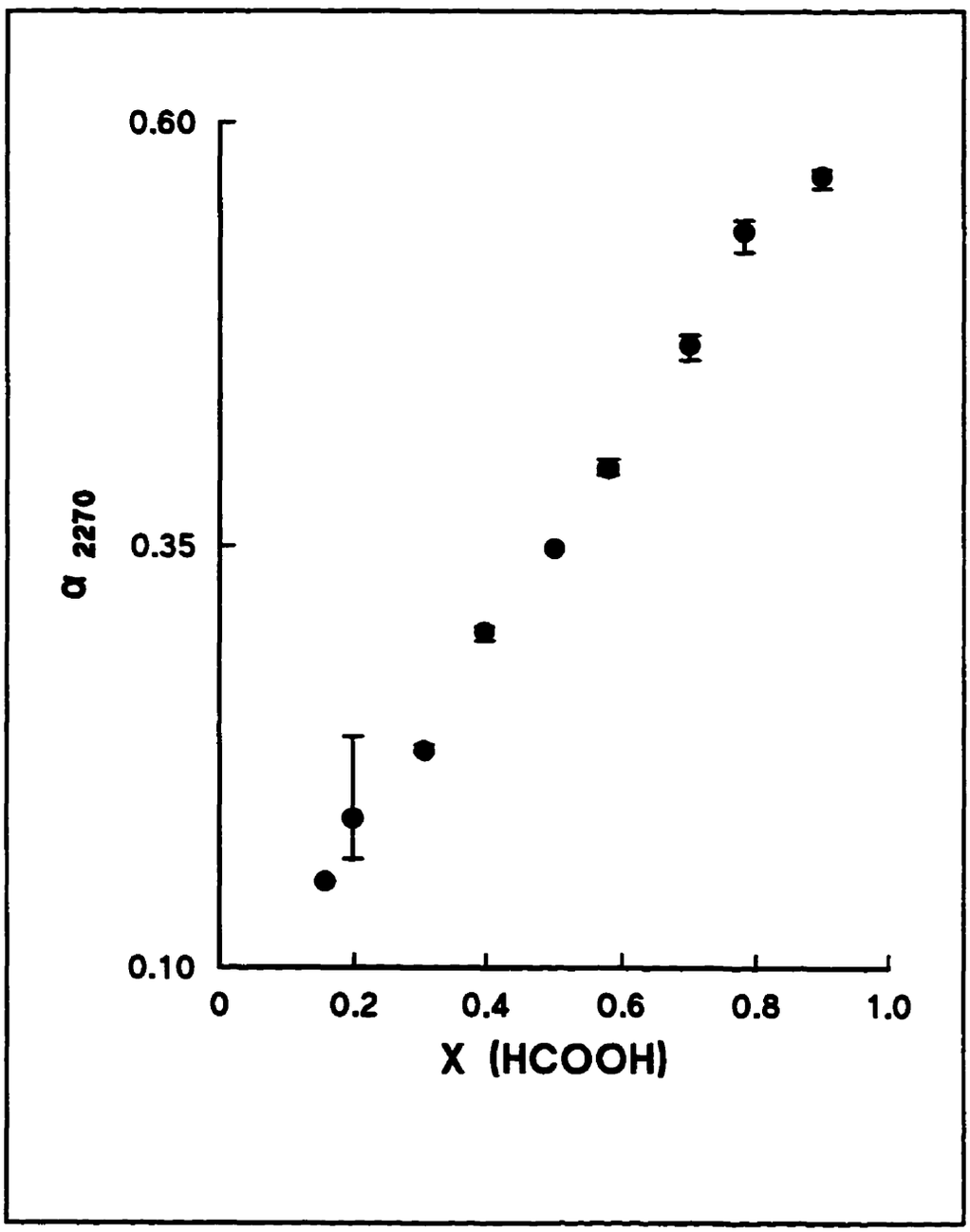

Fig. 3.13: Variation of the Fraction of the Total Intensity of the C≡N Stretch due to "Bound" Acetonitrile with Mole Fraction of Formic Acid.

Table 3.6: Fraction of Total Nitrile Intensity of 2270 cm^{-1} Band.

X(HCOOH)	α_{2270}
0.898	0.569
0.782	0.535
0.702	0.469
0.580	0.396
0.503	0.348
0.397	0.299
0.305	0.228
0.198	0.188
0.157	0.151

Having established the existence of a formic acid - acetonitrile association, the natural question to ask is, "how are these two molecules bound together?". One would expect acetonitrile to "bond" through the nitrogen atom as this atom possesses an electron lone pair. The development of the high frequency shoulder on the C≡N stretching band supports this belief. (The move to higher frequency has been explained by Fawcett (27) in the following way. The molecular orbital forming the bond to the electrophilic species (in this case, formic acid) has substantial nitrogen lone pair character. However, there are also considerable C≡N and C-C anti-bonding contributions. Because charge is removed from the anti-bonding orbital, the C≡N bond is strengthened and the bond shifts to higher frequency.) Unlike acetonitrile, formic acid has two possible sites for bonding: the carbon atom and the hydrogen of the OH group. If association were through the hydrogen atom, a change in the formic acid band at ~200 cm^{-1} (OH--H bend) might be anticipated. However, any changes in this region might be difficult to see. An alternative approach is to replace the acidic proton with a non-acidic group. Such a group (and the simplest) is the methyl group. If evidence is found of association (either through the carbonyl bands or the C≡N band), the association in the formic acid / acetonitrile system is most likely through the carbonyl group. Therefore, a solution of methyl formate in acetonitrile was studied.

A solution of methyl formate in acetonitrile (X(MF)~0.5) was prepared and the Raman spectrum collected. It is presented in Fig. 3.14. In the carbonyl stretching region

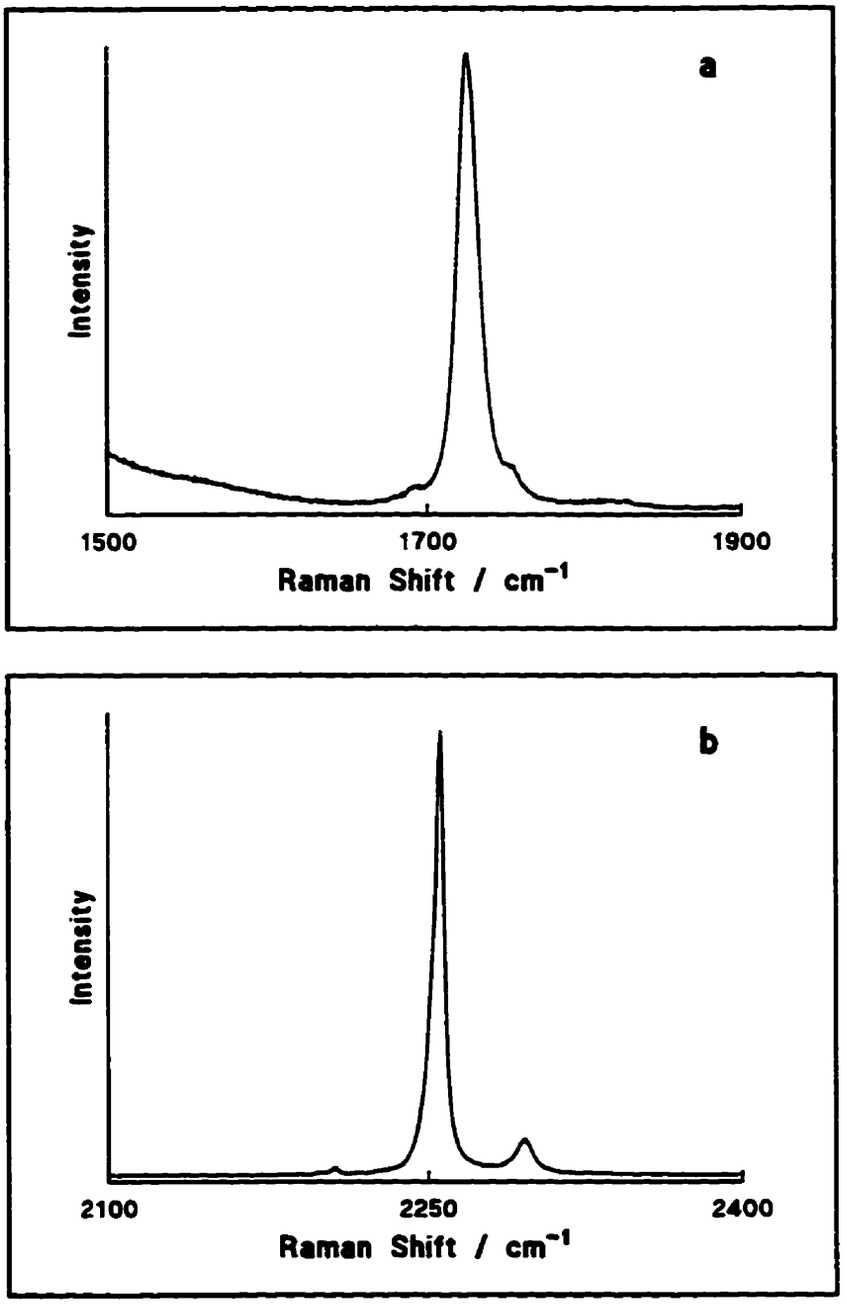

Fig. 3.14: Spectra of Solutions of Methyl Formate / Acetonitrile (X(MF)~0.5):
a) Carbonyl Region b) C≡N Region.

three bands, the strongest of which is at ~1720 cm^{-1}, are present. As an aside, this frequency is almost identical to the band maximum position of the anisotropic spectrum of pure formic acid. This observation may be quite significant. The spectrum of the carbonyl region is identical to that of pure methyl formate (Fig 4.1 and (28)). The C≡N stretching region of acetonitrile shows no change, unlike the formic acid spectra. These results suggest the interaction between the acetonitrile and formic acid occurs through the acidic hydrogen of the formic acid.

Having established (possibly) the nature of the interaction between acetonitrile and formic acid the next logical step is to try to determine the "co-ordination number" of the formic acid. This can be calculated by using the Job method or "method of continuous variations" (16). To do this, a suitable solvent must be found so the sum of the analytical concentrations of the two species can be held constant (i.e., C_T = C(HCOOH) + C(CH_3CN) = constant). Also, obviously, the solvent should not have overlapping bands with either species and both species should have a wide range of solubility. 1,4-dioxane appeared to fit the requirements quite nicely. Between 1500 cm^{-1} and 2600 cm^{-1} it has no bands of its own and formic acid and acetonitrile are quite soluble in it. In a preliminary experiment a small amount (~2.5 mL) of an HCOOH / CH_3CN solution (X(HCOOH) = 0.501) was added to ~2.5 mL of 1,4-dioxane. As seen in Fig. 3.15, some major changes occur in the spectrum. First, the relative intensity of the band at ~1730 cm^{-1} increases markedly while shifting to slightly lower frequency. Second, the shoulder

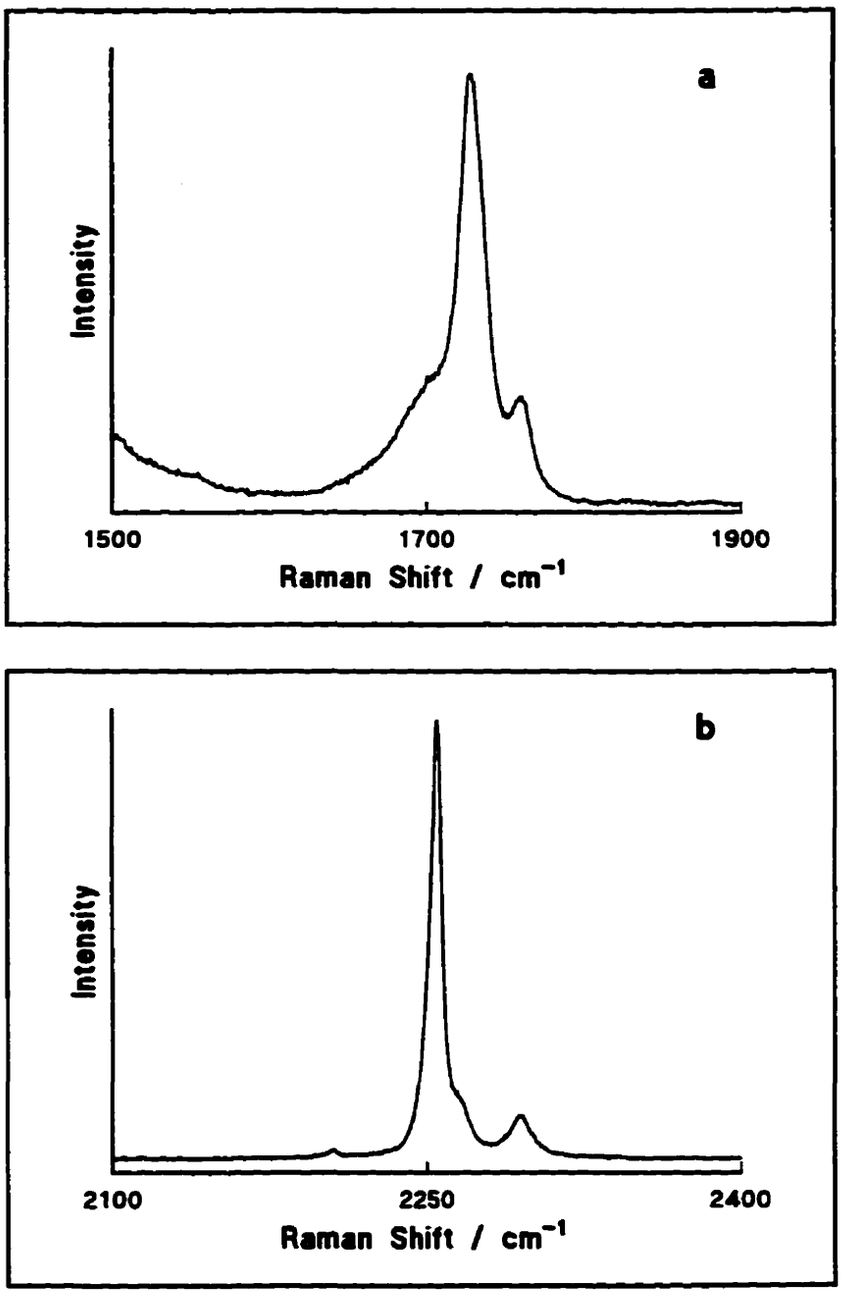

Fig. 3.15: (HCOOH + CH_3CN) / 1,4-dioxane:
a) Carbonyl Region b) C≡N Stretching Region.

at ~2270 cm^{-1} is greatly reduced in relative intensity (with respect to the 2255 cm^{-1} band). This suggests 1,4-dioxane is quite effective at reducing the interaction between acetonitrile and formic acid or that 1,4-dioxane competes with acetonitrile to solvate the formic acid. These preliminary results prompted a closer investigation of solutions of formic acid in 1,4-dioxane.

3.3.3 Formic Acid / 1,4-dioxane

A set of solutions of formic acid in 1,4-dioxane was prepared and the concentrations are summarized in Table 3.7. When the solutions were prepared, two observations were made. First, the mixing of the two liquids is exothermic. Second, the volume of the solution increases with mixing.

The spectra of formic acid in 1,4-dioxane are best discussed by breaking them into particular regions. The spectrum of pure 1,4-dioxane has already been reported by Malherbe and Bernstein (29) and a spectrum is shown here for completeness (Fig. 3.16a and Table 3.8). Assignments are taken from Malherbe and Bernstein and are based on C_{2h} symmetry, i.e., the chair conformation. A survey spectrum of HCOOH / 1,4-dioxane (X(HCOOH) = 0.509) is also presented (Fig. 3.16b).

Table 3.7: Summary of Concentrations for HCOOH / 1,4-dioxane.

Code	X(HCOOH)	C(HCOOH) / mol L^{-1}	C(1,4-dioxane) / mol L^{-1}
RB950227A	0.904	21.17	2.258
RB950227B	0.712	13.63	5.524
RB950227C	0.509	8.236	7.938
RB950227D	0.305	4.262	9.719
RB950227E	0.101	1.252	11.10

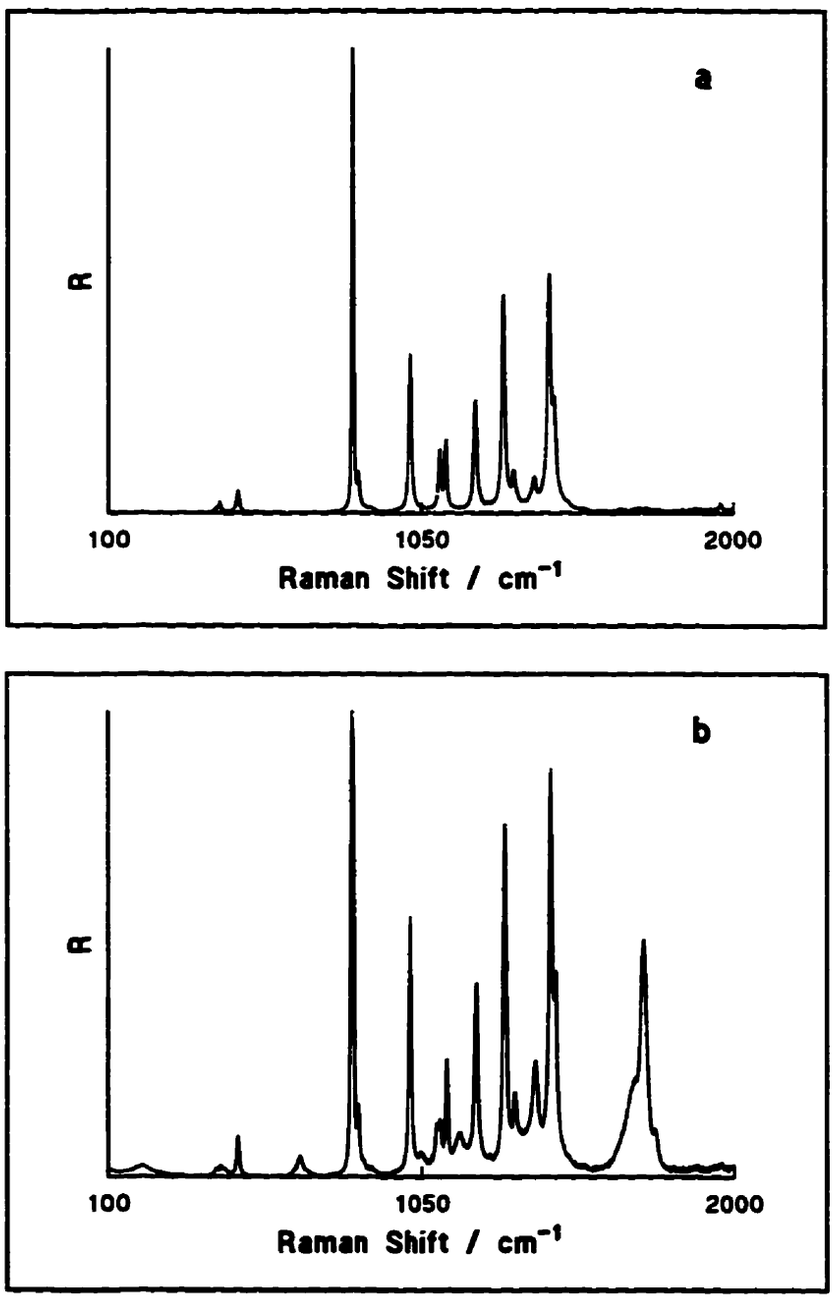

Fig. 3.16: Survey Spectra of:
a) 1,4-dioxane b) HCOOH / 1,4-dioxane (X(HCOOH) = 0.509).

Table 3.8: Assignment of 1,4-dioxane Spectrum (29).

Frequency / cm^{-1}	Assignment
422	ν_{10}, ring bending
433	ν_9, ring bending
486	ν_{36}, ring bending
834	ν_8, ring stretching
852	ν_6, rocking
946	ν_{34}, rocking
1015	ν_7, ring stretching
1109	ν_{35}, ring stretching
1127	ν_5, wagging
1216	ν_{33}, wagging
1303	ν_4, twisting
1334	$\nu_{25} + \nu_{28}$
1396	ν_{32}, twisting
1443	ν_3, deformation
1461	ν_{31}, deformation
2662	$\nu_3 + \nu_{33}$
2720	$\nu_{22} + \nu_{24}$
2748	$\nu_3 + \nu_4$
2855	ν_2, CH stretching
2889	$2\nu_3$
2966	ν_1, CH stretching

Between 100 and 950 cm^{-1} the most interesting effects occur between 400 and 500 cm^{-1}. In pure 1,4-dioxane three bands are present between 400 cm^{-1} and 500 cm^{-1}: at 419 cm^{-1} (ν_{10}, ring bend, A_g), 432 cm^{-1} (ν_9, ring bend, A_g), and 485 cm^{-1} (ν_{36}, ring bend, B_g). As formic acid is added to the system, a new band develops (see Fig 3.17). This band is first apparent at X(HCOOH) = 0.305 at a shift of 444 cm^{-1}. This new band, like the 432 cm^{-1} of pure 1,4-dioxane, is polarized. As the concentration of formic acid increases so does the relative intensity of this band. The shift also increases slightly to 450 cm^{-1}. At the same time the band of 1,4-dioxane at 432 cm^{-1} decreases and by X(HCOOH) = 0.903 the 432 cm^{-1} band has disappeared. The polarization characteristics of these three bands do not change with changing concentration of formic acid. Another region of interest is the O-C=O deformation region (650 - 750 cm^{-1}) of formic acid. As the formic acid is diluted, the effects seen here are almost identical to those seen in water. With dilution this band becomes more symmetrical and the high frequency shoulder less pronounced. The remaining two bands in this region (100 - 950 cm^{-1}) are from the 1,4-dioxane. The intense band at ~832 cm^{-1} is a ring stretching mode (ν_8, A_g) and the weaker shoulder at ~852 cm^{-1} is a CH_2 rocking mode (ν_6, A_g). They are unaffected by the presence of formic acid.

Between 900 and 1600 cm^{-1} 1,4-dioxane has many bands. Most of these (at 1127 cm^{-1}, 1217 cm^{-1}, 1304 cm^{-1}, 1397 cm^{-1}, 1441 cm^{-1} and 1459 cm^{-1}) have been assigned to various types of CH_2 bending modes. Of the remainder, two are ring stretching modes

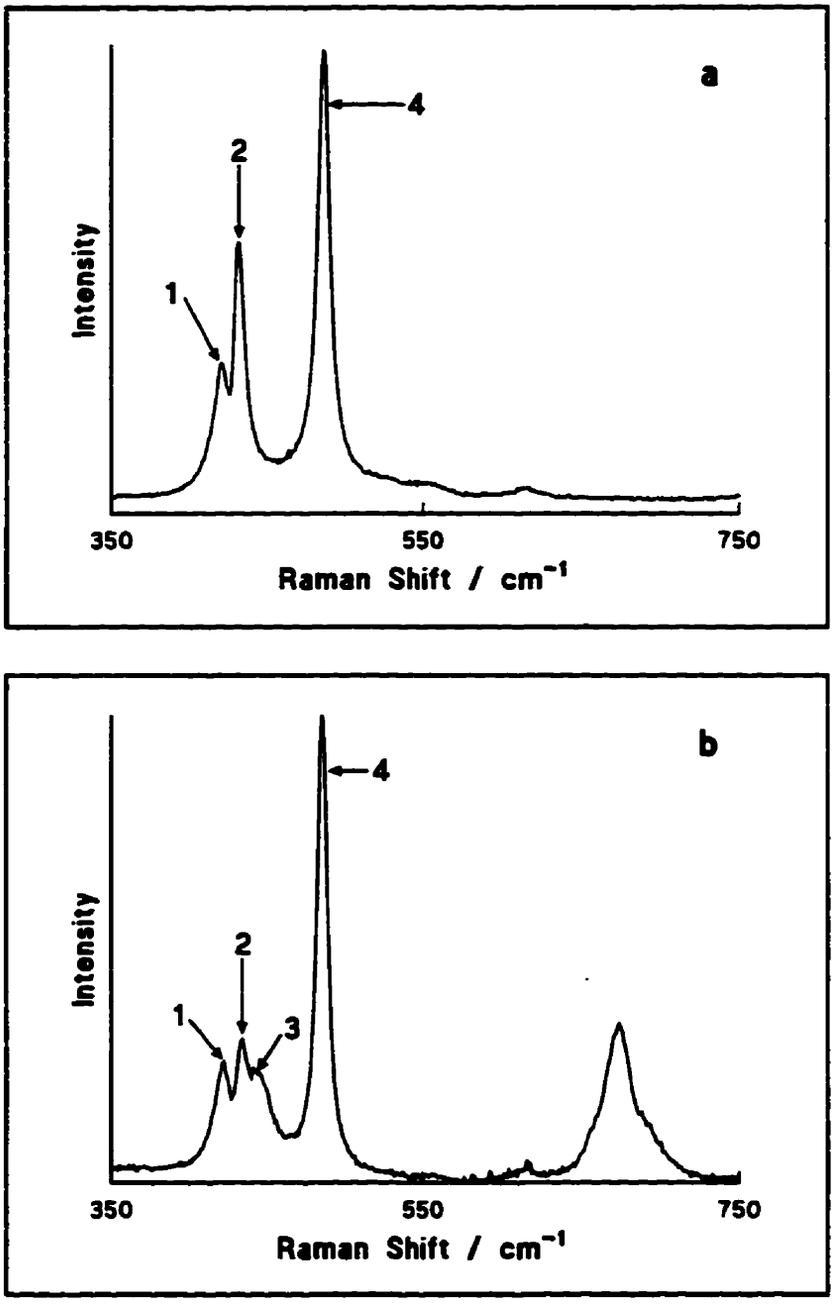

Fig. 3.17: a) 1,4-dioxane b) HCOOH / 1,4-dioxane
(X(HCOOH) = 0.509)
1 - 419 cm^{-1}; 2 - 432 cm^{-1}; 3 - 444 cm^{-1}; 4 - 485 cm^{-1}.

at 1014 cm^{-1} (ν_7, A_g) and 1108 cm^{-1} (ν_{35}, B_g) and one is a combination mode at 1335 cm^{-1} ($\nu_{25} + \nu_{28}$). The most interesting changes occur between 1090 cm^{-1} and 1150 cm^{-1} (Fig. 3.18). In this interval pure 1,4-dioxane has two peaks of almost equal intensity. With increasing formic acid concentration a new, depolarized peak at 1096 cm^{-1} forms. This peak is first apparent at X(HCOOH) = 0.305 and grows as the concentration of formic acid increases. At the same time the 1,4-dioxane mode at 1108 cm^{-1} decreases. Another change which can be seen in this region is the development of a band at 1166 cm^{-1}. This arises from formic acid and so its increase in intensity with increasing X(HCOOH) is hardly surprising. However, in pure formic acid it underlies a broad, asymmetrical profile ascribed to C-O stretching (see Fig. 3.1). The companion band in pure HCOOH is slightly more intense and centred at 1202 cm^{-1}. In the solutions in 1,4-dioxane this band (at ~1170 cm^{-1}) is distinct from the band at 1202 cm^{-1}. The band at 1202 cm^{-1} does not become apparent until X(HCOOH) = 0.712. The remaining bands in this region do not seem much affected.

The next important region studied was between 1500 and 1900 cm^{-1} (Fig. 3.19). In this region 1,4-dioxane has no bands of its own and all the bands arise from carbonyl stretching of the formic acid. Just as with the dilution of formic acid in acetonitrile, some very pronounced changes take place. At X(HCOOH) = 0.904 three underlying bands were obvious for the carbonyl contour. Unfortunately, the bandfitting was not very reliable for this solution when three-band fits were used. At lower concentrations four

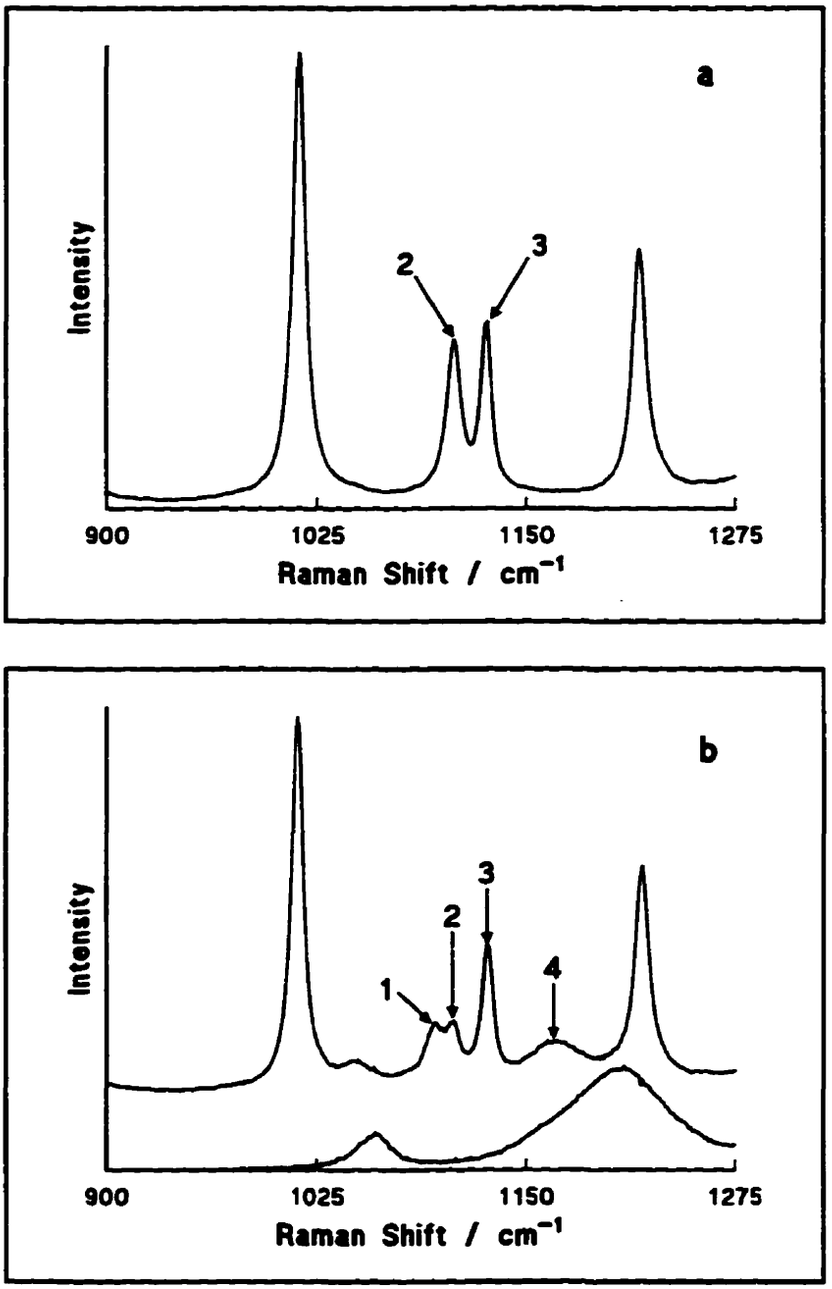

Fig. 3.18: a) Pure 1,4-dioxane
b) Upper Trace - X(HCOOH) = 0.509;
Lower Trace - Pure Formic Acid
1 - 1096 cm^{-1}; 2 - 1108 cm^{-1}; 3 - 1127 cm^{-1}; 4 - 1166 cm^{-1}.

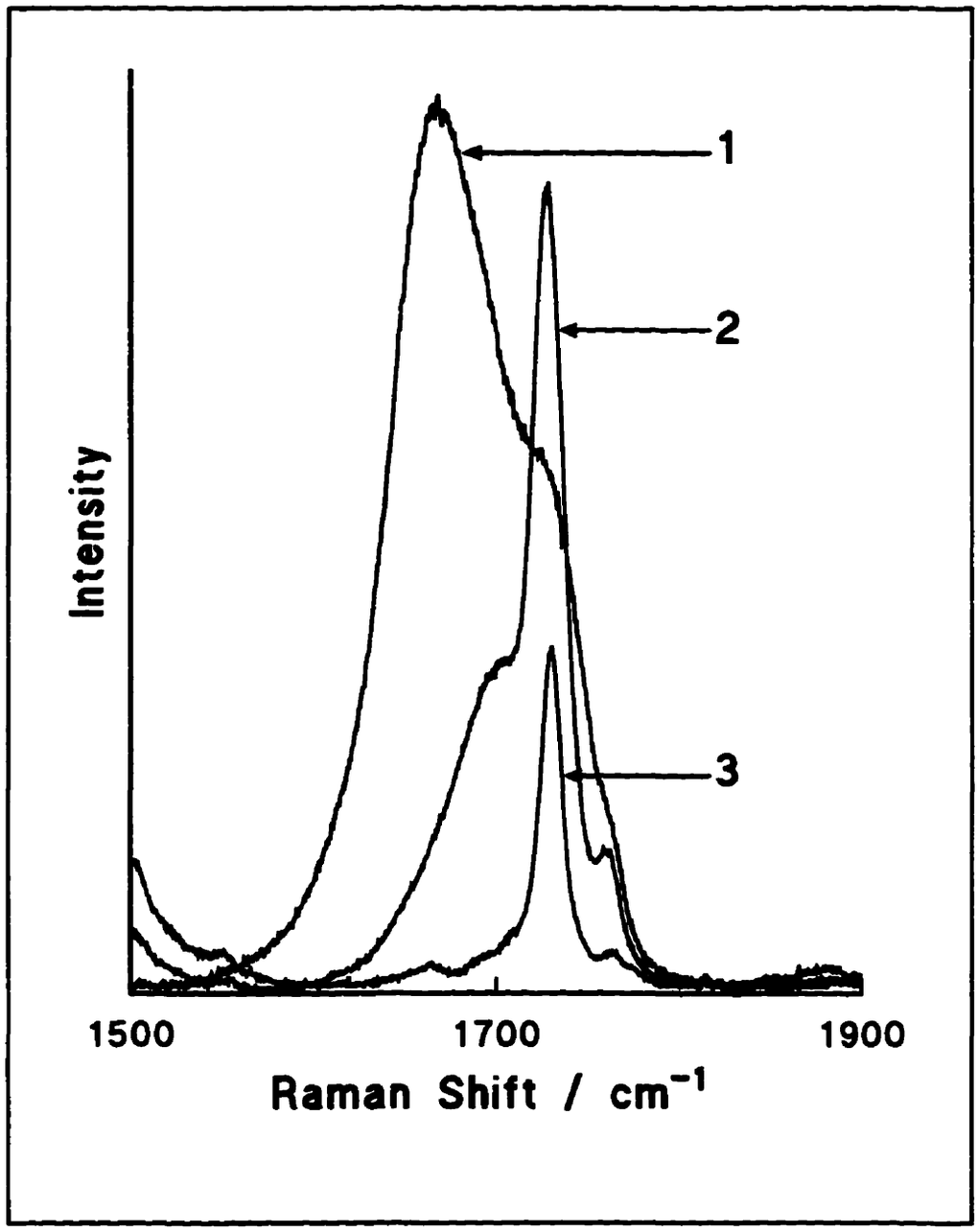

Fig. 3.19: Carbonyl Region of HCOOH / 1,4-dioxane
1 - X = 0.904; 2 - X = 0.509; 3 - X = 0.101.

bands clearly underlie the profile. As the formic acid is diluted, the band at ~1730 cm^{-1} becomes more and more prominent. In fact, for X(HCOOH) < 0.903 it is the most intense (as measured by fraction of total area) in the carbonyl region. Similarly, the maximum in $I_{\perp}$ of pure formic acid, the dominant peak of the HCOOH / CH_3CN solutions and the maximum in the methyl formate spectrum all occur between 1720 - 1740 cm^{-1} - a noteworthy observation. The band positions of the two higher bands (~1730 cm^{-1} and ~1764 cm^{-1}) are independent of the concentration of formic acid. Adopting the same convention for identifying the bands as used for the HCOOH / CH_3CN spectra, these are bands (c) and (d). Band (a) first rises in frequency and then decreases, passing a maximum at just over X(HCOOH) = 0.5. Band (b) shows a very small decrease in frequency as the concentration of formic acid increases (see Fig. 3.20a). As the formic acid becomes more concentrated the intensities of bands (a) and (b) increase while bands (c) and (d) decrease (see Fig. 3.20b). These results are similar to those for HCOOH / CH_3CN.

The results for HCOOH / 1,4-dioxane are quite instructive. First, the changes seen in the HCOOH / CH_3CN spectra are very similar to those seen for the HCOOH / 1,4-dioxane spectra so the spectral changes in the carbonyl region of the HCOOH / CH_3CN solutions are not unique to the HCOOH / CH_3CN system. Second, there is some evidence for an interaction between formic acid and 1,4-dioxane. This supposition rests entirely on the development of peaks at 444-450 cm^{-1} and at 1096 cm^{-1} and the simultaneous

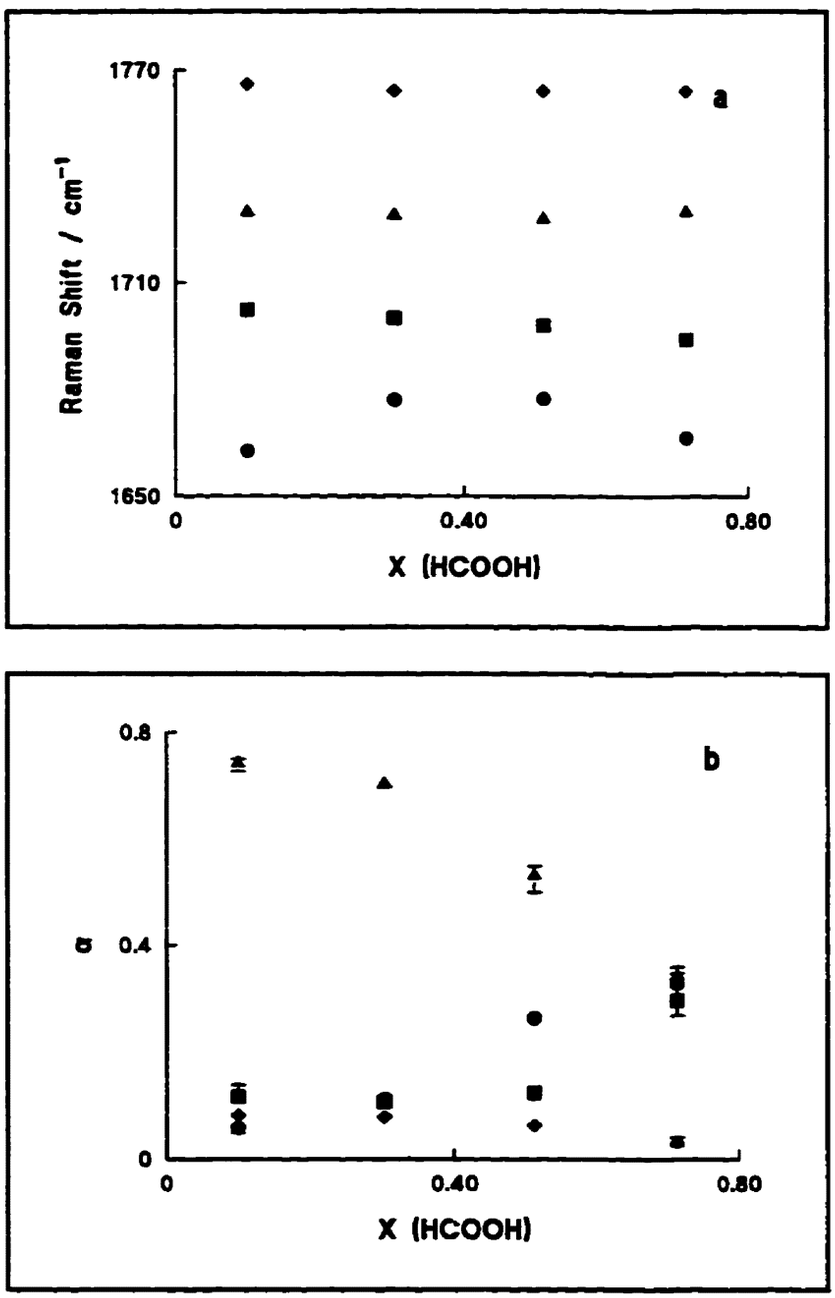

Fig. 3.20: Variation of the Band Parameters for Carbonyl Region of HCOOH / 1,4-dioxane:
a) Frequency b) Fraction of Total Intensity
● - Band a; ■ - Band b; ▲ - Band c; ♦ - Band d

decrease in peaks at 432 cm^{-1} and 1108 cm^{-1}. These two bands are ring bending and ring stretching modes, respectively. Considering any interaction between formic acid and 1,4-dioxane would occur through the oxygens on the 1,4-dioxane, it is not surprising these bands would be affected. The other two bands associated with ring vibrations (at ~832 cm^{-1} and 1014 cm^{-1}), which are far more intense, appear to be completely unaffected.

3.3.4 Formic Acid / Dichloromethane

Studies on formic acid in dichloromethane were originally undertaken to find a suitable solvent for a Job plot. Unlike acetonitrile and 1,4-dioxane, dichloromethane is unlikely to act as a Lewis base. Unlike water, it is a non-hydrogen bonded solvent. It is an aprotic, dipolar liquid. Furthermore, it does not have bands in the carbonyl region of formic acid. Also, formic acid and acetonitrile have a wide solubility range in dichloromethane. Because of all these properties, dichloromethane was included in this study. To begin, a series of binary solutions of formic acid and dichloromethane was prepared and the concentrations are summarized in Table 3.9.

As before, the carbonyl region of the formic acid was the most closely studied. At X(HCOOH) = 0.893 the spectrum is not much different from the spectrum of pure formic acid. A maximum at ~1661 cm^{-1} and a shoulder at ~1733 cm^{-1} are evident. High

Table 3.9: Concentration Summary for HCOOH / CH_2Cl_2 Solutions.

Code	X(HCOOH)	C(HCOOH) / mol L^{-1}	C(CH_2Cl_2) / mol L^{-1}
RB950316A	0.893	21.76	2.606
RB950316B	0.689	14.83	6.681
RB950316C	0.476	9.159	10.07
RB950316D	0.288	5.059	12.51
RB950316E	0.0998	1.626	14.57

frequency asymmetry exists on this envelope above ~1733 cm^{-1} but it is very slight. As the formic acid is diluted, the band at ~1661 cm^{-1} shifts to lower frequency by about 8 cm^{-1}. High frequency asymmetry appears on the band at 1661 cm^{-1} but with dilution this asymmetry decreases. The halfwidth of this band also decreases and the asymmetry is greatly reduced by X(HCOOH) = 0.476 (see Fig. 3.21a). Below X(HCOOH) = 0.476 some low frequency asymmetry appears on this band. At X(HCOOH) = 0.0998 the low frequency asymmetry has virtually disappeared but there is some high frequency asymmetry. With dilution the shoulder at 1733 cm^{-1} becomes progressively better defined and moves upward 12 cm^{-1} to ~1745 cm^{-1}. Throughout the concentration range, the band at 1733 - 1745 cm^{-1} continues to rise in relative intensity but is never the dominant peak. At X(HCOOH) = 0.0998, there are two distinct bands at ~1653 cm^{-1} and ~1745 cm^{-1} (see Fig. 3.21b) and there is also a very weak band at ~1788 cm^{-1}. The spectrum also suggests the presence of a weak band between 1653 cm^{-1} and 1745 cm^{-1}, but it is unknown from what this band arises.

The second region investigated in detail was 80 to 425 cm^{-1}. As previously stated, in pure formic acid this region contains a broad band that has been assigned by a number of workers, both theoretical (30-32) and (gas phase) experimental (33,34), to a mode involving hydrogen bonding. This region also includes a strong, sharp band from dichloromethane at ~284 cm^{-1}. As the formic acid is diluted, the broad band begins to change. A high frequency shoulder develops and grows in relative intensity (see Fig.

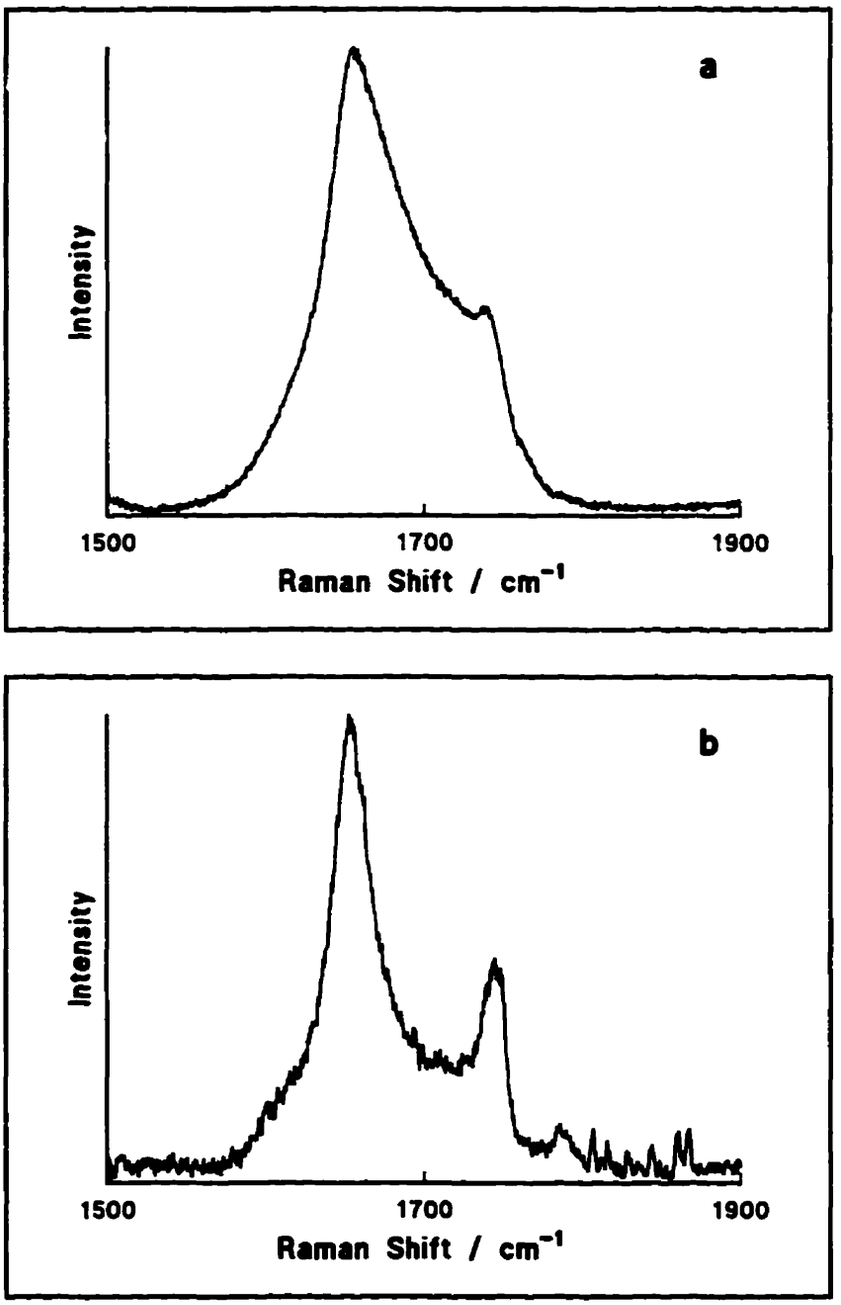

Fig. 3.21: Carbonyl Region of HCOOH / CH_2Cl_2:
a) X(HCOOH) = 0.476 b) X(HCOOH) = 0.0998.

3.22). The shoulder shifts to higher frequency with dilution. Unfortunately, at the most dilute concentration the new band is obscured by the far more intense band of the dichloromethane. The new band is also sharper than the original band. If the original band is really from hydrogen bonding, the changes seen in it are quite intriguing. One would expect dilution to have a pronounced effect on bands associated with hydrogen bonding. Of the four solvents used only the dichloromethane had any effect on this band.

Attempts were made to examine the bands of dichloromethane to see if any evidence could be found there for interaction between formic acid and dichloromethane. Unfortunately, the bands of dichloromethane are either too weak or the overlap with those of formic acid is too great to be of much use. The one exception is the band at ~284 cm^{-1}. This band shows no change with the presence of formic acid.

3.3.5 Discussion of Binary Results

When taken together, the results presented above for the binary systems of formic acid are quite enlightening.

The results for the HCOOH / H_2O system clearly indicate a phenomenon known as Resonance Energy Transfer (RET) is taking place. This effect arises from the coupling

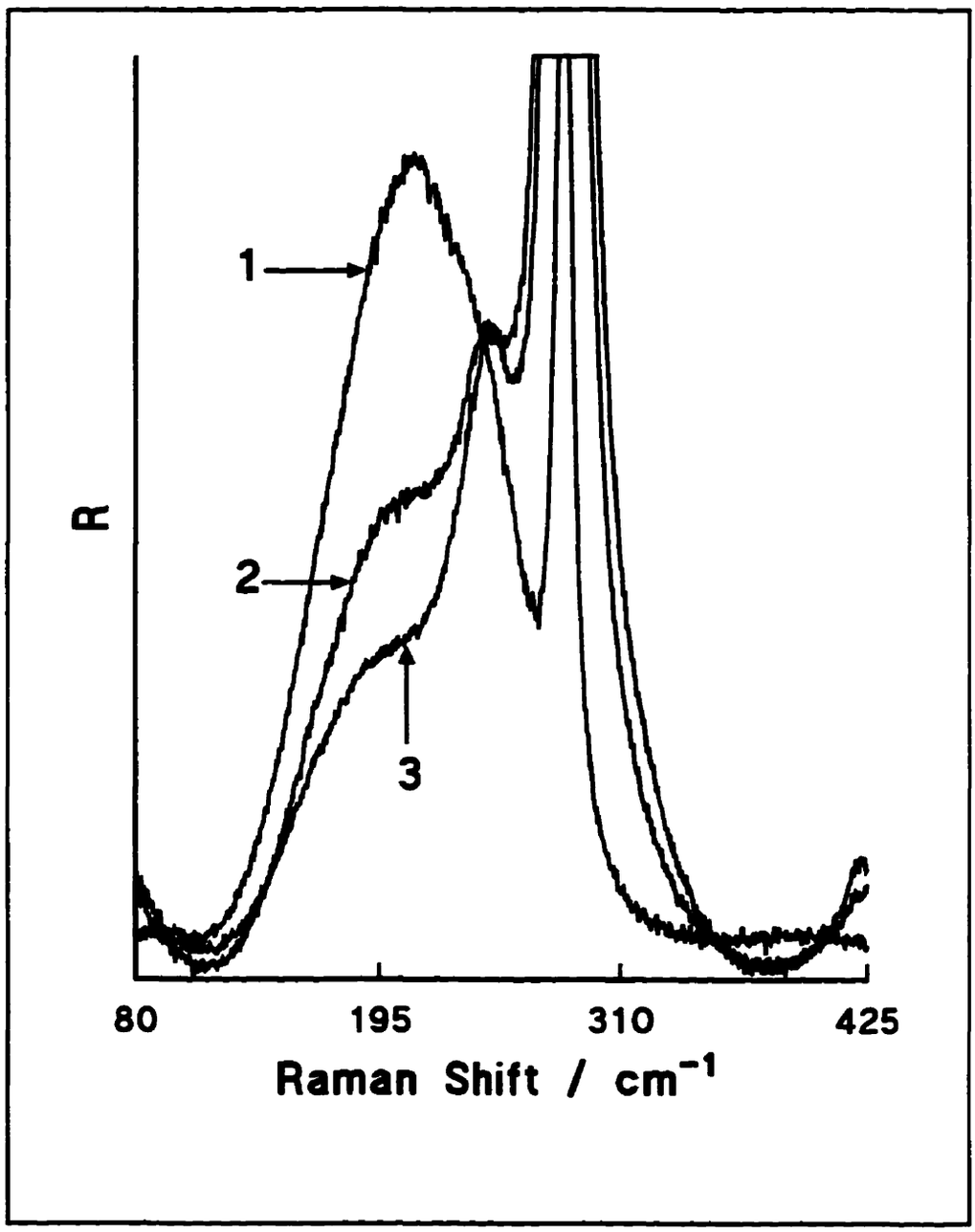

Fig. 3.22: Effect on "Association" Band of HCOOH of Dilution in CH_2Cl_2
1 - X(HCOOH) = 0.893 2 - X(HCOOH) = 0.476
3 - X(HCOOH) = 0.288.

of the transition dipole moments of two vibrational modes on two interacting species. Normally such an interaction indicates the presence of local order in the pure liquid induced by some intermolecular force such as dipole - dipole interaction or hydrogen bonding. RET usually manifests itself in the form of a non-coincidence effect (NCE) - a difference in the frequency maximum between the isotropic and anisotropic spectra. For liquids where the primary interaction is dipole - dipole (i.e., hydrogen bonding is absent) the non-coincidence effect is usually less than 15 cm^{-1}. N,N-dimethyl formamide (which is structurally similar to formic acid), for example, has one of the largest non-coincidence effects: ~14 cm^{-1} (35-37). Structurally, methyl formate is even more similar. The acid proton is replaced by a methyl group which, of course, precludes hydrogen bonding. As will be shown in chapter 4, the NCE of methyl formate is ~7 cm^{-1}. In pure formic acid the NCE is very large (~64 cm^{-1}). Very large NCE's are often found in liquids which exhibit hydrogen bonding such as HF (38) and alcohols (39,40). RET often broadens bands and the isotropic and anisotropic components of pure and aqueous formic acid are very broad compared to those of methyl formate. This evidence indicates a very strong intermolecular interaction between formic acid monomers in pure liquid formic acid to which hydrogen bonding makes a large contribution.

Acetonitrile and 1,4-dioxane are two solvents which are very different from water. Unlike water, they are aprotic and not hydrogen bonded. Also, they possess readily available lone pairs which may allow them to act as Lewis bases. Dilution in these

solvents has a dramatically different effect than dilution in water. The two most interesting peaks are those arising at the two higher frequencies: ~1737 cm^{-1} and ~1765 cm^{-1}.

First, consider the band at ~1730 - 1740 cm^{-1}. In acetonitrile its position does not vary much over the concentration range studied and averages to 1737 cm^{-1}. This band appears in 1,4-dioxane (~1729 cm^{-1}), dichloromethane (~1740 cm^{-1}), ether (~1735 cm^{-1}) (13) and as the anisotropic maximum in aqueous solutions (~1725 cm^{-1}). Furthermore, the C=O stretch in methyl formate is at ~1720 cm^{-1} (Table 4.4 and (28)). Because of its presence in the four solvents, this band likely does not arise from some HCOOH--solvent complex but from formic acid itself. Because the frequency of this peak is fairly close to the anisotropic maximum and close to the carbonyl frequency in pure methyl formate, this band is probably from "monomeric" (i.e., decoupled) formic acid. For acetonitrile and 1,4-dioxane this band becomes more intense (as measured by fraction of total carbonyl intensity) as the formic acid is diluted (see Fig. 3.23a). Furthermore, in both solvents the full width at half maximum (FWHM) shows a monotonic, major decrease with dilution (see Fig. 3.23b). This observation is also consistent with the hypothesis that RET is occurring in formic acid. As the active species is diluted, the coupling between individual units becomes less and less efficient. Therefore, the energy becomes "localized" on one of the monomeric units increasing the vibrational lifetime and narrowing the band of the decoupled monomer.

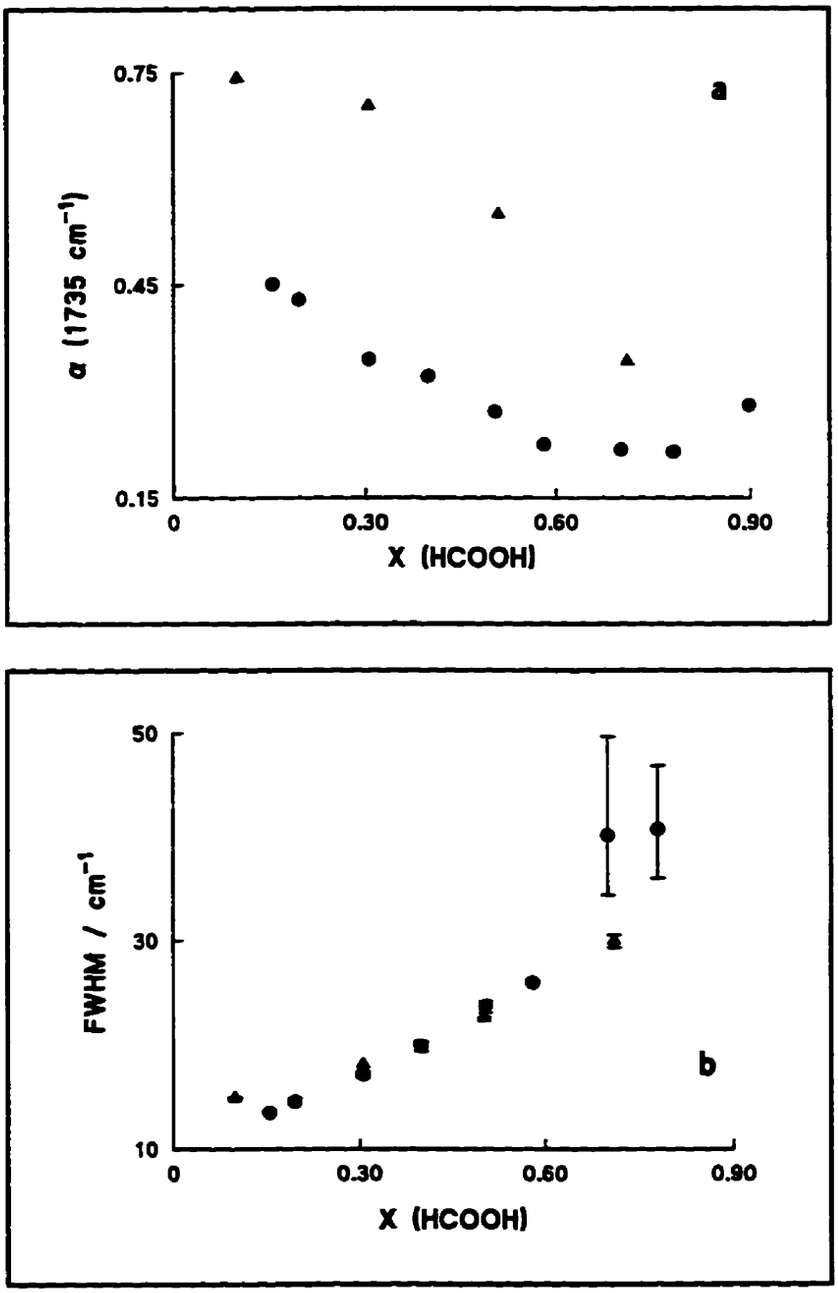

Fig. 3.23: Variation of the Band Parameters for 1735 cm^{-1} Band
a) Fraction of Total Intensity b) Full Width at Half Maximum
● - in Acetonitrile ▲ - in 1,4-dioxane.

The second band (at ~1765 cm^{-1}) is a little more difficult to interpret. This band is present in ether (13), acetonitrile, and 1,4-dioxane. It is not present in aqueous formic acid and there is no analogous peak in methyl formate. In dichloromethane its behaviour is quite peculiar. It appears as a weak shoulder at moderate formic acid concentrations but at X(HCOOH) = 0.0998 it has disappeared. In acetonitrile and 1,4-dioxane the intensity of this band increases as the formic acid is diluted (see Fig. 3.24a). However, in the acetonitrile solutions the intensity is higher and as the formic acid becomes more dilute the difference in intensity between the two solvents becomes even more noticeable. When (I_{1765} / I_{1735}) is plotted against mole fraction, different results for acetonitrile and 1,4-dioxane are obtained. In acetonitrile the relative intensity of the 1765 cm^{-1} band with respect to the 1735 cm^{-1} band steadily increases as the mole fraction of formic acid goes down, but in the 1,4-dioxane solutions the relative intensity is almost constant (see Fig. 3.24b). Because the relative intensity in acetonitrile increases, the two bands cannot arise from two different modes on the same "type" of formic acid. If this were so, the two bands would have a relative intensity independent of the concentration of formic acid. This band is never present in the aqueous solutions and disappears in the most dilute dichloromethane solutions, so it seems unlikely to arise purely from a formic acid species. In the acetonitrile and 1,4-dioxane solutions there is independent evidence to indicate the existence of a HCOOH--solvent complex, although, admittedly, in the case of 1,4-dioxane this evidence is not very strong. These pieces of evidence suggest the 1765 cm^{-1} band arises from a formic acid molecule "bound" to the solvent.

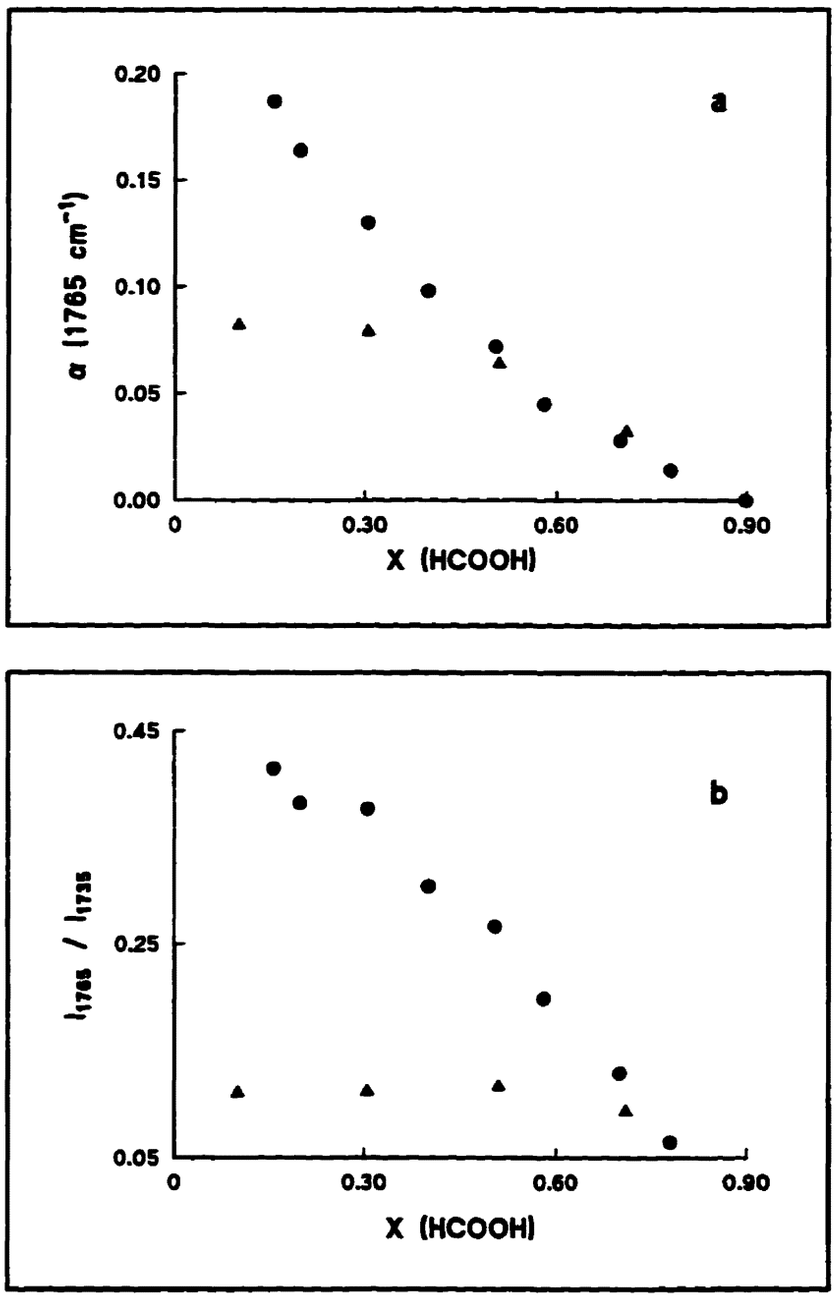

Fig. 3.24: Variation with X(HCOOH) of:
a) Fraction of Total Intensity b) I_{1765} / I_{1740}
for the 1765 cm^{-1} band

● - in Acetonitrile ▲ - in 1,4-dioxane.

Comparison of the results for acetonitrile and 1,4-dioxane reveals some important differences. At a similar formic acid concentration, the intensity of the 1765 cm^{-1} band with respect to the 1737 cm^{-1} is higher in acetonitrile than in 1,4-dioxane. This implies a greater degree of "complexation" of formic acid in acetonitrile. This may be partially explained by invoking simple steric arguments. In acetonitrile the nitrogen atom is at the end of the molecule and its lone pair is quite "exposed". In 1,4-dioxane the lone pairs are on oxygen atoms held in a six-membered ring. On either side of the oxygen atoms are 'CH_2' groups which might cause steric hindrance. Thus, in acetonitrile it may be easier for the formic acid to "attack" the lone pair. Further, the different levels of association may be a result of different electron donating abilities of the nitrogen and oxygen atoms.

The spectra of aqueous formic acid show no evidence of "bonding" between formic acid and water. Water is itself a hydrogen bonded liquid and it may be thermodynamically unfavourable to break the H_2O···H_2O and HCOOH···HCOOH hydrogen bonds to form H_2O···HCOOH hydrogen bonds. In acetonitrile and 1,4-dioxane this is not the case and the striking effects are seen. Crude thermodynamic evidence for this was found when the formic acid and 1,4-dioxane were mixed: heat was evolved (indicating the formation of new bonds) and $\Delta V_{mix.}$ was slightly positive.

The foregoing observations and discussion lead to the following model of formic

acid. In pure formic acid resonance energy transfer is occurring. Liquid formic acid, unlike liquid acetic acid, does not exist as discrete, long lived dimers or polymers. Instead, it exists as collections of monomeric units which interact by hydrogen bonding. This strong intermolecular interaction allows the transition dipole moments to couple giving the RET effect. The lifetimes of these interactions are probably quite short. If the formic acid is diluted in a solvent capable of acting as a Lewis base (e.g., acetonitrile or 1,4-dioxane) these hydrogen bonds may be ruptured and new ones formed with the base. This leads to the pronounced development of the 1737 cm^{-1} (from free monomer) and the 1765 cm^{-1} (from "bound" monomer) bands.

3.3.6 Formic Acid + Acetonitrile / Dichloromethane

Dichloromethane was chosen as the tertiary solvent to construct a Job plot in order to determine the "co-ordination number" of the acetonitrile - formic acid complex. It must be explicitly stated that the "co-ordination number" determined this way is for a formic acid - acetonitrile interaction in <u>dichloromethane</u>. In other solvents the "co-ordination number" could be different. Similarly, all the quantities calculated in this section are for a system of formic acid + acetonitrile in dichloromethane. In another tertiary solvent these quantities may also be different.

At this point it is instructive to have a short digression to discuss the Job method (sometimes called the "method of continuous variations") (16).

Consider a chemical reaction of the form:

$$M_aX_b \rightleftharpoons aM + bX$$

which can also be written as:

$$MX_n \rightleftharpoons M + nX$$

where n = b/a. If MX_n, M, and X have bands which are distinct, the "method of continuous variations" allows the determination of 'n' spectroscopically. In the formic acid - acetonitrile system the band at ~2270 cm^{-1} is assigned to the $HCOOH{\cdots}CH_3CN$ complex and is sufficiently distinct from the other bands that this method may be applied.

In applying the method of continuous variations the first step is to prepare a series of solutions such that the sum of the formal concentrations of 'M' and 'X' is constant:

$$C_M + C_X = C_T = constant \qquad [1]$$

The individual concentrations are then varied so each solution has a different ratio C_M : C_X. A quantity 'f' may be defined as:

$$C_X = fC_T \qquad [2]$$

and

$$C_M = (1 - f)\, C_T \qquad [3]$$

In any given mixture:

$$[M] = (1 - f)\, C_T - [MX_n] \qquad [4]$$

$$[X] = fC_T - n[MX_n] \qquad [5]$$

and the dissociation constant is given by:

$$K = \frac{(\,(1 - f)C_T - [MX_n]\,)(fC_T - n\,[MX_n])^n}{[MX_n]} \qquad [6]$$

$$K\,[MX_n] = (\,(1 - f)C_T - [MX_n]\,)(fC_T - n[MX_n])^n \qquad [7]$$

This equation implicitly shows how the concentration (and by extension, the intensity) varies with 'f'. The value of 'f' at which $[MX_n]$ is a maximum can be found by differentiating the above equation, setting the derivative equal to zero, and solving for 'f'. Differentiating the above equation gives:

$$\begin{aligned} K\,\frac{d\,[MX_n]}{df} = & \left(-C_T - \frac{d\,[MX_n]}{df}\right)(f\,C_T - n\,[MX_n])^n \\ & + (\,(1 - f)C_T - [MX_n]\,)\,(n\,(f\,C_T - n\,[MX_n]\,)^{n-1}\,) \\ & * \left(C_T - n\,\frac{d\,[MX_n]}{df}\right) \end{aligned} \qquad [8]$$

When the derivative is set to zero, this equation simplifies (after a little algebra) to:

$$1 - \frac{n\,(\,C_T - f_{max}C_T - [MX_n]\,)}{f_{max}C_T - n\,[MX_n]} = 0 \qquad [9]$$

and from this it is quite straightforward to show:

$$n = \frac{f_{max}}{1 - f_{max}} \qquad [10]$$

Thus, it is a fairly simple process to determine the value of 'n'. A plot of $\Gamma_{complex}$ (which depends linearly on [complex]) vs. 'f' should give a curve with a maximum at some value of 'f' between zero and one. From this value of 'f', 'n' can be calculated. For the studies involving CH_3CN and HCOOH, 'C_T' was set at ~5.04 M, 'M' was taken as HCOOH, and 'X' as CH_3CN.

There are some important points to consider when applying the method of continuous variations. The sharpness of the maximum reveals something of the nature of the complex. If it is only slightly dissociated, the maximum will be very well defined, but if the complex is very weak, the maximum will be poorly defined and it may be difficult to determine f_{max} precisely. This can be overcome by examining the data at high 'f' and at low 'f' and extrapolating the lines suggested by the data in these regions. The 'f' at which these lines intersect is f_{max}. Alternatively, an analytical function (e.g., a polynomial) can be fitted to the data and the maximum found by differentiation. The possible existence of several different complexes of the form MX_n is a further

complication. In the case of a formic acid - acetonitrile complex, the intensity of the 2270 cm^{-1} band depends only on the number of molecules of acetonitrile that are bound in a complex, not on the identity of the complex. It is, therefore, a "colligative" property. The intensity of the ~2270 cm^{-1} band could arise from the presence of several formic acid -acetonitrile complexes. If this is true, the Job plot is the superposition of the Job plots for each of the complexes. A Job plot with a poorly defined maximum or a plot with "structure" results.

The ternary solutions of acetonitrile, formic acid and dichloromethane were prepared in a similar fashion to the binary solutions. As mentioned above, the object in preparing solutions for a Job plot is to have a series of solutions in which the sum of the formal concentrations of the "reactants" is constant. To achieve this, the required volumes of formic acid and acetonitrile were measured with Mohr pipettes. The mass for each was also recorded. The 25 mL volumetric flasks were filled with dichloromethane and their masses were recorded. In this way the formal concentrations of all three species and the ratios of acetonitrile to formic acid are known. They are summarized in Table 3.10. The flasks were capped, wrapped with Parafilm and refrigerated. These solutions had a slightly positive ΔV_{mixing}.

To account for possible systemic errors such as variation in sample alignment, variations in detector response, etc., an intensity standard was used. For each solution,

Table 3.10: Concentrations for (HCOOH + CH_3CN) / CH_2Cl_2.

Code	C(HCOOH) / mol L^{-1}	C(CH_3CN) / mol L^{-1}	C_T / mol L^{-1}	f(CH_3CN)	C(CH_2Cl_2) / mol L^{-1}
RB950323A	4.504	0.523	5.026	0.104	12.36
RB950323H	4.025	1.024	5.049	0.202	12.26
RB950323I	3.511	1.531	5.042	0.304	12.06
RB950323B	3.019	2.021	5.040	0.401	12.06
RB950323C	2.466	2.537	5.003	0.507	11.98
RB950323D	2.033	3.018	5.050	0.598	11.83
RB950323E	1.510	3.537	5.047	0.701	11.73
RB950323F	1.015	4.036	5.051	0.798	11.64
RB950323G	0.480	4.534	5.014	0.904	11.58

Code	X(HCOOH)	X(CH_3CN)	X(CH_2Cl_2)	"R"[a]
RB950323A	0.259	0.030	0.711	8.612
RB950323H	0.233	0.059	0.708	3.931
RB950323I	0.205	0.090	0.705	2.293
RB950323B	0.177	0.118	0.705	1.494
RB950323C	0.145	0.149	0.705	0.972
RB950323D	0.120	0.179	0.701	0.674
RB950323E	0.090	0.211	0.699	0.427
RB950323F	0.061	0.242	0.697	0.251
RB950323G	0.029	0.273	0.698	0.106

Note:

a) "R" = C(HCOOH) / C(CH_3CN)

spectra were recorded in the 585 - 885 cm^{-1} region as well as in the C≡N stretching region. The 585 - 885 cm^{-1} region contains two strong bands of dichloromethane. The stronger of the two (at 703 cm^{-1}) was used as the intensity standard (see Fig. 3.25). For each solution the "relative integrated intensity" of the C≡N bands was calculated. The relative integrated intensity is defined as (41):

$$I^{r}_{analyte} = \left(\frac{I_{analyte}}{I_{standard}}\right) * C_{standard} \qquad [11]$$

The relative integrated intensity can then be directly related to the concentrations of the scattering species through:

$$I^{r}_{analyte} = J_{analyte} C_{analyte} \qquad [12]$$

where $J_{analyte}$ is the relative molar scattering coefficient.

The method of continuous variations was applied in the C≡N stretching region of the formic acid - acetonitrile solutions. The band at ~2270 cm^{-1} is assigned to the C≡N stretch of acetonitrile "bound" to the formic acid. Therefore, as outlined above, this band should pass through an intensity maximum as 'f' is varied. The variation of intensity of the ~2270 cm^{-1} band with 'f' is shown in Fig. 3.26 and in Table 3.11. The intensity does pass through a maximum but it is not particularly well defined. Two polynomials (cubic and quartic) were fitted to the Job Plot data:

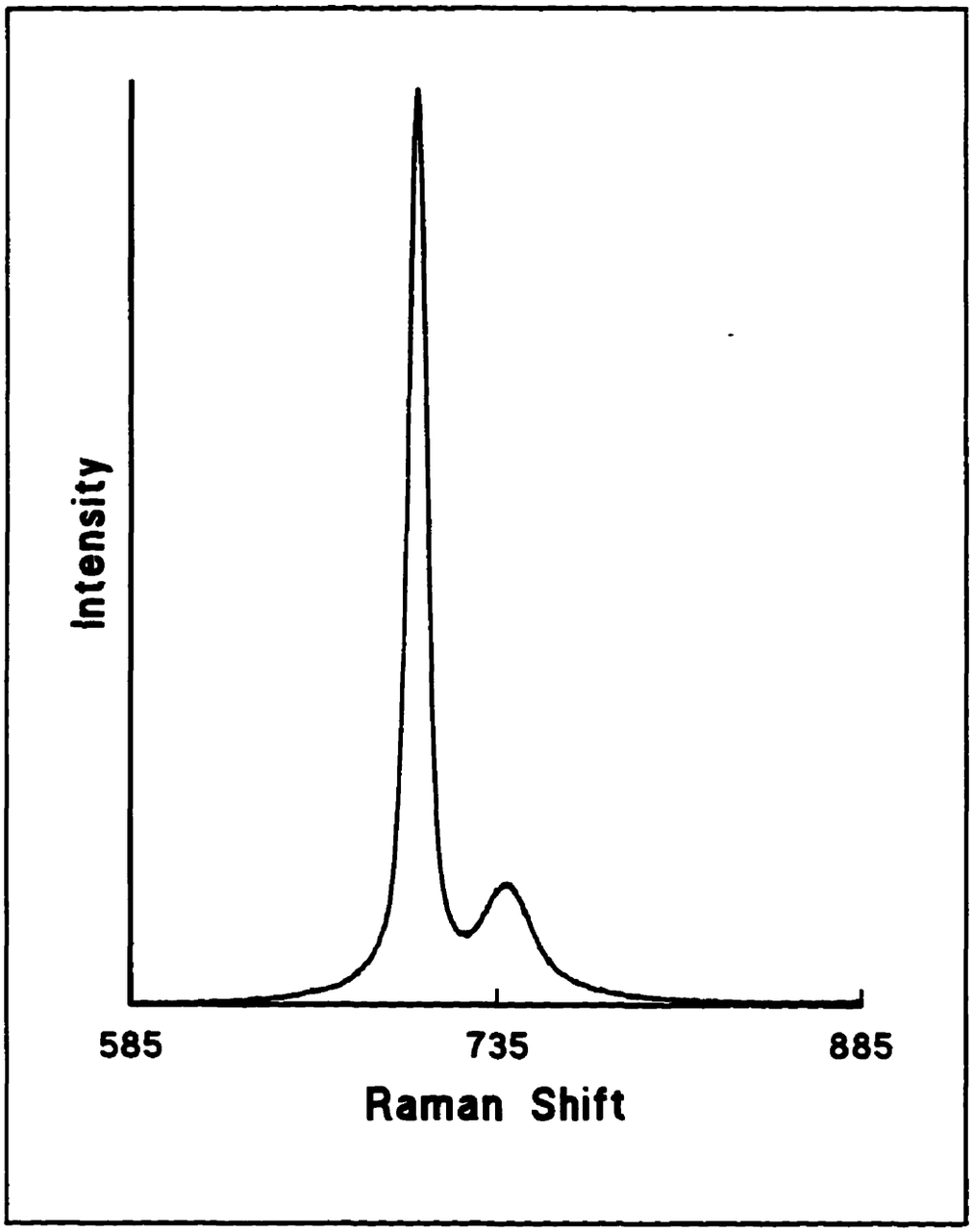

Fig. 3.25: ν_3 (703 cm^{-1}) and ν_9 (~736 cm^{-1}) Modes of CH_2Cl_2 in (HCOOH + CH_3CN) / CH_2Cl_2 ('f' = 0.507).

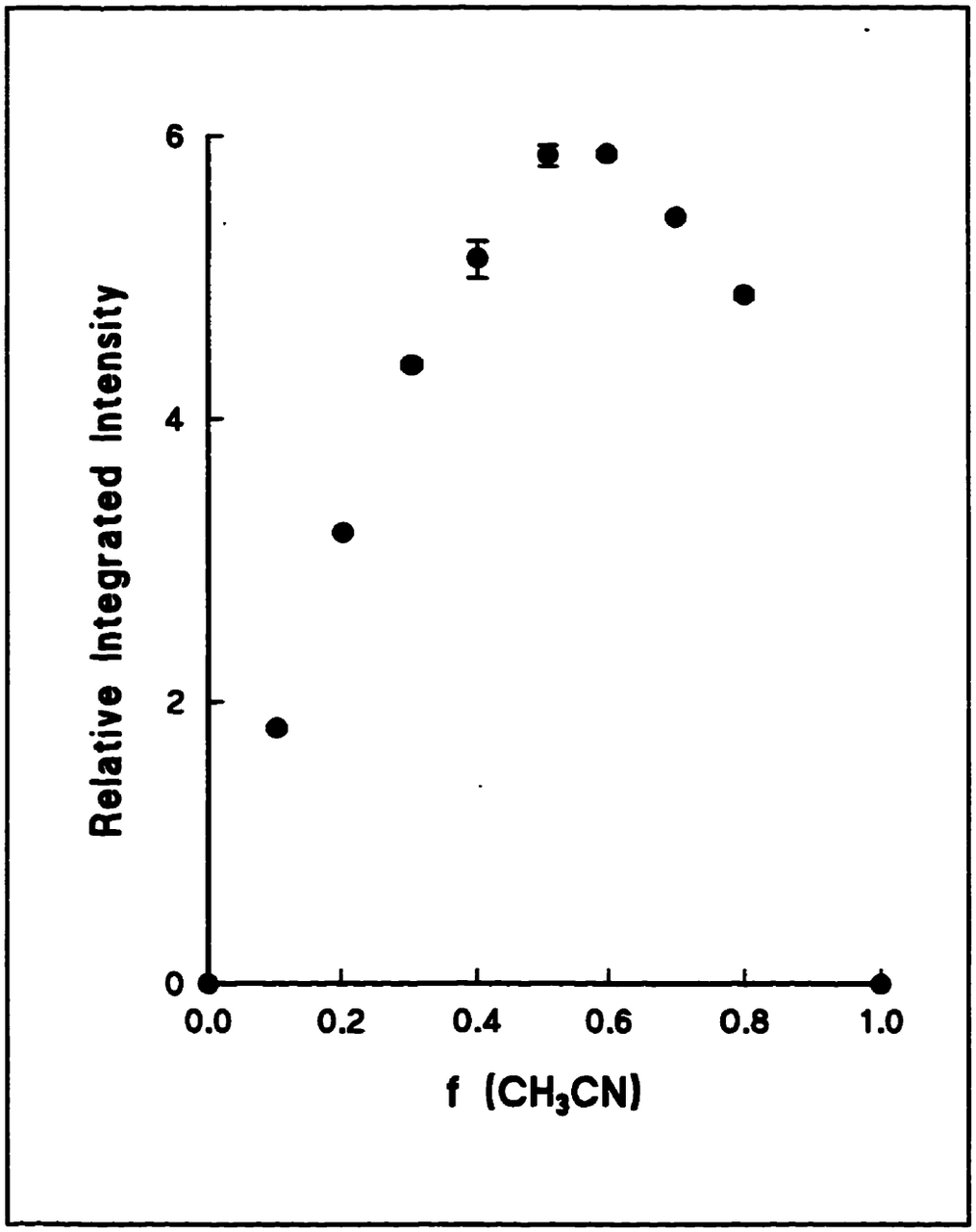

Fig. 3.26: Job Plot for the (HCOOH + CH_3CN) / CH_2Cl_2 System.

Table 3.11: Relative Integrated Intensities of the "Bound" Acetonitrile.

$f(CH_3CN)$	I_B^r
0.104	1.81
0.203	3.20
0.304	4.38
0.401	5.13
0.507	5.86
0.598	5.87
0.701	5.42
0.799	4.87

$$I_B^r = -15.257f^3 - 0.087f^2 + 15.324f + 0.116 \qquad r = 0.998$$

$$I_B^r = -20.232f^4 + 24.941f^3 - 24.833f^2 + 20.160f - 0.016 \qquad r = 0.999$$

The quartic fit does have a (very slightly) better correlation but the relative errors in the coefficients were much higher. The cubic polynomial gives n = 1.36 (i.e., HCOOH : CH_3CN = 3:4) while the quartic polynomial gives n = 1.47 (i.e., HCOOH : CH_3CN = 2:3). Obviously, then, ambiguity surrounds the true value of 'n'.

The question now, of course, is "what is the cause of this ambiguity?". The integrated intensity for the solution with f = 0.904 had an anomalously high value. This point was not used in the calculations but illustrated the possible limitations of the bandfitting program used in the analysis. This program, then, may contribute to the ambiguity surrounding 'n'. However, the biggest problem may lie in the assumption that there is only one complex. Possibly, a number of complexes is present. A combination of a 1:1 and a 1:2 complex could yield a distorted Job plot similar to that observed here.

Despite the difficulty in determining the value of 'n', another valuable quantity can be extracted from the data. This is the fraction, α, of acetonitrile which "reacts" to form the complex. More precisely, it is the fraction of acetonitrile which exists in a "bound" state. In order to determine this, it is necessary to determine the relationship between the molar scattering coefficients for "free" (J_F) and "bound" (J_B) acetonitrile.

In the C≡N stretching region of the HCOOH + CH_3CN solutions there are three bands. The high frequency band (~2270 cm^{-1}) is assigned to acetonitrile "bound" to formic acid. The remaining two bands underlie an asymmetrical band contour centred at about 2255 cm^{-1}. Even in pure acetonitrile the C≡N stretching band has some low frequency asymmetry. The asymmetry in the C≡N stretching band has been investigated by a number of workers who gave different explanations as to its meaning. Bulkin (42) suggested there was association of acetonitrile into dimers; the two bands arise from the dimer - monomer equilibrium. Griffiths (43) did not accept this, suggesting instead the spectral features "..arise from some unspecified molecular interaction which may well be localized on the C-C≡N part of the molecule..". Loewenschuss and Yellin (44) argued the spectral features were not due to an equilibrium between monomers and dimers but arise because of the existence of clusters in liquid acetonitrile. For the purpose of this discussion, this is a moot point. It indicates the low frequency asymmetry of the band at ~2255 cm^{-1} is not from an acetonitrile - formic acid or acetonitrile - dichloromethane interaction. Two bands were used to fit this envelope.

Assume the two bands underlying this asymmetric contour arise from the C≡N stretch of two "different" kinds of "free" acetonitrile. Let the concentrations of the two "forms" of free acetonitrile be $C_{A'}$ and $C_{A''}$ so that:

$$C_F = C_{A'} + C_{A''} \qquad [13]$$

where C_F = the total concentration of free acetonitrile.

Let

$$I^r_F = J_{A'} C_{A'} + J_{A''} C_{A''} \quad [14]$$

The integrated intensity of the asymmetrical contour is equal to the sum of the integrated intensities of the underlying bands. Therefore,

$$I_F = J_F C_F \quad [15]$$

The individual values of $C_{A'}$, $C_{A''}$, $J_{A'}$, and $J_{A''}$ are not known but are implicitly included in equation [15].

Let the concentration of "bound" acetonitrile be C_B. Under mass balance:

$$C = C_B + C_F \quad [16]$$

where C is the formal concentration of acetonitrile.

$$C_B = \frac{I^r_B}{J_B} \quad [17]$$

$$C_F = \frac{I^r_F}{J_F} \quad [18]$$

It is then possible to calculate J_F and J_B (cf. Campbell et al. (24)).

$$C = \frac{I^r{}_F}{J_F} + \frac{I^r{}_B}{J_B} \qquad [19]$$

$$\frac{I^r{}_F}{J_F} = C - \frac{I^r{}_B}{J_B} \qquad [20]$$

$$\frac{I^r{}_F}{C} = J_F - \frac{J_F}{J_B C} I^r{}_B \qquad [21]$$

Therefore, a plot of I_F / C vs. I_B / C should yield a line with a slope of J_F / J_B and an intercept of J_F. Such a plot is given in Fig. 3.27. Linear regression gives the following result:

$$I^r{}_F / C = 8.612 - 1.097\ (I^r{}_B / C) \qquad r = 0.981$$

From which $J_B = 7.85 \pm 1.32$ and $J_F = 8.61 \pm 0.41$.

Calculating 'α', the fraction of acetonitrile present in a "bound" state, is now a fairly simple matter. Mathematically, 'α' is defined as follows:

$$\alpha = \frac{C_B}{C} = 1 - \frac{I_F}{J_F C} \qquad [22]$$

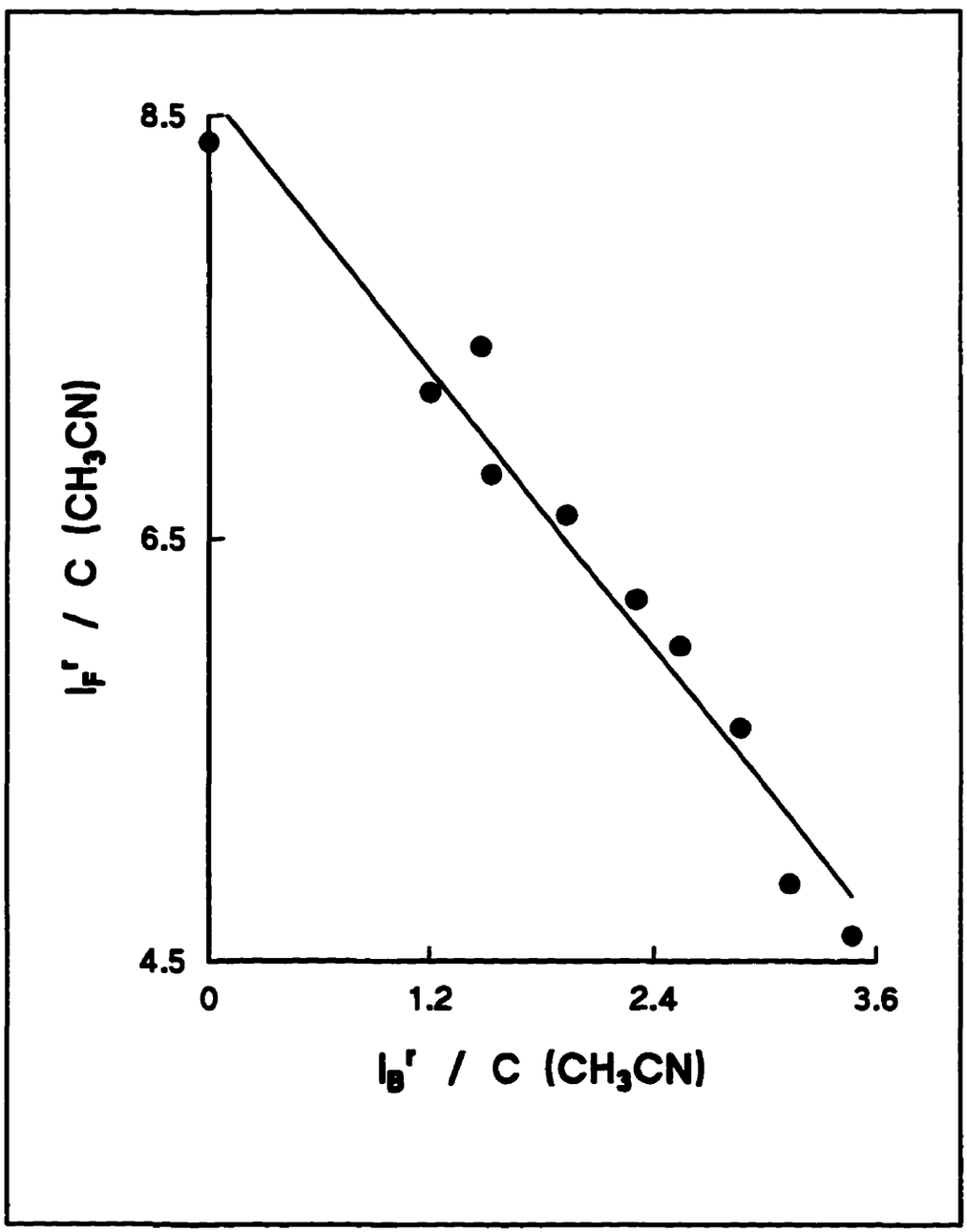

Fig. 3.27: Determination of J_B and J_F for the C≡N Bands in the (HCOOH + CH_3CN) / CH_2Cl_2 System.

Values of α are given in Table 3.12. A plot of 'α' versus 'f' is shown in Fig. 3.28a and shows a steady decrease in α as 'f' increases. An increasing 'f' is equivalent to an increasing $C(CH_3CN)$. Because the experiment is designed to hold the total formal concentration ($C_T = C(CH_3CN) + C(HCOOH)$) constant, C(HCOOH) must necessarily decrease. Therefore, $C(HCOOH) / C(CH_3CN)$ also decreases and so does the number of eligible "partners" per acetonitrile molecule. Consequently, the chances of a given acetonitrile molecule being in a "bound" state are lower. Ergo, 'α' decreases. Figure 3.28b shows the variation of 'α' as a function of 'R' (= $C(HCOOH) / C(CH_3CN)$). At high relative amounts of acetonitrile (i.e., low 'R'), 'α' is quite small. Initially, 'α' increases very rapidly with 'R' but begins to level off at higher values of 'R'.

An "equilibrium constant", "K", was calculated for the two possible complex stoichiometries (i.e., 2:3 and 3:4). The values of "K" were calculated on the basis of the general equation:

$$K = \frac{[complex]}{([HCOOH]_F)^a([CH_3CN]_F)^b} \qquad [23]$$

The concentration of "free" acetonitrile is obtained directly from the intensity and J_F. From it, the appropriate mole ratios, and the necessary mass balance, the concentrations of formic acid and the complex were calculated. The "equilibrium constants" are summarized in Table 3.13. Also included in Table 3.13 are "K" values assuming a 1:1 complex. A number of precedents exist in the literature (24,26,45-48) for assuming 1:1

Table 3.12: Summary of 'α' values for (HCOOH + CH_3CN) / CH_2Cl_2.

f(CH_3CN)	'R'	α
0.104	8.612	0.463
0.203	3.931	0.435
0.304	2.293	0.349
0.401	1.494	0.304
0.507	0.972	0.279
0.598	0.674	0.232
0.701	0.427	0.210
0.799	0.252	0.165

$$R = C_T(HCOOH) / C_T(CH_3CN)$$

α = fraction of acetonitrile present in a "bound" state

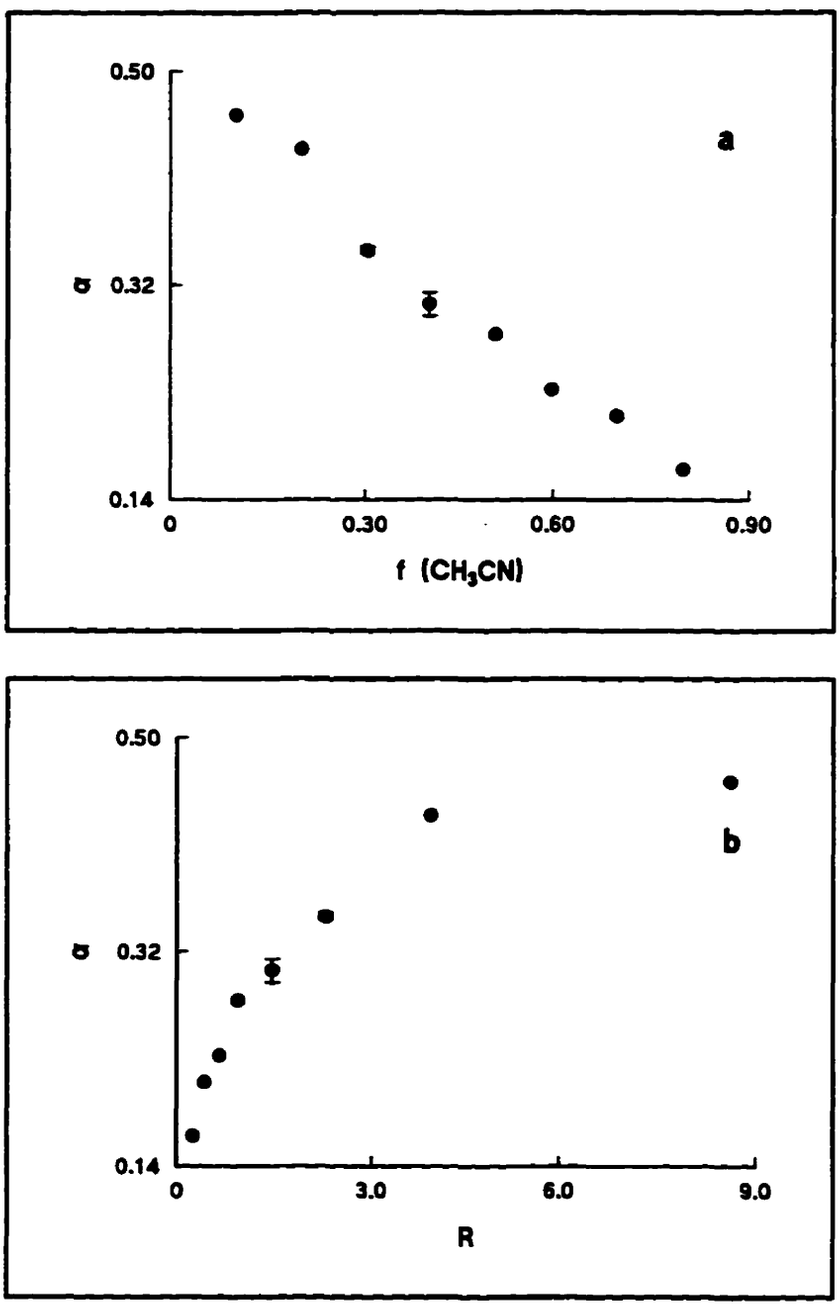

Fig. 3.28: Fraction of Bound Acetonitrile as a Function of: a) 'f' and b) 'R' for the (HCOOH + CH_3CN) / CH_2Cl_2 System.

Table 3.13: Values for "K" for Various Models of HCOOH + CH_3CN / CH_2Cl_2.

A) HCOOH : CH_3CN = 3:4

"f"	$[CH_3CN]_F$ / mol L^{-1}	$[HCOOH]_F$ / mol L^{-1}	[complex] / mol L^{-1}	"K"
0.104	0.28	4.32	0.061	0.050
0.203	0.58	3.69	0.11	0.052
0.304	1.00	3.11	0.13	0.043
0.401	1.41	2.56	0.15	0.043
0.507	1.83	1.94	0.18	0.050
0.598	2.32	1.51	0.18	0.050
0.701	2.79	0.95	0.19	0.070
0.799	3.37	0.52	0.17	0.096

B) HCOOH : CH_3CN = 2:3

"f"	$[CH_3CN]_f$ / mol L^{-1}	$[HCOOH]_F$ / mol L^{-1}	[complex] / mol L^{-1}	"K"
0.104	0.28	4.34	0.081	0.066
0.203	0.58	3.73	0.15	0.069
0.304	1.00	3.16	0.18	0.057
0.401	1.41	2.61	0.21	0.056
0.507	1.83	1.99	0.24	0.065
0.598	2.32	1.57	0.23	0.064
0.701	2.79	1.02	0.25	0.087
0.799	3.37	0.57	0.22	0.116

Table 3.13 continued.

C) HCOOH : CH_3CN = 1:1

"f"	$[CH_3CN]_F$ / mol L^{-1}	$[HCOOH]_F$ / mol L^{-1}	[complex] / mol L^{-1}	"K"
0.104	0.28	4.26	0.24	0.20
0.203	0.58	3.58	0.45	0.22
0.304	1.00	2.98	0.54	0.18
0.401	1.41	2.40	0.62	0.18
0.507	1.83	1.76	0.71	0.22
0.598	2.32	1.33	0.70	0.23
0.701	2.79	0.77	0.74	0.35
0.799	3.37	0.35	0.67	0.57

association between nitrile containing and 'OH' containing species, so these "K" values were calculated for comparison. Figure 3.29 illustrates "K" as a function of f(CH_3CN). At low values of 'f', the "K" value is nearly constant. Once 'f' is greater than approximately 0.6 the value of "K" increases sharply. In a study of ortho-cresol and acetonitrile in a binary system, Campbell, Park and Shurvell (24) also found a strong dependence of "K" on the concentrations of the species involved. A number of possible reasons for this can be advanced. First, concentrations were used to calculate "K" instead of activities. At the very high concentrations (on a thermodynamic scale) used here, this approximation may not be valid. Second, intensity has been assumed to be a linear function of concentration. Third, no allowance for possible self association of formic acid or acetonitrile has been made. In studies of methanol and acetonitrile Yarwood et al. (23,49) showed the necessity of doing just this. The dependence of "K" on 'f' and the ambiguous result for 'n' from the Job plot suggest the possibility of forming a mixture of complexes. Because the equilibrium constant increases sharply above f~0.6, the assumption of a single complex may break down at this point.

The average solvation number, $\bar{n}_{solv.}$, for formic acid was also calculated (see Table 3.14). The average solvation number is defined as:

$$\bar{n}_{solv.} = \frac{[CH_3CN]_B}{C(HCOOH)} \qquad [24]$$

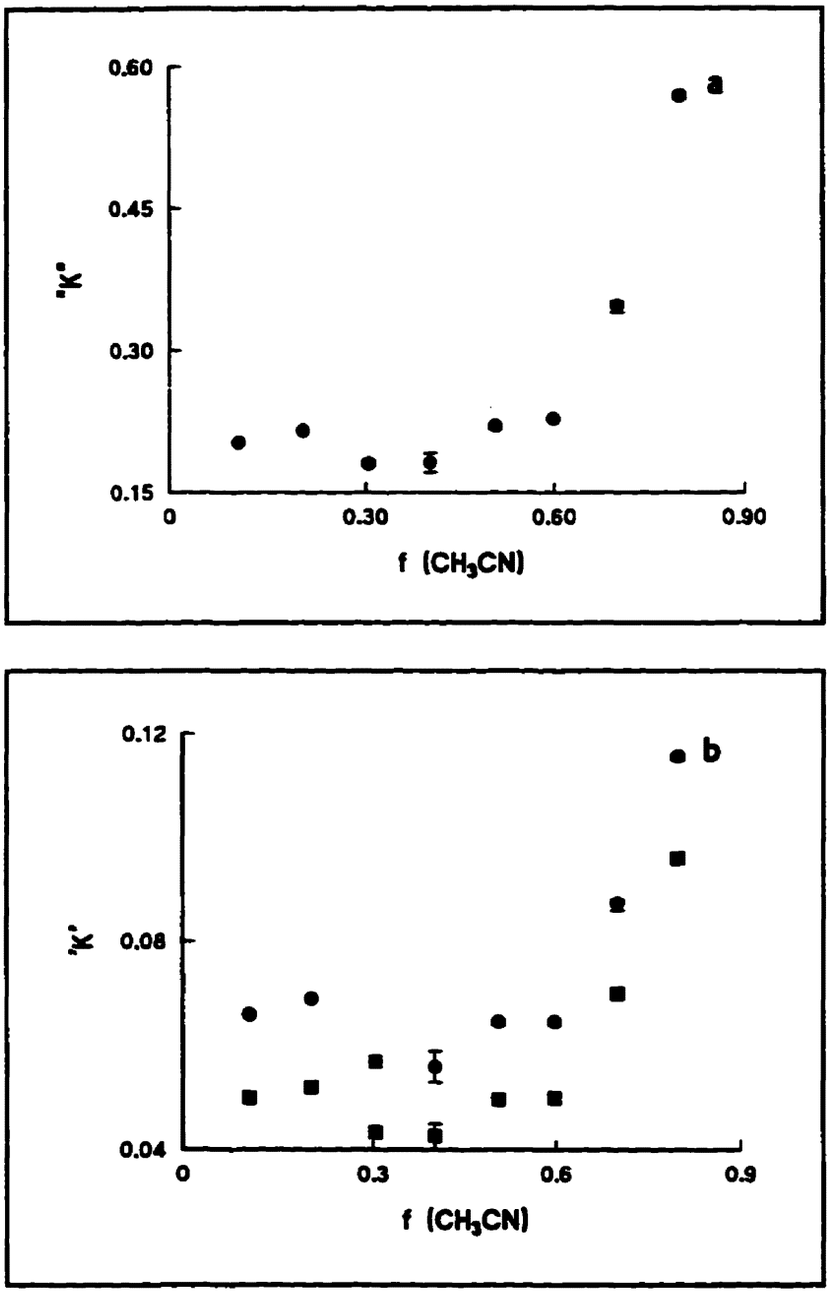

Fig. 3.29: "K" as a Function of 'f':
a) 1:1 Model
b) ● - 2:3 Model; ■ - 3:4 Model
for the (HCOOH + CH_3CN) / CH_2Cl_2 System.

Table 3.14: Average Solvation Numbers for (HCOOH + CH_3CN) / CH_2Cl_2.

C(HCOOH) / mol L^{-1}	C(CH_3CN) / mol L^{-1}	'f'	$[CH_3CN]_B$ / mol L^{-1}	$\bar{n}_{solv.}$
4.504	0.523	0.104	0.24	0.054
4.025	1.024	0.203	0.45	0.11
3.511	1.531	0.304	0.54	0.15
3.019	2.021	0.401	0.62	0.20
2.466	2.537	0.507	0.71	0.28
2.033	3.018	0.598	0.70	0.35
1.510	3.537	0.701	0.74	0.49
1.015	4.036	0.799	0.66	0.66

where

$[CH_3CN]_B$ = the concentration of "bound" acetonitrile

C(HCOOH) = total stoichiometric concentration of formic acid.

Figure 3.30 illustrates the dependence of $\bar{n}_{solv.}$ on $[CH_3CN]_F$. Not surprisingly, as $[CH_3CN]_F$ (and by extension, $C(CH_3CN)$) increases, so does the average solvation number.

While the studies of these solutions necessarily focused on the C≡N stretching region, spectra of the carbonyl region were also collected. The C=O stretch of formic acid is not nearly as good a scatterer as the C≡N stretch of acetonitrile. With this in mind and considering the relatively low concentrations of formic acid, the slits were opened to 200 μm. The spectra are shown in Fig. 3.31a. The changes in this region appear to be a "superposition" of the changes for HCOOH / CH_3CN and HCOOH / CH_2Cl_2. The two peaks at 1735 - 1740 cm^{-1} and ~1765 cm^{-1} become more and more prominent (as described previously) as the formic acid is diluted, consistent with the results from the binary solutions. Bandfitting was applied to these spectral contours. Unfortunately, the band overlap is quite severe and acceptable fits could not be obtained. Despite this, intensities of the ~1765 cm^{-1} band were estimated from peak heights. This is, admittedly, a rather crude means of obtaining intensities, but may be valid to a first approximation. The band at ~1765 cm^{-1} was previously assigned to "bound" formic acid. As such, the intensity of this band should have a linear dependence on the concentration of the complex. Figure 3.31b illustrates the dependence of I (1765 cm^{-1}) on [complex].

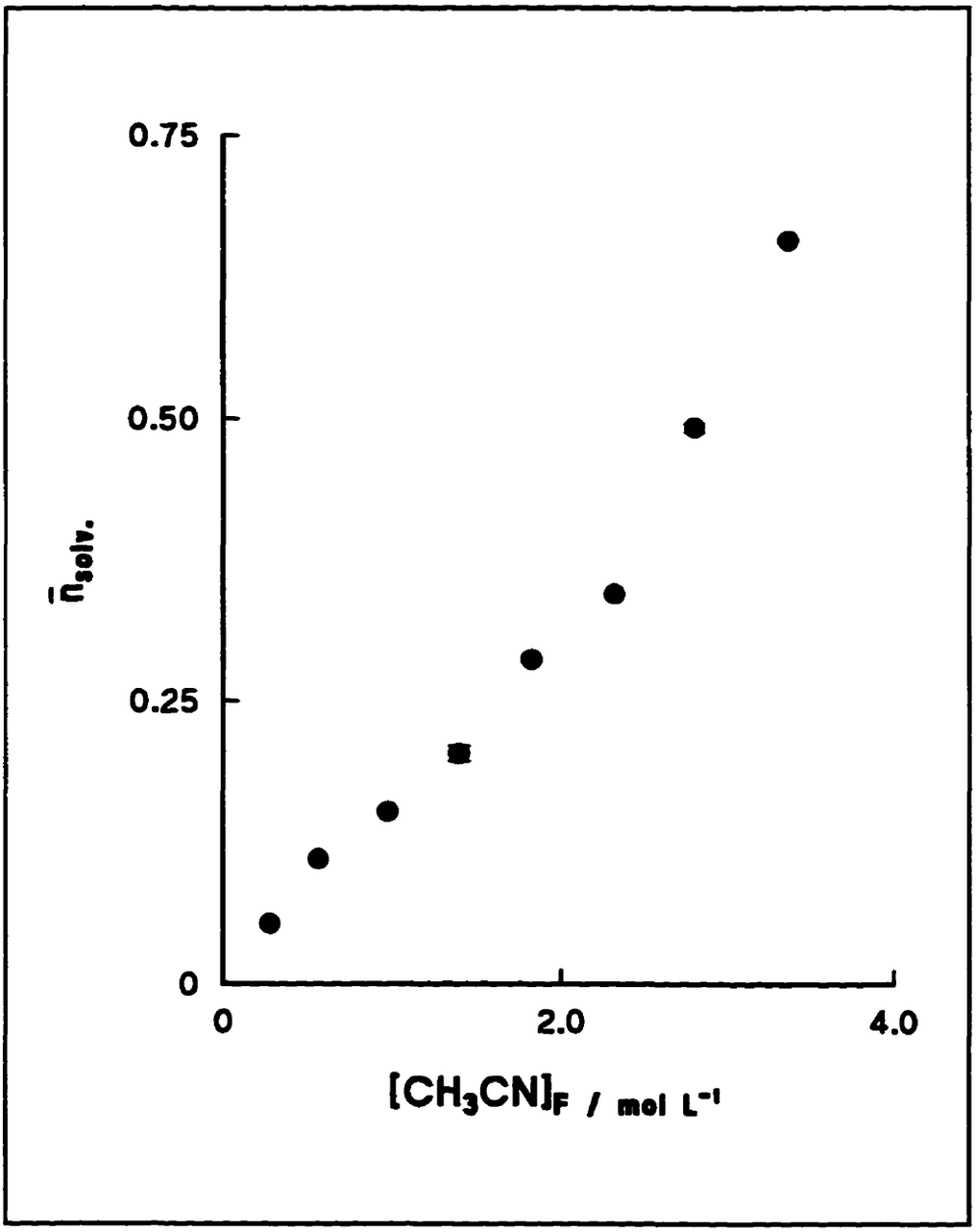

Fig. 3.30: Average Solvation Number of HCOOH in (HCOOH + CH_3CN) / CH_2Cl_2 versus $[CH_3CN]_F$.

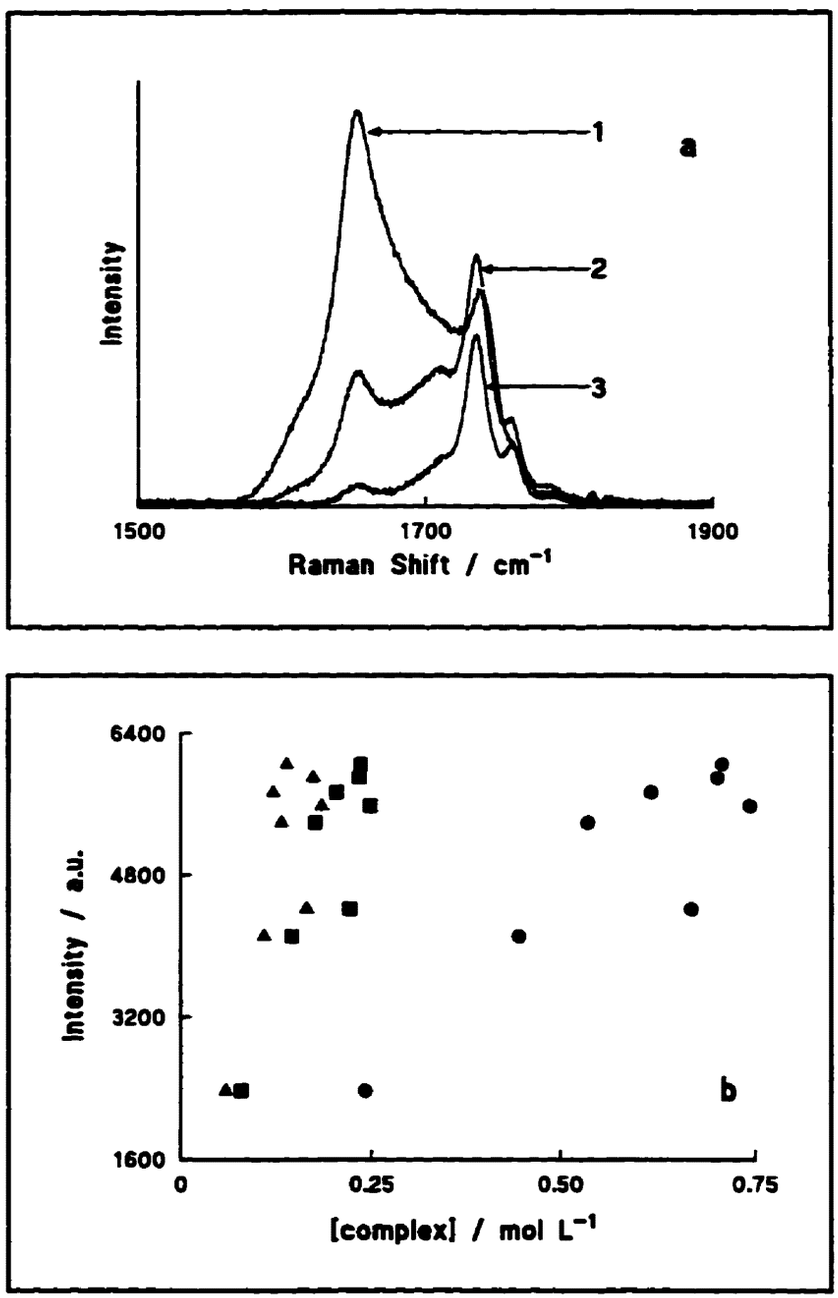

Fig. 3.31: a) Carbonyl Region of (HCOOH + CH_3CN) / CH_2Cl_2
1 - 'f' = 0.104; 2 - 'f' = 0.507; 3 - 'f' = 0.799
b) Intensity of 1760 cm^{-1} band versus [complex]
● - 1:1 Model; ■ - 2:3 Model; ▲ - 3:4 Model.

These are not relative intensities as defined by equation [11] but intensities from spectra normalized using the 702 cm^{-1} band of CH_2Cl_2. For each of the models the dependence appears to be roughly linear. The correlations are not particularly good ($r < 0.9$) but this may arise because of the peak height approximation. The apparent linear dependence of I (1765 cm^{-1}) on [complex] gives support to assigning the band at ~1765 cm^{-1} to "bound" formic acid.

3.4 Summary

This chapter describes studies of various solutions of liquid formic acid in an attempt to elucidate its structure. A second, serendipitous result was found: a pronounced effect on the acetonitrile spectrum indicative of a formic acid - acetonitrile complex.

Formic acid was studied in a number of solvents: water, acetonitrile, 1,4-dioxane and dichloromethane. The aqueous results are consistent with a phenomenon known as resonance energy transfer occurring in liquid formic acid. This, in turn, implies a degree of structural order in the liquid that allows the oscillators to couple. The hydrogen bonding present in the liquid formic acid facilitates this coupling and explains the large non-coincidence effect and great width of the bands in the carbonyl region. Dilution in acetonitrile and 1,4-dioxane leads to dramatic changes in the C=O band of formic acid.

The development of peaks at ~1730 cm^{-1} and ~1765 cm^{-1} arises from the breaking of the coupled monomers to form "isolated" monomers (~1730 cm^{-1} band) and the formation of a formic acid - solvent complex (~1765 cm^{-1} band). In solutions of formic acid in acetonitrile a new band (~2270 cm^{-1}) in the C≡N stretching region develops and is assigned to a formic acid - acetonitrile complex.

This complex was then studied in ternary solutions using dichloromethane as the solvent. The Job plot gave an ambiguous result. The molar scattering coefficients were calculated for the "free" and the "bound" acetonitrile and from these the fraction of acetonitrile existing in a "bound" state was calculated. This value decreases as the concentration of acetonitrile increases. The "equilibrium constant" for the reaction was also determined assuming several different formic acid : acetonitrile ratios. Unfortunately, for all the models the equilibrium constant is not constant. At lower concentrations of acetonitrile (< ~3.0 mol L^{-1}) it is nearly constant but above this concentration the value increases sharply. This may indicate some of the underlying assumptions are not valid or that, in solutions with high formal concentrations of acetonitrile, a mixtures of complexes is formed.

3.5 References

1. H. Susi, J. R. Scherer, *Spectrochim. Acta*, **1969** 25A 1243
2. D. Chapman, *J. Chem. Soc. B.* **1956** 225
3. S. Bratož, D. Hadži, N. Sheppard, *Spectrochim. Acta.* **1956** 8 249
4. G. E. Tomlison, B. Curnutte, C. E. Hathaway, *J. Mol. Spec.* **1970** 36 26
5. S. M. Blumenfeld, H. Fast, *Spectrochim. Acta.* **1968** 24A 1449
6. P. Waldstein, L. A. Blatz, *J. Phys. Chem.* **1967** 71 2271
7. H. Geisenfelder, H. Zimmerman, *Ber. Bunsenges. Phys. Chem.* **1963** 67 480
8. Z. Pajak, E. Szcześniak, *Chem. Phys. Lett.* **1977** 49 269
9. E. Constant, A. Lebrun, *J. Chim. Phys.* **1964** 61 163
10. G. I. Swan, *N.A.T.O. A.S.I. Sect. C* **1991** 329 139
11. A. A. Shubin, *Izv. Akad. Nauk. Ser. Fiz.* **1950** 14 442
12. R. J. Bartholomew, *M.Sc. Thesis*, **1992**, University of Waterloo
13. M. H. Brooker, *private communication*
14. J. Semmler, D. E. Irish, *J. Solution Chem.* **1988** 17 805
15. J. Semmler, D. E. Irish, *J. Mol. Liquids* **1990** 46 1
16. P. Job, *Ann. Chim. Phys.* **1928** 9 113
    L. Meites, H. C. Thomas, *Advanced Analytical Chemistry,* pp 297 - 298, McGraw Hill, New York, 1958
    M. T. Beck, *Chemistry of Complex Equilibria,* pp 86 - 89, Van Nostrand Reinhold Co., Toronto, 1970
17. J. Yarwood, *Ann. Rep. Prog. Chem. Sect. C,* **1990** 87 75
18. G. Fini, P. Mirone, *J. Chem. Soc. Faraday Trans.* **1974** 70 1776

19. M. H. Brooker, O. F. Nielsen, E. Praestgaard, *J. Raman Spec.* **1988** 19 71

20. Y-K. Sze, D. E. Irish, *Can. J. Chem.* **1975** 53 427

21. R. Lindemann, G. Zundel, *J. Chem. Soc. Faraday Trans. 2* **1972** 68 979

22. T. G. Chang, D. E. Irish, *J. Solution. Chem.* **1974** 3 161

23. M. Besnard, M. I. Cabaço, F. Strehle, J. Yarwood, *Chem. Phys.*, **1992** 163 103

24. J. M. Campbell, Y. S. Park, H. F. Shurvell, *Can. J. Appl. Spec.*, **1991** 36 147

25. B. Cohen, S. Weiss, *J. Phys. Chem.*, **1984** 88 3974

26. S. C. White, H. W. Thompson, *Proc. Roy. Soc.*, **1966** A291 460

27. W. R. Fawcett, G. Liu, T. E. Kessler, *J. Phys. Chem.* **1993** 97 9293

28. Z. Deng, D. E. Irish, *Can. J. Chem.* **1991** 69 1766

29. F. E. Malherbe, H. J. Bernstein, *J. Amer. Chem. Soc.*, **1952** 74 4408

30. I. Yokoyama, Y. Miwa, K. Machida, *J. Amer. Chem. Soc.*, **1991** 113 4408

31. I. Yokoyama, Y. Miwa, K. Machida, *J. Phys. Chem.*, **1991** 95 9740

32. Y-T Chang, Y. Yamiguchi, W. H. Miller, H. F. Schaefer III, *J. Amer. Chem. Soc.*, **1987** 109 7245

33. J. E. Bertie, K. H. Michaelian, *J. Chem. Phys.*, **1982** 76 886

34. R. C. Millikan, K. S. Pitzer, *J. Amer. Chem. Soc.*, **1958** 80 3515

35. V. M. Shelley, J. Yarwood, *Chem. Phys.*, **1989** 137 277

36. J. Jonas, H. D. Thomas, *J. Chem. Phys.*, **1989** 90 4632

37. V. M. Shelley, A. Talintyre, J. Yarwood, R. Buchner, *Faraday Discuss. Chem. Soc.*, **1988** 85 211

38. B. Desbat, P. V. Huong, *J. Chem. Phys.*, **1983** 78 6377

39. C. Perchard, J. P. Perchard, *Chem. Phys. Lett.*, **1974** 27 445

40. J. P. Perchard, *Chem. Phys. Lett.*, **1976** 44 169

41. D. E. Irish, T. Ozeki, in *Analytical Raman Spectroscopy*, Chap. 4 (J. G. Grasselli and B. J. Bulkin Eds.), John Wiley and Sons Inc., Toronto, 1991

42. B. J. Bulkin, *Helvet. Chim. Acta* **1969** 52 1348

43. J. E. Griffiths, *J. Chem. Phys.* **1973** 59 751

44. A. Loewenschuss, N. Yellin, *Spectrochim. Acta* **1975** 31A 207

45. S. S. Mitra, *J. Chem. Phys.* **1962** 36 3286

46. M. C. S. Lopes, H. W. Thompson, *Spectrochim. Acta* **1968** 24A 1367

47. J. C. F. Ng, Y. S. Park, H. F. Shurvell, *Spectrochim. Acta* **1992** 48A 1139

48. J. C. F. Ng, Y. S. Park, H. F. Shurvell, *J. Raman Spectrosc.* **1992** 23 229

49. S. S. Farwaneh, J. Yarwood, I. Cabaço, M. Besnard, *J. Mol. Liq.* **1993** 56 317

4. SOLUTIONS OF METHYL FORMATE

4.1 Introduction

Methyl formate is structurally very similar to formic acid; the acid proton being replaced by a methyl group. As illustrated in Table 4.1, such a small structural change leads to dramatic changes in the physical properties. Despite having a lower molar mass and a lower dipole moment, formic acid has much higher melting and boiling points. These differences are directly attributable to the hydrogen bonding present in formic acid. The hydrogen bonding has a profound effect on the spectrum which is illustrated in Figures 3.3 (C=O region of HCOOH) and 4.1 (see section 4.3).

By studying methyl formate some light may be shed on the problem of the liquid structure of formic acid. The isotropic and anisotropic spectra of formic acid reveal an unmistakeable non-coincidence effect (NCE, see Fig. 3.4) and this is one of the manifestations of resonance energy transfer (RET, see chapter 1). Unfortunately, the models developed to explain the NCE are not applicable to solutions where hydrogen bonding is present. Methyl formate is the nearest structural analogue to formic acid where hydrogen bonding is absent. Therefore, solutions of methyl formate were studied

Table 4.1: Comparison of the Physical Properties of Formic Acid and Methyl Formate (1).

	HCOOH	$HCOOCH_3$
Melting Point / °C	8.4	-99
Boiling Point / °C	100.7	31.5
Molar Mass / g mol^{-1}	46.03	60.05
Density / g ml^{-1}	$1.220^{20/4}$	$0.9742^{20/4}$
Index of Refraction	1.3714^{20}	1.3433^{20}
Dipole Moment (gas phase) / debye	1.41	1.77
Dielectric Constant	58.5 (16.5°C)	8.5 (20°C)

to gain a better understanding of the NCE and RET and to see how good the various models for the NCE are for solutions of methyl formate. Methyl formate is also of intrinsic interest because, despite its limited liquid range, it has been suggested as a possible solvent for lithium battery electrolytes (2).

Infrared (3-7) and Raman (8-10) studies of methyl formate have been reported. Two normal coordinate analyses have been performed on methyl formate (13,14) and its deuterated analogues (13). Most studied the vapour and liquid (3-6,9) states, but two have attempted to study the solid (7,9). The infrared (3,5) and Raman (9) spectra have been assigned and general agreement exists in the literature on these assignments. However, some slight disagreement over structure does exist. The first issue concerns the existence of two conformers of methyl formate. Microwave absorption experiments have established (11) that the C=O, C-O, and O-CH_3 bonds lie in a single plane. Within this structural restriction, two conformations are possible:

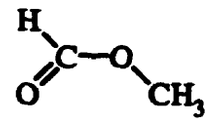

I

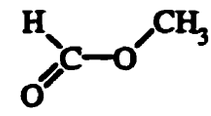

II

The literature is inconsistent about the application of the terms 'cis' and 'trans' to these conformers. Almost all workers (3-5,9,12) agree methyl formate exists only as conformer

I. However, Byrne et al. (6) argued for the presence of a small amount of conformer II. This argument was based on the presence of one band at 1768 cm^{-1} in CCl_4 solutions. Wilmshurst (3) had stated this band arose from a combination band (CH_3 symmetric bend + C-O bend). Harris et al. (9) based their Raman assignments on the exclusive presence of conformer I. The second issue is the existence of associated species. Wilmshurst suggested liquid methyl formate was a mixture of associated and unassociated molecules. Harris et al., however, stated no evidence existed in the Raman spectra to support this hypothesis.

The NCE has been studied in a wide variety of molecules. The majority of these systems have contained the carbonyl functional group. Ketones (15-18) and amides (19-22) have been the most frequently studied, but other molecules including liquid SO_2 (23), nitriles (24) and CS_2 (26), have also been studied. Almost no work has been done on esters. Therefore, a study of methyl formate (the very simplest ester!) was undertaken to study its NCE and to shine some light on the structure of liquid formic acid.

Resonance energy transfer not only causes a non-coincidence effect, it also affects the vibrational bandwidth. The bandwidth may be written as the sum of individual components (21):

$$\Gamma = \Gamma_{\phi} + \Gamma_{\pi} + 2\Gamma_{dd} \qquad [1]$$

where Γ_{dp} is the contribution from pure dephasing and Γ_{tr} is the dephasing contribution of RET . The third term arises from the "interference" of the first two and is only significant if the first two terms are of comparable magnitude and if there are statistical correlations between the processes. The sign of Γ_{dt} may be positive or negative, but this cannot be predicted from theory. Thus, depending on the sign, the band may be broadened or narrowed by resonant transfer. Therefore, dilution (which turns RET "off") can either broaden or narrow the band. If Γ_{dp} and Γ_{tr} are uncorrelated (i.e., $\Gamma_{dt} = 0$), then RET should always lead to band broadening.

Knapp (26), however, has argued that when resonant coupling is present, the band broadening or narrowing can be explained without considering the cross terms. The broadening or narrowing of bands is explained on the basis of the nature and rate of the fluctuations (of the molecule - bath interactions) that lead to dephasing. Knapp explained the effect on Raman band positions and widths from dephasing by using a model based on the concept of "reactive coupling" between an active site and a neighbouring site. The cross term, Γ_{dt}, was assumed to be zero. With this model "reactive coupling" is revealed by: a) a band shift to lower frequency (compared to the position at infinite dilution); b) asymmetry to the high frequency side of the isotropic band; c) broadening or narrowing of the band which depends on whether the fluctuations are rapid or slow compared with the "innate" vibrational dephasing rate. When the total amount of intersite coupling between the reference site and all other sites is varied (because of variations in diffusion

or molecular orientations), the presence of RET leads to a broadening of the band. If these variations are counteracted by other changes in the intersite interactions so that the total coupling is constant, RET will lead to a narrowing of the band. If this latter case is true, the removal of RET (by, for example, isotopic dilution) could lead to band broadening.

4.2 Experimental

The chemicals used in these experiments were: methyl formate, anhydrous, 99% (Aldrich), methyl d-formate, 99% (Cambridge Isotope Laboratories) and acetonitrile 99% (BDH). All the reagents were used without further purification. Methyl formate has a low boiling point, so it was kept refrigerated. Furthermore, to prevent decomposition or reaction with air, it was blanketed under argon.

Because of the small amount of available methyl d-formate, the solutions were made by successive dilution. 10 mL volumetric flasks were used. The required amount of methyl d-formate was measured with a graduated cylinder, added to the volumetric flask and its mass recorded. Methyl formate was then added to the mark and the solution weighed again. This solution then became the "stock" solution for the next highest concentration. Almost all of any given "stock" solution was used to prepare the next

concentration. Using this method, 12 solutions of methyl formate in methyl d-formate were prepared. The concentrations are given in Table 4.2.

Solutions of methyl formate in acetonitrile were prepared in much the same way as solutions of formic acid in acetonitrile (see section 3.2). Solutions were prepared in 25 mL volumetric flasks. The required volume of acetonitrile was pipetted using a Mohr pipette and the mass of the acetonitrile recorded. Methyl formate was added to the mark and its mass recorded. The acetonitrile was pipetted because the high volatility of methyl formate makes it difficult to pipette. The volumetric flasks were capped, wrapped with Parafilm and stored in a refrigerator. Nine solutions were prepared this way and the concentrations are given in Table 4.3.

A 5 mL glass syringe was used to fill the sample capillary tubes. For the solutions of methyl formate in acetonitrile there was sufficient solution to allow the rinsing of the syringe. However, for the methyl formate / methyl d-formate solutions this was not the case. For these solutions no rinsing was possible, so the syringe was dismantled and allowed to air dry. Because of the volatility of both species, this was judged to be adequate. Making a good seal on the capillary tube was essential to obtaining good spectra. Without a good seal, bubble formation (because of the high volatility of all the components) was a real problem. Additionally, allowing the sealed tubes to sit overnight seemed to alleviated this problem.

Table 4.2: Concentration Summary for MF / d-MF Solutions.

Solution	X(d-MF)	X(MF)
pure d-MF	1.000	0.000
RB951011A	0.885	0.115
RB951011B	0.766	0.234
RB950925A	0.643	0.357
RB951013B	0.559	0.441
RB951016A	0.496	0.504
RB951016B	0.443	0.557
RB950925D	0.393	0.607
RB951017A	0.342	0.658
RB950925E	0.299	0.701
RB951018A	0.239	0.761
RB950925F	0.221	0.779
RB950925G	0.116	0.884
pure MF	0.000	1.000

Table 4.3: Concentrations Summary for MF / Acetonitrile.

Solution	X(MF)	ϕ(MF)[a]
pure MF	1.00	1.00
RB950622A	0.899	0.910
RB950627A	0.799	0.820
RB950628A	0.699	0.727
RB950629A	0.594	0.627
RB950705A	0.494	0.528
RB950705B	0.434	0.467
RB950705C	0.296	0.325
RB950706A	0.199	0.221
RB950706B	0.095	0.107

a - volume fraction; see section 4.3.2.

All spectra were collected using the 514.5 nm line of an argon ion laser. The details of the spectrometer, laser, etc. are discussed in chapter 2. For the solutions of methyl formate in acetonitrile the laser power was 1.5 W. For the methyl formate / methyl d-formate solutions the power was reduced to 750 mW. Bubbles formed in the tube at higher laser powers. For all spectra, the mechanical slitwidth was set at 150 μm. Only the carbonyl region (1625 - 1825 cm^{-1}) was studied. All the spectra were recorded at 20°C. To collect the parallel and perpendicular spectra, a polarization analyzer was used. Details of this device are given in section 2.5. The orientations of the Polaroid film and the scrambler wedge were checked by running spectra of CCl_4 each day. The average values for the bands of CCl_4 were:

$$\rho_{218} = 0.782 \quad \rho_{314} = 0.774 \quad \rho_{459} = 0.022$$

which compare reasonably well to the theoretical values of 0.75, 0.75 and 0. These errors may arise from imperfections in the film, the wedge, or because the analyzer is not properly aligned with the slit and/or optic axis. Also, the theoretical values apply to isolated, non-interacting molecules.

4.3 Results and Discussion

Figure 4.1a shows a survey spectrum of methyl formate and assignments (taken form Harris (9)) are given in Table 4.4. The work presented in this chapter is concerned

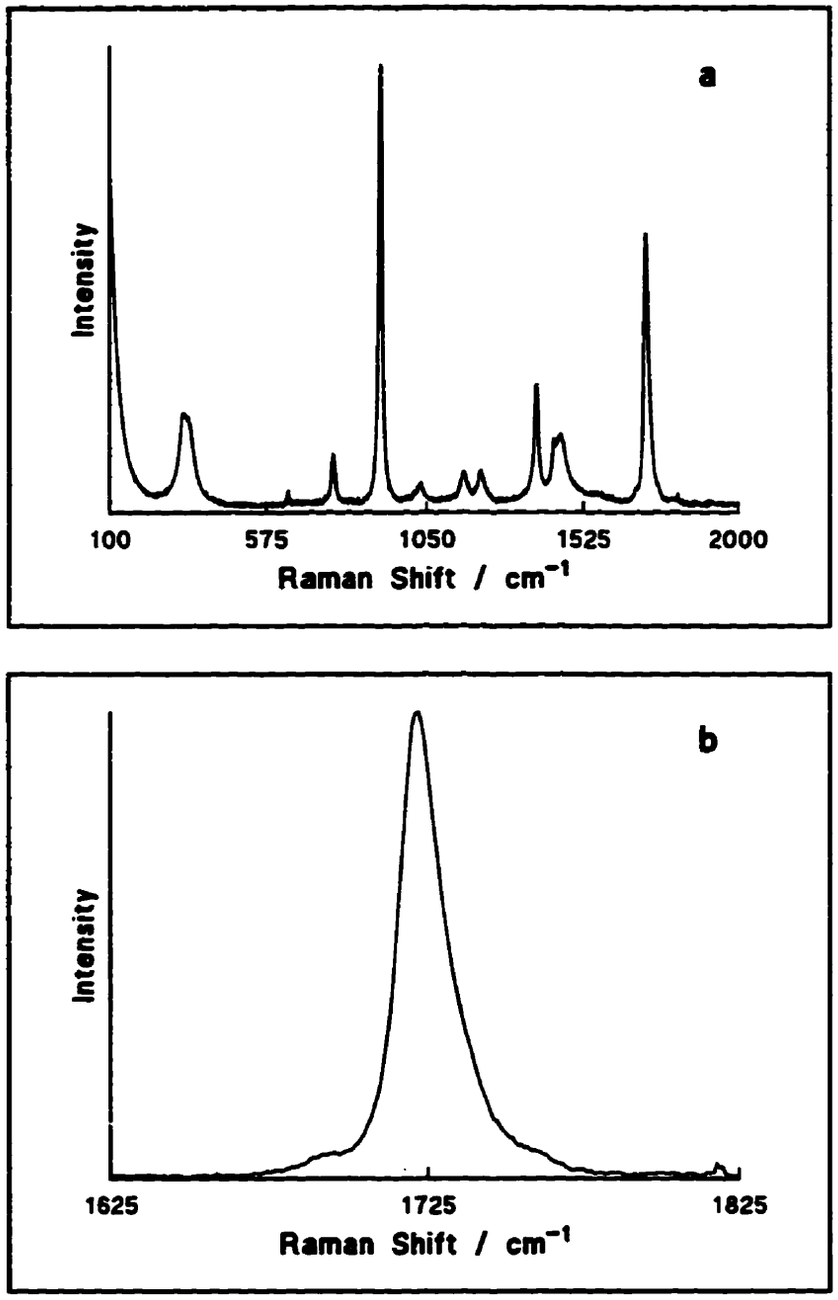

Fig. 4.1: a) Survey Spectrum of Methyl Formate
b) Carbonyl Region of Methyl Formate.

Table 4.4: Assignment of the Methyl Formate and Methyl d-Formate Spectra (2,9).

$HCOOCH_3$		$DCOOCH_3$	
Frequency / cm^{-1}	Assignment	Frequency / cm^{-1}	Assignment
3035	ν_1, CH_3 stretch	3038	ν_1, CH_3 stretch
2956	ν_2, ν_3, CH_3 and CH stretch	2958	ν_2, CH_3 stretch
1719	ν_4, C=O stretch	2223	ν_3, CD stretch
1454	ν_{14}, CH_3 deformation	1689	ν_4, C=O stretch
1434	ν_6, CH_3 deformation	1456	ν_{14}, CH_3 deformation
1379	ν_7, C-H in plane bend	1433	ν_6, CH_3 deformation
1211	ν_8, C-O stretch	1215	ν_8, C-O stretch
1162	ν_9, O-CH_3 in plane bend	1159	ν_9, O-CH_3 in plane bend
1030	ν_{16}, CH out of plane bend	1050	ν_7, C-D in plane bend
907	ν_{10}, O-CH_3 stretch	869	ν_{10}, O-CH_3 stretch
767	ν_{11}, O-C-O bend	849	ν_{16}, CD out of plane bend
338	ν_{17}, skeletal torsion	762	ν_{11}, O-C-O bend
323	ν_{12}, C-O-C bend	319	ν_{12}, ν_{17}, C-O-C bend skeletal torsion

exclusively with the behaviour of the carbonyl band at ~1720 cm^{-1}. This band is shown in more detail in Fig. 4.1b. Even a cursory look at the spectrum shows there are at least 3 bands in the carbonyl region: one strong, asymmetrical band at ~1720 cm^{-1} and two weak bands, one to higher frequency and one to lower frequency. Harris et al. (9) did not assign these bands. The bands are centred at ~1695 cm^{-1} and 1762 cm^{-1}. Byrne et al. (6) assigned a band at 1768 cm^{-1} to the C=O stretch of conformer II, but Harris assumed methyl formate to be entirely conformer I.

4.3.1 Methyl Formate / Methyl d-Formate

Raman spectra were recorded of 12 solutions of methyl formate (MF) in methyl d-formate (d-MF) plus pure MF and pure d-MF. As mentioned in the experimental section, the solutions were produced by successive dilution of the d-MF in methyl formate. The mole fractions of each solution are summarized in Table 4.2.

Figure 4.2 presents the isotropic and anisotropic spectra for pure MF and pure d-MF. The carbonyl band shifts from ~1720 cm^{-1} to ~1691 cm^{-1} with isotopic substitution. Unlike the MF, the d-MF has a prominent band ~1751 cm^{-1}. Harris (9) assigned this band to $2\nu_{10}$. Susi (5) observed similar spectral features with IR spectroscopy and suggested Fermi resonance was taking place.

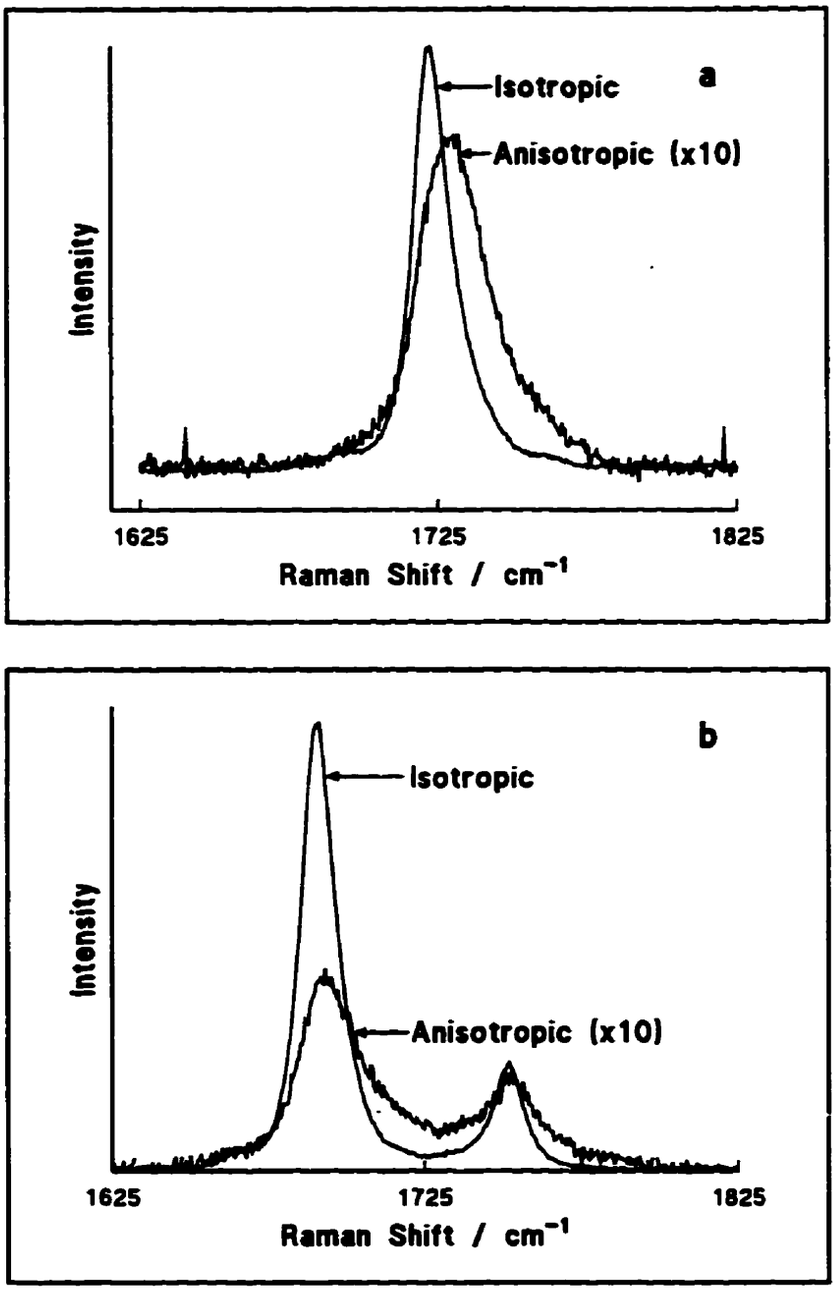

Fig. 4.2: Isotropic and Anisotropic Spectra:
a) Methyl Formate b) Methyl d-Formate.

Figure 4.3 shows the isotropic and anisotropic spectra of a solution of MF / d-MF (X(MF) = 0.504). Not unexpectedly, the carbonyl mode is strongly polarized. The band overlap of the carbonyl modes of the two isotopomers is significant but not severe. In order to study the behaviour of the spectral contour attributed to one or other of the isotopomers, the band parameters for the individual contours must be calculated. This was done by applying bandfitting (see section 2.6). The total contour was fitted with six bands. Then, the individual components of the C=O mode were added together to reconstruct the carbonyl contour of the isotopomer of interest. A comparison of the original spectrum and the reconstructed contour is shown in Fig. 4.4a and the individual band components for the complete contour are given in Fig. 4.4b. An example of the recombination procedure is shown for the C=O mode of MF (X(MF) = 0.504) in Fig. 4.5. The reconstructed contours were used for the subsequent data analysis.

The most obvious thing to extract from the re-constructed spectra is the position of the peak maximum in the isotropic and anisotropic spectra. The isotropic band is clearly asymmetric and more will be said about this later. The isotropic and anisotropic peak maxima (for MF) are summarized in Table 4.5. The isotropic band shows an obvious shift to higher frequency as the MF is diluted (see Fig. 4.6a). Yarwood (21) made the same observation for isotopic mixtures of N,N-dimethylformamide. In aqueous solutions of formic acid, a similar effect is seen. If a linear extrapolation is applied to the data an isotropic position of 1733 cm^{-1} is found at infinite dilution. Admittedly, no

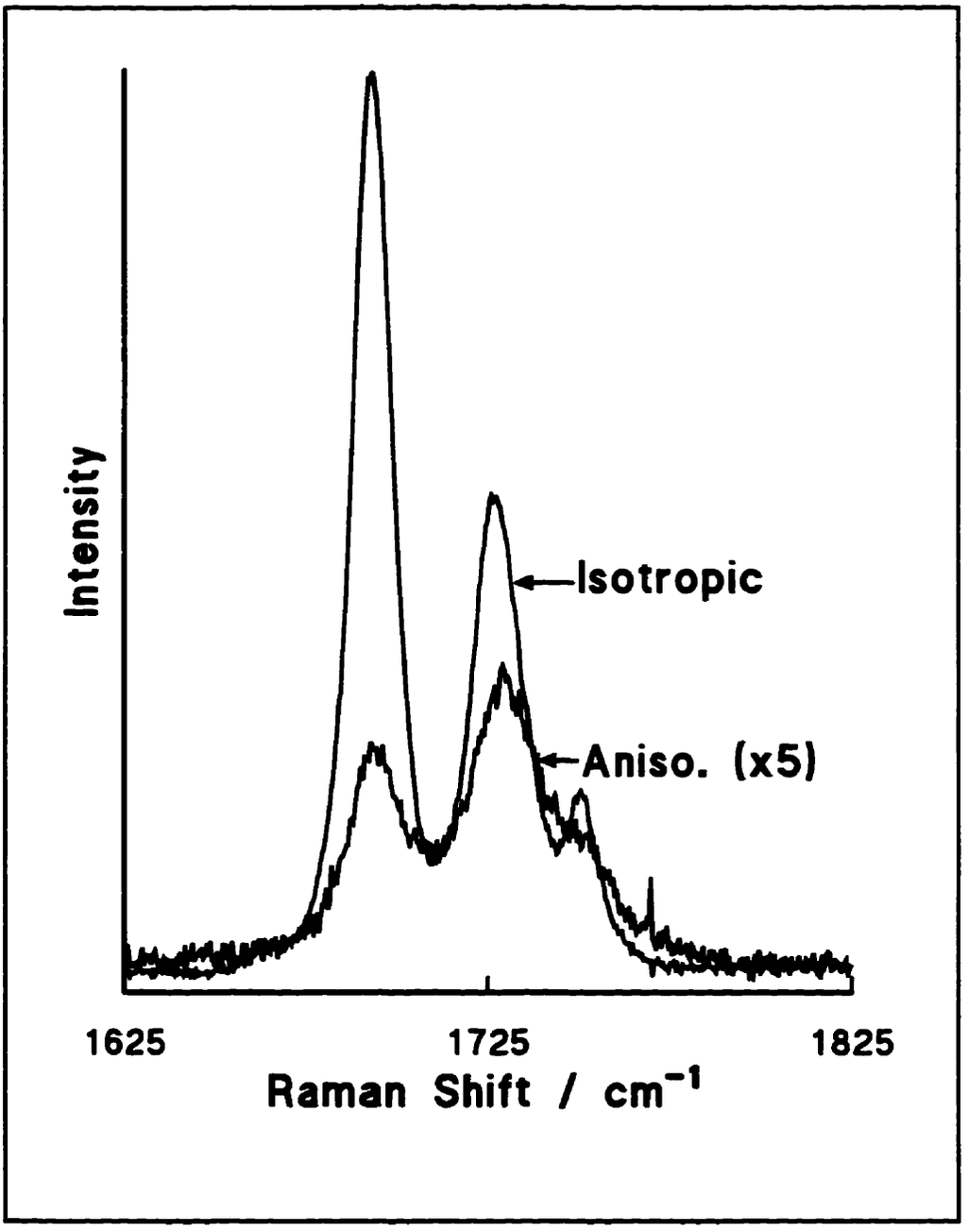

Fig. 4.3: Isotropic and Anisotropic Spectra of Methyl Formate / Methyl d-Formate (X(MF) = 0.504).

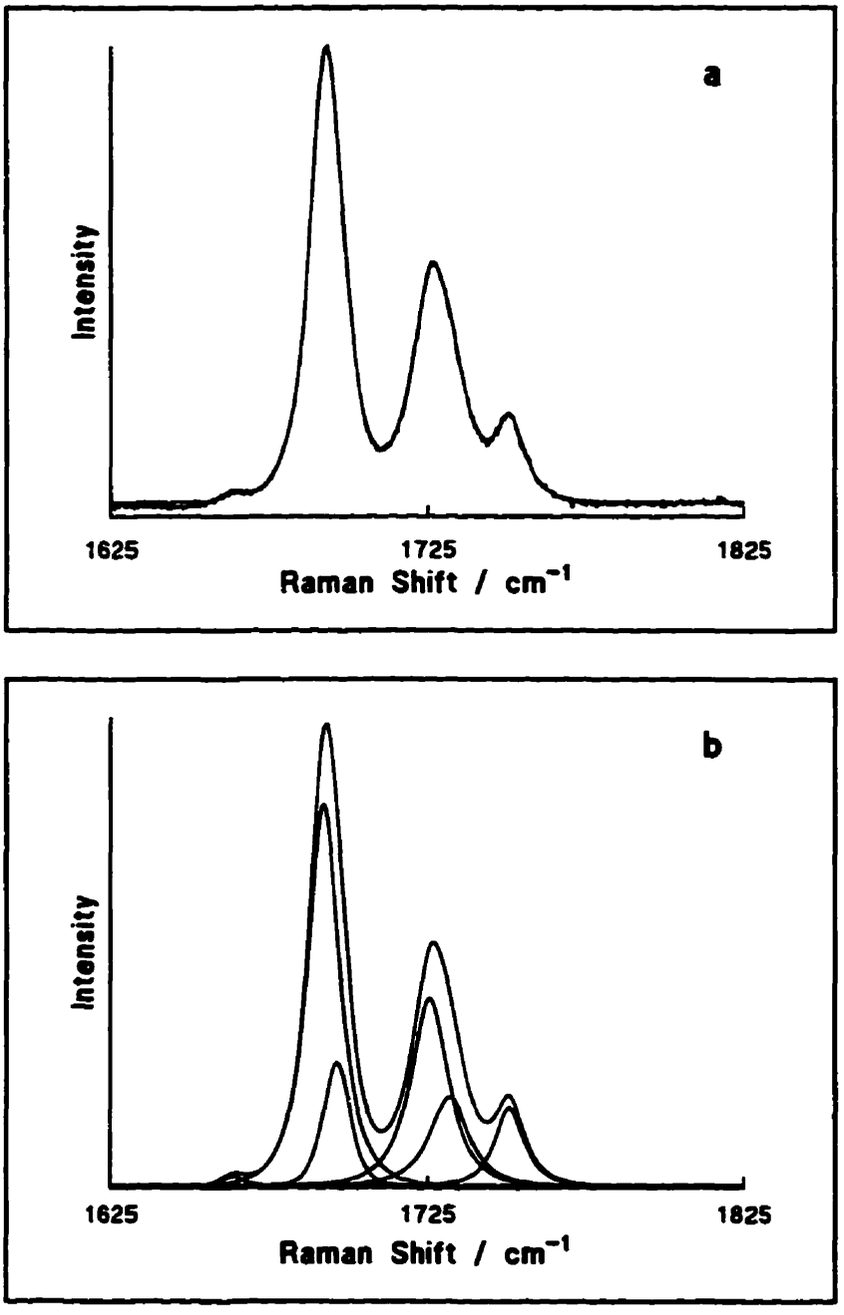

Fig. 4.4: Bandfitting Results for Methyl Formate / Methyl d-Formate (X(MF) = 0.504):
a) Overall Calculated Contour and Original Data
b) Overall Calculated Contour and Components.

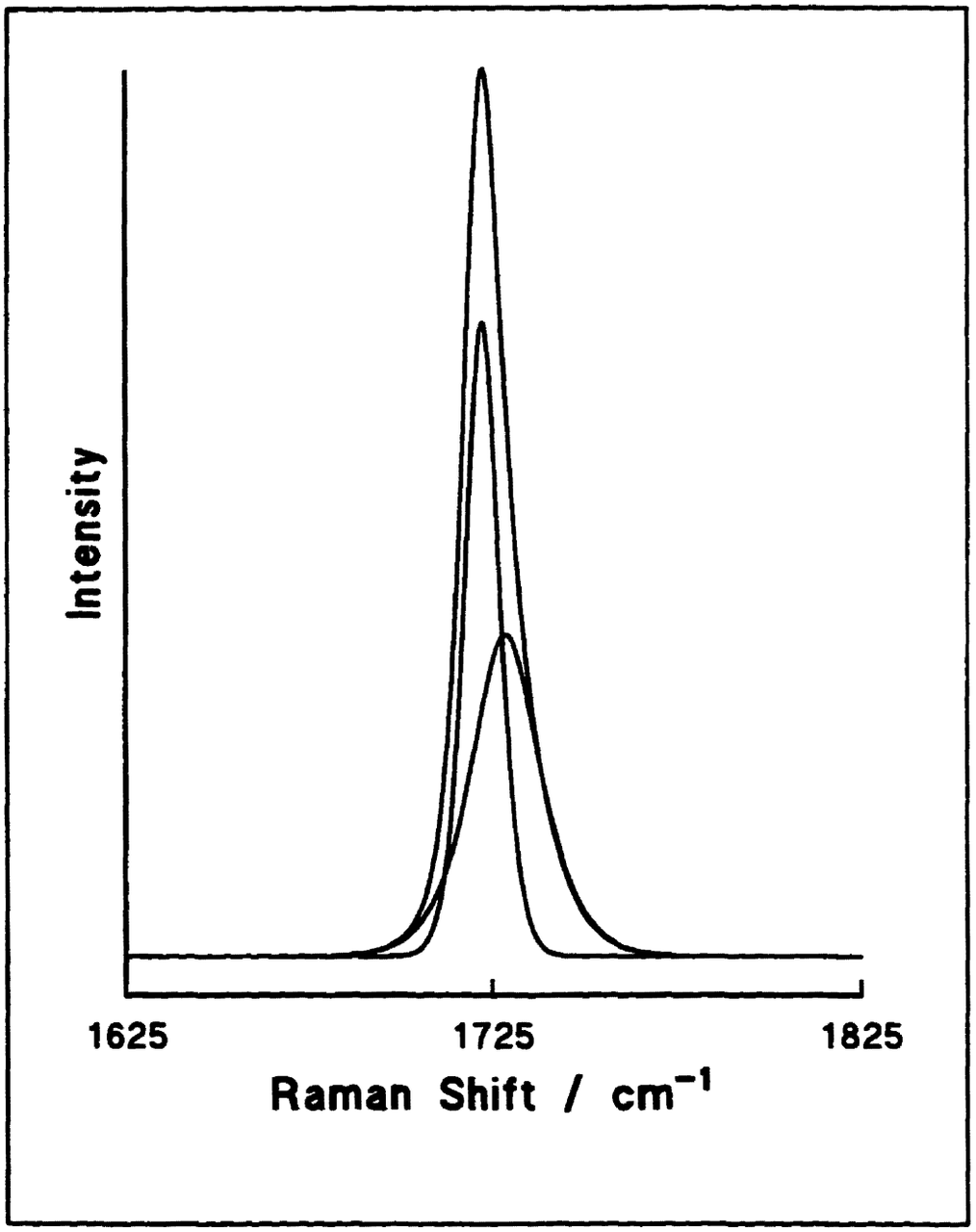

Fig. 4.5: Overall Calculated Contour and Component Bands for the Carbonyl Stretch of Methyl Formate / Methyl d-Formate (X(MF) = 0.504).

Table 4.5: Summary of the Band Positions for MF / d-MF.

X(MF)	$\nu_{iso.}$	$\nu_{aniso.}$	$\nu_{aniso.} - \nu_{iso.}$
0.115	$1731._9$	$1731._1$	$-0._8$
0.234	$1731._7$	$1731._9$	$0._2$
0.357	$1729._3$	$1730._1$	$0._8$
0.441	$1727._0$	$1729._0$	$2._0$
0.504	$1726._6$	$1730._2$	$3._6$
0.557	$1727._8$	$1731._5$	$3._7$
0.607	$1726._2$	$1730._3$	$4._1$
0.658	$1726._2$	$1730._7$	$4._5$
0.701	$1724._2$	$1729._0$	$4._8$
0.761	$1725._4$	$1730._8$	$5._4$
0.779	$1724._8$	$1729._9$	$5._1$
0.884	$1723._8$	$1729._1$	$5._4$
1.000	$1722._2$	$1729._1$	$7._0$

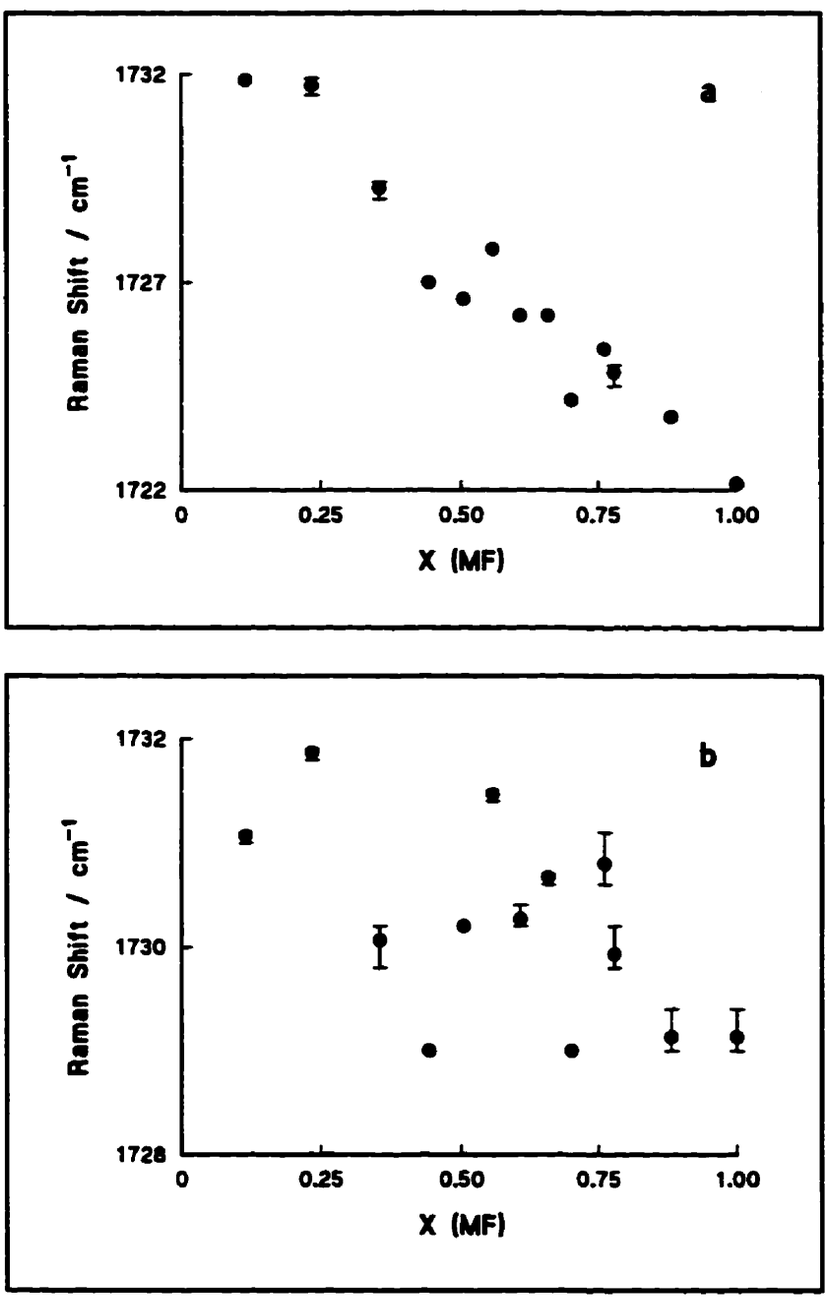

Fig. 4.6: Peak Positions for Methyl Formate / Methyl d-Formate: a) Isotropic b) Anisotropic.

theoretical basis exists for using a linear extrapolation on these data. However, the data do *suggest* a linear extrapolation is reasonable. The anisotropic peak data are not quite as "well behaved" (see Fig. 4.6b). Only the most optimistic eye would claim any definitive dependence on mole fraction. The (very) gross tendency, however, appears to be a slight shift to higher frequency as the MF becomes more dilute. This, too, is similar to the behaviour of formic acid (in water) where the anisotropic peak shifted, but only very slightly, to higher frequency. As an obvious consequence, the difference $\nu_{aniso.} - \nu_{iso.}$ (i.e., the NCE) decreases as the MF becomes more dilute. The differences are tabulated in Table 4.5 and plotted in Fig. 4.7. The plot shows the difference tends to zero (just as expected) as the concentration falls to zero.

A close look at the isotropic spectrum of MF shows the C=O band (at least in the reconstructed form, Fig. 4.5) is asymmetric on the "blue" side. Because of this asymmetry, Logan's theories (27,28) cannot be applied directly because the band maxima cannot be equated to the first moments. The band first moments, M, must be calculated and are given in Table 4.6. The more asymmetrical a band, the greater is the difference between the first moment and the band maximum. Figure 4.8 shows $M_{iso.} - \nu_{iso.}$ as a function of mole fraction of methyl formate. The isotropic band becomes more and more symmetrical as the methyl formate is progressively diluted. At fairly dilute (but non-zero) concentrations the difference is essentially zero indicating the band is symmetrical. More will be said below about this asymmetry.

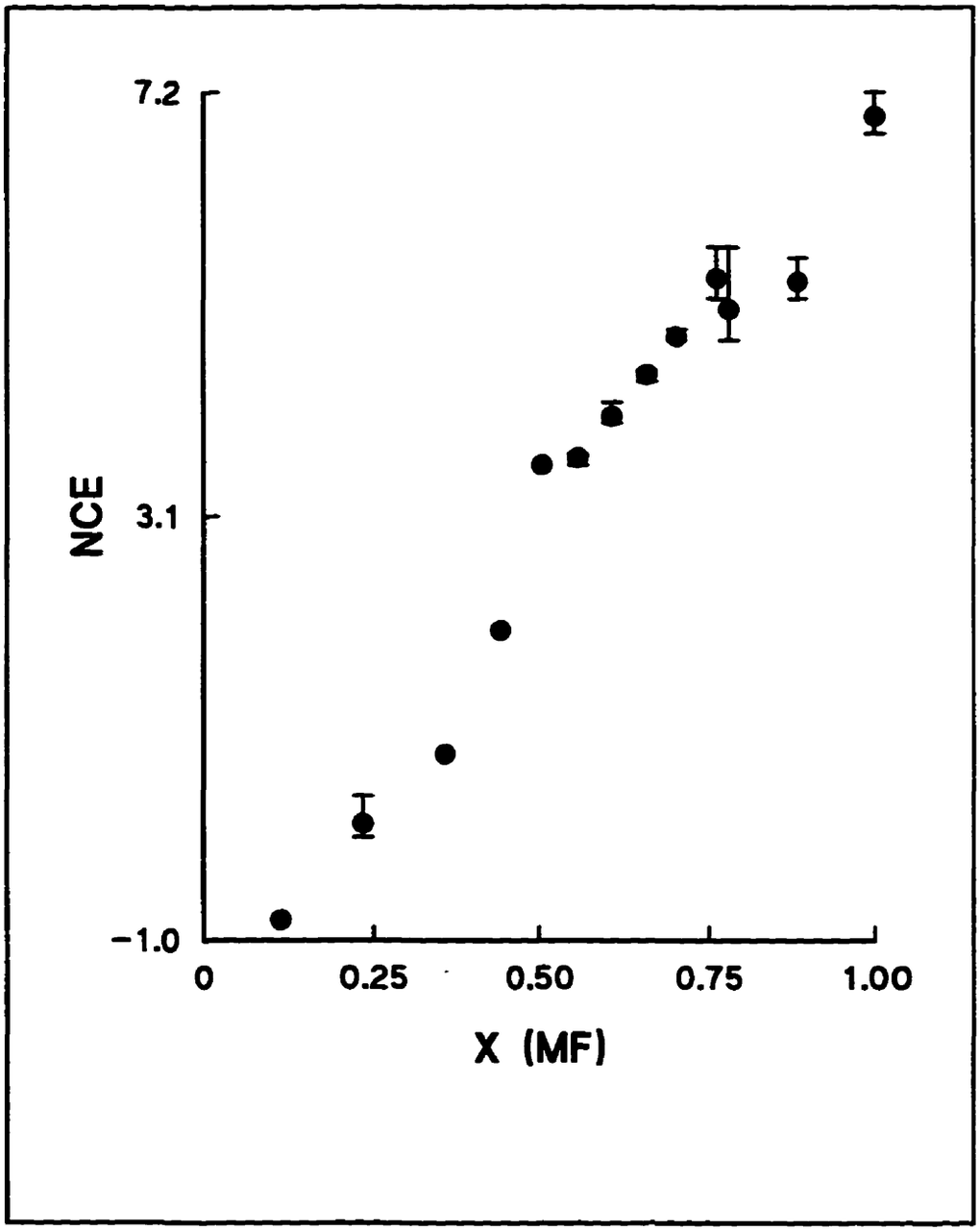

Fig. 4.7: Non-Coincidence Effect (= $\nu_{aniso.}$ - $\nu_{iso.}$) for Methyl Formate / Methyl d-Formate.

Table 4.6: Summary of the First Moments for MF / d-MF.

X(MF)	$M_{iso.}$	$M_{aniso.}$	$M_{aniso.} - M_{iso.}$
0.115	$1731._0$	$1731._2$	$0._2$
0.234	$1731._4$	$1731._6$	$0._2$
0.357	$1727._3$	$1730._3$	$3._0$
0.441	$1729._2$	$1730._1$	$0._9$
0.504	$1727._7$	$1729._0$	$1._3$
0.557	$1727._5$	$1730._5$	$3._0$
0.607	$1729._1$	$1731._5$	$2._4$
0.658	$1727._8$	$1730._8$	$3._0$
0.701	$1725._9$	$1729._0$	$3._1$
0.761	$1727._6$	$1730._8$	$3._2$
0.779	$1727._1$	$1730._1$	$3._0$
0.884	$1726._8$	$1729._3$	$2._5$
1.000	$1725._2$	$1729._3$	$4._1$

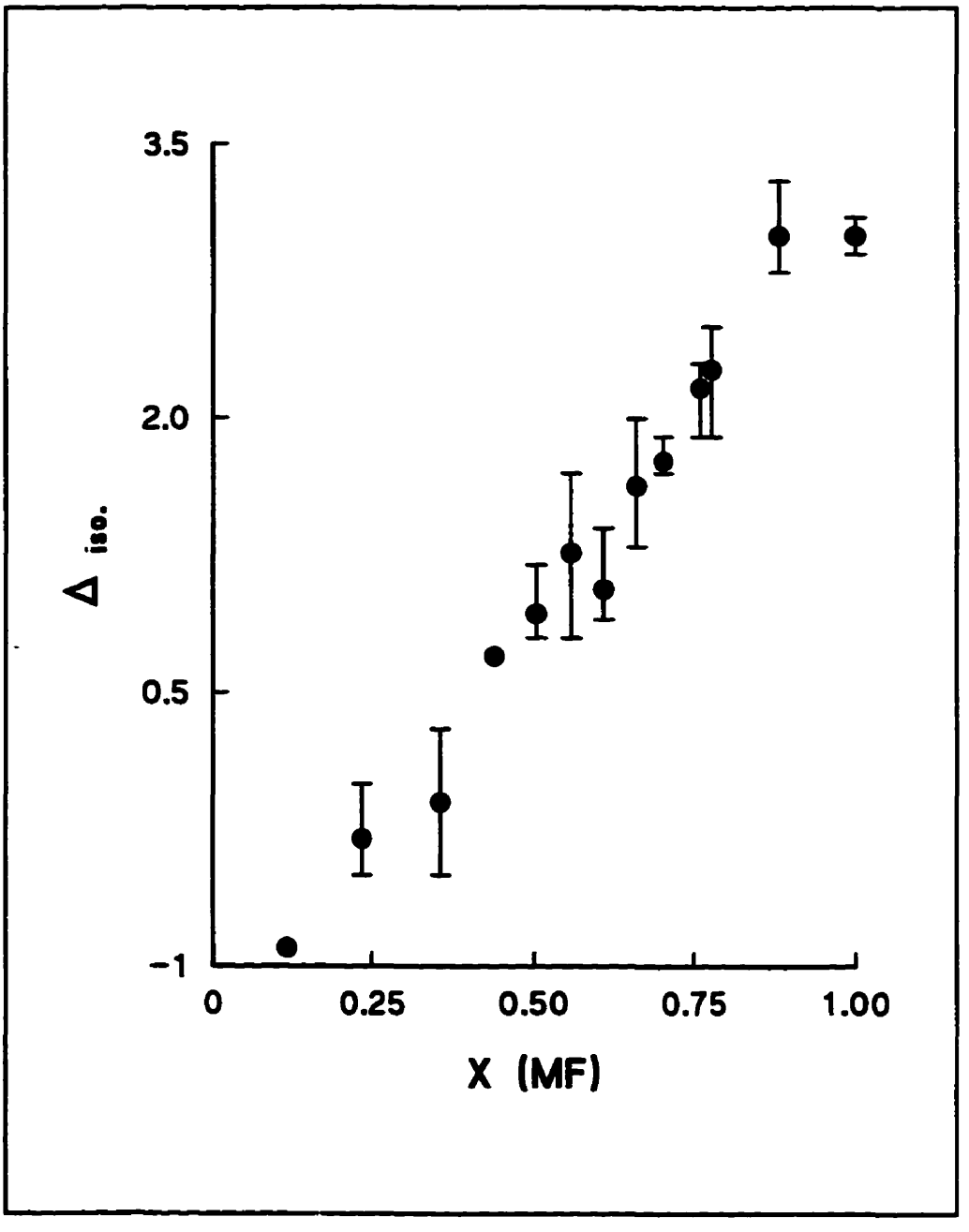

Fig. 4.8: $\Delta_{iso.}$ (= $M_{iso.}$ - $\nu_{iso.}$) vs. X(MF) for Methyl Formate / Methyl d-Formate.

For a simple isotopic dilution, Logan developed a model (27) (see section 1.3.4) to calculate the dependence of the NCE on mole fraction of the active species:

$$M_{aniso.} - M_{iso.} = \Delta_{neat} X \qquad [2]$$

where

$M_{aniso.}$	=	the anisotropic first moment
$M_{iso.}$	=	the isotropic first moment
Δ_{neat}	=	the splitting in the pure active species
X	=	mole fraction of the active species

A plot of $M_{aniso.}$ - $M_{iso.}$ versus X(MF) is given in Fig. 4.9. The splitting has a linear dependence on X(MF), but the correlation of the line is not very good. If the two points at X(MF) = 0.357 and X(MF) = 0.884 are neglected, the correlation is much improved (r = 0.939) and the equation of the line is given by:

$$M_{aniso.} - M_{iso.} = 5.1X - 0.658 \qquad [3]$$

In neat methyl formate the non-coincidence is 4.1 cm^{-1}. Within the confidence interval of the linear regression the slope is the same as Δ_{neat}. The intercept also lies within the confidence interval.

Lastly, the data show an important effect of dilution on the halfwidths of the bands. This is most pronounced for the isotropic band. Because it is asymmetric, the halfwidths at half height are different for the low ("red") frequency and high ("blue")

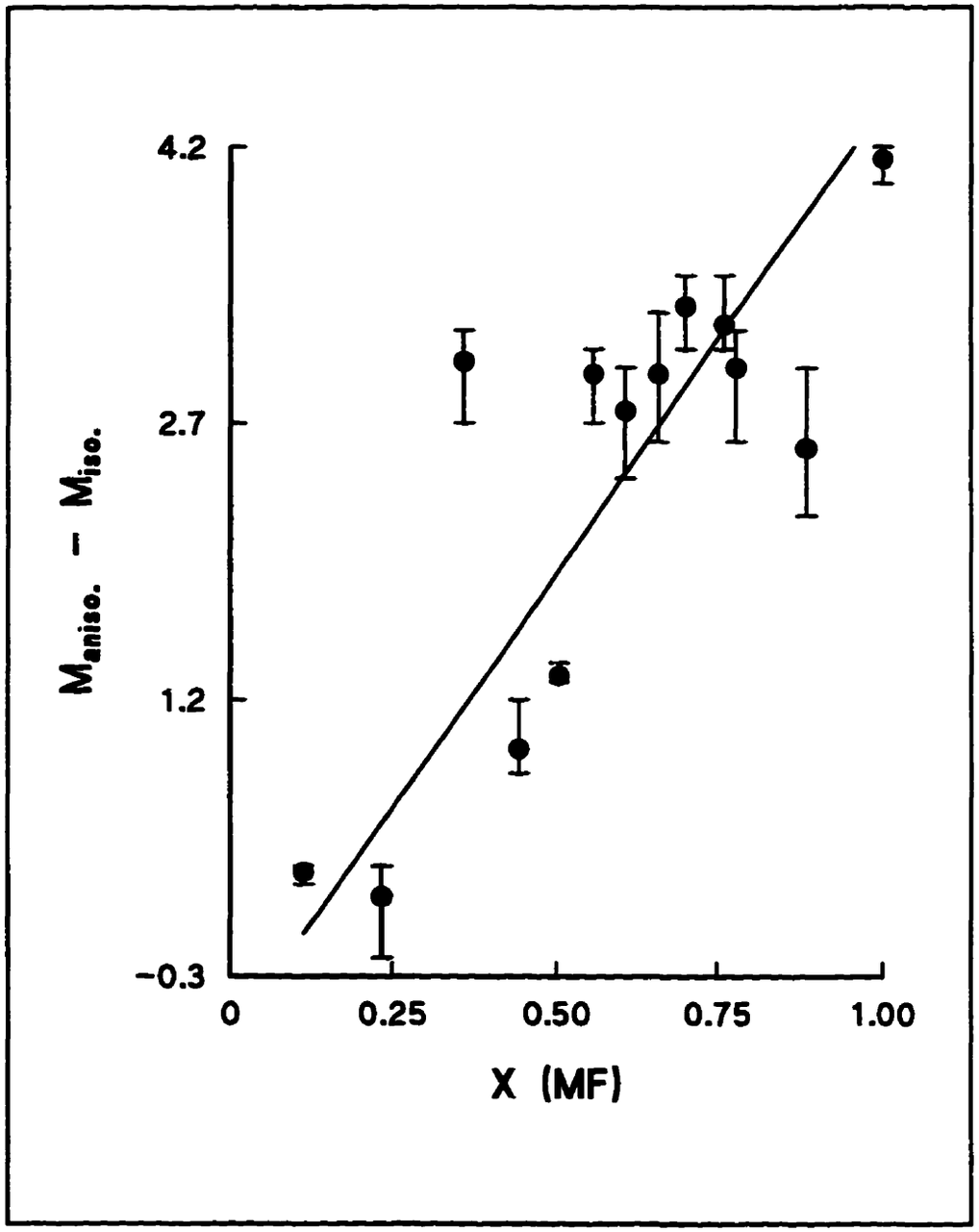

Fig. 4.9: Test of Logan's Model (26) for the NCE of Methyl Formate / Methyl d-Formate.

frequency sides of the band. Table 4.7 and Figure 4.10a show the variations of these two halfwidths as a function of mole fraction. At high MF concentrations the difference in the two values is quite large. As the MF is diluted, the high frequency halfwidth is virtually constant until X(MF)~0.5 at which point it falls dramatically. The low frequency halfwidth increases very slowly and then decreases slightly. The increase is only very slight and is surprising. Necessarily, then, the FWHM of the isotropic band initially increases as the MF is diluted. It rises to a maximum at X(MF)~0.5 and then falls quite steeply (Fig. 4.10b). An increase followed by a decrease in bandwidth is unusual. Normally, as the solute is diluted the resonance energy transfer becomes less and less effective because solute molecules in the solvation shell are replaced by solvent molecules. This should lead either to band broadening or narrowing, but not both.

The results for MF / d-MF can be summarized as follows. Firstly, the peak maximum of the isotropic band moves toward higher frequency as the MF is diluted. The data suggest a linear dependence. The anisotropic peak is not as definitive. Second, there is high frequency asymmetry on the isotropic band. The asymmetry decreases as the MF is diluted. Third, the NCE behaves just as predicted by Logan's model (27), i.e., it has a linear dependence on the mole fraction. Logan argued that RET was responsible for the NCE. Fourth, the FWHM of the isotropic band initially increases as the concentration decreases but falls dramatically for concentrations below X(MF)~0.5.

Table 4.7: HWHM's and FWHM's for MF / d-MF.

X(MF)	HWHM ("red") / cm^{-1}	HWHM ("blue") / cm^{-1}	FWHM / cm^{-1}
0.115	$7_{.3}$	$6_{.1}$	$13_{.4}$
0.234	$7_{.1}$	$6_{.4}$	$13_{.5}$
0.357	$7_{.9}$	$8_{.1}$	$16_{.0}$
0.441	$7_{.6}$	$8_{.9}$	$16_{.5}$
0.504	$7_{.5}$	$9_{.3}$	$16_{.8}$
0.557	$7_{.2}$	$9_{.3}$	$16_{.5}$
0.607	$7_{.2}$	$9_{.4}$	$16_{.6}$
0.658	$7_{.2}$	$9_{.3}$	$16_{.5}$
0.701	$6_{.9}$	$9_{.3}$	$16_{.2}$
0.761	$6_{.8}$	$9_{.3}$	$16_{.1}$
0.779	$6_{.6}$	$9_{.3}$	$15_{.9}$
0.884	$6_{.5}$	$9_{.3}$	$15_{.8}$
1.000	$6_{.4}$	$8_{.6}$	$15_{.0}$

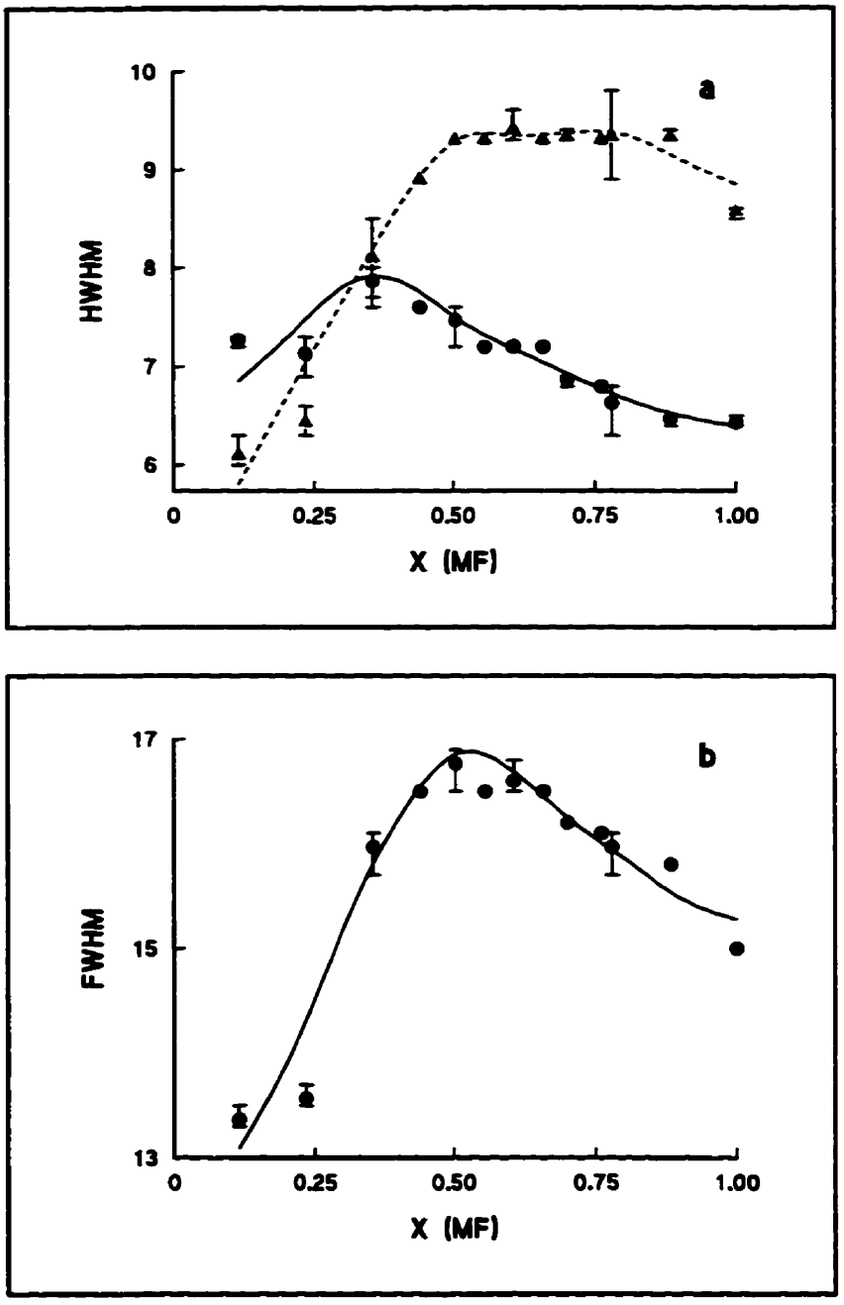

Fig. 4.10: Effect of Dilution on Bandwidth of Methyl Formate / Methyl d-Formate:
a) HWHM (solid line - low frequency HWHM, dashed line - high frequency HWHM) b) FWHM.

As mentioned above, the band of C=O in MF does show a shift to higher frequency with dilution and a very distinctive high frequency asymmetry. Under Knapp's (26) model this is evidence of reactive coupling in methyl formate. The loss of the asymmetry is also quite typical of this model. The behaviour of the FWHM of the isotropic band is rather unusual. Yarwood's (21) work on dimethyl formamide showed a steady increase in the HWHM as the dimethyl formamide was diluted. Yarwood argued this was consistent with Knapp's model because reactive coupling could lead to broadening or narrowing of the band with dilution. The behaviour of the FWHM does not conform with Knapp's model (26) for resonant coupling. At first it increases but then decreases having a fairly distinctive maximum at X(MF)~0.5. Clearly, this is not expected from Knapp's model. If the observation is real (as opposed to an artifact of bandfitting or experimental error), it implies a significant change in the nature of the intersite coupling. Initially (that is, for solutions concentrated in MF), the amount of coupling at a given reference site remains fixed. This leads to band broadening as the MF is diluted. At X(MF)~0.5 the amount of coupling is no longer fixed. Diffusional and re-orientational effects (as well as any other phenomena affecting the total amount of coupling) then cause variations in the total amount of vibrational coupling. As this happens, the band begins to narrow with dilution. An alternative explanation exists. Knapp's model is predicated on the assumption that the pure dephasing and the RET contributions to vibrational dephasing are uncorrelated (i.e., Γ_{dt} of equation [1] = 0). If Γ_{dt} is not zero, the band may be broadened or narrowed with dilution depending on the

sign of Γ_{dt}. For the methyl formate system these two dephasing mechanisms may, indeed, be correlated and the sign of Γ_{dt} may change with dilution.

So far the emphasis has been very much on the behaviour of the C=O band of methyl formate. The obvious question to ask, then, is, "what about the C=O band of methyl d-formate?". This band is centred at about 1690 cm^{-1} in pure d-MF (Fig. 4.2b) but with dilution shows a small shift to ~1698 cm^{-1} at X(d-MF) = 0.116. In pure d-MF the NCE is much smaller (~2.4 cm^{-1}) than in pure MF (~7.0 cm^{-1}). Yarwood's (21) results for dimethyl formamide showed the NCE for the two isotopomers to be nearly identical. Furthermore, unlike pure MF, the isotropic band of d-MF does not appear to have any high frequency asymmetry. However, a possible complication exists. Harris et al. (9) assigned the band at ~1751 cm^{-1} to $2\nu_{10}$. It has rather high intensity for an overtone band and this raises a question about the possibility of Fermi resonance with the C=O fundamental. Susi (5) assigned two bands at 1712 cm^{-1} and 1751 cm^{-1} (from infrared spectroscopy) to C=O stretching in Fermi resonance with a combination band (1441 + 304 cm^{-1}). Fermi resonance, of course, affects the intensities and frequencies of the bands involved. If Fermi resonance is occurring, any attempt to study the NCE of the C=O band is futile. For this reason, a detailed investigation of the C=O band of d-MF was not performed.

4.3.2 Solutions of Methyl Formate / Acetonitrile

The advantage of using acetonitrile as a solvent is that it has no bands which overlap those of the carbonyl region of methyl formate. This makes band resolution and reconstruction that much easier (see Fig. 4.11). Unfortunately, using non-isotopic dilution leads to greater theoretical complexity (27-30,33). Certain assumptions can no longer be made. That being said, the results for solutions of methyl formate in acetonitrile are qualitatively quite similar to those seen for MF / d-MF.

Ten solutions of methyl formate in acetonitrile were prepared and the concentrations are summarized in Table 4.3.

The dependences of the isotropic and anisotropic band positions on mole fraction are illustrated in Table 4.8 and Fig. 4.12. Qualitatively, the dependences are very similar to those seen in the isotopic dilution. The isotropic band position depends much more strongly on the mole fraction than the anisotropic band. For the isotopic dilution, a linear extrapolation gives an isotropic band position of 1733 ± 1.3 cm^{-1} at infinite dilution compared to 1730 ± 0.91 cm^{-1} in acetonitrile. When the statistical error limits are considered, these two values are virtually the same. The correlation of the line is not as good for the isotopic dilution and this is probably a result of greater bandfitting uncertainty. The dependence of the isotropic band position on mole fraction (i.e., the

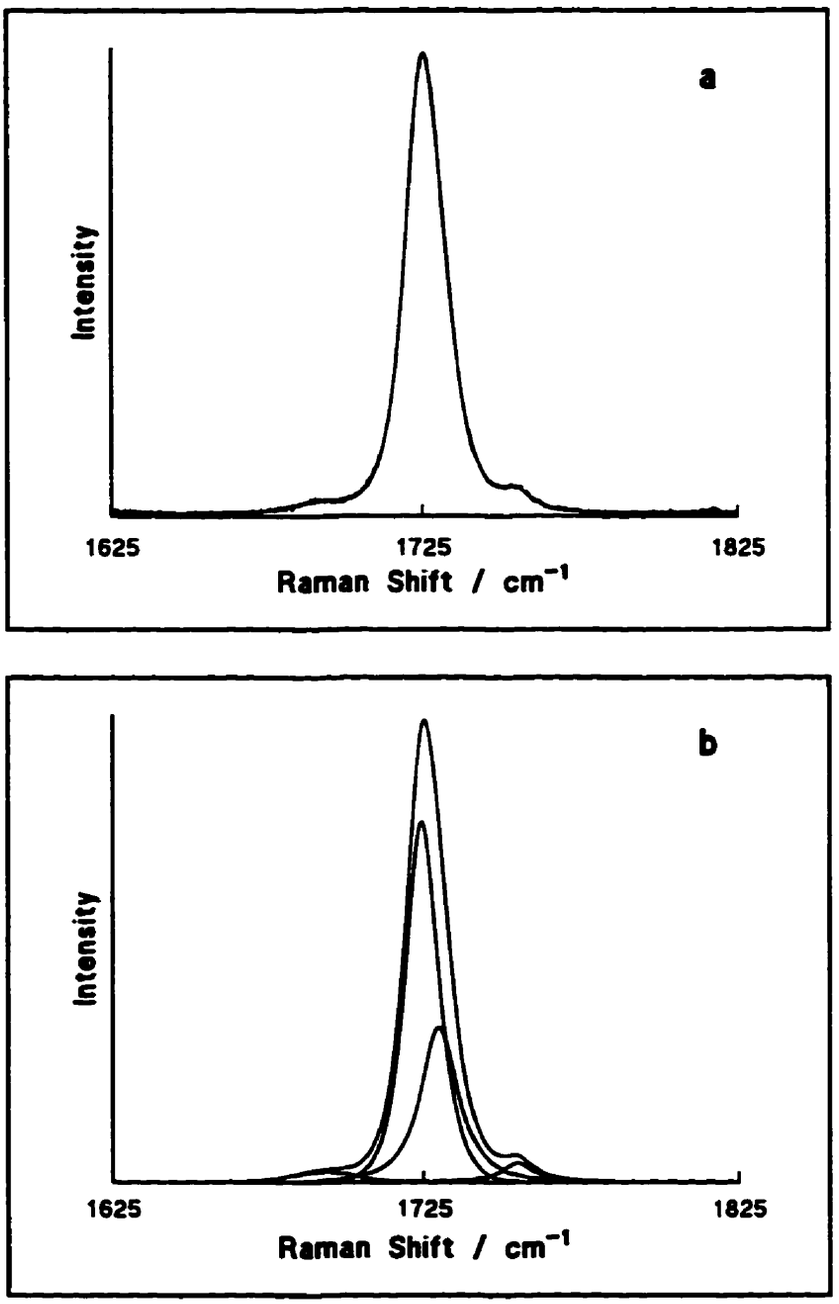

Fig. 4.11: Bandfitting in the Carbonyl Region of Methyl Formate / Acetonitrile (X(MF) = 0.494):
a) Overall Calculated Contour and Original Data
b) Overall Calculated Contour and Components.

Table 4.8: Summary of the Band Positions, NCE's and Relative NCE's for MF / Acetonitrile.

X(MF)	ϕ(MF)	$\nu_{iso.}$ / cm^{-1}	$\nu_{aniso.}$ / cm^{-1}	NCE / cm^{-1}	Rel. NCE
0.095	0.107	$1729._{-2}$	$1729._{-5}$	$0._{-3}$	0.05
0.199	0.221	$1728._{0}$	$1729._{-1}$	$1._{-1}$	0.16
0.296	0.325	$1727._{0}$	$1727._{-9}$	$0._{-9}$	0.14
0.434	0.467	$1726._{-2}$	$1729._{-8}$	$3._{-6}$	0.56
0.494	0.528	$1725._{-3}$	$1727._{-9}$	$2._{-6}$	0.40
0.594	0.627	$1724._{-9}$	$1728._{-2}$	$3._{-3}$	0.51
0.699	0.727	$1723._{-2}$	$1727._{-6}$	$4._{-4}$	0.67
0.799	0.820	$1722._{-5}$	$1727._{-3}$	$4._{-8}$	0.73
0.899	0.910	$1719._{-8}$	$1726._{-1}$	$6._{-3}$	0.96
1.00	1.00	$1719._{-4}$	$1725._{-9}$	$6._{-5}$	1.0

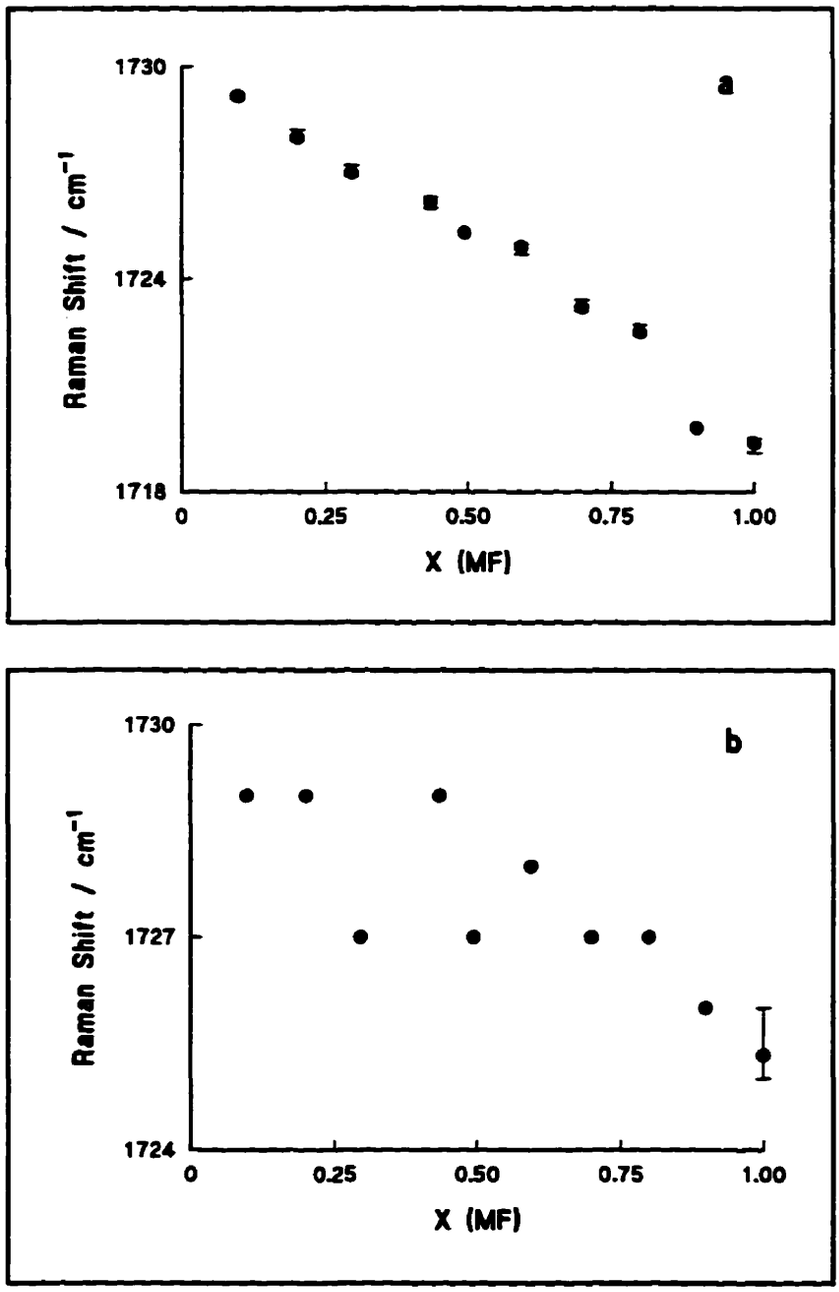

Fig. 4.12: Carbonyl Band Positions for Methyl Formate / Acetonitrile: a) Isotropic b) Anistropic.

slope of the line) is virtually the same for both the isotopic and non-isotopic dilutions. As with the solutions in d-MF, the NCE ($\nu_{aniso.} - \nu_{iso.}$) decreases as the MF is diluted (see Fig. 4.13). The RET is being "turned off" just as it was in the isotopic dilutions. However, the NCE disappears "faster" in the isotopic dilution. Imposing a linear fit on the data gives a slope of 8.9 ± 1.2 for the isotopic dilution but only 7.0 ± 1.4 for dilution in acetonitrile. Considering the error limits, however, these values are the same. This is an unfortunate result of the poor correlations on the lines. It seems reasonable to posit that the NCE decreases more rapidly with isotopic dilution than with non-isotopic dilution. The implication then becomes that RET is reduced / eliminated "quicker" (with respect to concentration) by isotopic dilution, for which solvent molecules are more similar in size and mass.

The ability of several models (presented in chapter 1) to describe the dependence of the NCE of MF on concentration was tested. To begin, however, the "relative splitting" must be defined. This quantity is given by:

$$\frac{\Delta(\phi)}{\Delta(\phi = 1)} \qquad [4]$$

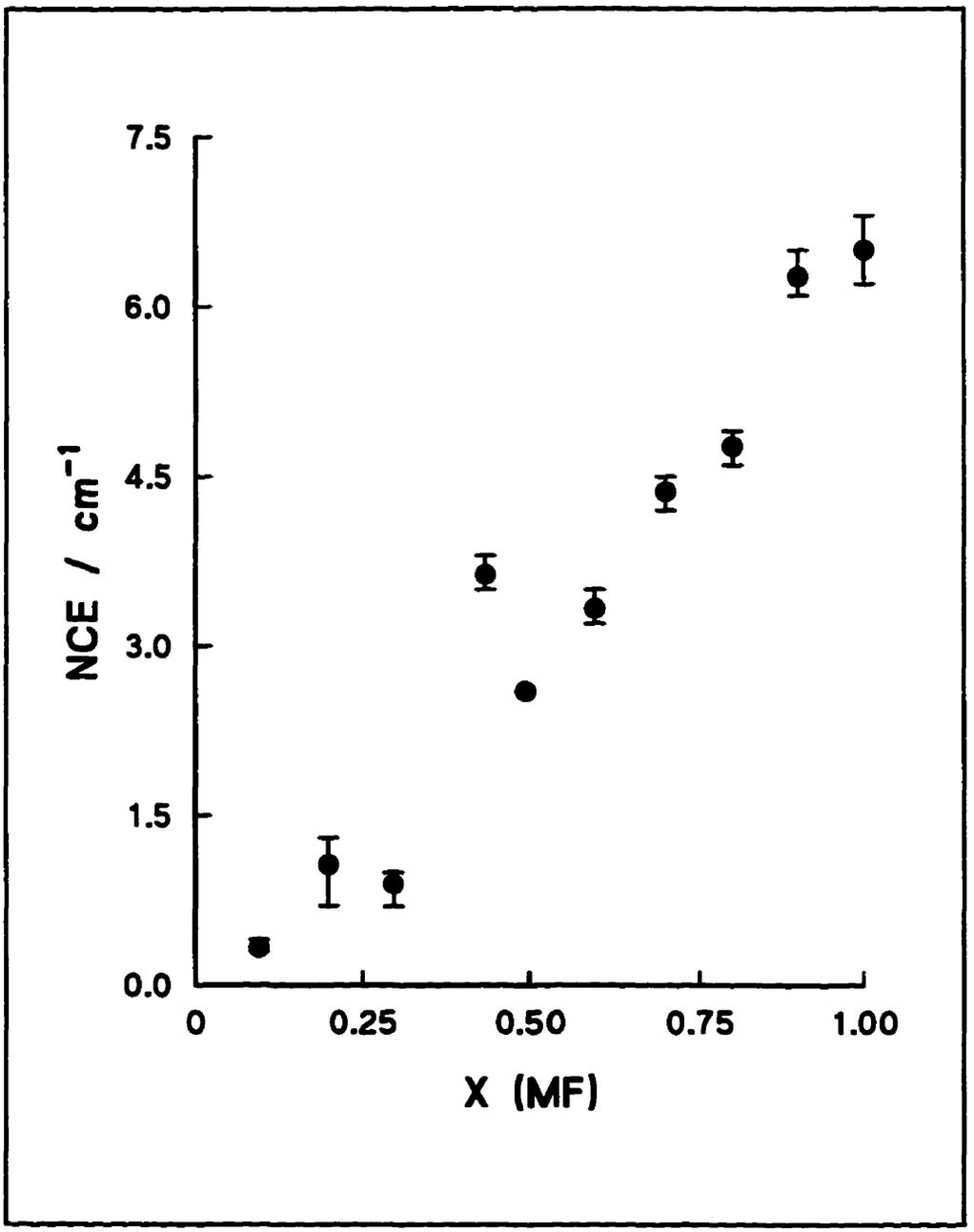

Fig. 4.13: NCE (= $\nu_{aniso.}$ - $\nu_{iso.}$) for Methyl Formate / Acetonitrile vs. Mole Fraction.

where

$\Delta(\phi)$	=	the splitting at a given volume fraction
$\Delta(\phi = 1)$	=	the splitting for the pure solute

All the models are based on using volume fraction as the concentration scale. This is to take advantage of the assumption that the dielectric constant can be written as a simple linear function of the concentration of the solute:

$$\epsilon = \epsilon_1(1-\phi) + \epsilon_2\phi \qquad [5]$$

where

ε_1	=	dielectric constant of the solvent
ε_2	=	dielectric constant of the solute
ϕ	=	volume fraction of the solute

All the models have also assumed ideal solutions (31). Therefore, all the concentrations on a mole fraction scale are easily converted to volume fractions using the densities of the solute and solvent. This conversion is given in Table 4.3. Obviously, the dielectric constants must also be known. The solutions were run at 20°C and at this temperature the dielectric constant of acetonitrile is 36.94 (32) and of methyl formate is 8.5 (1). The models of Fini and Mirone (15-17), McHale (29,30) and Mirone's modification (33) of McHale's model were examined. Logan's model (28) for non-isotopic dilution was not tested. This model assumes the hard sphere diameters of the solute and solvent are within 10%. Without knowing the hard sphere diameters, examining his model is pointless.

Fini and Mirone's model (15-17), an empirical derivation, gives the following dependence of splitting on volume fraction:

$$\Delta\nu = \Delta\nu_{max} \frac{\epsilon_2}{1-\phi_0} \frac{\phi-\phi_0}{\epsilon_2\phi+\epsilon_1(1-\phi)} \qquad [6]$$

for $\phi > \phi_0$

$$\Delta\nu = 0 \qquad [7]$$

for $\phi < \phi_0$

where $\phi$is some "threshold volume" below which there is no NCE. The first thing to do, then, is determine the threshold volume for MF / acetonitrile. The plot of $\Delta\nu$ versus ϕ (MF) was extrapolated using a linear fit to obtain ϕ_0 (see Fig. 4.14). The equation of the line is given by:

$$\Delta\nu = 7.07\ \phi - 0.678 \qquad r = 0.971$$

from which $\phi_0 = 0.096$. If the point at $\phi = 0.467$ (which appears to be anomalous, see Fig. 4.13) is neglected, the equation becomes:

$$\Delta\nu = 7.22\ \phi - 0.878 \qquad r = 0.985$$

and $\phi_0 = 0.122$. Figure 4.15 gives a comparison of the observed splitting and the splitting predicted by Fini and Mirone's model. Three predicted curves corresponding to $\phi_0 = 0$, 0.096 and 0.122 are plotted. The model fails badly. Other workers have found a fairly good agreement between their work and the model (18,20). In the examples given in Fini and Mirone's own paper (16), the dielectric constant of the solute was generally high

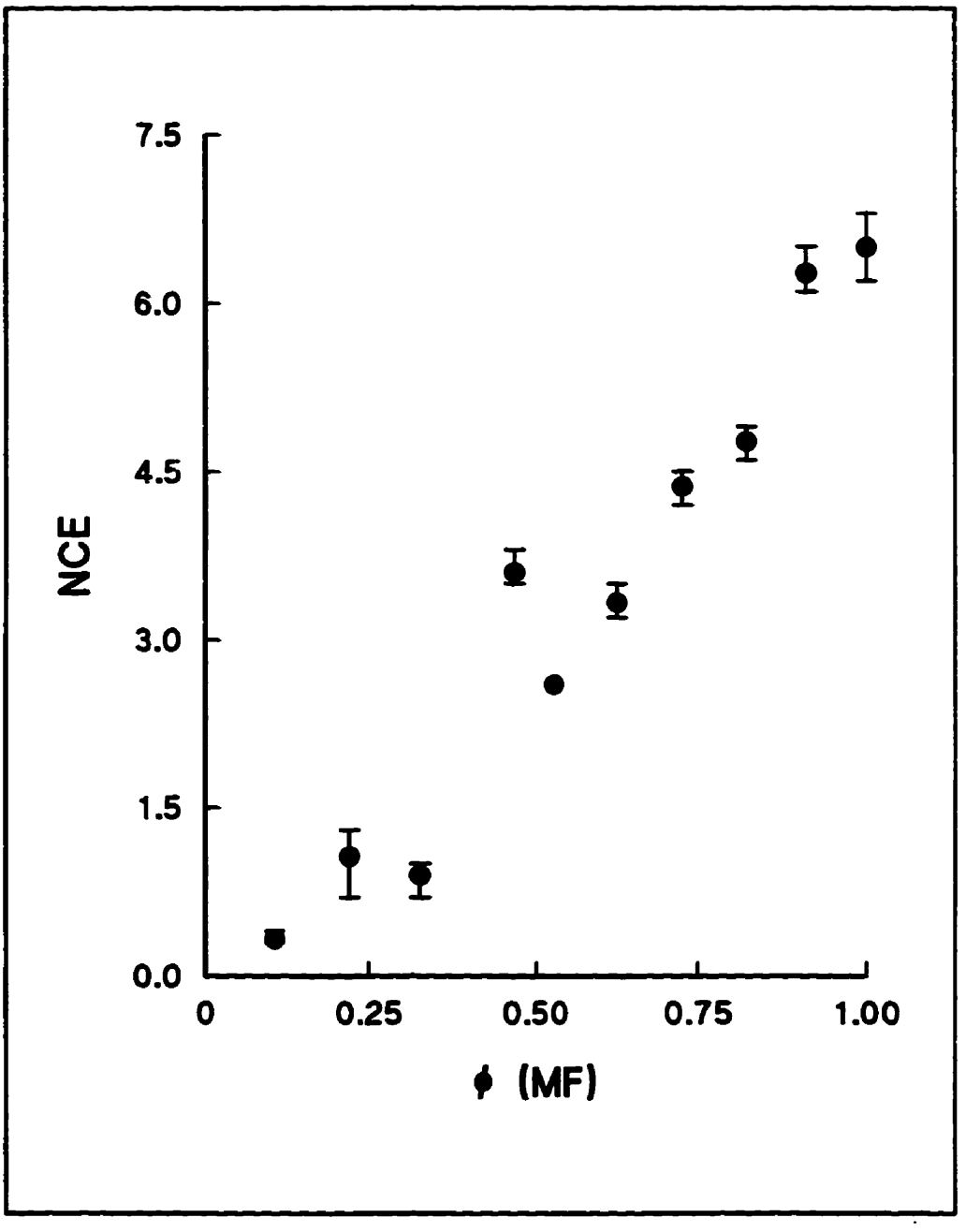

Fig. 4.14: NCE (= $\nu_{aniso.}$ - $\nu_{iso.}$) of Methyl Formate / Acetonitrile vs. Volume Fraction.

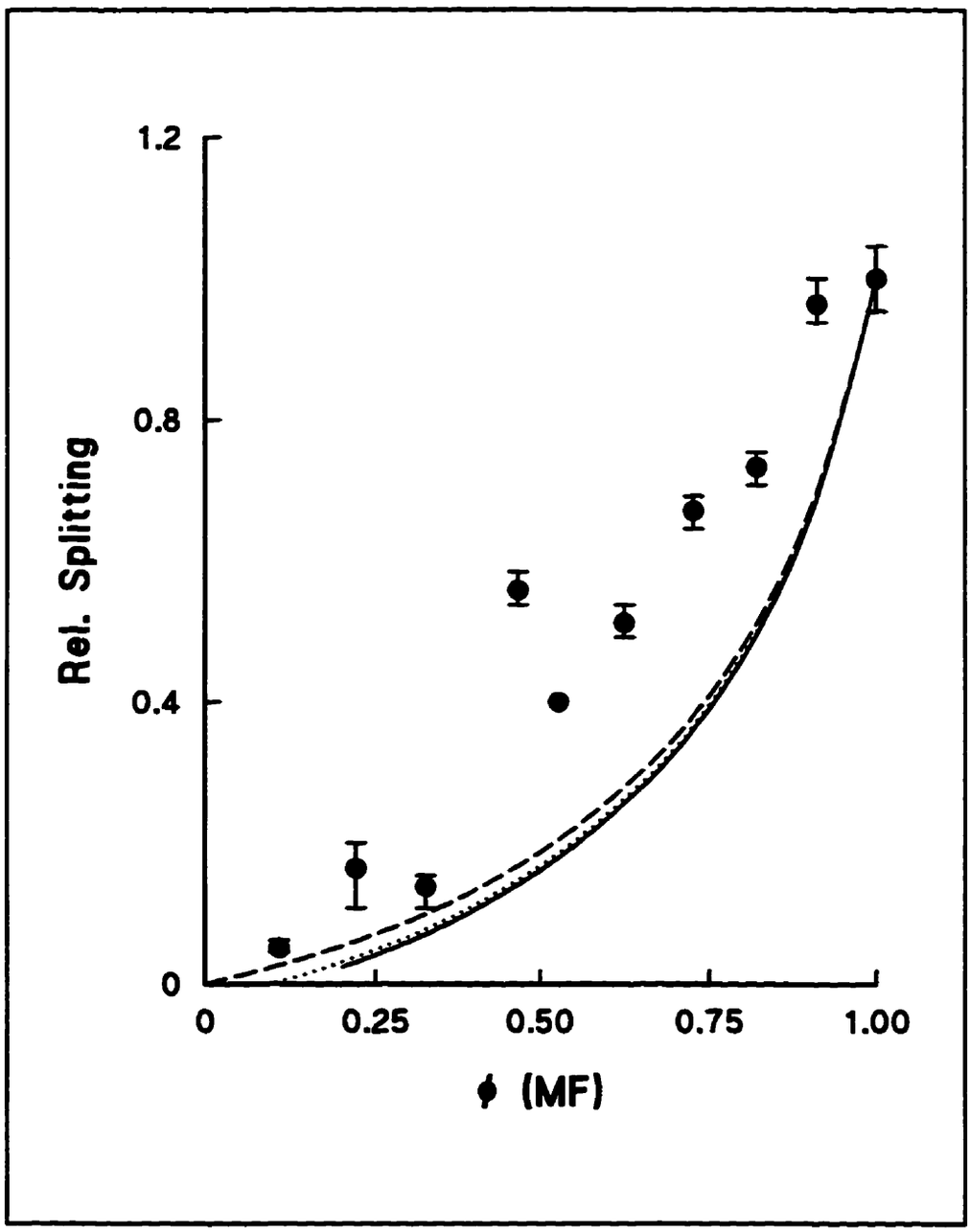

Fig. 4.15: Test of Fini and Mirone's Model (15-17) for the NCE of Methyl Formate in Acetonitrile:
Dashed Line: $\phi_0 = 0$; Dotted Line: $\phi_0 = 0.096$;
Solid Line: $\phi_0 = 0.122$.

of the solvent and several times the solvent was non-polar. Here, both the solute (MF) and the solvent (acetonitrile) are quite polar and the dielectric constant of MF is quite low relative to that of acetonitrile. Furthermore, the assumption of ideal solutions is suspect. To assume two liquids as polar as these two do not interact is probably not valid.

Figure 4.16 shows the theory of McHale (29,30) and Fig. 4.17 shows Mirone's modification (33) of McHale's theory. As an aside, Mirone's modification requires knowledge of the index of refraction of the solution. McHale's theory gives:

$$\frac{\Delta M}{\Delta M_{neat}} = \frac{\phi}{(\phi(1-x) + x)^2} \qquad [8]$$

$$x = \frac{\epsilon_1}{\epsilon_2} \qquad [9]$$

where

ΔM = the difference in the band first moments: $M_{aniso.} - M_{iso.}$

ΔM_{neat} = $M_{aniso.} - M_{iso.}$ for the pure liquid.

(see equations [33] - [35] of chapter 1). These values for methyl formate are summarized in Table 4.9. Mirone modified this equation to give

$$\frac{\Delta M}{\Delta M_{neat}} = \frac{1}{C}\left(\frac{n^2 + 2}{2\epsilon + n^2}\right)^2 \epsilon\, \phi \qquad [10]$$

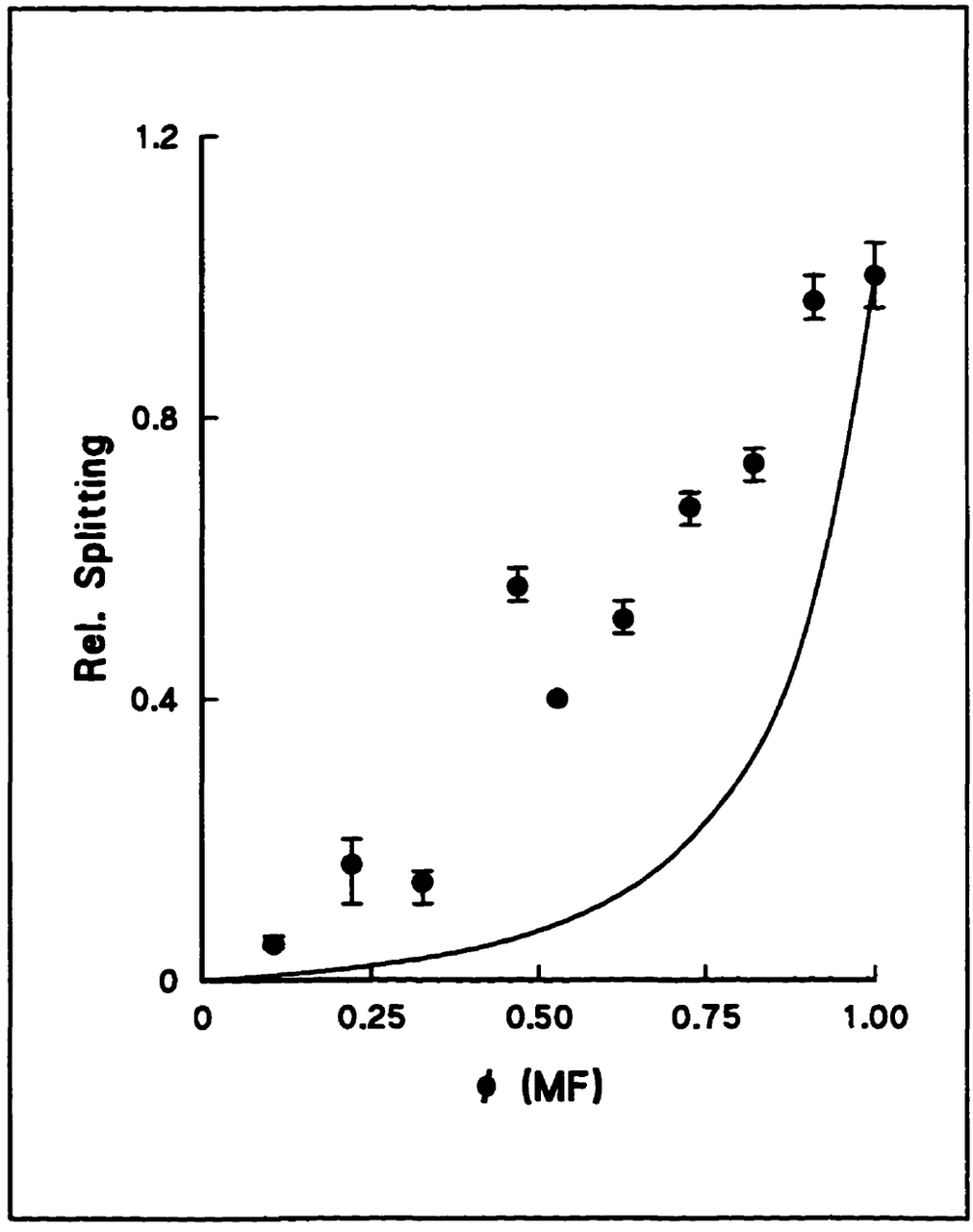

Fig. 4.16: Test of McHale's Model (29,30) of the NCE for Methyl Formate / Acetonitrile.

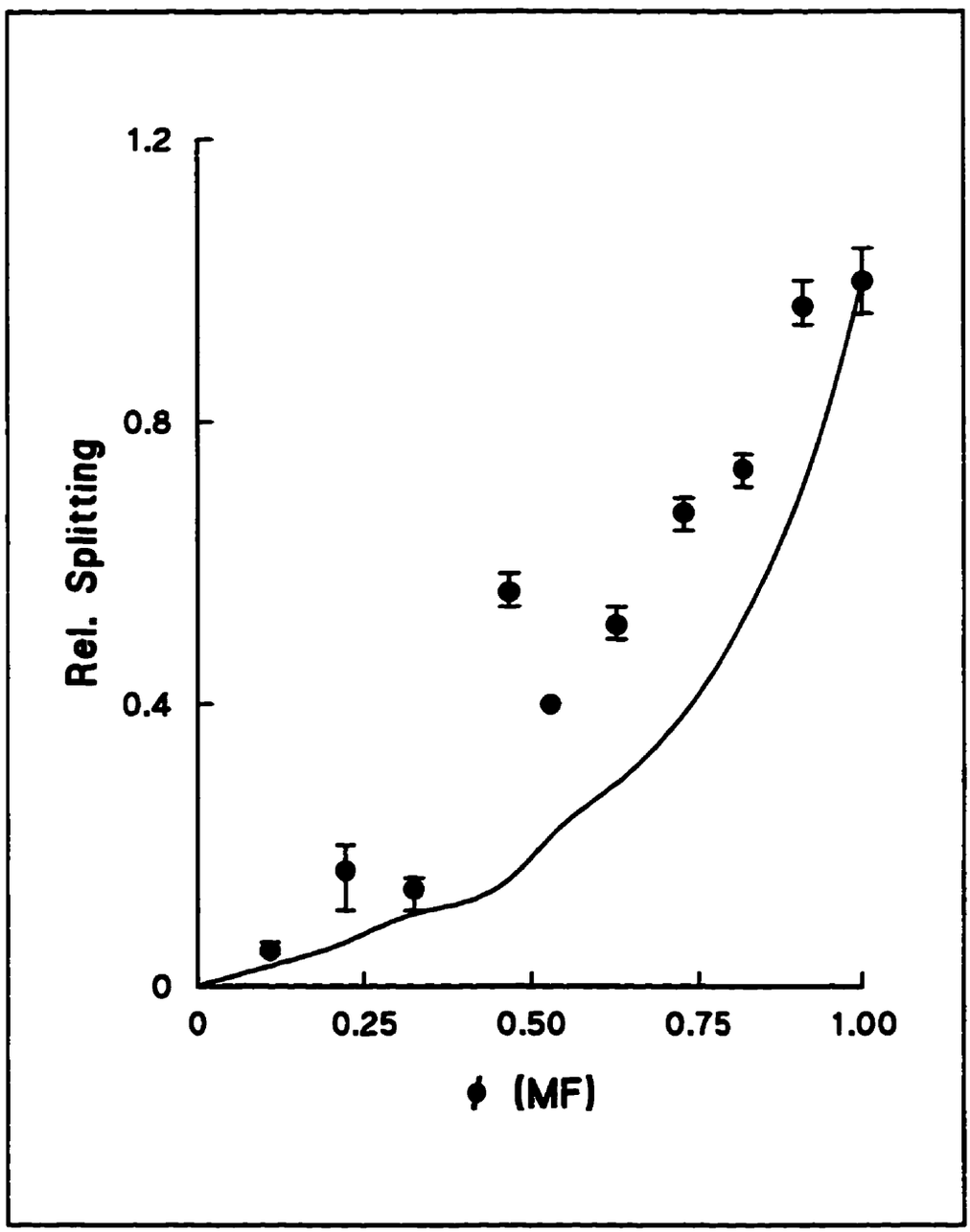

Fig. 4.17: Test of Mirone's (33) Modification of McHale's Model (29,30).

Table 4.9: Summary of the Band 1st Moments, NCE's and Relative NCE's for MF / CH_3CN.

X(MF)	ϕ(MF)	$M_{iso.}$ / cm^{-1}	$M_{aniso.}$ / cm^{-1}	NCE / cm^{-1}	Rel. NCE
0.095	0.107	$1728._6$	$1729._5$	$0._9$	0.25
0.199	0.221	$1727._4$	$1729._2$	$1._8$	0.50
0.296	0.325	$1726._9$	$1727._9$	$1._0$	0.26
0.434	0.467	$1726._5$	$1729._9$	$3._4$	0.93
0.494	0.528	$1726._3$	$1727._9$	$1._6$	0.45
0.594	0.627	$1726._5$	$1728._2$	$1._7$	0.47
0.699	0.727	$1725._6$	$1727._7$	$2._1$	0.58
0.799	0.820	$1724._9$	$1727._4$	$2._5$	0.69
0.899	0.910	$1722._5$	$1726._2$	$3._7$	1.03
1.00	1.00	$1722._3$	$1725._9$	$3._6$	1.0

where C is a constant given by:

$$C = \left(\frac{n_2^2 + 2}{2e_2 + n_2^2} \right)^2 e_2 \qquad [11]$$

(the subscript '2' designates values for the pure solute). Therefore, the refractive indices had to be measured. The refractive indices of MF and acetonitrile are virtually identical (1.3433 and 1.3423, respectively (1)). A plot of 'n' versus volume fraction is shown in Fig. 4.18 (and Table 4.10). This plot has considerable scatter but suggests the 'n' values maximize near X(MF) = 0.5. The "rippling" in the Fig. 4.17 is because of this scatter. As shown in Figs. 4.16 and 4.17 the behaviour of MF in acetonitrile does not conform with either one of these models. McHale (29) has stated her theory is only applicable in the "dilute solution regime" where aggregation is neglected. For a polar species such as methyl formate at the concentrations used here, this model may not be appropriate. Additionally, the ideal solution assumption has been made. Further, Torii (34) has shown, using Monte Carlo simulations, that in the case of acetone the dielectric screening approach of McHale is inadequate for explaining the NCE. Logan's (27,28) is better. In amending McHale's model, Mirone (33) made no assertions about the range of applicability.

The asymmetry present in the isotropic band of MF / d-MF is also present in the solutions of MF / acetonitrile. Just as before, the asymmetry (as measured by $M_{iso.} - \nu_{iso.}$)

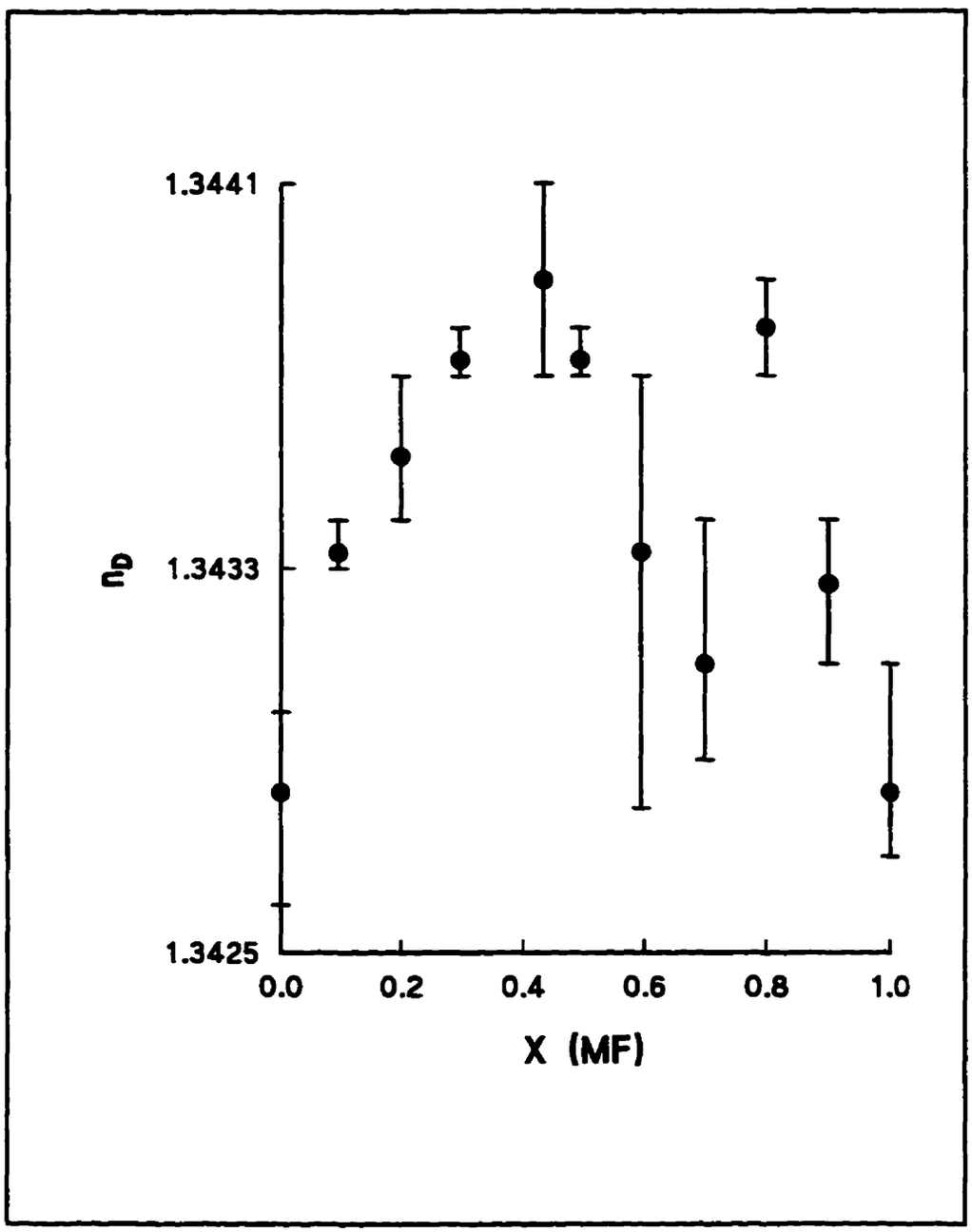

Fig. 4.18: Index of Refraction of Methyl Formate / Acetonitrile Solutions.

Table 4.10: Indices of Refraction of the MF / Acetonitrile Solutions.

X(MF)	ϕ(MF)	n
0.095	0.107	1.3433
0.199	0.221	1.3435
0.296	0.325	1.3437
0.434	0.467	1.3439
0.494	0.528	1.3437
0.594	0.627	1.3433
0.699	0.727	1.3431
0.799	0.820	1.3438
0.899	0.910	1.3432
1.00	1.00	1.3428

decreases as the MF is diluted (see Fig. 4.19). If a linear fit is imposed on the $M_{iso.}$ - $\nu_{iso.}$ versus X(MF) plot, the slope is 4.5 ± 0.75. For the isotopic dilution, however, the slope is 4.7 ± 0.47. Within the statistical errors the slopes are the same. Just as with the isotopic dilutions, the asymmetry of the band is vividly shown by comparing the two half-widths. The high frequency half-width is somewhat greater than the low frequency asymmetry (Fig. 4.20 and Table 4.11). This agrees with Knapp's model (26) in which high frequency asymmetry is seen for coupled oscillators. The "blue" half-width is also more strongly affected by dilution, decreasing quite rapidly below X(MF)~0.7.

The behaviour of the full-width at half maximum of the isotropic C=O band is somewhat different for the two solvents. In d-MF the FWHM initially rises and then, below X(MF)~0.5, falls rapidly. In acetonitrile the initial rise is much smaller. As mentioned above, within Knapp's model (26) this sort of behaviour is unexpected. Bands may broaden as the solute is diluted and Yarwood (21) observed this in solutions of dimethyl formamide. However, an initial increase followed by a decrease is unusual. In the case of the acetonitrile solutions, the largest FWHM reached is 15.5 cm^{-1} at X(MF) = 0.699 (see Table 4.11 and Fig. 4.20) This is just barely significant compared to the FWHM of pure MF (14.7 cm^{-1}). The largest FWHM for the isotopic dilution is 16.8 cm^{-1} at X(MF) = 0.504 (see Table 4.7 and Fig. 4.10) and this *is* significantly greater than the pure methyl formate. These results imply that vibrational dephasing follows a different mechanism in acetonitrile than in d-MF. The intermolecular potential and coupling

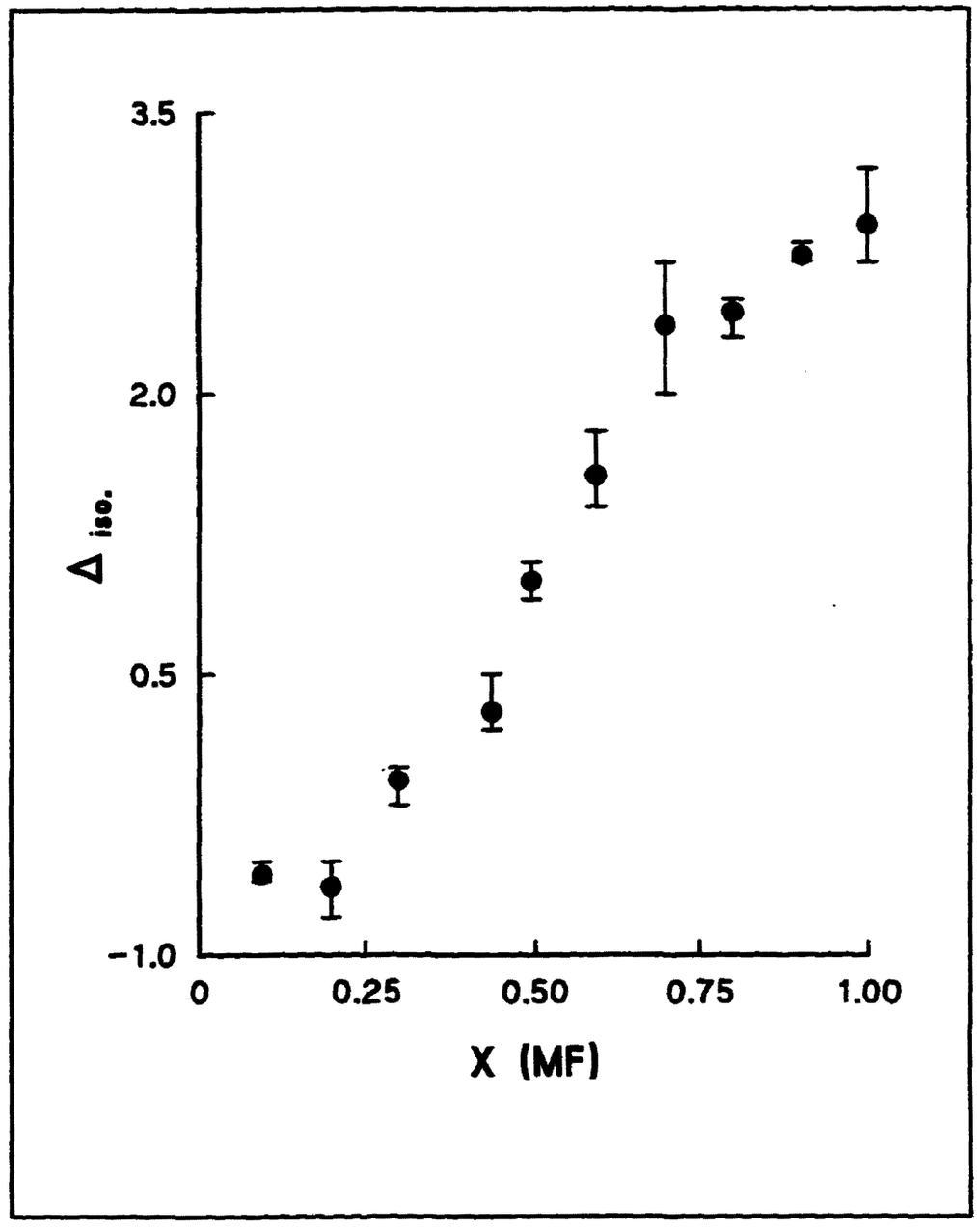

Fig. 4.19: $\Delta_{iso.}$ (= $M_{iso.}$ - $v_{iso.}$) vs. X(MF) for Methyl Formate / Acetonitrile.

between methyl formate molecules must be different in the two solvents. Interestingly, after the maximum bandwidth is reached it falls more sharply in acetonitrile than in d-MF. In acetonitrile, then, the concentration range over which the total amount of intersite coupling is fixed is quite small. Diffusional and orientational effects (as well as any other phenomena affecting the total amount of coupling) become significant at higher concentrations of methyl formate, leading to a decrease in bandwidth below these concentrations. Possibly, as explained in section 4.3.1, the pure dephasing and RET contributions to bandwidth are correlated (i.e., Γ_{dt} of equation [1] $\neq 0$) and the sign of Γ_{dt} may change with dilution.

The results for methyl formate in acetonitrile can be summarized as follows. First, the dilution of methyl formate leads to a progressive shift of the isotropic band to higher frequency. A linear extrapolation gives a Raman shift of 1730 cm^{-1} at infinite dilution. The high frequency asymmetry of the isotropic band decreases as the MF is diluted. These two observations are qualitatively identical to those seen for the isotopic dilution. The NCE decreases with dilution but does not conform to any of the three models tested. It must be said, however, that McHale's model (29,30) was derived for dilute solutions so its application here may be invalid. The FWHM of the isotropic band shows an initial (but very slight) increase followed by a decrease; different in degree from the FWHM behaviour in the isotopic studies where a clear maximum was observed.

Table 4.11: HWHM's and FWHM's for MF / AN.

X(MF)	HWHM ("red") / cm^{-1}	HWHM ("blue") / cm^{-1}	FWHM / cm^{-1}
0.095	$5._4$	$4._6$	$10._0$
0.199	$6._1$	$5._4$	$11._5$
0.296	$6._2$	$6._2$	$12._4$
0.434	$7._0$	$6._9$	$13._9$
0.494	$6._7$	$7._8$	$14._5$
0.594	$6._8$	$8._4$	$15._2$
0.699	$6._6$	$8._9$	$15._5$
0.799	$6._5$	$9._0$	$15._5$
0.899	$6._4$	$8._8$	$15._2$
1.000	$6._2$	$8._5$	$14._7$

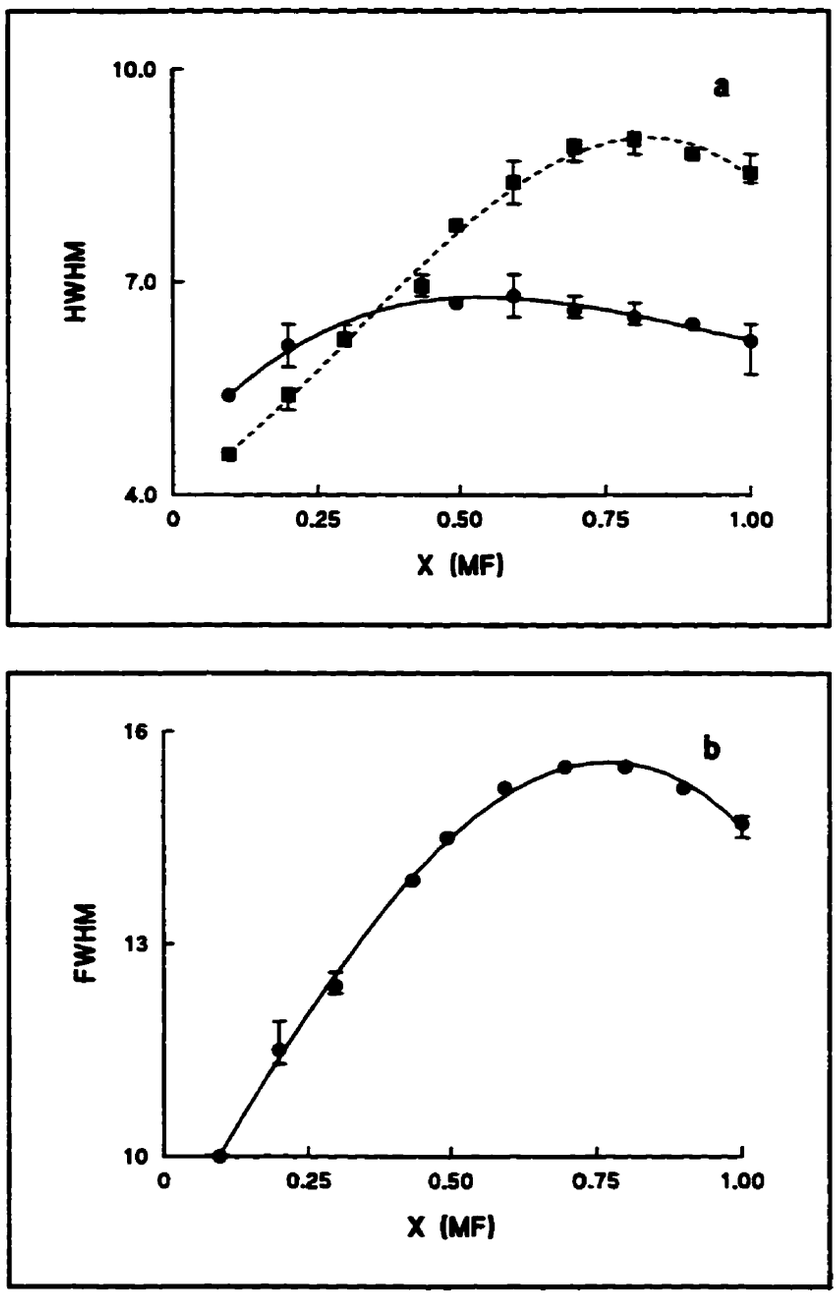

Fig. 4.20: Effect of Dilution on Bandwidth for Methyl Formate / Acetonitrile:
a) HWHM (solid line - low frequency HWHM, dashed line - high frequency HWHM) b) FWHM.

4.4 Summary

The results lead to some important conclusions about the nature of liquid methyl formate. Resonance Energy Transfer is one avenue for vibrational dephasing in organic liquids. It manifests itself most clearly in a non-coincidence of the isotropic and anisotropic peaks which decreases as the solute is diluted. A number of models (15-17,27-30,33) have been suggested to account for its dependence on concentration. The studies of methyl formate clearly indicate this effect is occurring in the liquid. The isotopic dilution studies conform with the theory of Logan (27) wherein the NCE has a linear dependence on mole fraction of the "active" species. Unfortunately, for the non-isotopic dilution (in acetonitrile), the NCE of methyl formate does not conform with any of the models tested. The reasons for this non-conformity are not known. It may, in part, be a result of assuming ideal solution behaviour. Fini and Mirone did suggest two reasons for possible failures of their model. First, the dielectric constant might not be a linear function of volume fraction. Second, specific, short range interactions might not be adequately described by the dielectric constant. In the case of McHale's model (29,30) application to solutions as concentrated as those used here is not likely valid. However, the NCE is decreased as the MF is diluted. In addition, the "rate" of the decrease of the NCE is greater for the isotopic dilution than for the non-isotopic dilution. Because the NCE disappears faster with isotopic dilution, the methyl formate oscillators are being

decoupled more quickly. Methyl d-formate is better at disrupting the preferential alignment required for RET to take place. Intuitively, this makes sense. A deuterated analogue should find it easier to penetrate the solvation shell than a completely "foreign" species.

One of the oddities of these results is the behaviour of the full-width at half maximum of the isotropic band. Under Knapp's (26) model RET can broaden *or* narrow a band even when pure dephasing and RET are uncorrelated. Yarwood (21) has found band broadening with isotopic dilution and explained it in terms of Knapp's model. For both the isotopic and non-isotopic dilutions, the FWHM first increases and then decreases. Thus, according to Knapp's model (26), the total amount of intermolecular coupling is constant for the concentrated solutions of MF and the C=O band broadens with dilution. At some concentration (X(MF)~0.5 for isotopic and X(MF)~0.7 for non-isotopic solutions) this is no longer, true and the band narrows with dilution. Alternatively, the pure dephasing and resonant energy transfer may be correlated (see equation [1]). Because the initial rise is smaller and the concentration at which narrowing begins is higher, the nature of the intermolecular potential for methyl formate molecules must be solvent dependent.

4.5 References

1. CRC Handbook of Chemistry and Physics, 1st Student Edition, CRC Press, Boca Raton, 1988
2. Z. Deng, *Ph.D. Thesis*, **1993**, University of Waterloo
3. J. K. Wilmshurst, *J. Mol. Spectrosc.* **1957** 1 201
4. T. Miyazawa, *Bull. Chem. Soc. Jpn* **1961** 34 691
5. H. Susi, T Zell, *Spectrochim. Acta* **1963** 19 1933
6. J. S. Byrne, P. F. Jackson, K. J. Morgan, N. Unwin, *J. Chem. Soc. Perkin Trans. 2* **1973** 845
7. J. E. Katon, N. L. Ranieri, *Spec. Lett.* **1978** 11 367
8. H. V. Venkatasetty, *J. Electrochem. Soc.* **1975** 122 245
9. W. C. Harris, D. A. Coe, W. O. George, *Spectrochim. Acta* **1976** 32A 1
10. Z. Deng, D. E. Irish, *Can. J. Chem.* **1991** 69 1766
11. R. F. Curl, *J. Chem. Phys.* **1959** 30 1529
12. E. Bock, *Can. J. Chem.* **1967** 45 2761
13. H. Susi, J. R. Scherer, *Spectrochim. Acta* **1969** 25A 1243
14. P. Matzke, O. Chacón, C. Andrade, *J. Mol. Struct.* **1971** 9 255
15. G. Fini, P. Mirone, *J. Chem. Soc. Faraday Trans.* **1974** 70 1776
16. P. Mirone, G. Fini, *J. Chem. Phys.* **1979** 71 2241
17. M. G. Giorgini, G. Fini, *J. Chem. Phys.* **1983** 79 639
18. M. Kamoun, P. Mirone, *Chem. Phys. Lett.* **1980** 75 287

19. H. D. Thomas, J. Jonas, *J. Chem. Phys.* **1989** 90 4144

20. V. M. Shelley, J. Yarwood, *Chem. Phys.* **1989** 137 277

21. V. Shelley, J. Yarwood, *Mol. Phys.* **1991** 72 1407

22. A. Mortensen, O. F. Nielsen, J. Yarwood, V. Shelley, *J. Phys. Chem.* **1994** 98 5221

23. M. Kamoun, *J. Raman Spectrosc.* **1979** 8 225

24. G. Fini, P. Mirone, *Spectrochim. Acta* **1976** 32A 625

25. S. L. Wallen, L. Nikiel, Y. Yi, J. Jonas, *Chem. Phys. Lett.* **1994** 82 229

26. E. W. Knapp, *J. Chem. Phys.* **1984** 81 643

27. D. E. Logan, *Chem. Phys.* **1986** 103 215

28. D. E. Logan, *Chem. Phys.* **1989** 131 199

29. J. L. McHale, *J. Chem. Phys.* **1981** 75 30

30. C. H. Wang, J. McHale, *J. Chem. Phys.* **1980** 72 4039

31. J. Yarwood, *private communication*

32. A. Würflinger, *Ber. Bunsenges Phys. Chem.* **1980** 84 653

33. P. Mirone, *J. Chem. Phys.* **1982** 77 2704

34. H. Torii, *J. Molec. Struct. (Theochem.)* **1994** 311 199

5. SUMMARY AND CONCLUSIONS

5.1 Formic Acid

Formic acid was studied in a number of solvents: water, acetonitrile, 1.4-dioxane and dichloromethane. Each of these solvents had a different effect on the spectrum of formic acid, although the spectra for the acetonitrile and 1,4-dioxane solutions were somewhat similar. For the aqueous solutions a very pronounced non-coincidence effect (which decreased as the formic acid was diluted) was seen. The size of the NCE (especially when compared to non-hydrogen bonded methyl formate) and the great width of the bands strongly suggest resonance energy transfer is occurring. The presence of RET implies considerable "structural order" (no doubt augmented by the hydrogen bonding) in the liquid which allows the individual oscillators to couple. Dilution in acetonitrile and 1,4-dioxane led to the development of two peaks at ~1735 cm^{-1} and at ~1765 cm^{-1}. The band at ~1735 cm^{-1} is almost coincident with the carbonyl frequency of dilute methyl formate. Because methyl formate is a "model" for non-hydrogen bonded formic acid, the ~1735 cm^{-1} band was assigned to "free" formic acid. The ~1765 cm^{-1} band does not appear in solutions of formic acid in water nor in solutions in dichloromethane. Because independent evidence existed for a formic acid--solvent

complex in acetonitrile and 1,4-dioxane solutions (perturbations in the spectra of pure acetonitrile and pure 1,4-dioxane), the band at ~1765 cm^{-1} was assigned to a formic acid···solvent complex.

For the formic acid / acetonitrile solutions, this complex was studied in more detail. A shoulder at ~2270 cm^{-1} developed on the C≡N stretch at ~2255 cm^{-1} and was assigned to the C≡N stretch of acetonitrile "bound" to formic acid. A Job Plot gave an ambiguous result. Equilibrium constants were calculated using several different stoichiometries. For all models the equilibrium constants increased dramatically at high formal concentrations of acetonitrile. The formation of more than one complex is possible and at the higher concentrations of acetonitrile a mixture of complexes may exist.

Future work on solutions of formic acid should focus on achieving a better understanding of the formic acid···acetonitrile complex. The most immediate question is the possibility of a mixture of complexes at high relative amounts of acetonitrile. The "Job" plot constructed from these experiments was based on rather high formal concentrations of both acetonitrile and formic acid. The preparation of a second Job plot with lower formal concentrations would be useful. Furthermore, it might help resolve the ambiguity concerning the co-ordination number. Solutions with a constant concentration of formic acid but varying concentrations of acetonitrile should also be studied. Such studies could shed some light on the question of the presence of more than one complex.

In addition to these immediate suggestions, the project could be expanded along two other lines. First, formic acid and its "association" with other nitriles (e.g., butyronitrile or acrylonitrile) could be examined. Second, the "association" of other carboxylic acids (e.g., acetic acid) and acetonitrile could be studied.

5.2 Methyl Formate

Originally, methyl formate was studied to gain a better understanding of the structure of liquid formic acid. This was not quite as successful as hoped. However, experiments on methyl formate did yield some important observations. First, the carbonyl band is much narrower and the non-coincidence effect is much smaller for methyl formate than for formic acid. Unlike methyl formate, formic acid can be expected to be extensively hydrogen bonded. The large differences in bandwidth and NCE (between formic acid and methyl formate) support this assertion. Second, in both acetonitrile and methyl d-formate the carbonyl band maximum at infinite dilution was ~1730 cm^{-1}, almost coincident with a band in solutions of formic acid. Consequently, the band at ~1735 cm^{-1} in formic acid was assigned to "free" formic acid monomer. Third, the spectrum of methyl formate in acetonitrile did not show any association between methyl formate and acetonitrile. Other than reducing the size of the NCE, the acetonitrile did not affect the carbonyl region of methyl formate. Furthermore, the C≡N stretch of acetonitrile was

unaffected. These observations led to the conclusion that (not surprisingly!) association between formic acid and acetonitrile occurs through the acid proton and the nitrogen of acetonitrile.

In addition to these observations, the experiments revealed some interesting facts about the structure of liquid methyl formate. A non-coincidence effect in methyl formate indicates resonance energy transfer is taking place in liquid methyl formate. The size of the NCE decreases as the methyl formate is diluted. Qualitatively, the behaviour of the isotropic band - a) a band shift to higher frequency with dilution; b) high frequency asymmetry which decreases with dilution; c) change of bandwidth with dilution - is consistent with Knapp's (1) model for "reactive coupling". For the isotopic dilution the methyl formate NCE effect shows reasonably good agreement with Logan's model (2). Unfortunately, the non-isotopic dilution shows very poor agreement with the models (3-8) tested. The existence of RET in liquid methyl formate suggests some significant short term, short range order in the liquid that allows the transition dipoles to couple. This short range order should not be interpreted as the formation of dimers in the "traditional" sense. If this were true, far more dramatic results would have been seen in the carbonyl region. The behaviour of the FWHM of methyl formate was also quite interesting. In both the isotopic and non-isotopic dilutions, the FWHM initially increased and then decreased. Under Knapp's model (1) this indicates the total amount of intermolecular coupling is initially constant but varies below some "threshold" concentration. The

variation of the FWHM was also different for the two different dilutions indicating (not surprisingly) that the intermolecular potential for methyl formate is solvent dependent. The behaviour of the bandwidths may also suggest that the pure dephasing and RET contributions to the bandwidth are not uncorrelated.

Expansion of the work on methyl formate could follow several paths. First, a different solvent for non-isotopic dilution could be used. Logan's model for isotopic dilution (2) was reasonably successful and the non-isotopic model (9) is an expansion (albeit a complex expansion) of the isotopic model. To do this, a solvent which has a hard sphere diameter within 10% of the hard sphere diameter of methyl formate must be found. The data needed to find such a solvent may be difficult to discover. Furthermore, in a different, non-isotopic, solvent methyl formate might conform with the other models (3-8). Second, the effect of ions on the NCE could be studied. Methyl formate has been suggested as a solvent for lithium battery electrolytes (10). Of course, ions must be added. A study of the NCE as a function of salt (e.g., $LiAsF_6$) concentration would be quite interesting. Replacing methyl formate molecules in the solvation shell with ions should disrupt the local order and lead to a decreased NCE. A third, broader, path is to study the NCE of other simple esters (e.g., methyl acetate).

5.3 References

1. E. W. Knapp, *J. Chem. Phys.* **1984** 81 643
2. D. E. Logan, *Chem. Phys.* **1986** 103 215
3. G. Fini, P. Mirone, *J. Chem. Soc. Faraday Trans.* **1974** 70 1776
4. P. Mirone, G. Fini, *J. Chem. Phys.* **1979** 71 2241
5. M. G. Giorgini, G. Fini, *J. Chem. Phys.* **1983** 79 639
6. J. L. McHale, *J. Chem. Phys.* **1981** 75 30
7. C. H. Wang, J. McHale, *J. Chem. Phys.* **1980** 72 4039
8. P. Mirone, *J. Chem. Phys.* **1982** 77 2704
9. D. E. Logan, *Chem. Phys.* **1989** 131 199
10. E. Plichta, M. Salomon, S. Slane, M. Uchiyama *J. Sol. Chem.* **1987** 16 225